INFORMATION TO USERS

This manuscript has been reproduced from the microfilm master. UMI films the text directly from the original or copy submitted. Thus, some thesis and dissertation copies are in typewriter face, while others may be from any type of computer printer.

The quality of this reproduction is dependent upon the quality of the copy submitted. Broken or indistinct print, colored or poor quality illustrations and photographs, print bleedthrough, substandard margins, and improper alignment can adversely affect reproduction.

In the unlikely event that the author did not send UMI a complete manuscript and there are missing pages, these will be noted. Also, if unauthorized copyright material had to be removed, a note will indicate the deletion.

Oversize materials (e.g., maps, drawings, charts) are reproduced by sectioning the original, beginning at the upper left-hand corner and continuing from left to right in equal sections with small overlaps. Each original is also photographed in one exposure and is included in reduced form at the back of the book.

Photographs included in the original manuscript have been reproduced xerographically in this copy. Higher quality 6" x 9" black and white photographic prints are available for any photographs or illustrations appearing in this copy for an additional charge. Contact UMI directly to order.

U·M·I

University Microfilms International
A Bell & Howell Information Company
300 North Zeeb Road, Ann Arbor, MI 48106-1346 USA
313/761-4700 800/521-0600

Order Number 9321164

Low-temperature pathways to Chevrel phases via reduced molybdenum sulfide cluster complexes

Hilsenbeck, Shane Jay, Ph.D.

Iowa State University, 1993

U·M·I
300 N. Zeeb Rd.
Ann Arbor, MI 48106

Low temperature pathways to Chevrel phases via reduced molybdenum sulfide cluster complexes

by

Shane Jay Hilsenbeck

A Dissertation Submitted to the
Graduate Faculty in Partial Fulfillment of the
Requirements for the Degree of
DOCTOR OF PHILOSOPHY

Department: Chemistry
Major: Inorganic Chemistry

Approved:

Signature was redacted for privacy.

In Charge of Major Work

Signature was redacted for privacy.

For the Major Department

Signature was redacted for privacy.

For the Graduate College

Iowa State University
Ames, Iowa

1993

TABLE OF CONTENTS

LIST OF FIGURES

PAPER 1.

PAPER 2.

PAPER 3.

LIST OF TABLES

PAPER 3.

GENERAL INTRODUCTION

Statement of Problem

Over the previous twenty years, ternary molybdenum chalcogenides of the general formula $M_xMo_8Y_8$ (M=ternary metal cation; Y=chalcogenide), known as Chevrel phases, have been extensively studied. Many of these compounds have been shown to be superconductors[1,2] as well as ion conductors.[3,4] However, more interest has developed concerning the use of these compounds as heterogeneous catalysts for hydrodesulfurization (HDS).[5-9]

The importance of this catalytic process is evidenced by the fact that over 60 million barrels of oil per day undergo HDS before further processing.[10] The predominant sulfur species are thiophenes[11] which undergo desulfurization as shown in equation 1:[12]

$$C_4H_4S + H_2 \xrightarrow[T=300\text{-}500°C]{\text{catalyst}} C_4H_x + H_2S \qquad (1)$$

The typical HDS catalyst is produced from molybdenum (or tungsten) oxides with a promoter metal such as cobalt (or nickel) supported on high surface area alumina (γ-Al_2O_3).[13] The precursor material is sulfided to form the "Co-Mo-S" catalyst which contains phases of MoS_2 and Co_9S_8.[14] Recently, a number of Chevrel phase compounds have been shown to possess higher HDS activities than the commonly

used Co-Mo-S catalysts. The Chevrel phases were also found to be more selective catalysts since these materials exhibited less 1-butene hydrogenation.[5-9]

The largest drawback concerning these Chevrel phase catalysts is their low surface area (0.1-1.5 m^2/g) relative to the supported Co-Mo-S catalysts on γ-Al_2O_3 (100 m^2/g). It is commonly observed in these types of catalytic processes that the activity increases with surface area; therefore, there is a need for the development of supported Chevrel phases.

The production of the Chevrel phases has generally involved solid state reactions at high temperatures (800-1200°C). This method has resulted in some difficulties in preparing stoichiometric, monophasic compounds. Further annealing or reaction at even higher temperatures has resulted in improvements in purity.[15] In order to produce supported Chevrel phase compounds, a variety of methods have been attempted including evaporation,[16] sputtering,[17] and chemical vapor transport.[18] Recently, though, lower temperature routes using polythiomolybdates and metal chlorides as solution precursors have been reported.[19,20] Also, the first example of an alumina-supported Chevrel phase compound has been published.[21] Likewise, a major focus of the McCarley research group has been on the preparation of $Mo_6S_8L_6$ cluster complexes as low temperature pathways to the Chevrel phases.

A similarity was noted that both molybdenum (II) halides and the Chevrel phases contain hexanuclear cluster units, although the overall structures are quite different. The structure of the Mo_6Y_8 unit is shown in Figure 1. This cluster consists of an octahedron of molybdenum atoms with eight triply bridging ligands (chalcogenide or

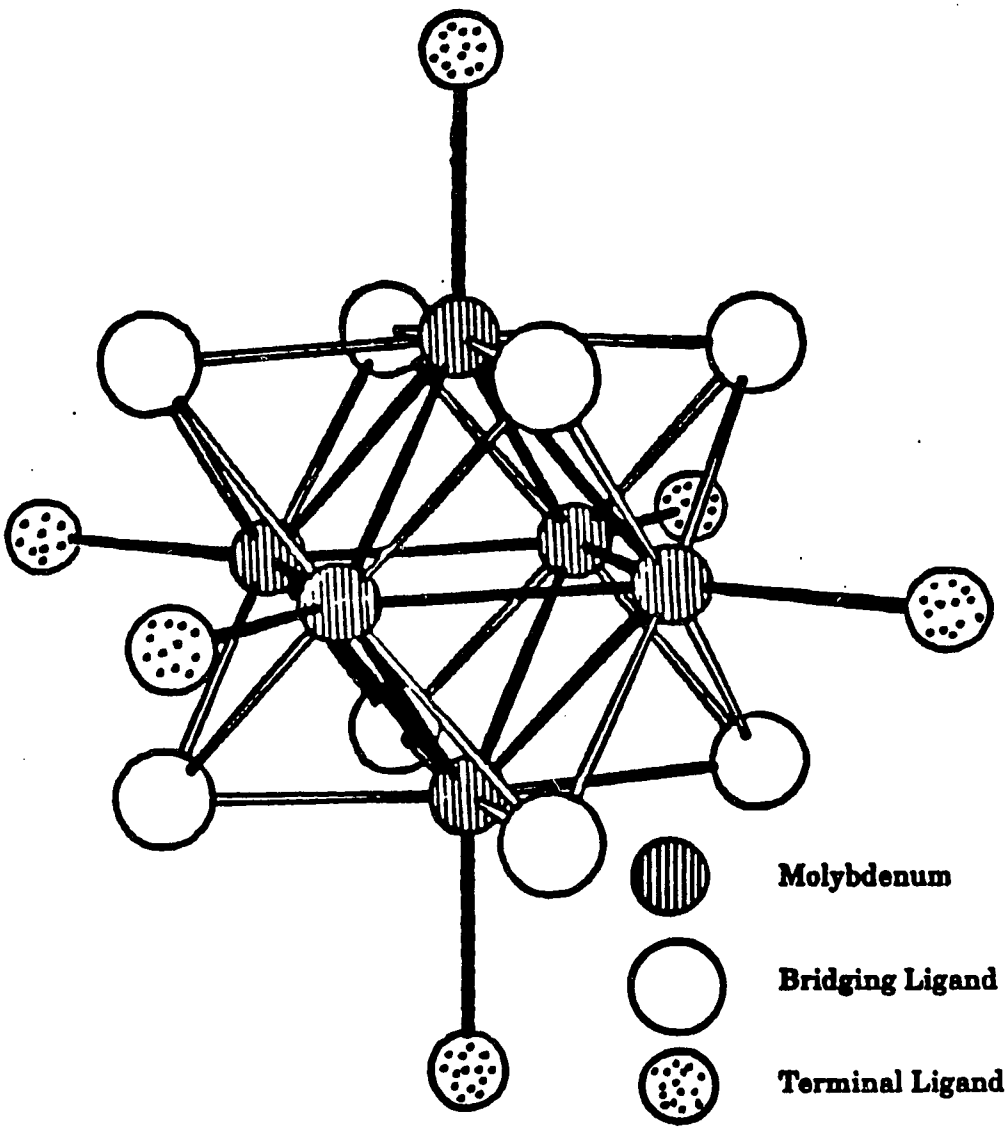

Figure 1. Structure of $Mo_6Y^i_8L^a_6$ cluster

halogen) capping each cube face. These bridging ligands are noted by Schäfer as "*i*" for "*inner.*" The six terminal positions located at the vertices of the octahedron are noted as "*a*" for "*ausser.*"[22] The hexanuclear molybdenum clusters can combine in various ways as evidenced in Figure 2. The *a-i* designation, which is evidenced in the Chevrel phases, signifies a ligand in the terminal position of one cluster that is shared through a bridging position of another cluster.

This structural similarity led to the exploration of mixed halide-chalcogenide systems. The first molecular chalcohalide, $[(pyH)_3(Mo_6Cl_7S)Cl_6]$, was reported by Michel and McCarley.[23] This $Mo_6SCl_7^{3+}$ cluster was prepared by the sulfidation of molybdenum (II) chloride (Mo_6Cl_{12}). Additional substitution of sulfur for chlorine into Mo_6Cl_{12} has resulted in a series of molecular complexes, $Mo_6S_xCl_{8-x}L_y$, where x varies from 3 to 8.[24-29] Reactions which produce incomplete replacement of the chlorine have shown mixtures of cluster products that possess a wide range of x values. The fully sulfided cluster complexes are better characterized as evidenced by the single crystal structure solutions for the triethylphosphine and tetrahydrothiophene adducts.[26-29] Concurrently, the triethylphosphine adduct has been reported by an unrelated synthetic procedure.[30,31]

The success in preparing hexamolybdenum sulfide cluster complexes through the sulfidation of molybdenum (II) chloride also led to the exploration of the tungsten analogues. This research has resulted in the preparation of structurally characterized adducts of the $W_6S_8L_6$ cluster unit where L is pyridine, triethylphosphine, and tetrahydrothiophene.[32]

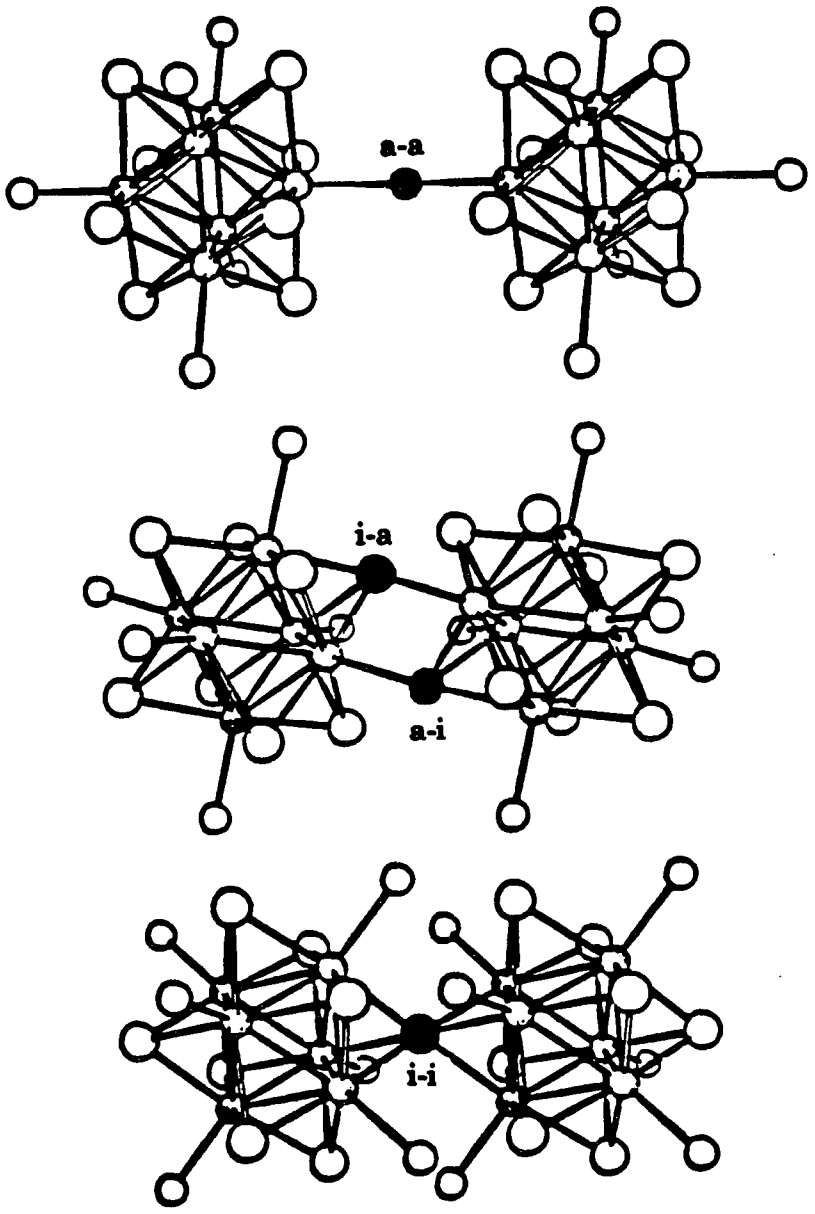

Figure 2. Possible ways that ligands can be shared between two $Mo_6Y^i_6L^a_6$ cluster units

The focus of this project has been to further develop the understanding of these hexamolybdenum sulfide cluster complexes and move toward the overall goal of a low temperature route to the Chevrel phases. Areas of investigation have included the preparation and characterization of new nitrogen-donor cluster complexes, the better characterization of previously synthesized complexes, the subsequent deligation and reaction of these cluster complexes in attempts to form Chevrel phase compounds, and the preparation of ternary molybdenum sulfides which resemble the Chevrel phases.

Explanation of Dissertation Format

This dissertation consists of three papers. Each paper is formatted for publication in a technical journal and the cited references are found at the end of each paper. A General Summary follows the three papers. The references cited in the General Introduction and Review of Previous Work are found at the end of the dissertation.

REVIEW OF PREVIOUS WORK

Chevrel Phases

In 1971, Chevrel *et al.* reported the existence of a new series of ternary molybdenum sulfides.[33] These materials, with the general formula $M_xMo_6Y_8$ (M=ternary metal, Y=chalcogen, $0 \leq x \leq 4$), have been found in about 160 different compounds and solid solutions with over 45 different ternary metal cations (as shown in Figure 3).[34] Chevrel phases have also been produced with both molybdenum and chalcogen substitution, where the metals (Nb, Ta, Re, Ru, Rh) replaced molybdenum ($Mo_{6-x}M_xY_8$) and Cl, Br, I, O were substituted for the chalcogen ($Mo_6Y_{8-x}X_x$).[2] Almost all of these compounds were synthesized directly from the ternary metal, chalcogen, and molybdenum (or binary chalcogenides) at 1000-1300°C with several annealings at 1000-1200°C. An exception is the metastable Mo_6S_8, which can only be prepared by indirect routes.[35,36]

There are generally two classes of compounds among the Chevrel phases. The first class corresponds to M being a small cation (Cu, Co, Fe, Ni) where the cation concentration is variable ($Cu_xMo_6S_8$, $1.8 \leq x \leq 4.0$). The large M cations (Pb, Sn, RE), where the cation concentrations are equal to 1.0 or have a very narrow domain ($Sn_xMo_6S_8$, $0.9 \leq x \leq 1.1$), make up the second class. Substitution of a second metal cation for the large cation can occur and results in a wide range of solid solutions.

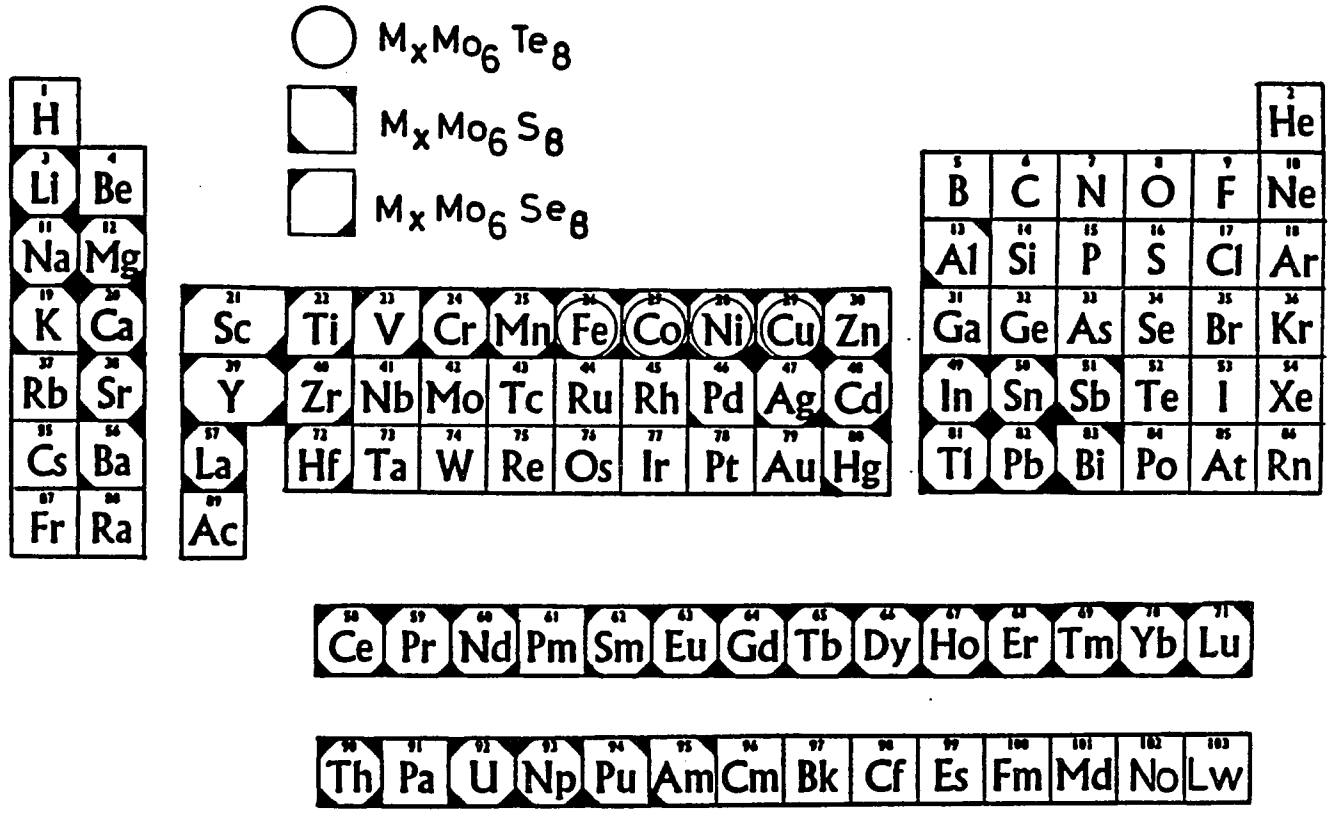

Figure 3. Periodic table showing the wide range of metals which can act as ternary cations in the Chevrel phase compounds

The first ternary molybdenum sulfide crystal structure was determined for $Ni_2Mo_6S_8$[37] and the observation was made that nearly all of these compounds crystallize in a hexagonal-rhombohedral structure ($R\bar{3}$) with α_R~90° and a_R~6.5Å. However, when the ternary metal is small and the metal concentration increases, several phases do undergo a triclinic distortion ($P\bar{1}$).[33] All of these structures are closely related to the Mo_6Y_8 unit and can be described as a three dimensional network of interlinked Mo_6Y_8 clusters. As shown in Figure 1, the cluster unit is a molybdenum octahedron with each face capped by one chalcogen. The actual structure shows an elongation along the ternary axis which results in a distortion of the molybdenum octahedron. Alternately described, the molybdenum atoms are slightly outside the face centers of the sulfur cube. The clusters are linked together such that each of the six bridging chalcogens not located on the ternary axis (three-fold axis in $R\bar{3}$) serves as a terminal ligand for one of the six neighboring clusters, as shown in Figure 4. The connectivity can be described as $(Mo_6Y_2^{i}Y_{6/2}^{i-a})Y_{6/2}^{a-i}$. This strong linkage can be evidenced by the short, covalent Mo-Y intercluster distances of 2.4-2.6 Å which are nearly as short as the intracluster Mo-Y distances and can result in direct, though weak, intercluster Mo-Mo interactions (3.1-3.4 Å).

This arrangement of the Mo_6Y_8 units leaves cavities in the chalcogen network as indicated by "1" and "2" in Figure 5. The largest cavity (site 1), with approximately cubic shape, lies at the origin of the rhombohedral cell. Much smaller holes (site 2) are found on either side of the large cavity (site 1). These cavities are all interconnected and form infinite channels along the rhombohedral axes. The large

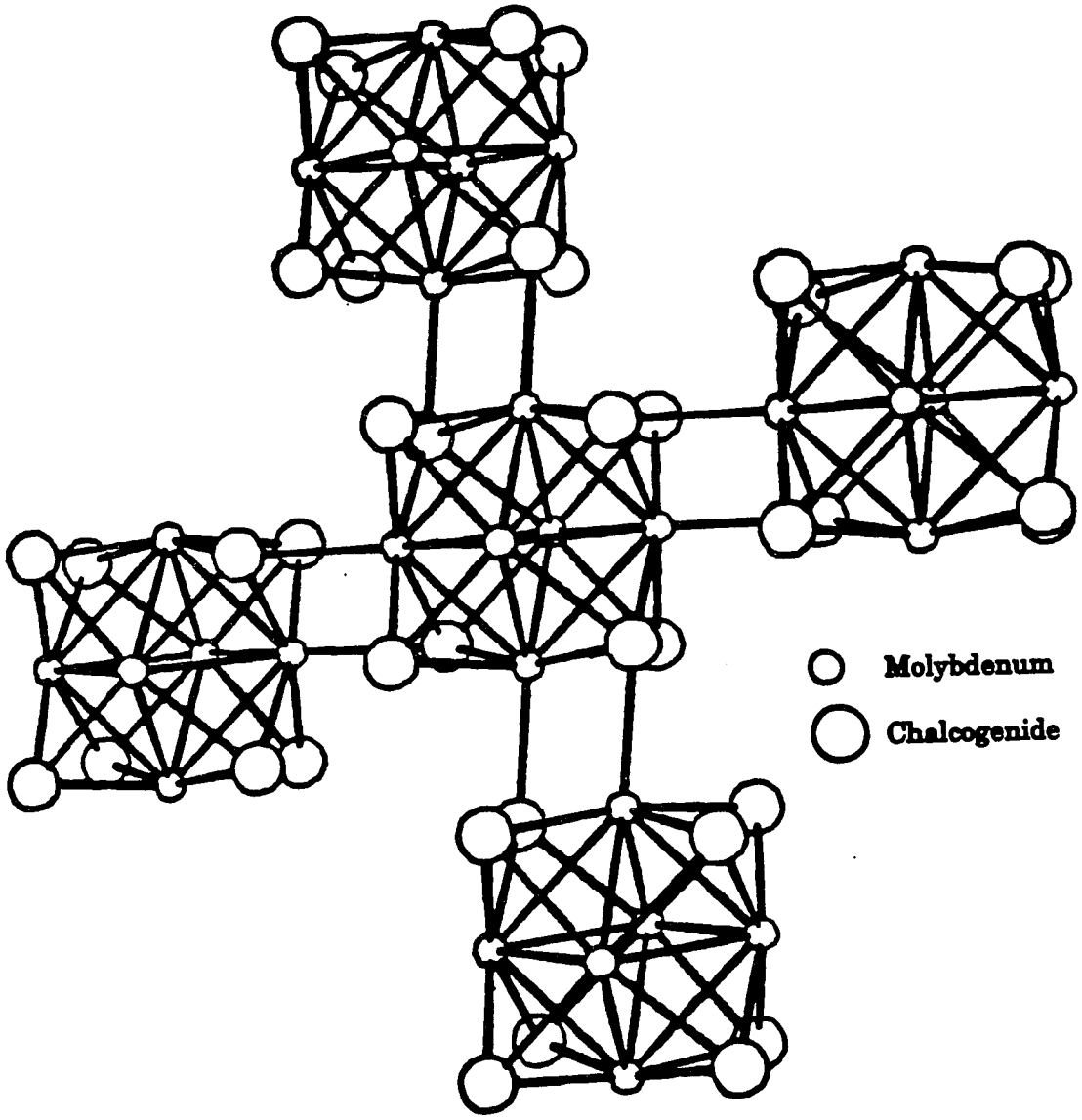

Figure 4. Structure of the Chevrel phases showing four of the six neighboring clusters

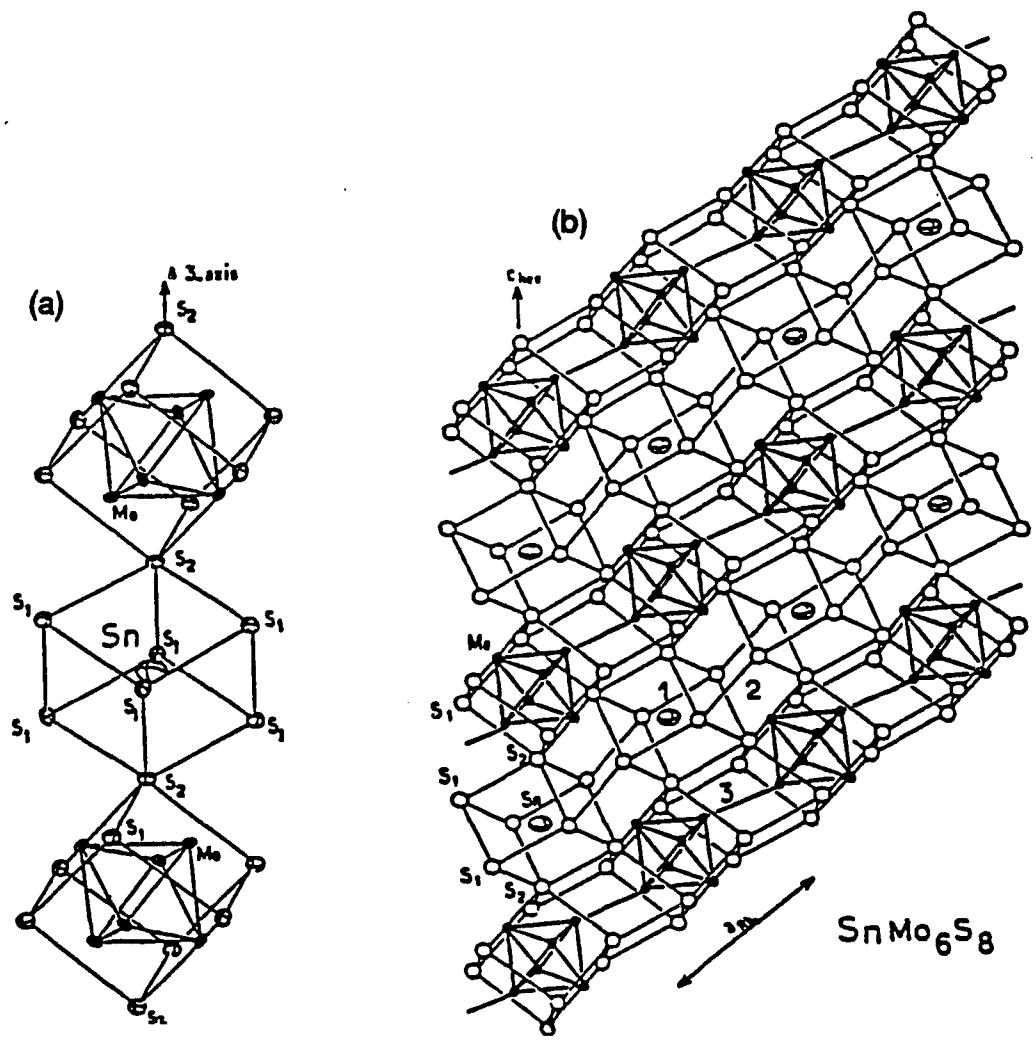

Figure 5. a) The stacking of the Mo_6S_8 units and S_8 cubic sites along the threefold axis. Here, the Sn atoms are located at the cell origin. b) View of the projection of the $SnMo_6S_8$ structure on the hexagonal $(11\bar{2}0)$ plane. Cavities can be noticed in the chalcogen atom network where sites 1 and 2 are partially filled by ternary metals and the intercluster Mo-Mo bond occurs through site 3.

metal atoms exclusively fill site 1 to yield stoichiometric (x~1) compounds, while the smaller cations occupy both types of sites. This resulting partial occupancy yields non-stoichiometric compounds (x>1).

The occupancy of these cavities by the ternary metal is the only overall structural difference between the binary and ternary Chevrel phases. Therefore, the ternary phase can be viewed as the insertion of metal cations into the binary lattice. This concept can be exhibited in the preparation of the metastable Mo_6S_8 phase via the acidic leaching of a small cation ternary molybdenum sulfide as shown in equation 2.[35,36]

$$M_xMo_6S_8 + 2x\ HCl \rightarrow Mo_6S_8 + x\ H_2 + x\ MCl_2 \quad (M=Co,\ Cu,\ Fe,\ Ni) \qquad (2)$$

The high ionic mobility of the small ternary metal cations allows for the relative ease of chemical or electrochemical insertion and removal at room temperature. A variety of metastable ternary Chevrel phases can be prepared from the reaction with the binary Mo_6S_8 phase as shown in equation 3.[3,38]

$$x\ M + Mo_6S_8 \rightarrow M_xMo_6S_8 \qquad (3)$$

electrochemical - Li, Na, small cations at 25°C
chemical - Li (n-BuLi) at 25°C
Hg at 350°C

Electrochemical insertion of large cations into the binary Mo_6S_8 phase has not succeeded; yet, thermal insertion is possible with higher temperatures (470°C) and long reaction times (1-3 weeks).[39]

The physical properties of the Chevrel phase compounds are greatly dependent on the ternary metal cation. This influence is the result of a transfer of valence electrons from the "ionic" metal to the electron-deficient, metallic Mo_6Y_8 component.[1] Band structure calculations[40,41] on the Chevrel phases have indicated that the conduction band is made up of E_g cluster HOMO's and lies just below the 24 electron gap. The calculations suggested that the addition of more electrons to the cluster via a higher cation concentration or higher cation charge would cause a decrease in the intracluster Mo-Mo distance. This trend was observed experimentally, as evidenced for $Pb_{0.92}Mo_6S_8$ - 2.710 Å and Mo_6S_8 - 2.807 Å.[2] Yvon has shown that the intercluster Mo-Mo distances increase with the addition of electrons via charge transfer.[1] From band structure calculations, the conduction band of E_g character possesses δ-type symmetry ($d_{x^2-y^2}$) and results in very little interaction with neighboring clusters.[40] Therefore, the addition of electrons causes strengthening of the intracluster bonding (cluster contraction) and concomitant lengthening of the intercluster Mo-Mo distances.

Magnetic properties and the conductance of these materials have also been found to be dependent on the type of ternary metal cation that is present. Magnetic susceptibility studies have shown that the addition of a diamagnetic cation (e.g. Cu^+,Pb^{2+}) results in an overall diamagnetic species with a residual temperature-independent paramagnetism. The addition of a magnetic metal cation (e.g. Fe^{2+},RE^{3+}) gives rise to Curie-Weiss behavior.[34] The ternary Chevrel phase compounds have all been found to be metallic conductors. The only materials

showing semiconductor behavior are the pseudobinary rhenium substituted molybdenum phases - $Re_4Mo_2Y_8$.[42] Even the 20 electron Mo_6Y_8 binary phases are metallic. This result agrees with the calculations which show that the conduction band is not purely E_g in character, but contains some chalcogenide p character and thus is not completely empty.[40] Many of the Chevrel phases also show superconductivity. This occurrence is greatly dependent on the bonding between clusters.[1]

HDS Studies on Chevrel Phases

The observed HDS activities permit the grouping of the sulfide Chevrel phases according to their cation sizes. The large cation compounds show high activities, while the small cation materials show much lower values.[5,6] Table 1 compares several Chevrel phase compounds with Co-Mo-S (commonly used HDS catalyst) and MoS_2.

Table 1. Thiophene hydrodesulfurization activities after 10 hour reaction at 400°C

	% thiophene conversion	HDS Rate ($x10^8$ mol/m^2s)
$Ho_{1.2}Mo_6S_8$	2.20	11.23
$PbMo_{6.2}S_8$	1.28	6.68
$SnMo_{6.2}S_8$	1.72	3.24
$Co_{1.6}Mo_6S_8$	0.47	1.02
$Co_{0.25}$-Mo-S	0.77	2.92
MoS_2	0.76	0.92

The most active phases involve large cations (Ho, Pb, Sn) which are generally considered poor "promoters", while the compounds containing Co and Ni - the two most common HDS promoters - are among the least active Chevrel phases. This result has been explained in that the large cations have little mobility which produces structural stability and thus catalytic stability.[5-8] The high mobility of the small cations, as observed in their high ion conductivity, allows these cations to "retreat" from the surface into the bulk structure. This movement makes the material less reactive and opens sites to surface oxidation and subsequent destabilization by forming MoS_2.

Alternative Routes to Chevrel Phases

An initial report by Sergent focused on the high temperature reduction of alkali metal intercalated molybdenum disulfides under a hydrogen atmosphere.[43] Later, Behlock *et al.* described the hydrogen reduction of lithiated molybdenum disulfide at 1000°C to prepare impure $Li_4Mo_6S_8$.[44] The platinum catalyzed reduction of MoS_2 with copper and nickel at 1000-1050°C was reported by Nanjundaswamy *et al.*[45]

More recently, the lower temperature solution precursor method using polythiomolybdates and metal chlorides has been explored as a pathway to the Chevrel phases. These solution precursors can then undergo hydrogen reduction at elevated temperatures as evidenced in equations 4 and 5.[19,20]

The reaction shown in equation 4 can also result in the preparation of Chevrel phase compounds with Pb, La, and Gd as the ternary metal cation. A MoS_2 impurity

phase is found in the final product of reaction 5. Subsequent work by Rabiller-Baudry *et al.* has resulted in the preparation of an alumina-supported Chevrel phase material.[21] This reaction also results in the production of a MoS_2 impurity phase.

$$2\ Cu(NH_3)Mo_3S_9 + 9\ H_2 \xrightarrow[4\text{-}5\ hrs]{1000°C} Cu_2Mo_6S_8 + 10\ H_2S + 2\ NH_3 \qquad (4)$$

$$2\ (NH_4)_2Mo_3S_{13} + 2\ CuCl_2 \cdot 2H_2O + 18\ H_2 \xrightarrow[20h]{600°C} Cu_2Mo_6S_8 + 4\ NH_3 + 4\ HCl + 18\ H_2S + 4\ H_2O \qquad (5)$$

Molecular Complexes of Hexamolybdenum Chalcogenides and Chalcohalides

Until quite recently, molecular complexes with the Mo_6Y_8 cluster unit seen in the Chevrel phases have not been found.[28-31] Prior to the establishment of the molecular Mo_6Y_8 units, only molecular complexes of mixed sulfide-chloride clusters had been observed. The first molecular chalcohalide was reported by Michel and McCarley.[23] The Mo_6SCl_7 cluster was prepared by the sulfidation of Mo_6Cl_{12} and isolated as crystals of $(pyH)_3[(Mo_6SCl_7)Cl_6]$ and $(pyH)_3[(Mo_6SCl_7)Cl_6]\cdot$ 3pyHCl. Since sulfur and chlorine are indistinguishable by x-ray diffraction, x-ray photoelectron spectroscopy (XPS) was used to determine that the sulfur atom occupied a bridging position in the cluster. The corresponding average intramolecular Mo-Mo bond distances of these two structures were equivalent (2.610 Å) and were found to agree quite well with values observed for the isoelectronic $Mo_6Cl_8^{4+}$ cluster of Mo_6Cl_{12} (2.613 Å)[46] and the $Mo_6SCl_7^{3+}$ unit of $Mo_6Cl_{10}S$ (2.615 Å).[47] These clusters which

possess 24 electrons for Mo-Mo bonding are all close to the estimated Mo-Mo single bond distance of 2.614 Å.

Michel also reported the crystal structure of what was believed to be $Mo_6S_6Cl_2(py)_6$.[24] This compound also showed no evidence for ordering of the sulfides and chlorides. The average intracluster Mo-Mo distance of 2.634 Å was close to the value estimated for a 22 electron cluster. Additional sulfidation of Mo_6Cl_{12} has yielded a series of mixed molybdenum chalcohalides with the general formula $Mo_6S_xCl_{8-x}L_y$ ($3 \leq x \leq 8$, y-variable) where incomplete sulfur substitution often leads to a mixture of cluster products.[24-29]

Recently, Saito *et al.* published the crystal structure of $Mo_6S_8(PEt_3)_6$ which was prepared by the reductive dimerization of trimeric Mo_3S_4 clusters:[30]

$$Mo_3S_7Cl_4 + 8\ PEt_3 \xrightarrow{\text{toluene}} Mo_3Cl_4(PEt_3)_5 + 3\ SPEt_3$$
$$2\ Mo_3S_4Cl_4(PEt_3)_5 + 4\ Mg \xrightarrow{\text{thf}} Mo_6S_8(PEt_3)_6 + 4\ MgCl_2 + 4\ PEt_3 \qquad (6)$$

The selenide analogue has been prepared by the same method, as well as, a report on the one electron reduction to form $[PPN][Mo_6Y_8(PEt_3)_6]$ (Y=S,Se; PPN=$(Ph_3P)_2N$).[31]

Concurrently, McCarley *et al.* reported on the successful preparation of a series of molecular compounds with the Mo_6S_8 cluster unit via sulfidation of Mo_6Cl_{12}.[28,29] Adducts of pyridine (py), propylamine ($PrNH_2$), triethylphosphine (PEt_3), and tetrahydrothiophene (tht) were prepared and the structures of the phosphine and thiophene complexes were determined. Either route resulted in an identical

$Mo_6S_8(PEt_3)_6$ complex as indicated by the same structure and bonding. The sulfidation of the Mo_6Cl_{12} cluster has a distinct advantage as a general preparation technique due to the range of adducts which can be prepared. Another advantage lies in the relative stability of the metal cluster during the sulfidation, as evidenced by very little, if any, cluster decomposition. The presence of the coordinating ligands appears to help stabilize the Mo_6S_8 cluster unit.

The synthetic route used to prepare the completely sulfided cluster unit is shown below in equation 7.

$$1\ Mo_6Cl_{12} + 8\ NaSH + 4\ NaOBu \xrightarrow[\text{reflux, 3d}]{\text{BuOH/py}} \xrightarrow[4d]{\text{MeOH wash}} Mo_6S_7Cl(py)_x \quad (7)$$

$$Mo_6S_7Cl(py)_x + 2\ NaSH \xrightarrow[\text{reflux, 2d}]{\text{BuOH/py}} \xrightarrow[4d]{\text{MeOH wash}} Mo_6S_8(py)_{\sim 4}$$

As shown in the reactions below, other adducts can be prepared from this pyridine complex via ligand exchange. From the crystal structures of the tetrahydrothiophene and triethylphosphine adducts, it is observed that the Mo_6S_8 cluster units are isolated with no intercluster interactions. The average intracluster Mo-Mo bond distances are 2.6584 Å for the phosphine adduct and 2.640 Å for the thiophene adduct. These bond lengths are quite close to the value of 2.662 Å which is estimated for a 20 electron octahedral cluster.

$$Mo_6S_8(py)_x + 6\ PEt_3 \rightarrow Mo_6S_8(Pet_3)_6 + x\ py$$

$$Mo_6S_8(py)_x + xs\ PrNH_2 \rightarrow Mo_6S_8(PrNH_2)_y + x\ py$$

$$Mo_6S_8(PrNH_2)_y + xs\ tht \rightarrow Mo_6S_8(tht)_6 + x\ py$$

Molecular Complexes of Hexatungsten Chalcogenides

Following the success in preparing the molecular Mo_6S_8 cluster unit, similar attempts were made to prepare the analogous tungsten complexes.[32] Complete substitution of the sulfide for chloride was achieved by using the stoichiometry of 1 W_6Cl_{12}: 12 NaSH: 6 NaOBu in neat pyridine. The resulting powder was poorly crystalline. However, single crystals of $W_6S_8(py)_6$ could be prepared by higher temperature (200°C) heating in pyridine. Ligand displacement of the pyridine adduct by triethylphosphine and tetrahydrothiophene produced crystalline molecular complexes also with the general formula $W_6S_8L_6$ (L=py, PEt_3, tht).

PAPER 1.

PREPARATION AND CHARACTERIZATION OF THE MOLECULAR $Mo_6S_8L_6$ CLUSTER COMPLEXES

INTRODUCTION

Ternary molybdenum chalcogenides of the general formula $M_xMo_6Y_8$ (M=ternary metal cation; Y=chalcogenide), known as Chevrel phases, have been extensively studied and have been shown to possess interesting physical and chemical properties.[1-6] These properties are related to the structures of the compounds which consist of Mo_6Y_8 clusters interlinked to form three-dimensional networks. The production of the Chevrel phases has generally involved solid state reactions at high temperatures (1000-1300°C). Recently, though, lower temperature routes using polythiomolybdates and metal chlorides as solution precursors have been reported.[7,8] Likewise, a major focus of the McCarley research group has been on the preparation of $M_6S_8L_6$ (M = Mo, W) cluster complexes as low temperature precursors to the Chevrel phases.[9-13]

The first step toward the synthesis of the Chevrel phases involved the preparation of these molecular cluster intermediates. Mo_6Cl_{12} was chosen as the starting complex since it is structurally similar to the Chevrel phases. This similarity is evidenced in that both materials possess a Mo_6Y_8 octahedral cluster unit. Complete substitution of sulfide for chloride was successfully accomplished without cluster decomposition via the reaction shown in equation 1.[10] Further reaction of this pyridine complex has led to the identification and structural characterization of the triethylphosphine and tetrahydrothiophene adducts.[9-11] Concurrently, the triethylphosphine adduct was prepared by another synthetic route.[14,15] Similar complexes

have also been prepared for the tungsten cluster unit - $W_6S_8L_6$ (L = pyridine, triethylphosphine, tetrahydrothiophene).[13]

$$1\ Mo_6Cl_{12} + 8\ NaSH + 4\ NaOBu \xrightarrow[\text{reflux, 3d}]{\text{BuOH/py}} \xrightarrow[4d]{\text{MeOH}} Mo_6S_7Cl(py)_x$$

$$Mo_6S_7Cl(py)_x + 2\ NaSH \xrightarrow[\text{reflux, 2d}]{\text{BuOH/py}} \xrightarrow[4d]{\text{MeOH}} Mo_6S_8(py)_{\sim 4} \qquad (1)$$

This paper will discuss the further developments in the characterization of the known $Mo_6S_8L_6$ cluster adducts. Secondly, the preparation and characterization of several nitrogen-donor complexes will be explored. The primary ligands that will be discussed are pyridine, propylamine, pyrrolidine, and piperidine.

EXPERIMENTAL

Materials

The reagents and products involved in this work appear to be air and moisture sensitive. Therefore, special precautions were taken to ensure the maintenance of a dry, inert atmosphere. All manipulations were performed by the use of an inert atmosphere drybox, a high-vacuum manifold, and Schlenk techniques, unless otherwise stated. All glassware was thoroughly dried prior to use by its placement in an oven at 140°C for at least 4 hours.

Mo_6Cl_{12} was prepared by the high temperature comproportionation method described by Koknat *et al.*[16] Sodium hydrosulfide (NaSH) was prepared by the method described by Brauer.[17] In this method, hydrogen sulfide gas was bubbled through a solution of sodium ethoxide in ethanol and the desired product precipitated by the addition of diethyl ether. Sodium butoxide (NaOBu) was prepared by the reaction of n-butanol with sodium metal, and used as the solid.

All solvents were purified and dried prior to use. Also, the solvents were deoxygenated by use of the freeze-thaw process: freeze to liquid nitrogen temperature, evacuate the gaseous material, and then thaw. This process was repeated three times prior to the distillation of the purified solvent onto 3 or 4 Å molecular sieves and storage under vacuum or a nitrogen atmosphere. Pyridine, 4-methylpyridine, n-propylamine, pyrrolidine, piperidine, tetrahydrothiophene, diethyl

ether, triethylphosphine, and benzonitrile were purified by refluxing over calcium hydride for at least 4 hours. Toluene and dichloromethane were refluxed over phosphorus pentoxide. Without heating, ethanol and 1-butanol were stirred with sodium metal. Methanol was dried by refluxing over sodium methoxide. When used, the solvents were vacuum distilled or syringed under a flowing nitrogen gas atmosphere.

Analytical Procedures

Molybdenum was determined gravimetrically either as the trioxide (if ternary metal cations were not present) or as the 8-hydroxyquinolate. For the trioxide method, samples were placed in tared crucibles and decomposed initially with dilute (3M) nitric acid. Concentrated nitric acid was then added to ensure complete oxidation and the samples evaporated to dryness. After ignition in a muffle furnace at 520°C, the resulting MoO_3 solid was weighed. For the 8-hydroxyquinolate method,[18] the samples were dissolved in basic solutions with the aid of hydrogen peroxide. The solutions were then neutralized with dilute sulfuric acid to pH = 4-6. Solutions of 5% EDTA and acetic acid/ammonium acetate buffer were added. The analyte, $MoO_2(ONC_9H_6)_2$, was precipitated by the addition of 8-hydroxyquinoline solution and filtered through tared filters. After washing with hot distilled water, the materials were dried to constant weight at 140°C.

Chlorine was determined by the potentiometric titration of neutralized solutions with a standardized silver nitrate solution. A silver/silver chloride electrode was used

as the working electrode and a silver electrode as the reference. The endpoint was determined by using the second derivative method.

Additional microanalyses for carbon, hydrogen, nitrogen, and sodium were obtained from Oneida Research Services.[19] The C,H,N analyses were found to be lower than expected based on the molybdenum analyses. This problem could arise from a loss of ligand prior to the analyses or from incomplete combustion since samples known to have excess ligand like pyrrolidine were always found to be ligand-deficient. Therefore, less confidence was placed in these elemental percentages.

Physical Measurements

Infrared spectroscopy

Infrared spectra (4000-200 cm^{-1}) were obtained by using an IBM IR/98 Fourier Transform Infrared Spectrometer and a Bomem MB-102 Fourier Transform Infrared Spectrometer manufactured by Hartmann and Braun. Samples were prepared as Nujol mulls and the mulls were pressed between cesium iodide plates. The sample chamber was continuously purged with dry, compressed air and reference spectra were collected in the empty chamber.

Raman spectroscopy

Raman spectra were obtained with the help of Jeanne Wynn in Professor Therese Cotton's group. A Spex Triplemate spectrometer with a Princeton Applied Research Corp. (PARC) intensified SiPD detector cooled to -40°C was used to record

the spectra. The excitation source was a Coherent Ar^+ 200 series laser at the wavelength of 514.5 nm and the scattered radiation was collected in a backscattering geometry. The laser power at the sample was approximately 30 mW and the integration time was 200 s. The Raman spectra were obtained at room temperature from solid samples packed in capillary tubes.

Nuclear magnetic resonance spectroscopy

Proton spectra were collected on the Nicolet NT-300 and Unity 500 MHz instruments. The samples were handled in an inert atmosphere solvent drybox and dissolved in deuterated benzene just prior to the NMR study. Two-dimensional NMR experiments - double quantum correlation spectroscopy (DQCOSY) and Nuclear Overhauser Effect spectroscopy (NOESY) - were performed on the Unity 500 MHz instrument by David Scott.

X-ray photoelectron spectroscopy

XPS spectra were collected by James Anderegg at room temperature with a Physical Electronics Industries 5500 multitechnique surface analysis system. This system was equipped with a hemispherical analyzer, a toroidal monochromator, and multichannel detector which sampled a 2 mm^2 area. The samples were placed on an indium substrate and excited with monochromatic Al K-α radiation (1486.6 eV) at the power of 300 W. The binding energies were calibrated with C 1s = 284.6 eV.

Ultraviolet-Visible spectroscopy

Electronic spectra were collected on a Shimadzu UV-2101PC UV-VIS scanning spectrophotometer located in Professor James Espenson's group. The samples were dissolved in toluene under a N_2 gas purge and examined over a 200-800 nm range. A toluene blank was used as the background and subtracted from the sample spectra.

X-ray powder diffraction

An Enraf Nonius Delft FR552 Guinier camera was used to obtain x-ray powder diffraction patterns. A General Electric XRD-5 generator with an AEG fine focus tube and a copper target were used to generate the x-rays. Air-sensitive samples were ground thoroughly and then placed between strips of cellophane tape in the drybox. Powdered NBS silicon was added as an internal standard.

Scanning Electron Microscopy-Energy Dispersive Spectroscopy (SEM-EDS)

This technique was employed to obtain qualitative elemental information on the sample. A Cambridge S-200 Scanning Electron Microscope coupled to a Tracor Northern Micro Z-II Energy Dispersive Spectrometer with a beryllium window was used. The samples were placed onto a metal disk backed with double-stick Scotch tape and then sputter-coated with gold or carbon. The molybdenum L series and sulfur K series peaks fell at almost identical energies and thus were not resolvable by this technique.

Synthetic Procedures

The general procedure for the preparation of the Mo_6S_8 cluster unit was developed by Laughlin.[10] This preparation involved the reaction of Mo_6Cl_{12}, NaSH, and NaOBu (1:8:4) to produce an incompletely sulfided (~1 Cl remaining) cluster. Upon further reaction with two equivalents of NaSH, the Mo_6S_8 cluster compound could be prepared. This two-step synthesis required extended MeOH extractions to remove the NaCl by-product after each reaction step. Therefore, modifications of this general procedure were explored in order to better facilitate a shorter preparative route.

Reactions with 1:10:5 stoichiometry

A typical reaction involved placing 4.00 g Mo_6Cl_{12} (4 mmol), 2.24 g NaSH (40 mmol), and 1.92 g NaOBu (20 mmol) into a 500 mL reaction flask. Under a nitrogen flow, 60 mL of 1-butanol and 20 mL of pyridine (py) were syringed into the reaction flask. The mixture was then refluxed for 2-4 days. After cooling, a dark brown solid and faint colored solution were separated by filtration. The solid was extracted with methanol for several days and dried *in vacuo*. Chlorine analyses for several of these reactions produced variable results of zero to one chlorine remaining. For the incompletely substituted products, further reaction with NaSH resulted in the desired product. Infrared spectra were obtained.

Reactions with 1:12:6 stoichiometry

The typical procedure is similar to the 1:10:5 reaction stated previously. In this preparation, 4.00 g Mo_6Cl_{12} (4 mmol), 2.69 g NaSH (48 mmol), and 2.30 g NaOBu (24 mmol) were placed in the reaction flask and 60 mL of 1-butanol and 15 mL of pyridine were added by syringe. The resulting brown/black solid showed no evidence of Cl by chlorine analyses. However, further study of this product by XPS indicated that sodium was present. This was confirmed by using SEM-EDS. Also, it was discovered that the pyridine and methanol contents were quite variable from one reaction to another. The pyridine-deficient (PD) product was found to be pyrophoric, insoluble in non-coordinating solvents, and amorphous to x-rays. Infrared spectra and elemental analyses were obtained. Analyses are given for the product of one procedure - Calc. for $Na_{0.8}Mo_6S_{8.4}(py)_2(MeOH)_1$: Na, 1.75%; Mo, 54.64%; C, 12.54%; H, 1.34%; N, 2.66%. Found : Na, 1.73%; Mo, 54.55%; C, 12.67%; H, 1.44%; N, 2.27%.

Reaction of $Na_{2y}Mo_6S_{8+y}(py)_x$ with pyridine

The PD compound was reacted in neat pyridine either at room temperature or under reflux conditions to produce a higher pyridine-coordinated material. A typical preparation involved the placement of 1.00 g of the pyridine-deficient compound into a 100 mL reaction flask and the syringing of 30 mL of pyridine onto the solids under a nitrogen flow. The mixture was refluxed for 1-2 days or stirred for 3-4 days and the result, after filtration, was a dark brown solid and a brownish solution. Infrared

spectra, Raman spectra, powder x-ray diffraction data and elemental analyses were obtained for the dark brown powder. The solid was found to contain sodium as detected by XPS. Analyses for the product of one procedure - Calc. for $Na_{1.5}Mo_6S_{8.75}(py)_6$: Na, 2.53%; Mo, 42.16%; C, 26.39%; H, 2.21%; N, 6.16%. Found: Na, 2.15%; Mo, 41.88%; C, 23.42%; H, 2.00%; N, 5.41%.

Crystals were grown from the brownish solution by reducing the volume and placing it in the refrigerator for several days.

Reaction of $Na_{2y}Mo_6S_{8+y}(py)_x$ with 4-methylpyridine

The PD compound (0.5 g) was placed in a 100 mL reaction flask and approximately 25 mL of 4-methlypyridine (4-Mepy) was vacuum-distilled onto the solid. The mixture was refluxed for 2 days and, upon filtering, a dark brown solid and light brown filtrate resulted. The solid, which was the major product, was insoluble in non-coordinating solvents. Infrared, Raman, and XPS spectra were obtained. Analyses for the product of one procedure - Calc. for $Na_{1.7}Mo_6S_{8.85}(4\text{-Mepy})_5$: Na, 2.87%; Mo, 42.20%; C, 26.42%; H, 2.59%; N, 5.13%. Found: Na, 2.77%; Mo, 41.55%; C, 24.89%; H, 2.43%; N, 4.48%.

Extended reactions at reflux conditions (4-5 days) resulted in a brown/black solid which was highly ligand deficient as evidenced by its infrared spectra and elemental analyses. Yet, this material could be extracted with neat n-propylamine to produce a black, "glassy" solid. Infrared spectra showed only propylamine coordination.

Ligand replacement reactions of the 4-methylpyridine adduct

A) **Pyridine.** The 4-Mepy adduct (0.10 g) was reacted with neat pyridine (25 mL) at room temperature for 2 days and produced a brown solid. Infrared spectra were obtained and showed only pyridine coordination.

B) **Propylamine.** The 4-Mepy adduct (1.00 g) was extracted with neat n-propylamine (30 mL) for approximately 1 day and resulted in complete dissolution of the solid. Upon drying under dynamic vacuum, a black, "glassy" solid was produced. Infrared spectra were obtained and showed only propylamine coordination.

C) **Triethylphosphine.** The 4-Mepy adduct (0.10 g) was reacted with an excess of triethylphosphine (0.20 mL) in toluene (25 mL) at reflux for 1 day and resulted in dissolution of the solid. Upon drying, a crystalline solid was obtained and its infrared spectra showed only triethyiphosphine (PEt_3) coordination.

D) **Pyrrolidine.** The 4-Mepy adduct (0.20 g) was reacted with neat pyrrolidine (20 mL) at reflux for 2 days and resulted in complete dissolution of the solid. After drying, a red solid was obtained and its infrared spectra showed only pyrrolidine (pyrr) coordination. A 1-day reaction under reflux resulted in incomplete substitution as evidenced by the infrared spectra showing both 4-methylpyridine and pyrrolidine coordination.

Reaction of $Na_{2y}Mo_6S_{8+y}(py)_x$ with n-propylamine

The PD compound was readily converted by extraction with neat n-propylamine. A typical preparation involved the placement of 2.0-3.0 g of $Na_{2y}Mo_6S_{8+y}(py)_x$ onto

the frit of an extractor and the distillation of 25-30 mL of n-propylamine ($PrNH_2$) into the receiving flask. After approximately 4-6 hours of extraction, the solid completely dissolved and provided a dark black/brown solution. After drying under dynamic vacuum, a black, "glassy" solid was obtained. This product, $Mo_6S_8(PrNH_2)_y$, showed variable propylamine content which was dependent upon amount of drying. Also, the propylamine adduct was amorphous to x-rays and insoluble in non-coordinating solvents. The compound was identified by infrared, Raman, and XPS spectra. SEM-EDS on the product indicated an absence of sodium, thus it was reasoned that the propylamine insoluble sodium sulfide by-product did remain on the frit after the extraction.

Reaction of $Mo_6S_8(PrNH_2)_y$ with pyrroildine

A typical preparation involved the placement of 0.50 g of the propylamine adduct into a 100 mL reaction flask and the vacuum distillation of 25-30 mL of pyrrolidine (pyrr) onto the solids. After refluxing for 1 day or stirring at room temperature for 3 days, the solid completely dissolved and a red/brown solid was obtained upon drying. The pyrrolidine content was found to be variable depending upon reaction conditions. Likewise, x-ray powder diffraction results indicated variability - from being amorphous to microcrystalline in nature. The pyrrolidine adduct was soluble in toluene and benzene. Infrared, Raman, UV-VIS, XPS, and NMR spectra and elemental analyses were obtained. Anal. Found: (RT) Mo, 47.55%; C, 20.74%; H, 3.94%; N, 5.60%; (reflux) Mo, 43.76%; C, 19.52%; H, 3.86%; N, 5.26%.

A small quantity of single crystals were grown by layering the solution with diethyl ether and allowing it to stand at room temperature for several days.

Reaction of $Mo_6S_8(PrNH_2)_y$ with piperidine

A typical preparation involved the placement of 0.3-0.5 g of the propylamine adduct into a 100 mL reaction flask and the vacuum distillation of 25-30 mL of piperidine (pip) onto the solids. After refluxing for 1 day or stirring at room temperature for 3 days, the solid completely dissolved and resulted in a red solid upon drying. The piperidine content was found to be variable depending upon reaction conditions. Likewise, x-ray powder diffraction results indicated variability - from being amorphous to microcrystalline in nature. The piperidine adduct was soluble in toluene, benzene, and chlorobenzene. Infrared, Raman, UV-VIS, XPS, and NMR spectra and elemental analyses were obtained. Anal. Found: (reflux) Mo, 39.39%; C, 25.73%; H, 5.15%, N, 5.70%.

Single crystals were grown by slowly reducing the volume of the solution and allowing it to stand at room temperature for several days.

The reaction of a larger quantity of the propylamine adduct (1.0-1.5 g) with 50-65 mL of neat piperidine, under the same conditions as discussed previously, resulted in the formation of a dark red solid and red/brown solution upon filtration. After drying under dynamic vacuum, the infrared spectra of both products indicated only piperidine coordination. The red solid could be rapidly dissolved in neat piperidine. Elemental analyses and NMR spectra indicated a large amount of uncoordinated piperidine.

Anal. Found: Mo, 29.39%; C, 34.06%; H, 6.21%; N, 7.52%. Range of values found for molybdenum analyses of products from different experiments: 29.26-34.18%.

Reaction of $Mo_6S_8(PrNH_2)_y$ with tetrahydrothiophene

Previously, this reaction was conducted by refluxing for 1 day and resulted in a small yield of crystalline $Mo_6S_8(tht)_6$ and a brown solid as the major fraction.[9] Attempts to improve the yield of the crystalline adduct were made by varying the reaction conditions. A typical reaction involved using 0.30-0.50 g of $Mo_6S_8(PrNH_2)_y$ and 30 mL of neat tetrahydrothiophene (tht).

Stirring at room temperature for 3-15 days resulted in mixed $PrNH_2$/tht products as identified by their infrared spectra. Extraction of the propylamine adduct with tht resulted in complete dissolution and, upon drying, produced a brown solid showing tht coordination; however, very little crystalline material was obtained. Refluxing for 2 hours resulted in a brown solid on the frit and red solid from the solution after filtration and drying under dynamic vacuum. Longer reaction times (4 hours -1 day) led to larger amounts of the insoluble brown solid.

This brown solid was found to be insoluble in non-coordinating solvents and amorphous to x-rays. Infrared, Raman, and XPS spectra and elemental analyses were obtained. Anal. Found: Mo, 47.72%; C, 13.19%, H, 2.18%. The range of values found for molybdenum analyses of products from different experiments: 46.48-48.03%. The crystalline solid was identified by its infrared spectra and further studied by XPS and Raman spectroscopy.

Ligand replacement reactions of the tetrahydrothiophene adduct

A) **Propylamine.** The tht adduct (0.2-0.4 g) was reacted with neat n-propylamine (25-30 mL) at reflux for 1 day or room temperature for 5 days and resulted in complete dissolution of the solid. After drying, the blackish product showed only propylamine coordination in its infrared spectra.

B) **Pyridine.** The tht adduct (0.6 g) was reacted with neat pyridine (25 mL) at room temperature for 3 days and resulted in a brown/black solid for which the infrared spectra showed only pyridine coordination.

C) **Triethylphosphine.** The tht adduct (0.20 g) was allowed to react with 6 equivalents of triethylphosphine (0.14 mL) in dichloromethane (25 mL) at room temperature for 1 day and resulted in complete dissolution of the solid. The black product showed only triethylphosphine coordination in its infrared spectra.

Reaction of $Mo_6S_8(PrNH_2)_y$ with thiophene

Previously, the reaction between the pyridine adduct and thiophene was studied.[27] In this reaction, 0.50 g of $Mo_6S_8(PrNH_2)_y$ was placed into a 100 mL reaction flask and approximately 40 mL of thiophene distilled onto the solid and refluxed for 2 days. The resulting brownish powder showed only propylamine coordination in the infrared spectra and indicated that no reaction had occurred.

Reaction of $Mo_6S_8(PrNH_2)_y$ with various nitrile ligands

Attempts were made to prepare a complex with more labile ligands by forming nitrile adducts. A variety of nitriles were explored including acetonitrile, propionitrile, butyronitrile, and benzonitrile. The reactions with acetonitrile, propionitrile, and butyronitrile were studied in neat nitrile and with the addition of trifluoromethanesulfonic acid. A typical reaction involved placing 0.3 g of $Mo_6S_8(PrNH_2)_y$ into a 100 mL reaction flask and the distillation of 30 mL of nitrile onto the solid. When used, the acid (0.15 mL, 6 equiv.) was added by syringe and the mixture was refluxed for 1-2 days. The result, upon filtration, was complete dissolution of the solid and upon drying an oily residue often resulted. This residue could be broken by the addition of toluene and a brownish-black solid was obtained. Infrared spectra were obtained on the products. These nitrile reactions without the addition of acid exhibited only propylamine coordination as observed in the infrared spectra and the addition of the acid resulted in coordination of triflate anions ($CF_3SO_3^-$) instead of the desired nitrile. The reaction of benzonitrile in toluene produced a mixed nitrile/propylamine complex.

A typical reaction involved the placement of 0.5 g of $Mo_6S_8(PrNH_2)_y$ into a 100 mL reaction flask and the distillation of approximately 10 mL of benzonitrile (PhCN) and 25 mL of toluene onto the solid. The mixture was refluxed for 2-3 days and, upon filtering and vacuum drying, a blackish solid was recovered. The product was identified by its infrared spectra and elemental analyses were obtained. Anal. Found: Mo, 43.96%; C, 22.02%; H, 2.12%; N, 3.89%.

X-ray Structure Determinations

The x-ray data collection and structure solutions were carried out by Victor G. Young, Jr. at the Iowa State Molecular Structure Laboratory on a Siemens P4/RA diffractometer. Refinement calculations were performed on a Digital Equipment Corp. Micro VAX 3100/76 computer using SHELXTL-PLUS direct methods programs.[20] The crystallographic data are summarized in Table 1.

Structure determination for $Mo_6S_8(py)_8 \cdot 1.65$ py

Single crystals were grown from the reaction of the pyridine-deficient compound with neat pyridine at reflux for 1-2 days. The obtained filtrate was placed in a refrigerator for several days and crystals slowly formed. Crystals were found of two different morphologies - irregularly shaped brown chunks and brown cubes. The vast majority of crystals observed were chunky in nature. A large, irregularly shaped chunk crystal was quickly selected and, while in oil, the edges trimmed to a box-like shape. The crystal, with dimensions of 0.35 x 0.35 x 0.15 mm, was then attached to the tip of a glass fiber and mounted on the Siemens P4/RA diffractometer for data collection at -50 ± 1°C. The cell constants for data collection were determined from reflections found by a rotation photograph. Graphite-monochromated Cu radiation (k = 1.54178 Å) was employed to collect data in the range $4° < 2\theta < 115°$, using the θ-2θ scan technique. Three standard reflections, measured every 97 reflections, showed some intensity variation during data collection which led to the application of a correction based on the decay. A total of 7110 unique reflections were collected

Table 1. Summary of crystal data, intensity collection, and structure refinement

compound	$Mo_6S_8(py)_6 \cdot 1.65py$	$Mo_6S_8(py)_6 \cdot 2py$	$Mo_6S_8(pip)_6 \cdot 7pip$	$Mo_6S_8(pyrr)_6 \cdot 1pyrr$
formula	$C_{38.25}H_{38.25}Mo_6N_{7.65}S_8$	$C_{40}H_{40}Mo_6N_8S_8$	$C_{65}H_{143}Mo_6N_{13}S_8$	$C_{28}H_{63}Mo_6N_7S_8$
formula weight	1437.2	1464.9	1939.1	1330.0
crystal system	triclinic	cubic	tetragonal	tetragonal
space group	$P\bar{1}$	$Pa\bar{3}$	$I\bar{4}$	$I4_1/a$
a, Å	11.580 (5)	16.994 (2)	19.421 (2)	29.933 (4)
b, Å	12.170 (6)	-	-	-
c, Å	21.995 (9)	-	22.584 (3)	23.697 (8)
α, deg	75.94 (3)	90	90	90
β, deg	88.94 (3)	90	90	90
γ, deg	62.61 (3)	90	90	90
V, $Å^3$	26574. (2)	4908.2 (12)	8518. (2)	21231. (11)
Z	2	4	8	16
calc. density, g/cm^3	1.794	1.980	1.510	1.574
F(000)	1396	2860	4008	9792
crystal size, mm	0.35 x 0.35 x 0.15	0.12 x 0.12 x 0.12	0.50 x 0.40 x 0.35	0.45 x 0.40 x 0.12
abs. coeff., mm^{-1}	14.479	1.865	1.096	14.375
diffractometer	Siemens P4/RA	Siemens P4/RA	Siemens P4/RA	Siemens P4/RA
λ, Å	1.54178	0.71073	0.71073	1.54178
temperature, K	223	228	223	213
scan method	θ-2θ	θ-2θ	θ-2θ	θ-2θ
2θ range, deg	4-115	4-50	4-60	4-115

Table 1. (continued)

compound	$Mo_6S_8(py)_6 \cdot 1.65py$	$Mo_6S_8(py)_6 \cdot 2py$	$Mo_6S_8(pip)_6 \cdot 7pip$	$Mo_6S_8(pyrr)_6 \cdot 1pyrr$
range of h,k,l	0-12,-11-13,-23-23	0-20,0-20,-20-0	0-27,0-27,0-31	0-32,0-32,0-25
total data	7531	4858	6726	7686
unique data	7110	1460	6713	7147
data observed[a]	3332	695	5008	4168
param. refined	470	100	402	326
data/parameter	7.1	6.9	12.5	12.8
abs. correction	semi-empirical	N/A	semi-empirical	semi-empirical
trans. factors	0.5323-1.0000	N/A	0.7307-0.8647	0.0001-1.0000
R[b]	0.0750	0.0381	0.0317	0.0675
R_w[c]	0.0941	0.0351	0.0366	0.0911
quality of fit[d]	3.09	0.99	1.24	2.91
largest shift, esd	0.310	0.030	0.122	2.161
diff. peaks, e/Å^3	+2.10, -1.70	+0.51, -0.63	+0.75, -0.74	+1.25, -0.73

[a]Reflections are considered as observed when $F > 6.0\ \sigma(F)$

[b]$R = \Sigma \mid |F_o|-|F_c| \mid / \Sigma |F_o|$

[c]$R_w = [\ \Sigma\ \omega\ \{|F_o|-|F_c|\}^2 / \Sigma\ \omega\ |F_o|^2\ ]^{1/2}$; $\omega = 1/\sigma^2\ \{|F_o|\}$

[d] Quality of fit $= [\ \Sigma\ \omega\ \{|F_o|-|F_c|\}^2 / \{\ N_{obs}-N_{parameters}\}\ ]^{1/2}$

and 3332 of them were considered as observed with $F > 6.0\ \sigma(F)$. Lorentz and polarization corrections were applied. A series of azimuthal reflections were collected in order to apply a semi-empirical absorption correction.[20] The agreement factor for the averaging of reflections was 6.2%.

The triclinic space group $P\bar{1}$ was chosen based on the lack of systematic absences and intensity statistics. However, the mosaic spread of these crystals indicated that solvent loss might have contributed to a poorer than average specimen for data collection. The unit cell parameters were a = 11.580 (5) Å, b = 12.170 (6) Å, c = 21.995 (9) Å, α = 75.94 (3)°, β = 88.94 (3)°, γ = 62.61 (3)°, and Z = 2. The lattice was triclinic, but also appeared to be pseudo C-centered monoclinic with a = 21.615 Å, b = 11.580 Å, c = 21.995 Å, α = 88.94°, β = 105.30°, and γ = 88.986°.

All non-hydrogen atoms were placed directly from the E-map. These atoms were refined with isotropic or anisotropic thermal parameters depending on whether the thermal parameters were positive, definite. The hydrogens of the coordinated pyridines were refined as riding-atoms with a 0.96 Å ideal distance from the host atom and with individual isotropic thermal parameters. Approximately 1 2/3 pyridine solvent molecules were found for every one cluster unit. The lower than expected occupancy of one of the two solvent sites might be explained as arising from solvent loss.

The major problem in this structure is the double orientation of coordinated pyridine ring 1. The close proximity of the nitrogen and the para-carbon in the two orientations required the use of an idealized-hexagon, rigid body (C-C, 1.395 Å) with

isotropic thermal parameters. The partially occupied pyridine site was also refined as a rigid body, because it was ill-behaved as well. The structure was finally refined to R = 0.0750 and R_w = 0.0941. The final electron density difference map showed the largest peak with 2.10 e/Å^3 and the largest hole with -1.70 e/Å^3. The atomic coordinates and equivalent isotropic thermal parameters of the non-hydrogen atoms are given in Table 2, and the anisotropic thermal parameters of the non-hydrogen atoms are shown in Table 3.

Structure determination for $Mo_6S_8(py)_6 \cdot 2\ py$

Due to the difficulties encountered in accurately describing the disorder in the triclinic structure, another attempt at data collection for the pyridine adduct was explored. The Siemens P4/RA diffractometer radiation source was changed to molybdenum K_α radiation (k = 0.71073 Å). A brown cubic crystal, with dimensions of 0.12 x 0.12 x 0.12 mm, was attached to the tip of a glass fiber and data collection proceeded at -45 ± 1°C. The cell constants for data collection were determined from reflections found by a rotation photograph. Graphite-monochromated Mo radiation was employed to collect data in the range 4° < 2θ < 55°, using the θ-2θ scan technique. Three standard reflections, measured every 97 reflections, showed some intensity variation during data collection which led to the application of a correction based on the decay. A total of 1460 unique reflections were collected and 600 of them were considered as observed with F > 6.0 σ(F). Lorentz and polarization corrections were applied. Although a series of azimuthal reflections were collected

Table 2. Atomic coordinates and equivalent isotropic thermal parameters ($Å^2$) of the non-hydrogen atoms for $Mo_6S_8(py)_6 \cdot 1.65$ py

Atom	X	Y	Z	U_{eq}, $(Å^2)^a$
Mo1	0.5706 (3)	0.4047 (3)	0.1947 (1)	0.044 (2)
Mo2	0.6724 (3)	0.3459 (3)	0.3123 (1)	0.041 (1)
Mo3	0.4354 (3)	0.5392 (3)	0.2721 (1)	0.042 (1)
Mo4	0.4657 (3)	0.3260 (3)	0.3543 (1)	0.041 (1)
Mo5	0.6032 (3)	0.1919 (3)	0.2759 (1)	0.043 (1)
Mo6	0.3658 (3)	0.3841 (3)	0.2370 (1)	0.042 (1)
S1	0.6330 (8)	0.5451 (8)	0.2337 (4)	0.049 (4)
S2	0.2498 (8)	0.5088 (8)	0.3121 (4)	0.045 (4)
S3	0.4066 (8)	0.1841 (8)	0.3151 (4)	0.049 (5)
S4	0.5029 (8)	0.2575 (8)	0.1678 (4)	0.047 (4)
S5	0.7877 (8)	0.2242 (8)	0.2377 (4)	0.048 (4)
S6	0.6889 (8)	0.1489 (8)	0.3847 (4)	0.043 (4)
S7	0.3469 (8)	0.5806 (8)	0.1642 (4)	0.052 (4)
S8	0.5342 (8)	0.4737 (8)	0.3812 (4)	0.046 (4)
N1[b]	0.6367 (42)	0.4352 (45)	0.0971 (18)	0.042 (24)
C11[b]	0.5649	0.5302	0.0592	0.049 (19)
C12[b]	0.5976	0.5743	-0.0014	1.324 (440)
C13[b]	0.7020	0.5035	-0.0240	0.051 (25)
C14[b]	0.7737	0.3785	0.0139	0.101 (34)
C15[b]	0.7411	0.3444	0.0745	0.040 (17)
N1'[b]	0.6308 (38)	0.4640 (44)	0.0969 (17)	0.036 (17)
C11'[b]	0.6286	0.5801	0.0667	0.063 (20)
C12'[b]	0.6482	0.6057	0.0032	0.089 (28)
C13'[b]	0.6701	0.5153	-0.0303	0.230 (85)
C14'[b]	0.6723	0.3993	-0.0002	0.339 (111)
C15'[b]	0.6526	0.3727	0.0634	0.076 (23)

[a]Equivalent isotropic U defined as one-third of the trace of the orthogonalized U_{ij} tensor ($U_{eq} = \frac{1}{3} \Sigma_i \Sigma_j U_{ij} a_i^* a_j^* a_i a_j$)

[b]Positions are the result of a rigid body refinement of the pyridine ring

Table 2. (continued)

Atom	X	Y	Z	U_{eq}, (Å^2)
N2	0.8555 (24)	0.3264 (25)	0.3578 (11)	0.045 (14)
C21	0.8744 (38)	0.3225 (32)	0.4157 (21)	0.074 (22)
C22	0.9761 (35)	0.3259 (37)	0.4448 (18)	0.075 (23)
C23	1.0654 (31)	0.3379 (38)	0.4077 (21)	0.077 (24)
C24	1.0507 (32)	0.3489 (36)	0.3457 (18)	0.071 (21)
C25	0.9518 (33)	0.3397 (31)	0.3239 (21)	0.071 (21)
N3	0.3337 (25)	0.7490 (23)	0.2700 (12)	0.043 (13)
C31	0.2098 (36)	0.8226 (35)	0.2518 (15)	0.060 (21)
C32	0.14226(45)	0.9467 (41)	0.2531 (18)	0.080 (25)
C33	0.2039 (51)	1.0017 (38)	0.2765 (22)	0.097 (28)
C34	0.3316 (46)	0.9345 (42)	0.2964 (21)	0.089 (30)
C35	0.3963 (35)	0.7945 (36)	0.2920 (19)	0.065 (22)
N4	0.4015 (24)	0.2774 (23)	0.4540 (11)	0.043 (13)
C41	0.3656 (32)	0.3615 (35)	0.4922 (22)	0.078 (23)
C42	0.3279 (36)	0.3375 (35)	0.5469 (14)	0.066 (21)
C43	0.3154 (37)	0.2302 (40)	0.5691 (15)	0.074 (25)
C44	0.3541 (35)	0.1412 (35)	0.5317 (15)	0.068 (21)
C45	0.3943 (33)	0.1681 (35)	0.4751 (15)	0.061 (20)
N5	0.7062 (25)	-0.0158 (22)	0.2769 (13)	0.046 (13)
C51	0.6528 (37)	-0.0753 (34)	0.2536 (14)	0.057 (20)
C52	0.7230 (52)	-0.2088 (38)	0.2539 (18)	0.087 (30)
C53	0.8421 (45)	-0.2833 (41)	0.2782 (20)	0.074 (25)
C54	0.9013 (36)	-0.2302 (35)	0.3043 (21)	0.076 (22)
C55	0.8296 (39)	-0.0971 (38)	0.3008 (17)	0.070 (26)
N6	0.1790 (27)	0.4028 (30)	0.1923 (13)	0.059 (17)
C61	0.1704 (41)	0.3049 (38)	0.1827 (22)	0.092 (26)
C62	0.0493 (58)	0.3288 (60)	0.1480 (27)	0.142 (22)
C63	-0.0498 (65)	0.4311 (62)	0.1360 (29)	0.156 (25)
C64	-0.0472 (57)	0.5281 (54)	0.1437 (26)	0.132 (20)
C65	0.0686 (43)	0.5180 (41)	0.1792 (23)	0.116 (30)

Table 2. (continued)

Atom	X	Y	Z	U_{eq}, (Å^2)
N7	0.9220 (38)	0.1597 (42)	0.5935 (16)	0.091 (25)
C71	0.9350 (42)	0.0532 (48)	0.5794 (20)	0.112 (28)
C72	0.8426 (44)	0.0390 (46)	0.5521 (19)	0.089 (28)
C73	0.7263 (35)	0.1299 (40)	0.5469 (17)	0.071 (22)
C74	0.7023 (43)	0.2479 (42)	0.5594 (18)	0.093 (26)
C75	0.7999 (46)	0.2575 (38)	0.5807 (16)	0.072 (24)
N8	0.0146 (46)	0.1412 (63)	0.8779 (25)	0.145 (18)
C81[c]	0.1231	0.0340	0.8681	0.145 (18)
C82[c]	0.2471	-0.0029	0.8961	0.145 (18)
C83[c]	0.2625	0.0674	0.9338	0.145 (18)
C84[c]	0.1540	0.1746	0.9437	0.145 (18)
C85[c]	0.0300	0.2115	0.9157	0.145 (18)

[c]Positions are the result of a rigid body refinement and also show partial occupancy

Table 3. Anisotropic thermal parameters[a] (x 10^3 Å^2) of the non-hydrogen atoms for $Mo_6S_8(py)_6 \cdot 1.65$ py

Atom	U_{11}	U_{22}	U_{33}	U_{12}	U_{13}	U_{23}
Mo1	35 (2)	58 (2)	33 (2)	-16 (2)	10 (1)	-17 (2)
Mo2	29 (2)	57 (2)	33 (2)	-14 (1)	7 (1)	-16 (2)
Mo3	34 (2)	54 (2)	33 (2)	-14 (1)	7 (1)	-14 (1)
Mo4	31 (2)	53 (2)	29 (2)	-11 (1)	5 (1)	-12 (1)
Mo5	33 (2)	53 (2)	34 (2)	-11 (1)	5 (1)	-17 (1)
Mo6	31 (2)	57 (2)	33 (2)	-14 (1)	5 (1)	-16 (2)
S1	43 (6)	56 (5)	40 (6)	-17 (4)	4 (4)	-14 (5)
S2	32 (5)	52 (5)	42 (6)	-11 (4)	10 (4)	-18 (4)
S3	44 (6)	64 (6)	43 (6)	-26 (5)	11 (5)	-19 (5)
S4	43 (6)	61 (5)	30 (5)	-14 (4)	2 (4)	-18 (4)
S5	31 (5)	60 (5)	37 (6)	-9 (4)	3 (4)	-16 (4)
S6	38 (5)	48 (5)	30 (5)	-13 (4)	5 (4)	-6 (4)
S7	38 (5)	57 (5)	38 (5)	-8 (4)	- 9 (4)	-3 (4)
S8	36 (5)	60 (5)	43 (5)	-19 (4)	9 (4)	-23 (5)
N2	37 (16)	74 (19)	20 (16)	-28 (14)	-3 (13)	-3 (14)
C21	72 (29)	56 (22)	89 (35)	-27 (21)	24 (25)	-18 (23)
C22	55 (25)	114 (32)	47 (24)	-34 (24)	-22 (21)	-19 (22)
C23	23 (20)	119 (33)	93 (35)	-42 (22)	-5 (21)	-18 (27)
C24	31 (21)	106 (30)	50 (26)	-21 (20)	-20 (18)	-1 (22)
C25	51 (24)	68 (23)	103 (34)	-32 (20)	32 (24)	-31 (23)
N3	35 (17)	50 (16)	43 (18)	-17 (14)	9 (14)	-14 (14)
C31	65 (27)	72 (25)	32 (21)	-21 (22)	-2 (19)	-17 (19)
C32	97 (36)	69 (29)	32 (24)	-14 (27)	11 (22)	5 (20)
C33	114 (44)	42 (23)	87 (39)	3 (26)	61 (34)	-19 (24)
C34	101 (39)	90 (33)	101 (39)	-59 (31)	43 (33)	-38 (30)
C35	43 (23)	85 (28)	84 (31)	-34 (22)	37 (22)	-46 (25)

[a]The coefficients U_{ij} of the anisotropic thermal parameter expression are defined as:
$\exp [-2\pi^2 (U_{11}h^2a^{*2} + U_{22}k^2b^{*2} + U_{33}l^2c^{*2} + 2U_{12}hka^*b^* + 2U_{13}hla^*c^* + 2U_{23}klb^*c^*)]$

Table 3. (continued)

Atom	U_{11}	U_{22}	U_{33}	U_{12}	U_{13}	U_{23}
N4	44 (16)	48 (15)	29 (15)	-16 (13)	4 (12)	-8 (12)
C41	39 (22)	73 (25)	132 (42)	-31 (20)	6 (24)	-35 (27)
C42	92 (30)	86 (26)	19 (18)	-40 (23)	45 (20)	-18 (18)
C43	89 (31)	120 (34)	17 (19)	-55 (28)	27 (20)	-16 (21)
C44	81 (28)	80 (25)	27 (21)	-42 (22)	10 (19)	22 (19)
C45	67 (25)	83 (26)	29 (20)	-27 (21)	19 (17)	-22 (18)
N5	28 (16)	34 (14)	53 (19)	8 (12)	5 (14)	-17 (13)
C51	80 (28)	78 (25)	21 (19)	-41 (23)	11 (18)	-19 (18)
C52	161 (51)	65 (28)	41 (26)	-54 (31)	21 (29)	-19 (22)
C53	88 (36)	58 (27)	68 (32)	-25 (26)	35 (27)	-23 (24)
C54	44 (24)	52 (24)	105 (38)	-10 (20)	38 (24)	-4 (23)
C55	91 (33)	93 (31)	64 (28)	-72 (28)	54 (26)	-28 (25)
N6	47 (19)	91 (23)	41 (19)	-34 (18)	17 (15)	-17 (17)
C61	66 (31)	61 (27)	134 (45)	-26 (24)	3 (28)	-10 (27)
C65	90 (37)	67 (28)	142 (49)	-9 (26)	-57 (34)	5 (29)
N7	86 (30)	130 (34)	60 (25)	-43 (27)	34 (22)	-50 (25)
C71	62 (32)	117 (41)	53 (30)	43 (28)	15 (24)	-19 (28)
C72	71 (33)	125 (39)	56 (30)	-24 (31)	-13 (25)	-41 (28)
C73	38 (24)	102 (31)	57 (26)	-13 (22)	0 (19)	-34 (23)
C74	87 (35)	92 (33)	45 (27)	0 (26)	-39 (24)	-9 (23)
C75	95 (34)	80 (27)	26 (22)	-23 (27)	17 (22)	-27 (20)

in order to apply an absorption correction, it was determined that none was necessary. The agreement factor for the averaging of reflections was 3.8%.

The cubic space group $Pa\bar{3}$ was chosen based on systematic absences and intensity statistics. The unit cell parameter was a = 16.994 (2) Å and Z = 4. All non-hydrogen atoms were placed directly from the E-map. These atoms were refined with anisotropic thermal parameters. The hydrogens of the coordinated pyridines were refined as riding-atoms with an ideal distance of 0.96 Å from the host atom and with individual isotropic thermal parameters.

The one solvent molecule was disordered about a three-fold axis (8c). All sites were properly modelled to account for this disorder by refining each position as 5/6 carbon and 1/6 nitrogen. The Mo_6S_8 cluster unit was centered on a $\bar{3}$ position (4b). The structure was finally refined to R = 0.0381 and R_w = 0.0351. The final electron density difference map showed the largest peak with 0.51 e/Å^3 and the largest hole with -0.63 e/Å^3. The atomic coordinates and equivalent isotropic thermal parameters of both the non-hydrogen and hydrogen atoms are given in Table 4, and the anisotropic thermal parameters of the non-hydrogen atoms are shown in Table 5.

Structure determination for $Mo_6S_8(pip)_6 \cdot 7$ pip

Single crystals were grown from the reaction of the propylamine adduct with neat piperidine at reflux for 2 days. By slowly reducing the volume of the filtrate and allowing the solution to stand at room temperature for several days, reddish-brown crystals were obtained. An irregularly shaped crystal, with dimensions of 0.50 x 0.40

Table 4. Atomic coordinates and equivalent isotropic thermal parameters ($Å^2$) of the non-hydrogen and hydrogen atoms for $Mo_6S_8(py)_6 \cdot 2\ py$

Atom	X	Y	Z	U_{eq}, $(Å^2)^a$
Mo	0.0578 (1)	0.5870 (1)	0.0345 (1)	0.034 (1)
S(1)	0.1025 (2)	-0.3975 (2)	-0.1025 (2)	0.045 (1)
S(2)	0.1665 (2)	0.4942 (2)	0.0598 (2)	0.041 (1)
N	0.1279 (6)	0.6934 (5)	0.0771 (5)	0.044 (3)
C(1)	0.0959 (8)	0.7485 (7)	0.1235 (8)	0.063 (5)
C(2)	0.1355 (10)	0.8098 (8)	0.1533 (9)	0.080 (6)
C(3)	0.2115 (11)	0.8169 (8)	0.1387 (10)	0.099 (8)
C(4)	0.2478 (9)	0.7641 (9)	0.0901 (9)	0.087 (7)
C(5)	0.2036 (8)	0.7016 (8)	0.0624 (7)	0.063 (5)
C(11)[b]	0.3851 (14)	0.5076 (14)	0.0749 (20)	0.169 (14)
N(11)[b]	0.3851 (14)	0.5076 (14)	0.0749 (20)	0.169 (14)
C(12)[b]	0.4408 (19)	0.5194 (19)	0.1225 (11)	0.147 (14)
N(12)[b]	0.4408 (19)	0.5194 (19)	0.1225 (11)	0.147 (14)
H(1A)	0.0402	0.7422	0.1301	0.035 (27)
H(2A)	0.1078	0.8412	0.1912	0.086 (51)
H(3A)	0.2364	0.8589	0.1672	0.053 (31)
H(4A)	0.3003	0.7823	0.0799	0.144 (67)
H(5A)	0.2317	0.6657	0.0291	0.082 (47)
H(11A)[b]	0.3501	0.4635	0.0787	0.180
H(12C)[b]	0.4446	0.4844	0.1667	0.150

[a]Equivalent isotropic U defined as one-third of the trace of the orthogonalized U_{ij} tensor ($U_{eq} = \frac{1}{3} \Sigma_i \Sigma_j U_{ij} a_i^* a_j^* a_i a_j$)

[b]Disordered positions

Table 5. Anisotropic thermal parameters[a] (x 10^3 Å^2) of the non-hydrogen atoms for $Mo_6S_8(py)_6 \cdot 2\ py$

Atom	U_{11}	U_{22}	U_{33}	U_{12}	U_{13}	U_{23}
Mo	33 (1)	34 (1)	36 (1)	-5 (1)	1 (1)	2 (1)
S(1)	45 (1)	45 (1)	45 (1)	-7 (1)	7 (1)	7 (1)
S(2)	36 (2)	45 (2)	43 (2)	-2 (1)	0 (1)	0 (1)
N	51 (6)	44 (6)	37 (6)	-15 (5)	-2 (4)	11 (5)
C(1)	52 (9)	48 (7)	88 (10)	-5 (7)	-13 (7)	2 (7)
C(2)	86 (11)	47 (9)	107 (13)	-21 (9)	-17 (10)	-13 (9)
C(3)	130 (17)	61 (11)	105 (15)	-65 (12)	-58 (13)	21 (9)
C(4)	72 (11)	89 (12)	100 (13)	-55 (10)	-27 (10)	37 (10)
C(5)	59 (9)	74 (9)	58 (8)	-24 (8)	1 (7)	16 (7)
C(11)	81 (15)	178 (25)	247 (32)	-71 (15)	-34 (17)	99 (24)
N(11)	81 (15)	178 (25)	247 (32)	-71 (15)	-34 (17)	99 (24)
C(12)	122 (21)	237 (34)	82 (14)	-42 (20)	-21 (14)	51 (16)
N(12)	122 (21)	237 (34)	82 (14)	-42 (20)	-21 (14)	51 (16)

[a]The coefficients U_{ij} of the anisotropic thermal parameter expression are defined as:
$\exp [-2\pi^2 (U_{11}h^2a^{*2} + U_{22}k^2b^{*2} + U_{33}l^2c^{*2} + 2U_{12}hka^*b^* + 2U_{13}hla^*c^* + 2U_{23}klb^*c^*)]$

x 0.35 mm, was attached to the tip of a glass fiber and mounted on the Siemens P4/RA diffractometer for data collection at -50 ± 1°C. The cell constants for data collection were determined from reflections found by a rotation photograph. Graphite-monochromated Mo radiation (k = 0.71073 Å) was employed to collect data in the range $4° < 2\theta < 60°$, using the θ-2θ scan technique. Three standard reflections, measured every 97 reflections, showed some intensity variation during data collection which led to the application of a correction based on the decay. A total of 6713 unique reflections were collected and 5008 of them were considered as observed with $F > 6.0\ \sigma(F)$. Lorentz and polarization corrections were applied. A series of azimuthal reflections were collected in order to apply a semi-empirical absorption correction. The agreement factor for the averaging of reflections was 2.2%.

The tetragonal space group $I\bar{4}$ was chosen based on systematic absences and intensity statistics. Two other space groups were possible, I4/m and I4, but neither provided the basis for a reasonable starting model. The unit cell parameters were found to be a = 19.421 (2) Å, c = 22.584 (3) Å, and Z = 8.

All non-hydrogen atoms were placed directly from the E-map. These atoms were refined with anisotropic thermal parameters, except for the disordered piperidine molecule (discussed further below). The hydrogens of the coordinated piperidines were refined as riding-atoms with C-H distances equal to 0.96 Å and with N-H distances of 0.85 Å and with fixed isotropic thermal parameters.

The asymmetric unit was found to be $Mo_3S_4(pip)_3 \cdot 3.5$ pip, where three of the solvent piperidine molecules were well-behaved, but the remaining half-piperidine

molecule was disordered. This disorder occurred about a crystallographic two-fold axis and was modelled with atoms C(71), N(71), C(72), N(72), C(73), and N(73). The carbon/nitrogen atoms of this solvent molecule were given occupancies with the 0.83333:0.16667 ratio. Hydrogen atoms were placed with an occupancy of 0.83333. These C-C and C-N bond lengths were constrained to be 1.5200 (1) Å in order to get near convergence. Thermal parameters of like atoms were constrained to have the same value. The largest shifts in the final cycle of refinement were due to oscillations in these thermal parameters, yet the result was close to convergence.

The three ligand piperidine groups were found in the chair conformation. Likewise, the three well-behaved solvent piperidine molecules were also in the chair conformation. However, the disordered piperidine molecule once joined with its symmetry equivalent displayed the boat conformation. The Mo_6S_8 cluster unit was centered on a 2-fold position (4e). The structure was finally refined to R = 0.0317 and R_w = 0.0366. The final electron density difference map showed the largest peak with 0.75 e/Å^3 and the largest hole with -0.74 e/Å^3. The atomic coordinates and equivalent isotropic thermal parameters of the non-hydrogen atoms are given in Table 6, and the anisotropic thermal paramters of the non-hydrogen atoms are shown in Table 7.

Structure determination for $Mo_6S_8(pyrr)_6 \cdot 1$ pyrr

Single crystals were grown from the reaction of the propylamine adduct with neat pyrrolidine at reflux for 2 days. The filtrate was layered with diethyl ether and the

Table 6. Atomic coordinates and equivalent isotropic thermal parameters ($Å^2$) of the non-hydrogen atoms for $Mo_6S_8(pip)_6 \cdot 7$ pip

Atom	X	Y	Z	U_{eq}, $(Å^2)^a$
Mo(1)	0.4925 (1)	0.5961 (1)	0.2664 (1)	0.019 (1)
Mo(2)	0.4323 (1)	0.4947 (1)	0.2071 (1)	0.019 (1)
Mo(3)	0.4319 (1)	0.4951 (1)	0.3248 (1)	0.019 (1)
S(1)	0.4937 (1)	0.5900 (1)	0.1581 (1)	0.024 (1)
S(2)	0.3809 (1)	0.4018 (1)	0.2662 (1)	0.024 (1)
S(3)	0.4943 (1)	0.5879 (1)	0.3744 (1)	0.025 (1)
S(4)	0.3671 (1)	0.5795 (1)	0.2660 (1)	0.023 (1)
N(1)	0.4753 (2)	0.7144 (2)	0.2624 (3)	0.028 (1)
C(11)	0.5289 (3)	0.7531 (3)	0.2320 (4)	0.044 (2)
C(12)	0.5114 (4)	0.8299 (3)	0.2251 (4)	0.053 (3)
C(13)	0.4963 (5)	0.8261 (4)	0.2826 (4)	0.069 (4)
C(14)	0.4397 (5)	0.8224 (4)	0.3144 (4)	0.065 (4)
C(15)	0.4587 (5)	0.7456 (4)	0.3193 (4)	0.056 (3)
N(2)	0.3531 (3)	0.4816 (3)	0.1310 (2)	0.025 (1)
C(21)	0.3780 (3)	0.5029 (4)	0.0729 (3)	0.036 (2)
C(22)	0.3307 (4)	0.4833 (5)	0.0217 (3)	0.052 (3)
C(23)	0.2590 (5)	0.5142 (5)	0.0325 (4)	0.064 (3)
C(24)	0.2327 (4)	0.4908 (5)	0.0929 (3)	0.055 (3)
C(25)	0.2834 (3)	0.5094 (4)	0.1421 (3)	0.044 (2)
N(3)	0.3456 (3)	0.4902 (3)	0.3949 (2)	0.028 (2)
C(31)	0.3385 (5)	0.5498 (5)	0.4320 (4)	0.076 (4)
C(32)	0.2740 (5)	0.5446 (6)	0.4728 (5)	0.095 (5)
C(33)	0.2723 (5)	0.4798 (9)	0.5091 (4)	0.117 (7)
C(34)	0.2806 (6)	0.4231 (7)	0.4700 (5)	0.106 (6)
C(35)	0.3458 (4)	0.4257 (5)	0.4304 (4)	0.075 (4)

[a]Equivalent isotropic U defined as one-third of the trace of the orthogonalized U_{ij} tensor ($U_{eq} = \frac{1}{3} \Sigma_i \Sigma_j U_{ij} a_i^* a_j^* a_i a_j$)

Table 6. (continued)

Atom	X	Y	Z	U_{eq}, (Å^2)
N(4)	0.3325 (4)	0.3205 (3)	0.1369 (3)	0.056 (2)
C(41)	0.3571 (6)	0.2771 (7)	0.0910 (5)	0.103 (5)
C(42)	0.3082 (7)	0.2490 (9)	0.0540 (5)	0.144 (8)
C(43)	0.2482 (6)	0.2190 (6)	0.0834 (5)	0.099 (5)
C(44)	0.2253 (7)	0.2621 (9)	0.1347 (7)	0.166 (9)
C(45)	0.2709 (7)	0.2920 (7)	0.1657 (6)	0.143 (7)
N(5)	-0.0226 (4)	0.2757 (3)	0.1930 (3)	0.048 (2)
C(51)	-0.0883 (5)	0.3074 (4)	0.2052 (5)	0.068 (4)
C(52)	-0.1000 (5)	0.3680 (4)	0.1628 (5)	0.065 (3)
C(53)	-0.0417 (5)	0.4184 (4)	0.1686 (4)	0.055 (3)
C(54)	0.0272 (5)	0.3821 (5)	0.1623 (5)	0.069 (4)
C(55)	0.0321 (5)	0.3218 (4)	0.2037 (5)	0.066 (3)
N(6)	0.6418 (3)	0.2881 (3)	0.1626 (3)	0.038 (2)
C(61)	0.7124 (4)	0.2751 (4)	0.1757 (4)	0.051 (3)
C(62)	0.7294 (5)	0.2017 (5)	0.1673 (5)	0.067 (3)
C(63)	0.7130 (5)	0.1778 (5)	0.1053 (4)	0.070 (4)
C(64)	0.6414 (5)	0.1986 (5)	0.0882 (4)	0.071 (4)
C(65)	0.6265 (4)	0.2737 (5)	0.1002 (3)	0.057 (3)
C(71)[b]	0.5620 (13)	0.0202 (12)	0.0392 (12)	0.252 (13)
N(71)[b]	0.5620 (13)	0.0202 (12)	0.0392 (12)	0.252 (13)
C(72)[b]	0.5422 (12)	-0.0556 (12)	0.0403 (9)	0.197 (9)
N(72)[b]	0.5422 (12)	-0.0556 (12)	0.0403 (9)	0.197 (9)
C(73)[b]	0.4811 (16)	-0.0607 (15)	-0.0016 (12)	0.321 (18)
N(73)[b]	0.4811 (16)	-0.0607 (15)	-0.0016 (12)	0.321 (18)

[b]Disordered positions

Table 7. Anisotropic thermal parameters[a] (x 10^3 Å^2) of the non-hydrogen atoms for $Mo_6S_8(pip)_6 \cdot 7pip$

Atom	U_{11}	U_{22}	U_{33}	U_{12}	U_{13}	U_{23}
Mo(1)	20 (1)	17 (1)	21 (1)	0 (1)	0 (1)	-1 (1)
Mo(2)	20 (1)	19 (1)	19 (1)	0 (1)	-1 (1)	0 (1)
Mo(3)	20 (1)	20 (1)	19 (1)	-1 (1)	1 (1)	0 (1)
S(1)	27 (1)	23 (1)	22 (1)	1 (1)	-2 (1)	4 (1)
S(2)	21 (1)	22 (1)	28 (1)	-5 (1)	0 (1)	-1 (1)
S(3)	28 (1)	25 (1)	23 (1)	0 (1)	0 (1)	-6 (1)
S(4)	21 (1)	23 (1)	26 (1)	3 (1)	0 (1)	1 (1)
N(1)	29 (2)	21 (2)	35 (3)	1 (2)	0 (3)	0 (3)
C(11)	39 (3)	22 (3)	72 (5)	-4 (3)	6 (5)	5 (4)
C(12)	45 (4)	26 (3)	87 (7)	-7 (3)	8 (5)	7 (4)
C(13)	67 (5)	25 (3)	116 (10)	3 (4)	-23 (6)	-19 (5)
C(14)	102 (8)	23 (4)	72 (6)	15 (4)	13 (6)	-9 (4)
C(15)	82 (6)	28 (4)	59 (5)	11 (4)	13 (5)	-7 (4)
N(2)	30 (3)	25 (3)	21 (2)	0 (2)	-3 (2)	-1 (2)
C(21)	37 (4)	50 (4)	19 (3)	-3 (3)	-4 (3)	4 (3)
C(22)	63 (5)	73 (6)	21 (3)	-6 (5)	-13 (3)	-6 (4)
C(23)	74 (6)	65 (6)	52 (5)	7 (5)	-45 (5)	-4 (4)
C(24)	35 (4)	75 (6)	54 (5)	8 (4)	-17 (4)	-15 (5)
C(25)	35 (4)	52 (5)	44 (4)	7 (3)	-14 (3)	-10 (4)
N(3)	20 (3)	42 (3)	23 (2)	1 (2)	1 (2)	2 (2)
C(31)	50 (5)	99 (8)	78 (7)	-27 (5)	36 (5)	-55 (6)
C(32)	58 (6)	133 (11)	95 (8)	-33 (7)	54 (6)	-72 (8)
C(33)	42 (5)	287 (20)	21 (4)	-35 (9)	7 (4)	-15 (8)
C(34)	73 (7)	146 (12)	101 (9)	32 (8)	43 (7)	99 (9)
C(35)	48 (5)	106 (8)	71 (6)	22 (5)	22 (5)	61 (6)

[a]The coefficients U_{ij} of the anisotropic thermal parameter expression are defined as:
$\exp [-2\pi^2 (U_{11}h^2a^{*2} + U_{22}k^2b^{*2} + U_{33}l^2c^{*2} + 2U_{12}hka^*b^* + 2U_{13}hla^*c^* + 2U_{23}klb^*c^*)]$

Table 7. (continued)

Atom	U_{11}	U_{22}	U_{33}	U_{12}	U_{13}	U_{23}
N(4)	76 (5)	47 (4)	44 (4)	-25 (4)	1 (4)	-6 (3)
C(41)	73 (7)	141 (11)	96 (9)	-45 (8)	25 (7)	-66 (9)
C(42)	143 (13)	210 (17)	78 (8)	-111 (13)	57 (9)	-70 (10)
C(43)	137 (11)	95 (8)	67 (7)	-76 (8)	16 (7)	-23 (6)
C(44)	147 (15)	195 (17)	156 (14)	-104 (14)	99 (12)	-108 (14)
C(45)	170 (14)	134 (12)	124 (11)	-110 (11)	100 (11)	-96 (10)
N(5)	70 (4)	24 (3)	51 (4)	7 (3)	-4 (3)	-2 (3)
C(51)	65 (6)	41 (4)	97 (8)	-10 (4)	18 (6)	-2 (5)
C(52)	53 (5)	37 (4)	104 (8)	9 (4)	-6 (5)	-16 (5)
C(53)	69 (6)	27 (4)	69 (6)	-6 (4)	6 (5)	3 (4)
C(54)	69 (6)	50 (5)	87 (7)	-19 (5)	18 (6)	-8 (5)
C(55)	60 (5)	41 (4)	98 (7)	10 (4)	-24 (5)	-16 (5)
N(6)	36 (3)	41 (3)	36 (3)	7 (3)	1 (3)	-5 (3)
C(61)	52 (5)	60 (5)	42 (4)	5 (4)	-9 (4)	-3 (4)
C(62)	55 (5)	61 (6)	86 (7)	27 (5)	-16 (5)	6 (5)
C(63)	82 (7)	48 (5)	80 (7)	17 (5)	22 (6)	-18 (5)
C(64)	67 (6)	94 (8)	53 (5)	3 (5)	-10 (5)	-34 (6)
C(65)	54 (5)	77 (6)	40 (4)	32 (5)	-9 (4)	-8 (4)

solution was allowed to stand at room temperature for several days. After this time, a small number of reddish-brown, rectangular crystals were obtained. A crystal was attached to the tip of a glass fiber and mounted on the Siemens P4/RA diffractometer for data collection at -60 ± 1°C. The cell constants for data collection were determined from reflections found by a rotation photograph. Graphite-monochromated Cu radiation (k = 1.54178 Å) was employed to collect data in the range $4° < 2\theta < 115°$, using the θ-2θ scan technique. Three standard reflections, measured every 97 reflections, showed some intensity variation during data collection which led to the application of a correction based on the decay. A total of 7147 unique reflections were collected and 4168 of them were considered as observed with $F > 6.0\ \sigma(F)$. Lorentz and polarization corrections were applied. A series of azimuthal reflections were collected in order to apply a semi-empirical absorption correction. The agreement factor for the averaging of reflections was 6.8%.

The tetragonal space group $I4_1/a$ was chosen based on systematic absences. The unit cell parameters were a = 29.933 (4) Å, c = 23.697 (8) Å, and Z = 16. The Mo, S, and N atoms were placed directly from the E-map. Some carbons were also found, however, several of the pyrrolidine rings were difficult to model due to disorder and resulted in incomplete rings. Attempts to model this disorder by rigid-body methods also failed.

The structure was composed of two-half molecules that are related by symmetry. The Mo, S, and N atoms were refined with anisotropic thermal parameters. The carbons were refined with anisotropic thermal parameters, if possible, but many could

only be refined isotropically. The observed disorder arose from the flexing of individual pyrrolidine rings. Cluster 1 was centered on a two-fold position (8e) and cluster 2 was on an inversion center (8d). The best structure refinement gave R = 0.0675 and R_w = 0.0911. The atomic coordinates and equivalent isotropic thermal parameters of the non-hydrogen atoms are listed in Table 8, and the anisotropic thermal parameters of the non-hydrogen atoms are shown in Table 9.

Table 8. Atomic coordinates and equivalent isotropic thermal parameters ($Å^2$) of the non-hydrogen atoms for $Mo_6S_8(pyrr)_6 \cdot 1$ pyrr

Atom	X	Y	Z	U_{eq}, $(Å^2)^a$
Mo11	0.4758 (1)	0.7132 (1)	-0.0033 (1)	0.052 (1)
Mo12	0.4748 (1)	0.7132 (1)	-0.1149 (1)	0.051 (1)
Mo13	0.4481 (1)	0.7850 (1)	-0.0599 (1)	0.052 (1)
Mo21	0.1916 (1)	0.7298 (1)	-0.2367 (1)	0.057 (1)
Mo22	0.2672 (1)	0.7285 (1)	-0.1788 (1)	0.062 (1)
Mo23	0.2643 (1)	0.6948 (1)	-0.2818 (1)	0.065 (1)
S11	0.4061 (2)	0.7147 (2)	-0.0586 (2)	0.058 (2)
S12	0.5474 (2)	0.7181 (2)	-0.1629 (2)	0.064 (2)
S13	0.5484 (2)	0.7184 (2)	0.0435 (2)	0.059 (2)
S14	0.5024 (2)	0.6505 (2)	-0.0595 (2)	0.062 (2)
S21	0.2257 (2)	0.6615 (2)	-0.2018 (3)	0.080 (3)
S22	0.1664 (2)	0.8017 (2)	-0.2743 (3)	0.077 (3)
S23	0.3064 (2)	0.7997 (2)	-0.1671 (3)	0.074 (2)
S24	0.1989 (2)	0.7624 (2)	-0.1423 (3)	0.081 (3)
N11	0.4505 (7)	0.6699 (6)	0.0696 (7)	0.082 (9)
C111	0.4023 (10)	0.6563 (20)	0.0678 (19)	0.290 (35)
C114	0.4694 (16)	0.6208 (13)	0.0838 (16)	0.240 (27)
N12	0.4389 (7)	0.6689 (6)	-0.1793 (8)	0.075 (8)
C121	0.4204 (10)	0.6268 (9)	-0.1569 (11)	0.107 (14)
C122	0.4268 (17)	0.5958 (15)	-0.2019 (19)	0.251 (24)
C123	0.4481 (19)	0.6248 (17)	-0.2572 (24)	0.327 (34)
C124	0.4694 (11)	0.6537 (14)	-0.2299 (11)	0.205 (24)
N13	0.3840 (6)	0.8262 (6)	-0.0664 (9)	0.072 (8)
C131	0.3917 (12)	0.8701 (12)	-0.0986 (20)	0.179 (25)
C132	0.3591 (24)	0.8877 (22)	-0.0718 (31)	0.410 (52)
C133	0.3386 (25)	0.8548 (24)	-0.0220 (36)	0.506 (79)
C134	0.3614 (16)	0.8307 (24)	-0.0159 (20)	0.496 (67)

[a]Equivalent isotropic U defined as one-third of the trace of the orthogonalized U_{ij} tensor ($U_{eq} = \frac{1}{3} \Sigma_i \Sigma_j U_{ij} a_i^* a_j^* a_i a_j$)

Table 8. (continued)

Atom	X	Y	Z	U_{eq}, ($Å^2$)
N21	0.1192 (6)	0.7063 (6)	-0.2266 (7)	0.070 (8)
C211	0.0907 (8)	0.7353 (10)	-0.1918 (12)	0.102 (13)
C212	0.0840 (21)	0.7103 (19)	-0.1415 (30)	0.130 (24)
C213	0.0720 (24)	0.6609 (23)	-0.1828 (31)	0.155 (29)
C214	0.1102 (8)	0.6621 (10)	-0.1948 (22)	0.254 (34)
N22	0.2898 (6)	0.7041 (8)	-0.0942 (9)	0.099 (10)
C221	0.2935 (15)	0.6550 (14)	-0.0813 (19)	0.229 (22)
C222	0.2842 (15)	0.6603 (14)	-0.0175 (19)	0.227 (21)
C223	0.2852 (13)	0.7016 (13)	0.0108 (18)	0.190 (17)
C224	0.2726 (12)	0.7230 (13)	-0.0432 (16)	0.169 (15)
N23	0.2792 (10)	0.6274 (8)	-0.3380 (19)	0.195 (22)
C231	0.2988 (20)	0.6025 (22)	-0.3049 (30)	0.397 (43)
C232	0.3136 (21)	0.5642 (19)	-0.3287 (25)	0.323 (38)
C233	0.2961 (19)	0.5744 (20)	-0.3869 (26)	0.268 (26)
N31	0.7981 (18)	0.6590 (22)	0.0219 (26)	0.355 (28)
C311	0.7918 (27)	0.6072 (29)	0.0372 (36)	0.361 (39)
C312	0.7586 (23)	0.5892 (24)	0.0836 (32)	0.314 (33)
C313	0.7662 (22)	0.6505 (27)	0.0957 (29)	0.303 (30)
C314	0.7840 (25)	0.6981 (27)	0.0792 (34)	0.351 (37)

Table 9. Anisotropic thermal parameters[a] (x 10^3 Å^2) of the non-hydrogen atoms for $Mo_6S_8(pyrr)_6 \cdot 1$ pyrr

Atom	U_{11}	U_{22}	U_{33}	U_{12}	U_{13}	U_{23}
Mo11	58 (1)	59 (1)	40 (1)	-8 (1)	1 (1)	0 (1)
Mo12	54 (1)	60 (1)	40 (1)	2 (1)	-1 (1)	-5 (1)
Mo13	53 (1)	61 (1)	43 (1)	1 (1)	0 (1)	-5 (1)
Mo21	52 (1)	76 (1)	44 (1)	-3 (1)	-1 (1)	5 (1)
Mo22	55 (1)	84 (1)	49 (1)	-6 (1)	-4 (1)	11 (1)
Mo23	59 (1)	75 (1)	61 (1)	3 (1)	-2 (1)	-4 (1)
S11	52 (3)	72 (4)	50 (4)	-7 (3)	2 (3)	-7 (3)
S12	66 (4)	76 (4)	50 (4)	4 (3)	10 (3)	-1 (3)
S13	69 (4)	70 (4)	39 (3)	-5 (3)	-5 (3)	8 (3)
S14	73 (4)	54 (4)	59 (4)	-1 (3)	-1 (3)	0 (3)
S21	74 (4)	80 (4)	85 (5)	-8 (4)	-11 (4)	19 (4)
S22	61 (4)	88 (5)	81 (5)	3 (3)	-9 (3)	3 (4)
S23	61 (4)	101 (5)	60 (4)	-8 (4)	-3 (3)	-9 (4)
S24	71 (4)	125 (6)	49 (4)	-2 (4)	4 (3)	-12 (4)
N11	112 (17)	91 (15)	44 (12)	-27 (13)	10 (11)	2 (11)
C111	55 (19)	586 (91)	246 (49)	-71 (35)	-1 (25)	288 (57)
C114	382 (63)	200 (38)	137 (33)	229 (43)	-17 (37)	-51 (29)
N12	108 (16)	51 (12)	65 (14)	-5 (11)	-25 (12)	-2 (10)
C121	153 (29)	98 (22)	70 (20)	-33 (21)	-30 (19)	-19 (17)
C124	162 (32)	377 (59)	77 (23)	-176 (37)	67 (23)	-150 (32)
N13	53 (12)	78 (14)	86 (16)	23 (11)	-16 (11)	-31 (12)
C131	105 (29)	121 (33)	312 (62)	9 (26)	-10 (34)	46 (37)
C134	308 (66)	995 (184)	186 (52)	525 (103)	-69 (48)	-96 (80)
N21	77 (14)	96 (15)	36 (11)	4 (12)	16 (10)	1 (10)
C211	68 (17)	159 (28)	79 (21)	-12 (18)	-8 (16)	2 (20)
C214	30 (16)	92 (25)	640 (99)	-4 (17)	-43 (34)	132 (42)
N22	63 (14)	149 (22)	84 (17)	-16 (14)	-3 (12)	5 (16)
N23	130 (24)	80 (18)	374 (58)	52 (18)	-61 (30)	21 (27)

[a]The coefficients U_{ij} of the anisotropic thermal parameter expression are defined as:
$\exp [-2\pi^2 (U_{11}h^2a^{*2} + U_{22}k^2b^{*2} + U_{33}l^2c^{*2} + 2U_{12}hka^*b^* + 2U_{13}hia^*c^* + 2U_{23}klb^*c^*)]$

RESULTS AND DISCUSSION

Sulfidation Reactions

Previous research on sulfide substitution into the $Mo_6Cl_8^{4+}$ cluster units (Mo_6Cl_{12}) showed that NaSH was a good sulfiding agent. The use of a proton acceptor (OBu^-) in 1-butanol also led to a greater and more facile sulfide substitution.[21] Laughlin showed that the 1:6:4 (Mo_6Cl_{12}:NaSH:NaOBu) stoichiometry could produce $Mo_6S_6Cl_2(py)_4$ and that completely sulfided Mo_6S_8 cluster compounds could be prepared by the following two-step reaction sequence:[10]

$$1\ Mo_6Cl_{12} + 8\ NaSH + 4\ NaOBu \xrightarrow[\text{reflux, 3d}]{\text{BuOH/py}} \xrightarrow[4d]{\text{MeOH wash}} Mo_6S_7Cl(py)_x$$

$$Mo_6S_7Cl(py)_x + 2\ NaSH \xrightarrow[\text{reflux, 2d}]{\text{BuOH/py}} \xrightarrow[4d]{\text{MeOH wash}} Mo_6S_8(py)_{\sim 4}$$

Based on the observation that an excess of sulfiding agent was needed in order to produce a completely sulfur-substituted product, research was initiated into reactions with an increasing sodium hydrosulfide content. Reactions with the 1:10:5 stoichiometry resulted in products with a small, but variable, chlorine content (0-1 Cl) remaining. The far-infrared spectra of the completely sulfided materials (Figure 1) showed the absence of Mo-Cl stetching modes as compared to Mo_6Cl_{12}. Very weak, but detectable, pyridine coordination bands at 629 and 431 cm^{-1} and a broad Mo-S stretching vibration centered at 384 cm^{-1} were also observed. The location of this Mo-S mode was indicative of the Mo_6S_8 cluster unit and the broad nature of the band showed the material was amorphous.

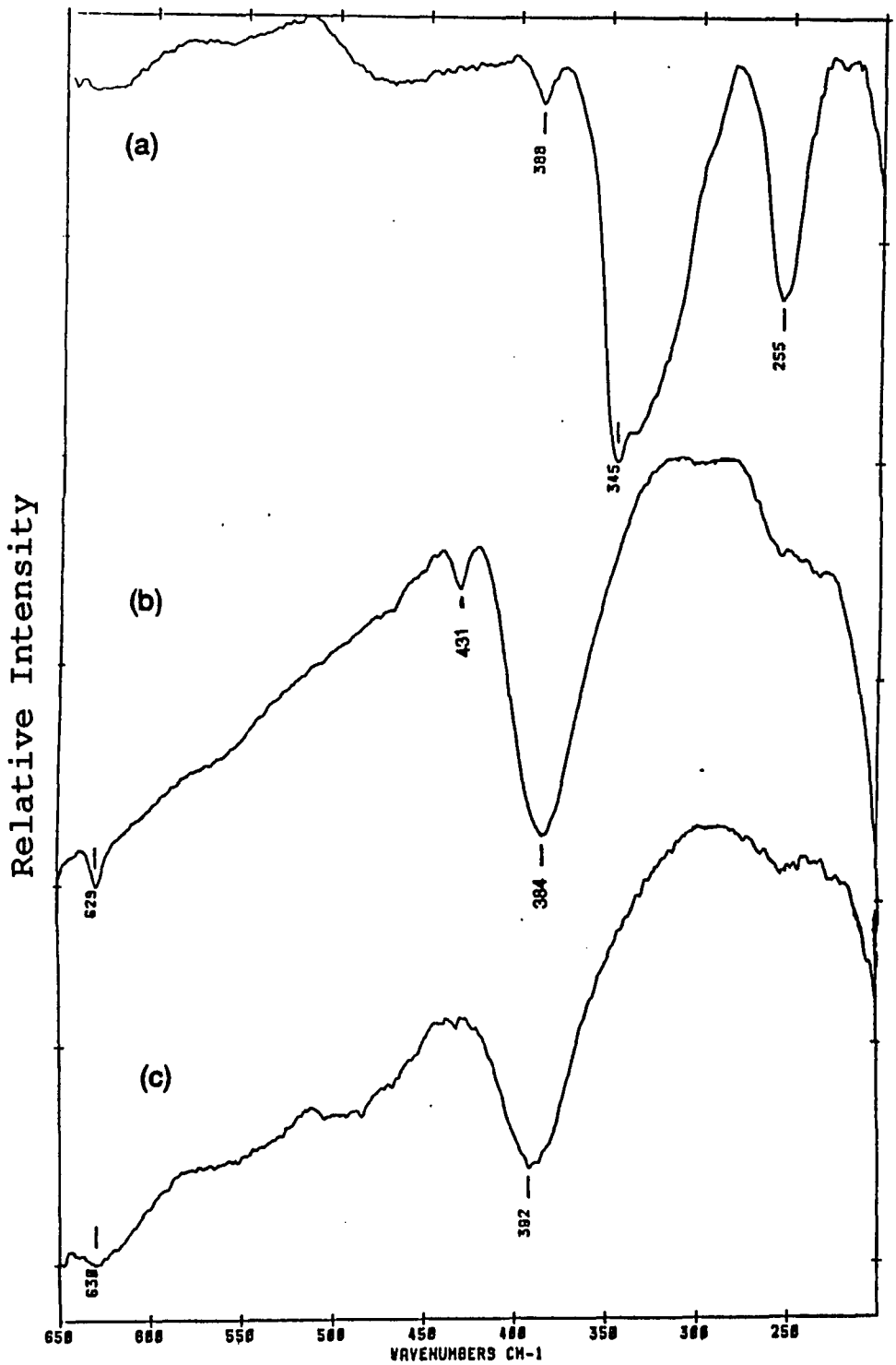

Figure 1. Far-infrared spectra (Nujol) of Mo_6Cl_{12} (a) and the pyridine adducts obtained from the 1:10:5 (b) and 1:12:6 (c) reactions

By increasing the reaction stoichiometry to 1:12:6 (Mo_6Cl_{12}:NaSH:NaOBu), a one-step procedure for the preparation of the Mo_6S_8 cluster unit resulted. The brown/black product was highly pyridine deficient as indicated by the weak pyridine bands in the infrared spectrum (Figure 2). Pyridine coordination can be evidenced at 1597, 1213, 750, and 690 cm^{-1} in the mid-IR region. Again, a broad Mo-S stretching mode was present and centered about 392 cm^{-1}. Examination of this compound by both XPS and SEM-EDS indicated the presence of sodium. Elemental analyses resulted in the formulation of this pyridine-deficient product as $Na_{0.8}Mo_6S_{8.4}(py)_2(MeOH)$. Infrared bands for methanol were not observed; however, the presence of methanol was based on higher than expected carbon and hydrogen results and on the fact that methanol was observed in the ternary sodium molybdenum sulfides (discussed in Paper 3). The pyridine and methanol contents were found to be variable from one reaction to another. Thus, this pyridine-deficient compound will be referred to as $Na_{2y}Mo_6S_{8+y}(py)_x$. The reactivity of this compound with the atmosphere was also found to be variable. Materials with less pyridine were more reactive (pyrophoric).

Further SEM-EDS analysis of the pyridine-deficient compounds prepared by previous workers also indicated that sodium (not sodium chloride) was present. Based on these observations, it appears that intercluster Mo-S interactions are formed more favorably than the terminal pyridine coordination under these reaction conditions. This results in disordered materials with extended Mo-S-Mo intercluster bonding similar to that in the Chevrel phase compounds. Retention of the Mo_6S_8

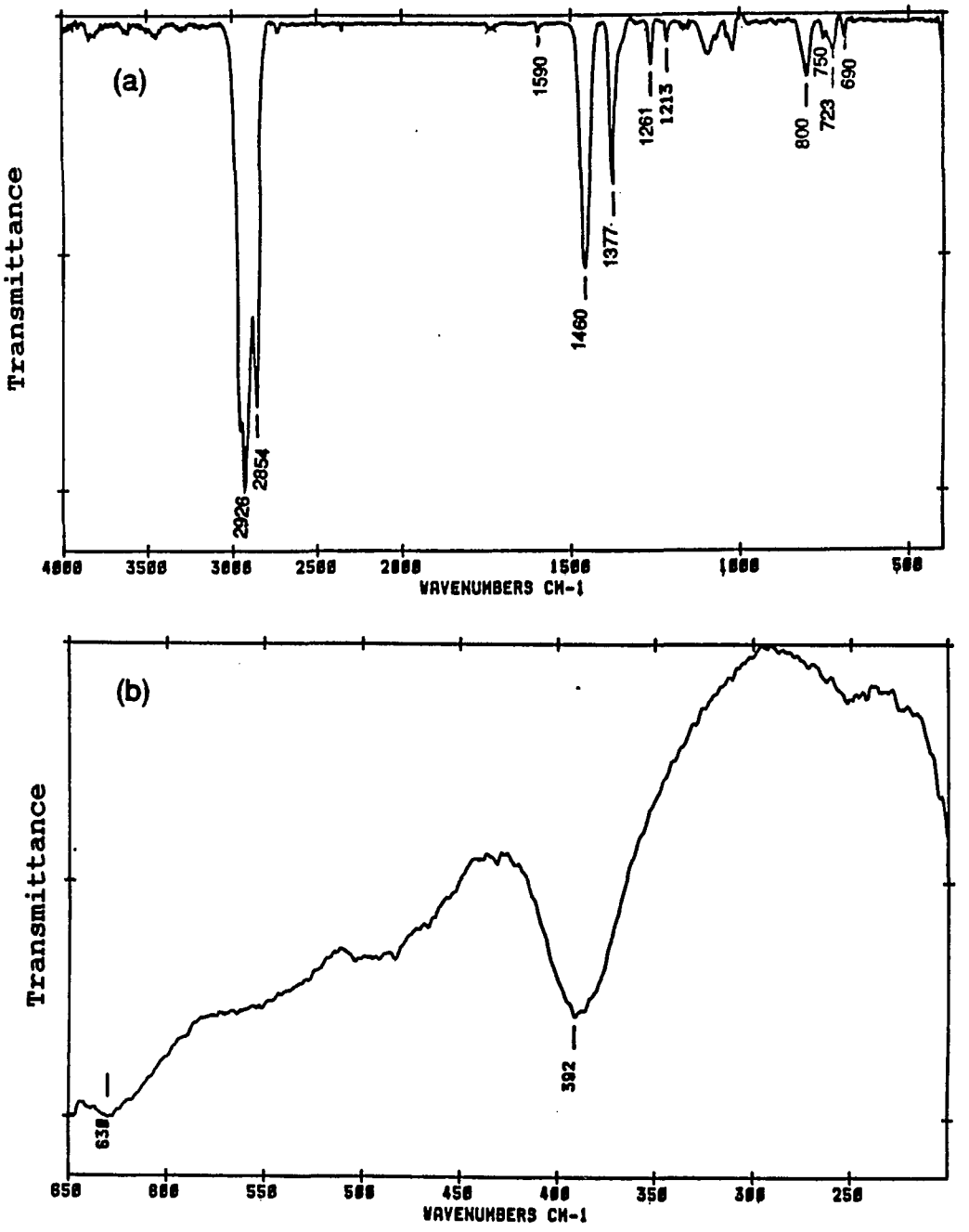

Figure 2. Mid-infrared (a) and far-infrared (b) spectra (Nujol) of the pyridine adduct from the 1:12:6 reaction with Mo_6Cl_{12}, NaSH, and NaOBu.

cluster unit could be unambiguously proven by the rapid reaction of this pyridine-deficient material with n-propylamine and the further ability to form crystalline $Mo_6S_8L_6$ cluster complexes with triethylphosphine, tetrahydrothiophene, pyrrolidine, and piperidine.

Crystalline $Mo_6S_8(py)_6$

The pyridine-deficient material was found to be somewhat soluble in pyridine and, upon further reaction in neat pyridine, a brown solid and brown solution were formed. The brown solid from this pyridine reaction was also somewhat pyridine soluble. Greater solubility was observed in coordinating solvents like n-propylamine and piperidine. Mid- and far-infrared spectra for the brown solid are shown in Figure 3. Coordinated pyridine is evidenced by the characteristic bands in the mid-IR region. In the far-IR region, there occur two separate pyridine bands at 629 and 612 cm^{-1} which are due to coordinated and "free" pyridine in the solid. Support for this conclusion can be found in the pyrrolidine and piperidine compounds which also contain both coordinated and "free" ligands even after drying overnight under dynamic vacuum. The narrow band resulting from the Mo-S stretching vibration at 378 cm^{-1} indicated that the material had some degree of crystallinity. This was evidenced in the x-ray powder diffraction pattern which showed a few weak lines at low two-theta values. Single crystals containing $Mo_6S_8(py)_6$ were obtained by the slow reduction of the solvent volume from the filtrate and refrigeration for several days.

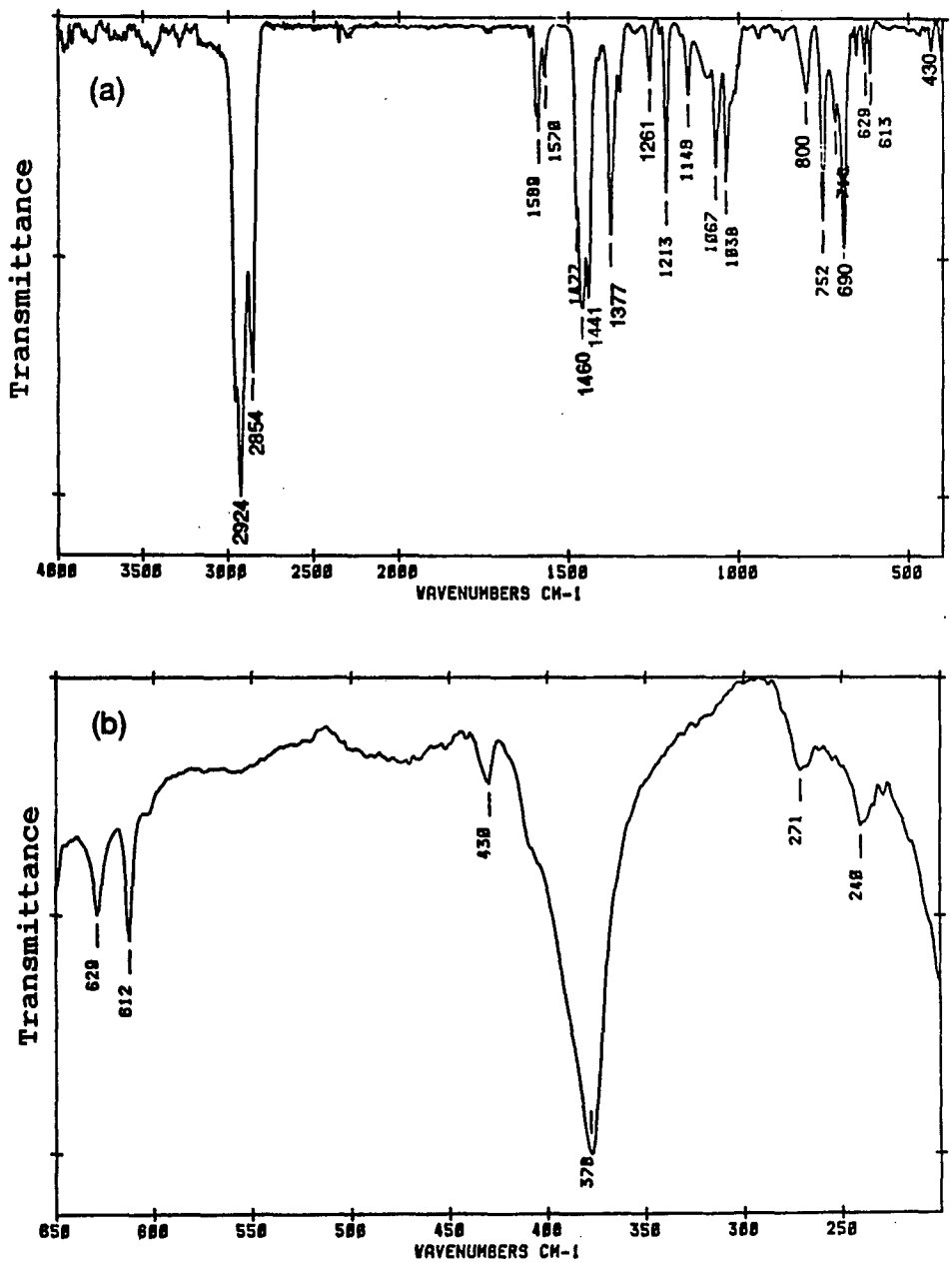

Figure 3. Mid-infrared (a) and far-infrared (b) spectra (Nujol) of the pyridine adduct from the reaction between $Na_{2y}Mo_6S_{8+y}(py)_x$ and neat py

The chemistry of the tungsten analogues showed few similarities.[13] The hexapyridine adduct could be prepared by the reaction of W_6Cl_{12}, NaSH, and NaOBu in a 1:12:6 ratio in neat pyridine. The resulting product was a red, relatively air-stable material which was almost completely insoluble in pyridine. Crystals were grown by a sealed tube reaction at 200°C in pyridine. In comparison, the reaction of Mo_6Cl_{12} in neat pyridine led to incomplete sulfidation, thus 1-butanol was used with added pyridine. The use of the same reaction stoichiometry resulted in a product generally formulated as $Na_{2y}Mo_6S_{8+y}(py)_x$ where excess Na_2S was present. This brown pyridine-deficient material was somewhat soluble in pyridine and, with further reaction in neat pyridine, crystals of the pyridine adduct could be grown out of the solution. These brown crystals contained pyridine as solvent of crystallization. Based on these observations, the reaction chemistry of the molybdenum and tungsten sulfide clusters are quite different. When it comes to exploring reaction behavior, however, the comparison of these reaction products would prove interesting.

Ligand Exchange Reactions

Earlier research into ligand exchange reactions focused on the preparation of the triethylphosphine, propylamine, and tetrahydrothiophene adducts. The triethylphosphine complex was produced by a simple exchange reaction of the pyridine adduct with triethylphosphine in toluene and resulted in a crystalline solid. Upon further study, it was found that n-propylamine was much more labile than pyridine and thus made an excellent candidate for ligand exchange. This was exhibited for the

tetrahydrothiophene adduct. Starting with the propylamine adduct resulted in a more facile reaction and formation of a crystalline product. However, the study of the reactivity of either the pyridine or propylamine adducts has been limited.

Some exploration has been made into the ligand substitution reactions of the tungsten analogues.[13] Initial differences were found, since the pyridine adduct $W_6S_8(py)_6$ was completely insoluble in n-propylamine. However, exchange reactions produced the triethylphosphine and tetrahydrothiophene adducts from the pyridine cluster complex. From the crystal structure data, bond order calculations of the metal-ligand bond strengths indicated that the metal-nitrogen bonds of coordinated pyridine were at least as weak as, if not weaker than, the metal-sulfur bonds in coordinated tetrahydrothiophene. The calculations also showed that the metal-phosphorus bonds of coordinated triethylphosphine were the strongest. These results seemed to indicate that the best materials for subsequent deligation should be the nitrogen-based ligands.

4-Methylpyridine

Further study into the reactivity of the pyridine-deficient material with 4-methylpyridine resulted in the formation of the 4-Mepy adduct. The mid- and far-infrared spectra for this adduct are shown in Figure 4. The mid-IR region shows bands attributable to 4-methylpyridine; especially identifiable are the strong bands at 1612 and 491 cm^{-1}. In the far-IR region, the bands at 491 and 397 cm^{-1} are due to two ring torsion modes for 4-methylpyridine and the band at 384 cm^{-1} is the Mo-S

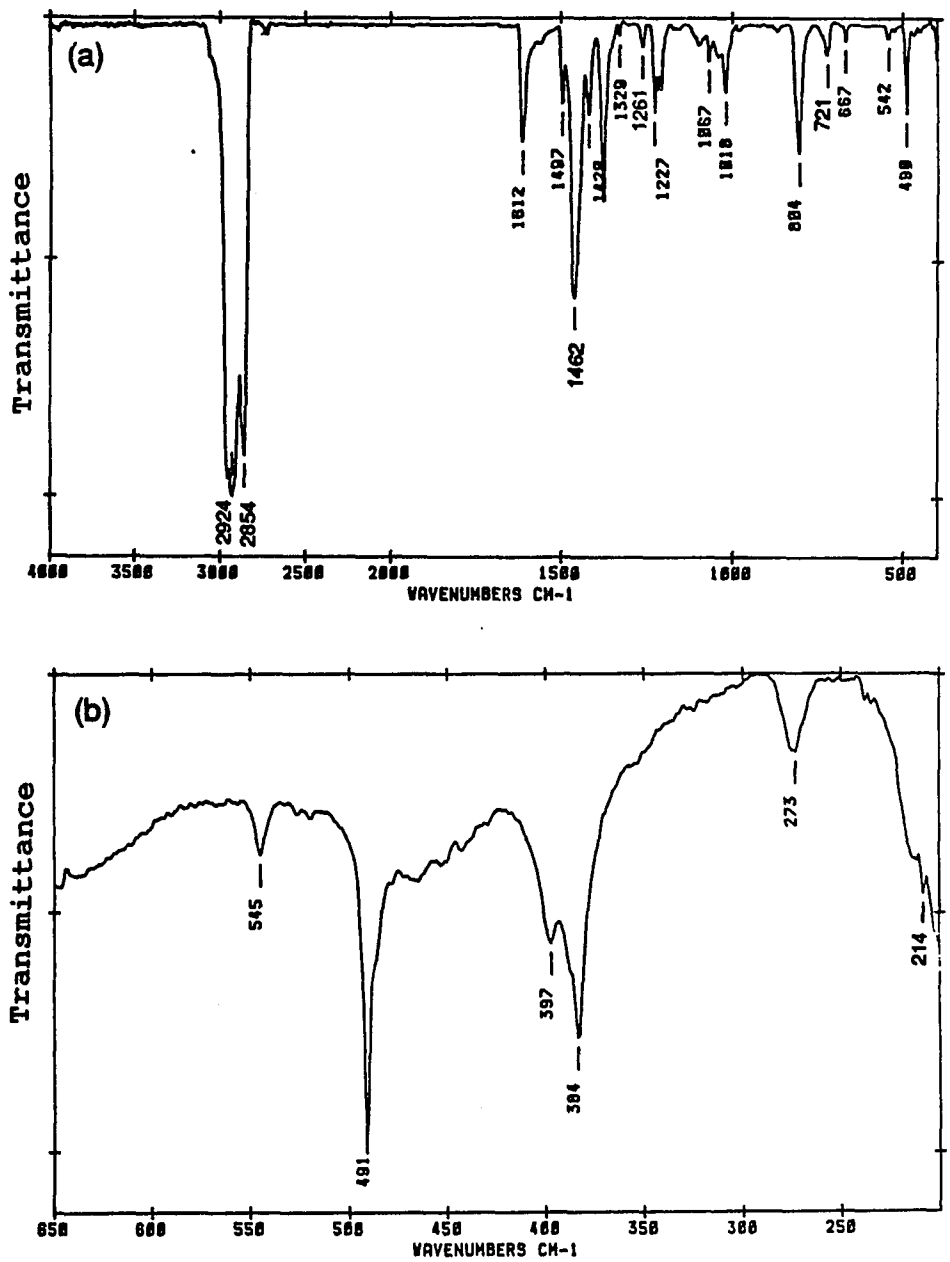

Figure 4. Mid-infrared (a) and far-infrared (b) spectra (Nujol) of the 4-Mepy adduct from the reaction between $Na_{2y}Mo_6S_{8+y}(py)_x$ and 4-methylpyridine

stretching mode. The presence of the band at 273 cm^{-1} is most likely due to the Mo-N stretching mode and is observed for all of the nitrogen-based ligands in the range of 265-276 cm^{-1}. The x-ray powder diffraction pattern resulted in several weak lines at low two-theta values which indicated some crystallinity for the solid. Attempts to grow single crystals from the filtrate have not succeeded.

Extended reactions of the 4-Mepy adduct under reflux in neat 4-methylpyridine resulted in deligation and the formation of intercluster Mo-S interactions. The infrared spectrum showed only very weak bands attributable to 4-methylpyridine and a broad Mo-S mode centered about 396-400 cm^{-1}. Under these reaction conditions, the interactions must be weak and random in nature since extraction of this material with n-propylamine results in the formation of the propylamine adduct. Thus, similar behavior to the pyridine-deficient compound occurred.

Ligand replacement reactions of the 4-methylpyridine adduct show that this ligand can be exchanged to produce the pyridine, propylamine, triethylphosphine, and pyrrolidine adducts as identified by their respective infrared spectra. The reactivity of this compound is similar to the pyridine-deficient material, but neither is as reactive as the propylamine complex.

Propylamine

The pyridine-deficient material can be readily extracted with n-propylamine to form the propylamine adduct. Previous study on the propylamine adduct had shown that the degree of coordination was greatly dependent upon drying conditions.

Longer drying under dynamic vacuum resulted in greater ligand loss as indicated in the elemental analyses. The reaction product appeared crystalline; however, it was glassy as evidenced by its amorphous x-ray powder diffraction pattern. The amorphous nature is also observed in the infrared spectra of this complex. As shown in Figure 5, the far-IR region contains the broad Mo-S stretching mode centered at 384 cm^{-1}. The mid-IR region shows bands attributable to propylamine coordination. Also, a very weak N-H stretching band can be observed at about 3170 cm^{-1}. Attempts to prepare single crystals by slow reduction of volume have not succeeded because of the high solubility in neat n-propylamine and then subsequent ligand loss and precipitation. Also, layering of the solution with diethyl ether or toluene has not produced the desired single crystals. However, the ease of deligation and the reactivity of the propylamine adduct does make this material an excellent intermediate for further ligand exchange reactions.

The propylamine adduct has been reacted with a wide range of coordinating solvents like pyridine, 4-methylpyridine, pyrrolidine, piperidine, and tetrahydrothiophene to produce the corresponding cluster complexes. The reactions are much more facile with the propylamine adduct as compared to identical reactions with the pyridine-deficient compound.

Pyrrolidine

The pyrrolidine adduct can be easily formed by the reaction of the $PrNH_2$ adduct with neat pyrrolidine; however, single crystals could only be prepared by layering the

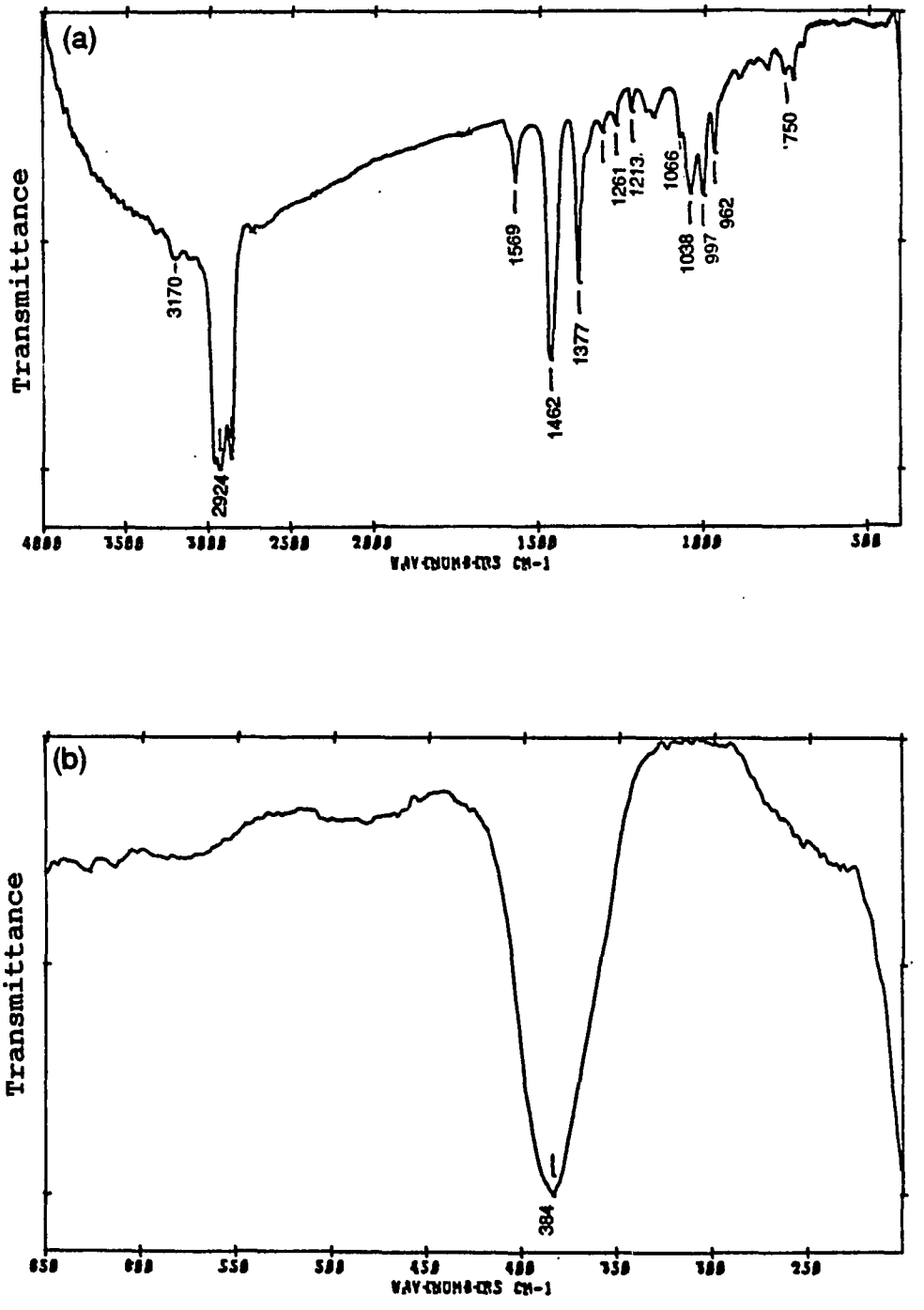

Figure 5. Mid-infrared (a) and far-infrared (b) spectra (Nujol) of the propylamine adduct from the extraction of $Na_{2y}Mo_6S_{8+y}(py)_x$ with neat propylamine

filtrate with diethyl ether. The pyrrolidine adduct was found to be soluble in toluene and was the first readily soluble nitrogen-ligated cluster complex. Over time, though, some solid slowly precipitated out of the toluene solution. This solubility opened avenues for characterization by UV-VIS and NMR spectroscopy. The UV-VIS data are summarized in Table 10. Neither peak in the electronic spectrum is believed to be arising from the HOMO-LUMO transition. Earlier studies on $Mo_6S_8(PEt_3)_6$ indicated that this $T_{1u} \rightarrow E_g$ transition occurred at 991 nm.[15] The higher energy absorptions at 491 and 289 nm were not assigned. A broad shoulder at about 340 nm is also observed in the UV-VIS spectrum of the triethylphosphine adduct. Similar higher energy bands at about 340 and 500 nm can be noted for the pyrrolidine and piperidine adducts; however, the near-infrared region was not examined for the band around 1000 nm.

Table 10. UV-VIS data for toluene soluble cluster complexes

$Mo_6S_8L_6$ clusters	Peak 1 (nm)	Peak 2 (nm)
pyrr	498	342.5
pip	500	341
PEt_3	491	289

Elemental analyses indicated that the pyrrolidine adduct still contained excess pyrrolidine (~1 pyrr) even after drying under a dynamic vacuum. This observation was confirmed by NMR. The NMR spectrum (Figure 6) showed the presence of bands attributable to both free and coordinated pyrrolidine. The α-CH_2 resonance

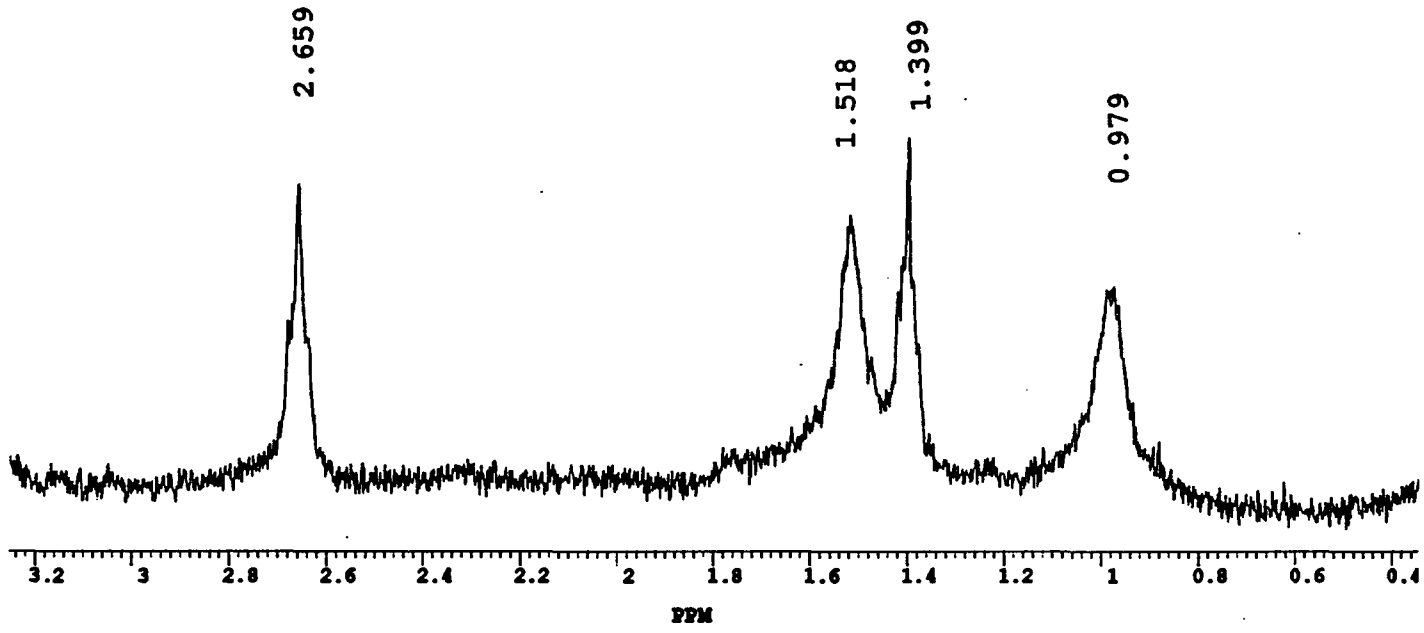

Figure 6. Proton NMR spectrum (300 MHz) of pyrrolidine adduct in deuterated benzene showing coordinated pyrr at 1.518 and 0.979 ppm and free pyrr at 2.659 and 1.399 ppm

has been reported at 2.78 ppm and the β-CH_2 resonance at approximately 1.60 ppm for free pyrrolidine in deuterated chloroform.[22] The spectrum of the adduct run in deuterated benzene showed the free ligand α-CH_2 peak at 2.66 ppm and the β-CH_2 peak at 1.41 ppm. Also, broad bands attributable to coordinated pyrrolidine were identified at 1.52 ppm and 0.98 ppm. Further efforts in making proton assignments were not attempted.

The infrared spectrum for the pyrrolidine adduct is shown in Figure 7. Distinct bands attributable to pyrr are found at 1070, 1029, and 904 cm^{-1}. The band from the N-H stretching mode is present at 3194 cm^{-1} and the Mo-S stretching band is found at 381 cm^{-1}. The peak at 273 cm^{-1} is thought to result from a Mo-N stretching mode.

Piperidine

Results for the piperidine complex were similar to those of pyrrolidine. The piperidine adduct was prepared by the reaction of the $PrNH_2$ adduct with neat piperidine. By slow reduction of the filtrate volume and standing at room temperature, crystalline material was obtained in larger quantities than for the pyrrolidine adduct. Also, the piperidine adduct was much more soluble in toluene than the pyrrolidine complex and showed even greater solubility in chlorobenzene. The infrared spectrum for the piperidine adduct is shown in Figure 8. The complex exhibits a distinctive IR band located at 869 cm^{-1} and the Mo-S stretching vibration is present at 382 cm^{-1}. N-H stretching modes are also found in this spectrum at 3287 and 3214 cm^{-1} for the free and coordinated ligand, respectively.

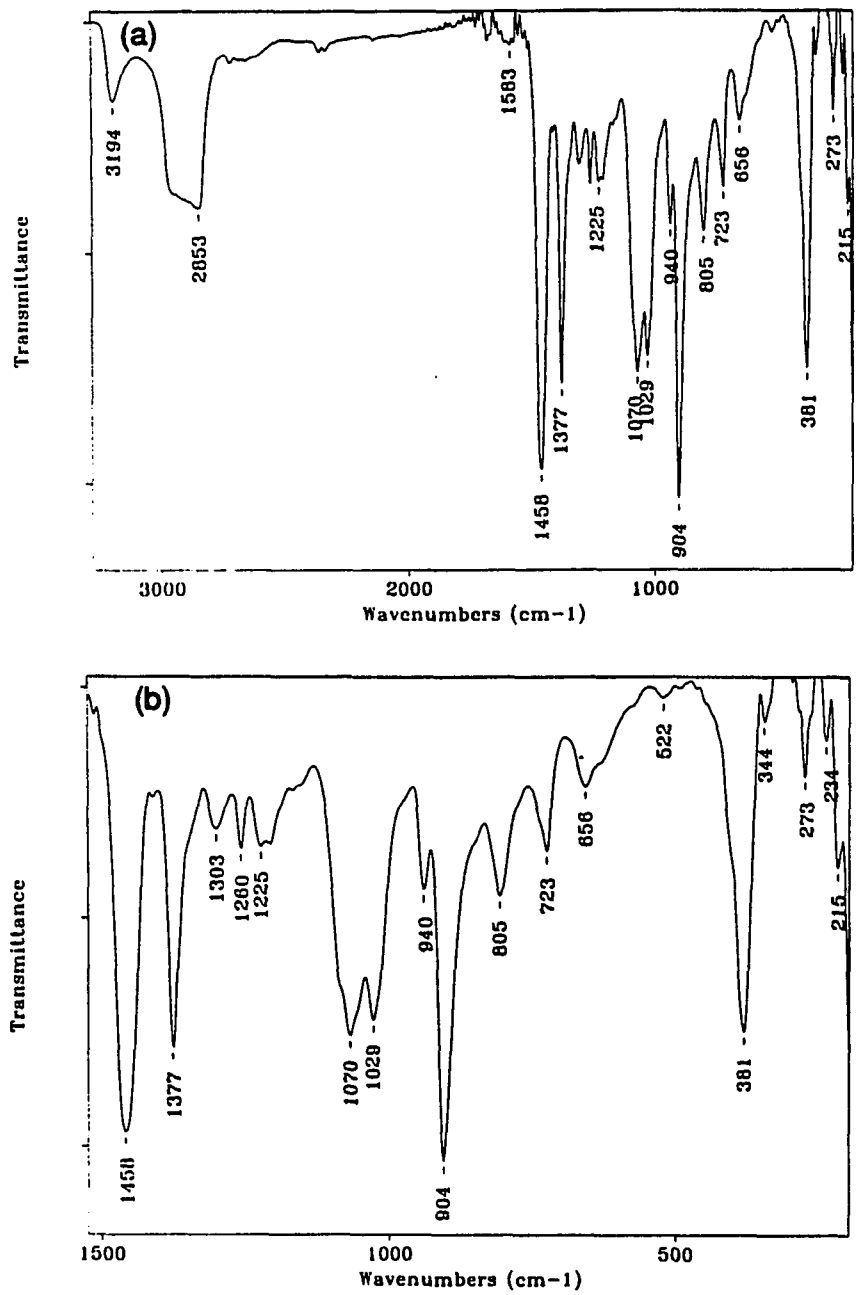

Figure 7. Mid/far-infrared spectrum (Nujol) of the pyrrolidine adduct from the reaction of $Mo_6S_8(PrNH_2)_y$ with neat pyrrolidine. The entire spectrum (a) and the region from 1500-200 cm^{-1} (b) are shown.

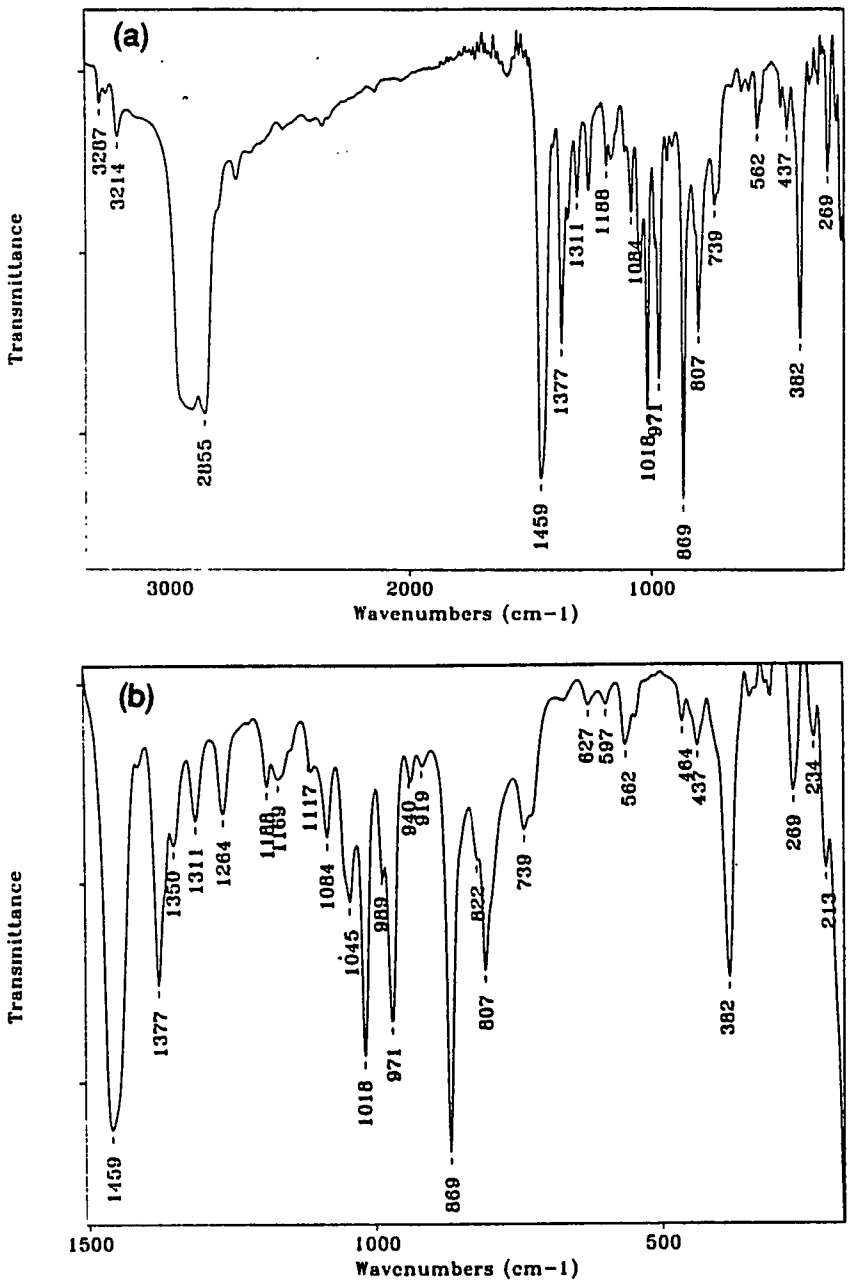

Figure 8. Mid/far-infrared spectrum (Nujol) of the piperidine adduct from the reaction of $Mo_6S_8(PrNH_2)_y$ and neat piperidine. The entire spectrum (a) and the region from 1500-200 cm^{-1} (b) are shown.

As observed in Table 10, the UV-VIS values are very similar to the pyrrolidine and triethylphosphine complexes. Like the results for the pyrrolidine adduct, elemental analyses for the piperidine adduct indicated excess ligand present even after drying under dynamic vacuum. While the pyrrolidine adduct indicated 1 excess ligand, the piperidine adduct indicated 4-7 excess ligands present. Therefore, a proton NMR study was undertaken to identify and then make assignments of the free and coordinated piperidine protons.

NMR study on piperidine adduct

Literature values for the free piperidine resonances were reported for α-CH_2 at 2.77 ppm (s) and for β & γ-CH_2 at 1.52 ppm (d) in deuterated chloroform.[23] The initial spectrum at 300 MHz in deuterated benzene (Figure 9a) showed the presence of free piperidine bands at 2.61 and 1.39 ppm, as well as, coordinated piperidine bands forming a doublet at 3.90 & 3.85 ppm and unresolved multiplets at 3.25-3.07 ppm and 1.11-0.85 ppm. Further information was gained from a proton decoupling experiment.

Irradiation at the doublet (3.87 ppm) resulted in changes in all of the multiplets and the observation of a peak shoulder arising at 1.31 ppm. The presence of this shoulder near the β,γ peak of free piperidine was observed in all of the irradiation experiments. Further irradiation at 3.17 and 3.05 ppm resulted in the doublet becoming a singlet (3.89 ppm) and changes in intensity and splitting of the multiplet at 0.90-0.85 ppm. Irradiation at free α-CH_2 (2.59 ppm) showed no change in the

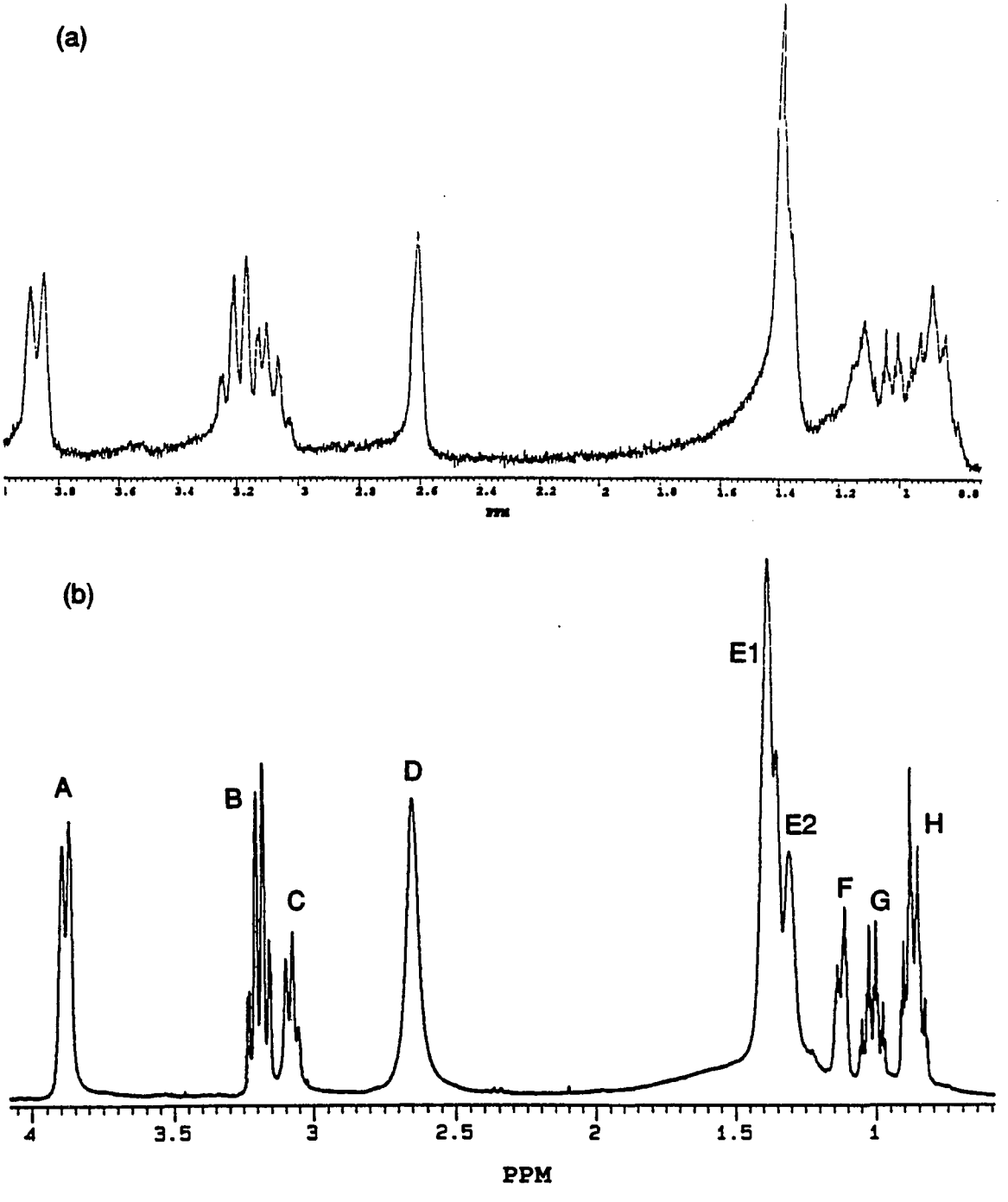

Figure 9. Proton NMR spectra of the piperidine adduct in C_6D_6 showing spectra collected on Nicolet 300 MHz NMR (a) and Unity 500 MHz NMR (b). Spectrum (b) is labelled as to peak assignments discussed in text.

coordinated peaks. Finally, irradiation at 1.11 and 0.88 ppm resulted in changes in the doublet and multiplets at 3.25-3.07 ppm. These results indicated that a great deal of interaction was occurring between the various piperidine hydrogens. Also, the presence of a shoulder on the free β,γ peak most likely resulted from a coordinated pip band intermixed with the free band, rather than the separation of the free peak into its two components.

The system was studied using a higher field instrument (500 MHz NMR) in order to produce further peak separation and aid in proton assignments. The spectrum (Figure 9b) is labelled for peak identification. The free piperidine bands are D at 2.65 ppm (α-CH_2) and E1 at 1.38 ppm (β,γ-CH_2) and the coordinated piperidine bands are labelled as A,B,C,E2,F,G,H. The spectrum showed greater resolution as indicated by (1) two distinct multiplets - B at 3.23-3.15 ppm and C at 3.10-3.06 ppm, (2) the "shoulder" on the free β,γ peak (E1) at 1.35 ppm possibly due to resolution of free γ-CH_2 protons, and (3) the three distinct multiplets - F at 1.14-1.11 ppm, G at 1.06-0.97 ppm, and H at 0.91-0.82 ppm.

Peak integration values were used to form some general conclusions about the ratio of free to coordinated piperidine ligands. Based on literature data, peak D was determined to be arising from the free piperidine α-protons (α-CH_2) and it was assumed that the multiplets A (3.90-3.87 ppm) and B (3.23-3.15 ppm) were the result of the two differing coordinated piperidine α-protons (axial and equatorial). Also, it was assumed that these cluster complexes were of the general formula $Mo_6S_8(pip)_6 \cdot x$ pip which resulted in 24 α-H for coordinated pip and 4x α-H for free pip. Then

using the relative integrals from integration, the amount of free piperidine could be calculated. The initial NMR experiment on the 300 MHz NMR indicated 4.3 free pip and the experiment on the 500 MHz NMR showed 5.0 free pip. Molybdenum analyses on this compound resulted in 29.39% Mo or approximately 13 piperidines. Also, knowing that the ratio of free α-H to free β,γ-H was 4 to 6, the contribution of coordinated piperidine to peak E could be calculated. The results show that peak E is composed of about 55% free (E1) and 45% coordinated (E2) piperidine.

Two-dimensional NMR was implemented in order to gain further information concerning the proton assignments. The techniques employed were double quantum correlation spectroscopy (DQCOSY) which studied through-bond coupling interactions and Nuclear Overhauser Effect spectroscopy (NOESY) which studied through-space coupling interactions. The NMR spectra are shown in Figures 10 to 12, the results tabulated in Table 11, and proton assignments formulated in Figure 13. The proton NMR spectrum for the two-dimensional experiments (Figure 10) showed several differences from the previous spectrum on the 500 MHz instrument (Figure 9b). The presence of bands at 3.45-3.32 ppm resulted from methanol which was used to clean the NMR tube prior to use. Also, there is a marked difference in the free piperidine peaks between the two spectra. The free α-CH_2 peak (D) is smaller in size for Figure 10 and it is completely absent in the two-dimensional spectra. The spectral differences for the free piperidines can also be noticed for the free β,γ peak at 1.38 ppm. In Figure 10, the peak is dominated by the coordinated piperidine band E2 as observed by the doublet. These results might be due to the short time interval

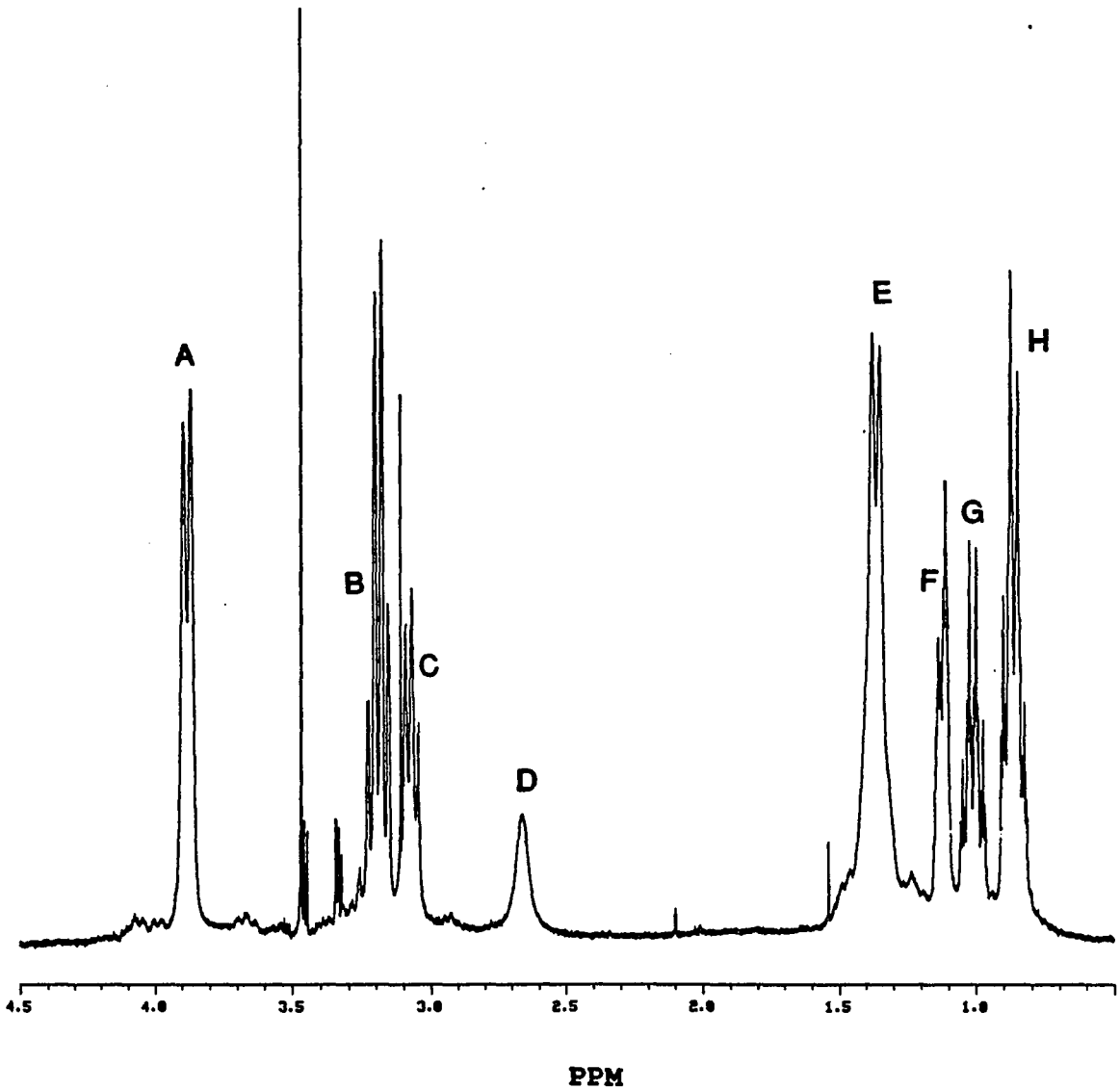

Figure 10. Proton NMR spectrum (500 MHz) of piperidine adduct in C_6D_6 collected during 2-dimensional DQCOSY and NOESY experiments

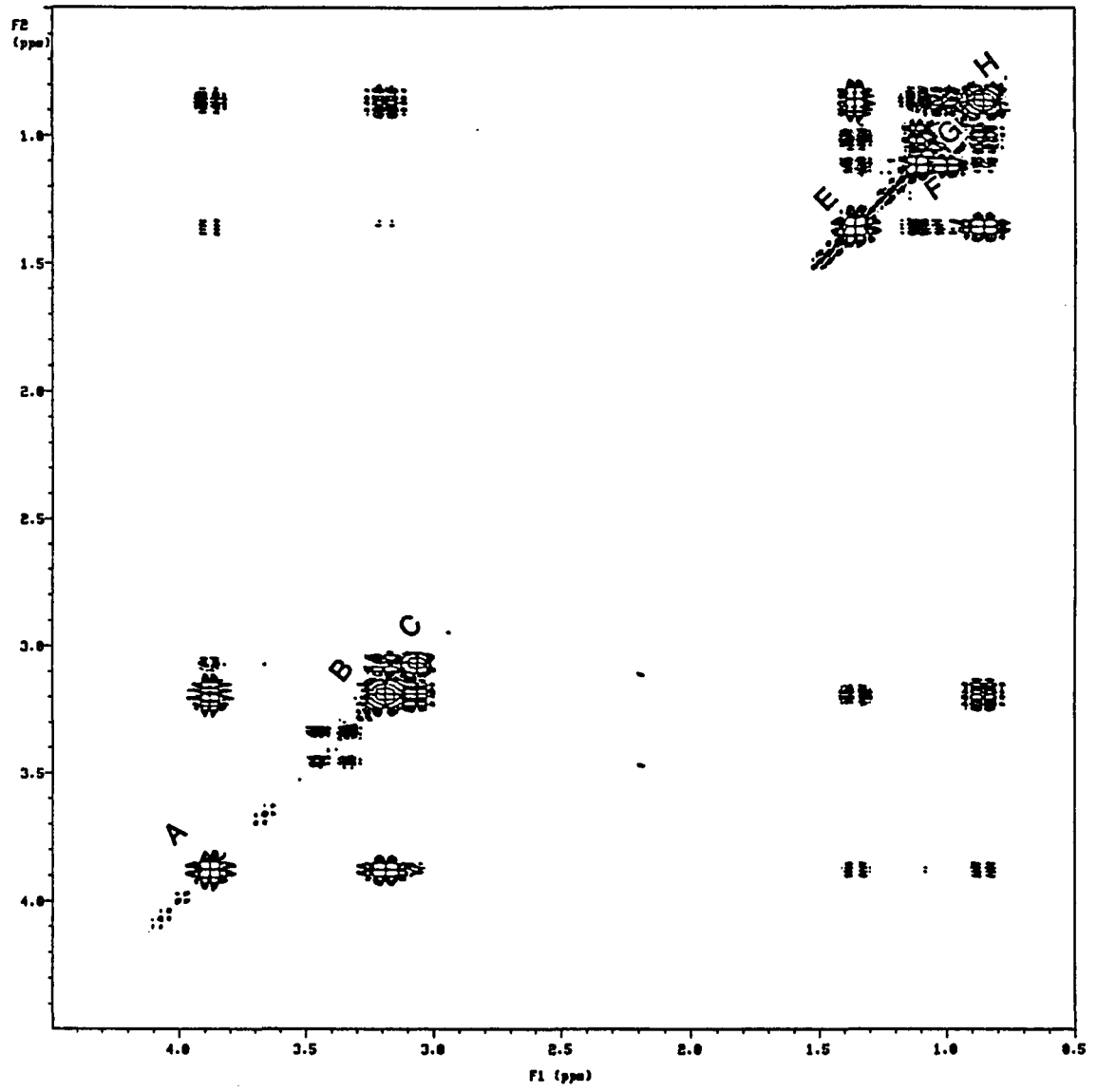

Figure 11. Double quantum correlation spectroscopy (DQCOSY) spectrum of the piperidine adduct showing through-bond interactions. The peaks on the diagonal are labelled as in Figure 10 and the presence of off-diagonal peaks indicates the occurrence of coupling interactions between the labelled peaks.

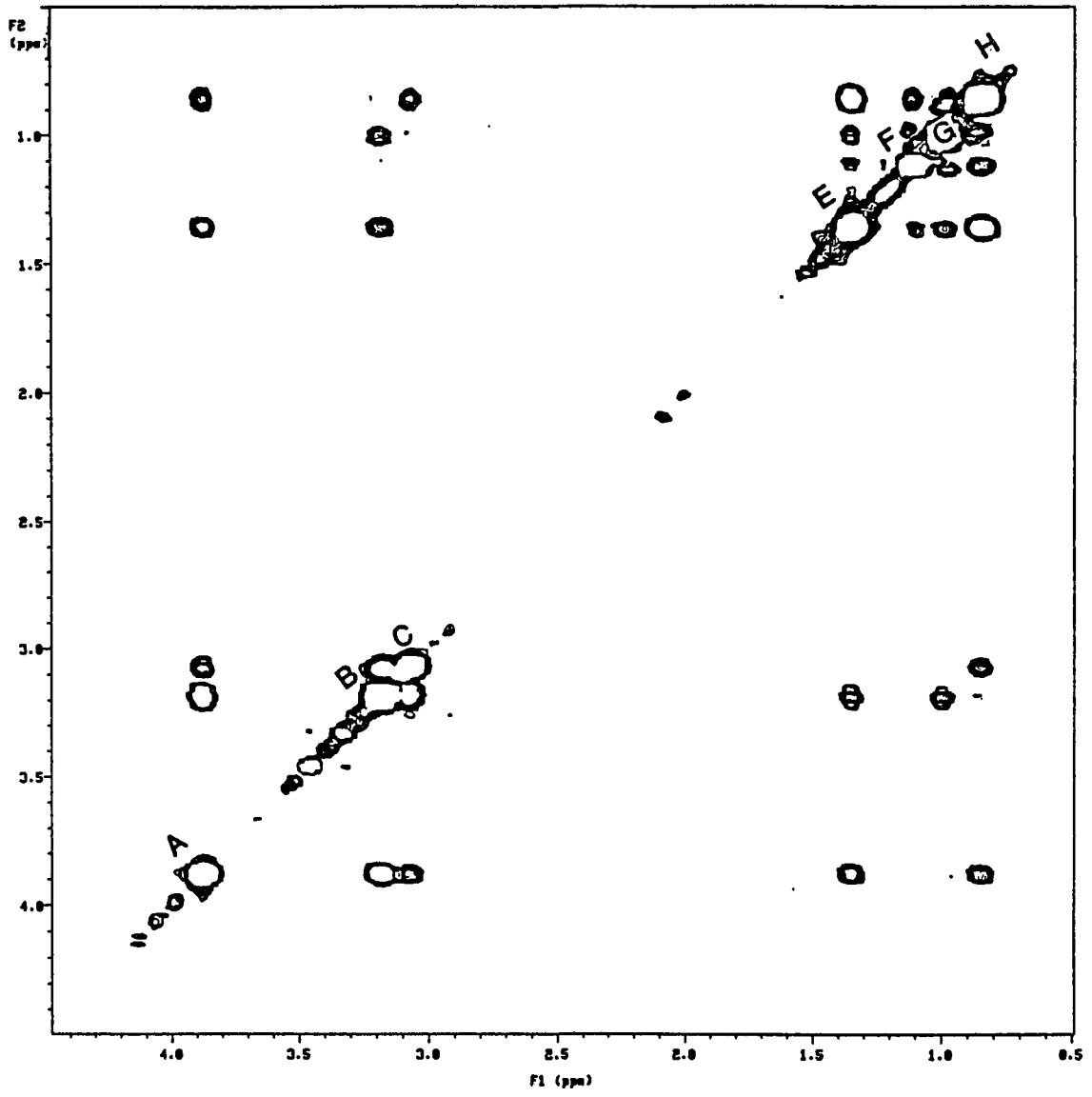

Figure 12. Nuclear Overhauser Effect spectroscopy (NOESY) spectrum of the piperidine adduct showing through-space interactions. The peaks on the diagonal are labelled as in Figure 10 and the presence of off-diagonal peaks indicates the occurrence of through-space coupling between the labelled peaks.

Table 11. Through-bond (DQCOSY) and through-space (NOESY) interactions observed in two-dimensional NMR spectra shown in Figures 11 and 12. E signifies the interaction of peak E2.

	A	B	C	D	E	F	G	H
DQCOSY	B,C,E,H	A,C,E,H	A,B	---	A,B,F,G,H	E,G,H	E,F,H	A,B,E,F,G
NOESY	B,C,E,H	A,C,E,G	A,B,H	---	A,B,F,G,H	E,G,H	B,E,F,H	A,C,E,F,G

A - equatorial α
B - axial α
C - NH proton (axial)
D - free α
E1- free β,γ
E2- axial β
F - axial γ
G - equatorial γ
H - equatorial β

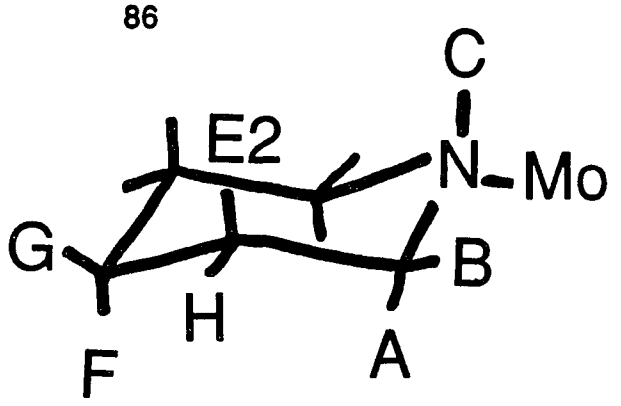

Figure 13. Proton assignments for coordinated piperidine were formulated based on the results of the DQCOSY and NOESY experiments and are shown In the structural diagram

between pulses relative to a longer spin-lattice relaxation time, T_1. This would result in an incomplete relaxation process for the free piperidine and reduction of the peak.

The crystal structure of the adduct showed that the coordinated piperidine was present in the chair conformation and that the ligand was bonded to molybdenum exclusively through the equatorial position. If fast conformational exchange between boat and chair conformations was occurring in solution, a broadening of the coordinated peaks would be expected; but this was not observed.

In the following discussion, the reference to proton E signifies the coordinated piperidine proton referred to previously as E2. As noted in Table 11, similarities in the DQCOSY interactions could be observed for protons A & B, E & H, and F & G. Proton C interacts only with protons A & B which indicates that it must arise from the N-H proton. Likewise, A & B interact with C and E & H which leads to their assignment as the α-hydrogens. Integration showed that peaks C,F,G were all about one-half the value of the other peaks and thus they were assigned as single protons.

Also, protons F & G interact only with each other and E & H which leads to their assignment as the γ-hydrogens. The remaining protons, E & H, are therefore β-hydrogens and interact with both the α- and γ-hydrogens as expected.

A qualitative discussion will be attempted concerning the observed splittings in the NMR spectra for the piperidine adduct. In order to gain a better understanding of the coupling which is occurring in this system, modelling should be explored. The splitting of peak A into a doublet can be reasoned from much stronger coupling of the axial-axial protons between A and E than for the axial-equatorial interaction between A and B. Likewise, the observed doublet in Figure 10 of the E peak (E2) could arise from the same interaction with A. Peak F should also show this strong axial-axial coupling and results in a pattern that somewhat resembles a doublet. The other peaks show much more complicated splitting patterns due to smaller differences in coupling between equatorial-equatorial and equatorial-axial protons. In the DQCOSY spectrum for peak C, there is a much greater interaction between B & C than between A & C, which could lead to something between a doublet and a triplet. No explanation has been developed concerning peaks B, G, and H which all somewhat resemble quartets.

Tetrahydrothiophene

Previous research concerning the tetrahydrothiophene adduct resulted in the report of the molecular structure of crystals grown from the filtrate.[9] However, no discussion was made of the predominant product - the insoluble brown solid.

Analyses on this product indicated that the material was highly ligand deficient and the x-ray powder pattern showed that it was amorphous. A comparison of the far-infrared spectra for the crystalline product and the tht-deficient complex is given in Figure 14. The deficient material has a much larger bandwidth which is again indicative of an amorphous material. Also, a peak indicating tht coordination is present at 515 cm^{-1}.

The yields of the crystalline $Mo_6S_8(tht)_6$ reported previously were never greater than 5-10%. Therefore, attempts were made to improve the yields of the crystallline material by varying the reaction conditions. It was discovered that heating was necessary in the reaction of $Mo_6S_8(PrNH_2)_y$ with tht to produce complete exchange; stirring at room temperature for up to 15 days produced only mixed $PrNH_2$/tht complexes. Extraction of the propylamine adduct with neat tht resulted in complete dissolution and the formation of very small amounts of crystalline material in the warmed receiving flask. Upon drying, however, the brown product was not crystalline in nature. The formation of the crystalline material in the warmed flask indicated a solubility limit which was reached and thus crystals formed from the solution. The best results were observed by refluxing for the short time period of 1-2 hours. The red crystalline material could be obtained from the filtrate in similar yields to that found previously. Longer heating (4-24 hours) resulted in larger amounts of the brown amorphous material. Thus, no improvement has been made on increasing the yield of the crystalline tht product.

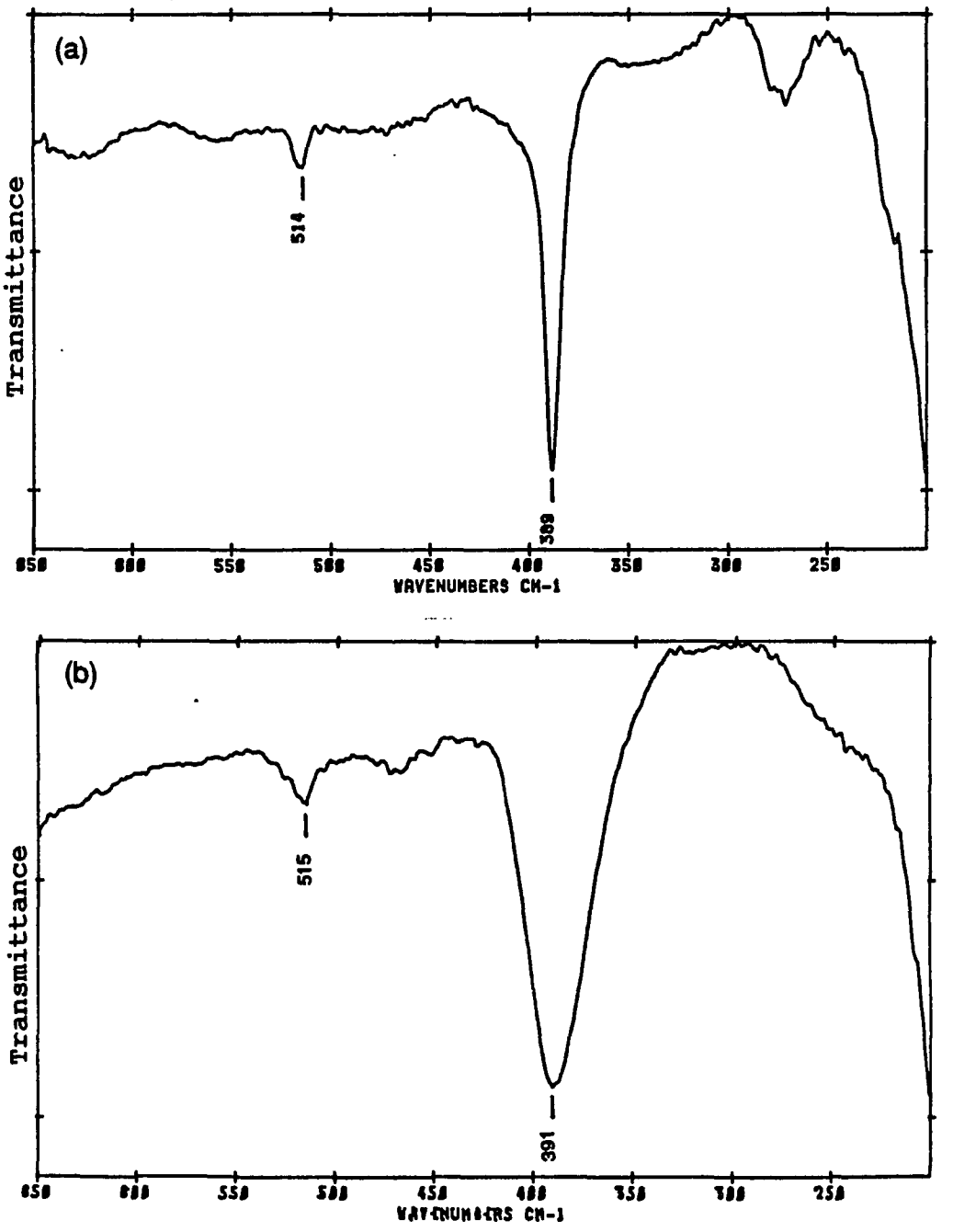

Figure 14. Far-infrared spectra (Nujol) of the tetrahydrothiophene adducts for the crystalline $Mo_6S_8(tht)_6$ (a) and the tht-deficient solid (b)

Ligand replacement reactions of the tht-deficient complex showed that this ligand could be exchanged for propylamine, pyridine, and triethylphosphine. The products were identified by their respective infrared spectra.

Thiophene

Previously, attempts were made to prepare the thiophene-bound complex starting from the pyridine-deficient compound. The results indicated that the thiophene adduct was not formed. However, studies using thiophene complexes as models for hydrodesulfurization prompted further interest in preparing this adduct. Numerous attempts at the reaction of the propylamine complex with neat thiophene did not result in formation of the desired product. The infrared spectra showed only propylamine coordination and thus indicated that no reaction had occurred.

Nitriles

In an attempt to form more labile complexes, research focused on the preparation of nitrile adducts. A variety of nitriles were explored including acetonitrile, propionitrile, butyronitrile, and benzonitrile. The reactions were studied in neat nitrile and with the addition of trifluoromethanesulfonic acid. The use of acetonitrile, propionitrile, and butyronitrile produced an unreacted propylamine complex as identified by the infrared spectra. The addition of the acid resulted in coordination of the triflate anion ($CF_3SO_3^-$) instead of the desired nitrile. The reaction with benzonitrile in toluene produced a propylamine complex with included benzonitrile.

The infrared spectrum of this product is shown in Figure 15. The benzonitrile C≡N mode is observed at 2223 cm^{-1} and other distinctive bands are identified at 756 and 547 cm^{-1}. The propylamine bands are found at 1567, 1067, 1041, and 999 cm^{-1}. As noticed in the far-IR region, the Mo-S stretching mode is centered at 390 cm^{-1}, the Mo-N stretch is at 261 cm^{-1}, and possibly a Mo-Mo stretch at 236 cm^{-1}. The x-ray powder diffraction pattern was indicative of an amorphous material and the elemental analyses also indicated a ligand-deficient complex.

Infrared Spectroscopy

The use of this technique was the first step in identification of the reaction products and has proven to be an effective tool for the characterization of the Mo_6S_8 cluster complexes. Characteristic bands for the coordinated organic ligands could be identified and are tabulated in Table 12. Also, characteristic bands for Mo-S, Mo-N and Mo-Mo modes have been observed.

As shown previously in Figure 1, the formation of the Mo_6S_8 unit can be observed by the loss of Mo-Cl modes at 345 and 255 cm^{-1} and the appearance of the Mo-S vibration at 384-392 cm^{-1}. The presence of the cluster unit was later confirmed by other techniques, but infrared spectroscopy results in a simple tool for identification of Mo_6S_8 cluster complexes.

The reaction to form the pyridine adduct produced an infrared spectrum (Figure 3) showing characteristic bands for pyridine coordination. Previous studies have resulted in the identification and assignment of these pyridine vibrations in molecular

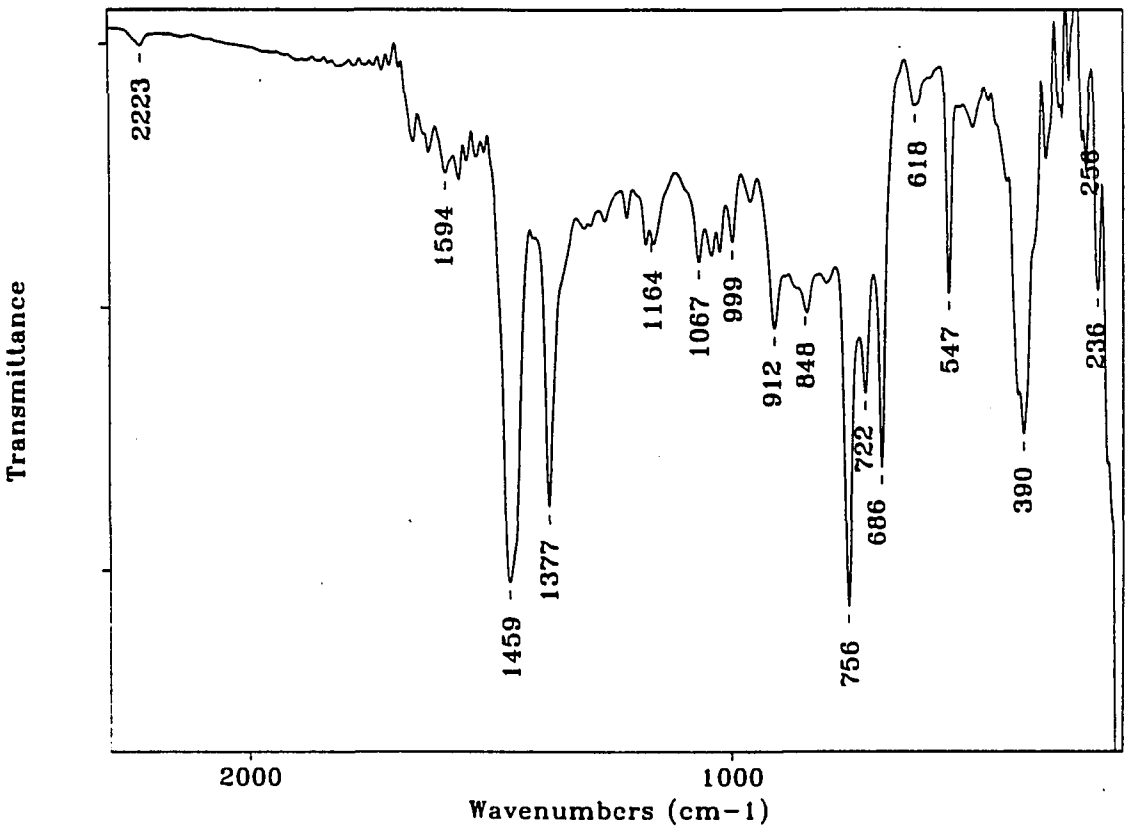

Figure 15. Mid/far-infrared spectrum (Nujol) for the reaction of $Mo_6S_8(PrNH_2)_y$ with benzonitrile in toluene. Bands for coordinated propylamine and for included benzonitrile are observed in this spectrum.

Table 12. Infrared absorption frequencies (cm^{-1}) of the molecular Mo_6S_8 cluster complexes

py	4Mepy	$PrNH_2$	pyrr	pip	tht	PEt_3	PhCN
1589(m)[a]	1612(m)	3170(vw)	3194(m)	3214(w)			2223(w)
1570(w)		1568(m)	1583(w)	1593(w,br)			1594(w)
1477(w,sh)	1497(w)						
1441(ms)	1420(w)			1350(sh)		1414(m)	
	1329(vw)		1303(w)	1311(w)	1306(m)		
1261(w)	1227(m)		1260(w)	1264(w)	1269(m)		
1213(m)	1217(vw)	1213(vw)	1225(w)	1188(w)	1254(m)	1249(m)	
1148(w)	1207(vw)		1209(w)	1169(w)	1130(m)		1175(w)
				1117(w,sh)		1135(w,b)	1158(w)
1067(m)	1067(w)	1066(vw)	1070(s)	1084(w)	1070(ms)		
1038(m)		1038(m)	1029(s)	1045(m)	1035(vw)	1032(s)	
1009(vw)	1018(m)			1018(s)	1023(vw)		1026(w)
		997(m)		989(w,sh)		998(m)	
		962(mw)	940(m)	971(s)	957(m)	974(w)	
			904(s)	940(w)			912(w)
		860(vw)		869(s)	879(ms)		842(w)
800(w)	804(m)		805(m)	807(ms)	808(m)	804(w)	
752(ms)		750(w)		739(w)		760(s)	756(s)
690(m)	667(vw)		656(w)	627(w)	667(w)	715(s)	686(ms)
629(w)		627(w)		597(w)		666(w)	618(w)
612(w)	545(vw)		522(vw)	562(w)	515(m)	622(m)	547(m)
	491(m)			464(w)	472(vw)	404(m)	
430(w)	397(w)			437(w)		390(s)	401(w,sh)
378(s)	384(s)	384(s,br)	381(s)	382(s)	389(s)	364(m)	390(s)
271(w)	273(w)	265(br)	273(w)	269(w)	272(w)	334(m)	261(w)
240(w)			234(vw)	234(w)		236(w)	236(w)
	214(vw)		215(w)	213(w)		217(vw)	

[a]Relative intensities given in parentheses: s=strong, m=medium, w=weak, v=very, sh=shoulder, br=broad

complexes.[24,25] The mid-IR vibrations have generally been found to be either carbon-carbon (ring modes) or carbon-hydrogen in nature. Two characteristic modes of coordinated pyridine are found in the far-infrared region. The band at about 625 cm^{-1} was identified as an in-plane ring bending mode and the band at 420 cm^{-1} as an out-of-plane bending mode. For the pyridine adduct of the Mo_6S_8 cluster, these modes arise at 629 and 430 cm^{-1}, respectively. However, also present in the spectrum is a band at 612 cm^{-1}.

Similar observations have been noted for the tungsten analogues.[13] The extra band was found in samples that possessed higher than expected elemental analyses for carbon and hydrogen, and was explained as the presence of free pyridine in the product. For $W_6S_8(py)_6$, only one band was observed at 634 cm^{-1}. The free pyridine ring modes have been reported at 601 and 403 cm^{-1}.[24,25] Van der Waals bonding interactions between the pyridines could result in the observed inclusion of "free" pyridine in the complex. This interaction should lead to a slight shifting of the "free" pyridine as observed by the band at 612 cm^{-1} and the shoulder at 415 cm^{-1}.

Evidence for included pyridine in the Mo_6S_8 cluster complex is noted from the observation of pyridine as solvent of crystallization in the crystalline material. Trapping of "free" ligand has been observed for the pyrrolidine and piperidine complexes, however, this is most likely due to hydrogen bonding interactions. The band at 271 cm^{-1} has been assigned as a Mo-N stretching mode. All of the nitrogen-ligated complexes exhibit this band in the range of 265-276 cm^{-1}. Also, the band at 240 cm^{-1} may be tentatively assigned as a Mo-Mo stretching mode. Previous

research has shown that a Mo-Mo stretching mode might be assigned to a band at approximately 230 cm^{-1} for $Mo_6X_8Y_6$ (X=Cl,Br; Y=Cl,Br,I) compounds.[26]

Infrared spectroscopy has been used to observe ligand exchange reactions as evidenced by the preparation of the 4-methylpyridine adduct from the pyridine-deficient compound. Figure 4 shows the resulting spectra and the frequencies are listed in Table 12. Upon 4-Mepy coordination, the absorption frequencies exhibit a complete change from the values for the pyridine complex. These frequencies for coordinated 4-Mepy match values found in previously assigned complexes,[27] and show very little shifting from the frequencies observed for the free ligand.[28] The mid-IR bands have been attributed to carbon-carbon and carbon-hydrogen modes (like pyridine). The far-IR spectrum shows distinct bands at 545 cm^{-1} due to a ring deformation mode and two ring torsion modes at 491 and 397 cm^{-1}. The Mo-S stretching mode is observed at 384 cm^{-1}, the Mo-N stretch at 273 cm^{-1}, and the suggested Mo-Mo stretch at 214 cm^{-1}.

The propylamine adduct exhibits a characteristic mid-infrared spectrum as shown in Figure 5. Coordination results in noticeable shifting in the absorption frequencies from those noted for free n-propylamine.[29] However, peak assignment information can be gained from a previous study of coordinated propylamine complexes.[30] Various N-H and C-N-H modes can be evidenced in the spectrum as follows: symmetric stretch at 3170 cm^{-1}, bending at 1568 (in-plane) and 627 cm^{-1} (out-of-plane), twisting at 1213 cm^{-1}, and wagging at 750 cm^{-1}. A C-N mode is observed at 1066 cm^{-1}, a C-C stretch at 997 cm^{-1}, and two CH_3 rocking modes at 1038 and 860

cm^{-1}. The broad Mo-S stretching vibration is present at 384 cm^{-1} and a broad Mo-N mode (not very detectable from the spectrum shown) at 265 cm^{-1}.

The infrared spectrum for the pyrrolidine adduct (Figure 7) exhibits bands distinctive for pyrrolidine coordination. These bands are similar to previously reported pyrrolidine complexes[31] and show noticeable shifting from the spectrum of the free ligand.[32] The N-H stretching mode at 3194 cm^{-1} and the Mo-N stretch at 273 cm^{-1} are similar to the reported modes at 3187 and 265 cm^{-1}, respectively.[33] The distinctive Mo-S stretching vibration is found at 381 cm^{-1} and a weak Mo-Mo stretching mode may be associated with one of the bands observed at 235 or 214 cm^{-1}.

The infrared spectrum of the piperidine adduct is shown in Figure 8. Coordination of piperidine results in very little shifting of the absorption frequencies as compared to the free ligand.[32,34] Bands attributable to N-H or C-N-H modes are present at 3214, 1311, 1264, 869, and 739 cm^{-1} with the remaining modes being carbon-carbon or carbon-hydrogen in nature. The Mo-S stretch is observed at 382 cm^{-1}, the Mo-N stretch at 269 cm^{-1}, and a Mo-Mo stretch at either 234 or 213 cm^{-1}. The presence of excess piperidine in this complex can be observed by the N-H stretching mode present at 3287 cm^{-1} which is nearly the same frequency as observed for the free ligand.[32]

The infrared spectra for the tetrahydrothiophene and triethylphosphine adducts of the Mo_6S_8 cluster unit have been reported previously.[9] Similar spectra have been observed for the tungsten analogues,[13] however, little discussion has been made

concerning the spectra. Comparable values have been noted for the absorption frequencies of free tetrahydrothiophene[35] and the previously reported tht complexes.[36] The bands in the mid-infrared region (1306-808 cm^{-1}) are generally due to CH_2 vibrations (wag, twist, and rock) along with carbon-carbon stretching modes. The far-IR bands at 515, 472, and 272 cm^{-1} result from ring deformation modes and the Mo-S stretch is present around 389 cm^{-1}.

The infrared spectrum for the triethylphosphine adduct is shown in Figure 16. The absorption frequencies observed for this adduct are similar to those found in previous studies. A comparison of the mid-IR region (1416-733 cm^{-1}) for free and coordinated PEt_3 showed that these bands were mainly due to the various C-H modes (wagging and rocking).[37] The bands in the far-IR region were found to be due to a carbon-phosphorus stretch (624 cm^{-1}) and several CCP bending modes at 404, 364, and 334 cm^{-1}.[38] The Mo-S stretch is present at 390 cm^{-1} and the peak at 236 cm^{-1} is probably either a Mo-Mo stretch, or, a weak CCP bending mode which has been reported to occur around 245-270 cm^{-1}. The band at 217 cm^{-1} might also be assigned as a Mo-Mo mode.

The usefulness of infrared spectroscopy can be observed for the spectrum shown in Figure 15. Bands for both propylamine and benzonitrile are found in this spectrum. The weak propylamine modes at 1564, 1067, 1041, and 998 cm^{-1} are indicative of the coordinated ligand. The modes for benzonitrile are similar in value to free benzonitrile bands.[39] Upon coordination, the C≡N stretching mode should shift to higher wavenumbers due to strengthening of the C≡N bond by bonding of the nitrogen

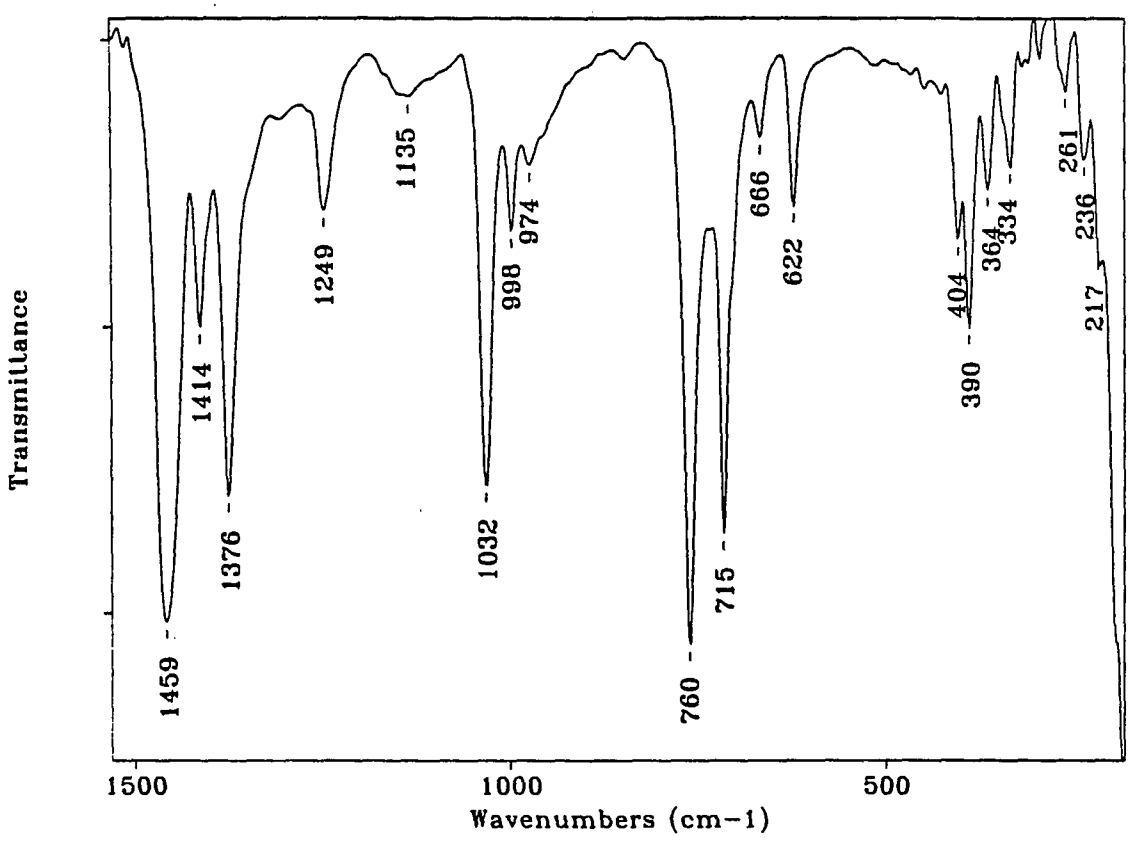

Figure 16. Mid/far-infrared spectrum (Nujol) of the crystalline triethylphosphine adduct from the reaction of the pyridine-deficient compound with triethylphosphine in dichloromethane.

lone pair. This shifting has been observed; where, upon coordination, the band moved from 2231 to 2257 cm^{-1}.[40] In the reaction with propylamine, the band is found at 2223 cm^{-1} which is very close to the free benzonitrile value. Based on this observation, it can reasonably be assumed that the benzonitrile present in this reaction is not coordinated; therefore, it is included in the material.

Raman Spectroscopy

Infrared spectroscopy was found to lose significance during deligation studies because the Mo-S stretching mode broadened and was lost in the background of the spectrum. Therefore, it was difficult to observe if the cluster unit was still present after the heating and deligation. The technique of Raman spectroscopy was explored in order to gain information about the Mo_6S_8 cluster complexes prior to the deligation studies and after deligation (which will be discussed further in Paper 2). Initial interest focused on the crystalline complexes of piperidine, tetrahydrothiophene, and triethylphosphine.

A spectrum of the crystalline piperidine adduct is shown in Figure 17. In this spectrum, the most distinguishing feature is the sharp peak at 408 cm^{-1} which can be attributed to the Mo-S A_{1g} stretching mode. This peak assignment results from reported assignments for MoS_2[41] and other molybdenum sulfide complexes.[42-43] The observed peaks for the MoS_2 spectrum were found at 409 (A_{1g}), 383 ($E_{2g}{}^1$), 287 (E_{1g}), and 118 ($E_{2g}{}^2$) cm^{-1}. Only a limited number of Raman spectra have been reported for molybdenum sulfide complexes. In the study of a group of cyanothio-

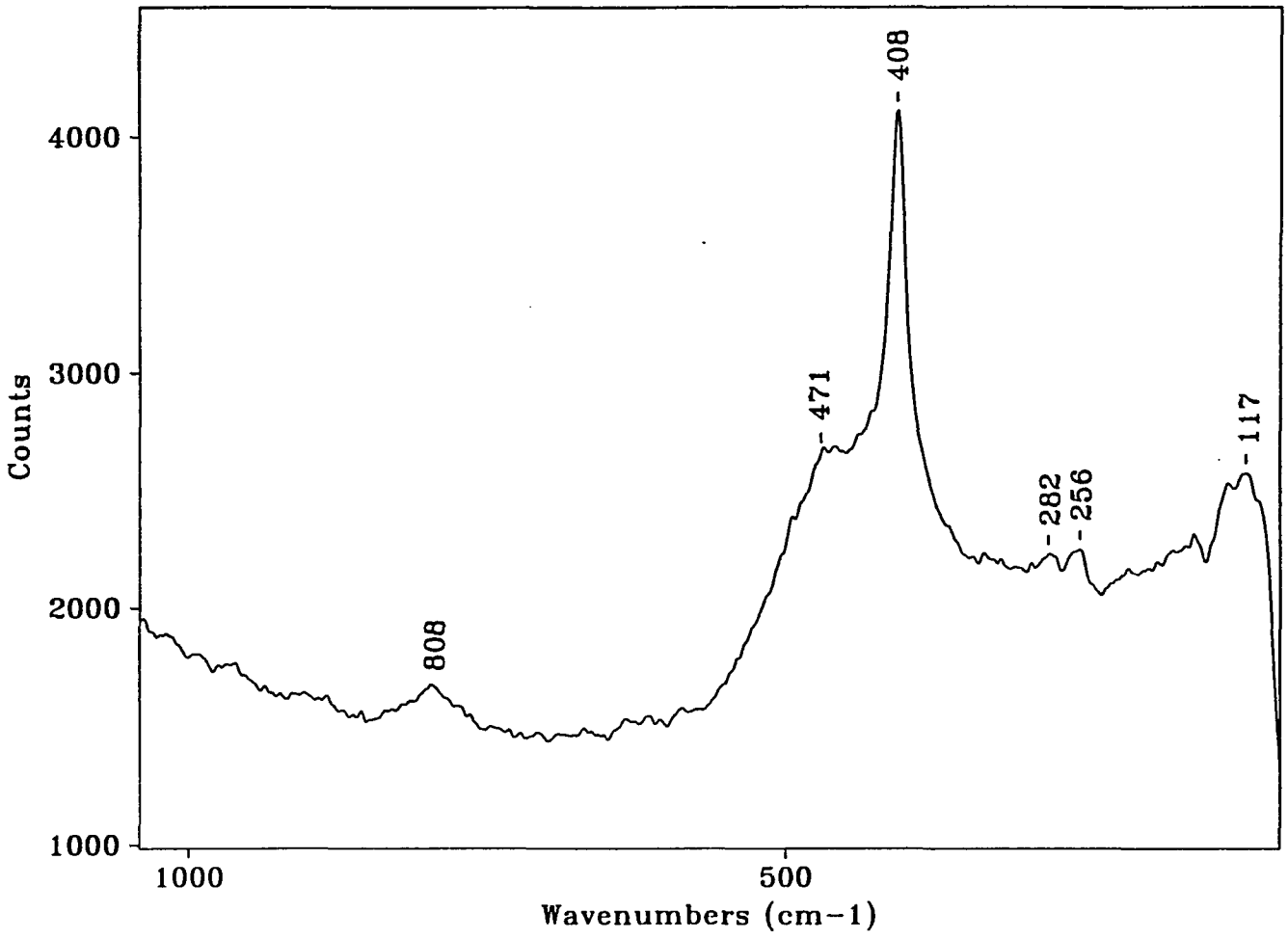

Figure 17. Raman spectrum of the piperidine adduct exhibiting the sharp Mo-S A_{1g} mode at 408 cm^{-1} characteristic of a crystalline Mo_6S_8 cluster complex.

molybdates,[42] a complex with a Mo_4S_4 core (Mo^{III}) exhibited a Mo-S A_1 mode at 372 cm^{-1} and Mo-Mo modes at 228 (A_1) and 192 (E) cm^{-1}. Also, there was a report[43] concerning a complex containing the MoS_4^{2-} unit that showed a Mo-S A_1 mode at 440 cm^{-1}.

Based on these reports showing that the predominant mode is due to the Mo-S A_1 interaction, the assignment of the peak at 408 cm^{-1} was rather straightforward. However, further assignments are, at best, rather speculative. For this cluster, the idealized octahedral symmetry would result in Raman active modes of A_{1g}, E_g, and T_{2g} for both the Mo-S and Mo-Mo interactions and produce mixing. Therefore, the shoulder band at 471 cm^{-1} could be due to the Mo-S stretching modes of either E_g or T_{2g} types. The bands at 256 and 282 cm^{-1} are possibly Mo-Mo E_g modes. The band at 117 cm^{-1} could be Mo-S E_g or Mo-Mo type modes. Finally, the band at 808 cm^{-1} is most likely the first overtone of the Mo-S A_{1g} mode.

The Raman spectra of the nitrogen-ligated Mo_6S_8 cluster complexes are shown in Figures 18 and 19. In Figure 18, all of the spectra show the presence of the Mo-S A_{1g} band at 408-414 cm^{-1}. Also, as the crystallinity of the material decreases, a broadening of the band can be observed. The crystalline piperidine adduct shows the sharpest peak, while the microcrystalline pyrrolidine, pyridine and 4-methylpyridine bands are weaker and broader. The other bands discussed previously at about 120, 270, 470, and 820 cm^{-1} are still present, even though they cannot be detected in this figure. Figure 20 shows the similar Raman spectra for the crystalline tetrahydrothiophene and triethylphosphine adducts with the Mo-S A_{1g} mode at 414 cm^{-1}. The

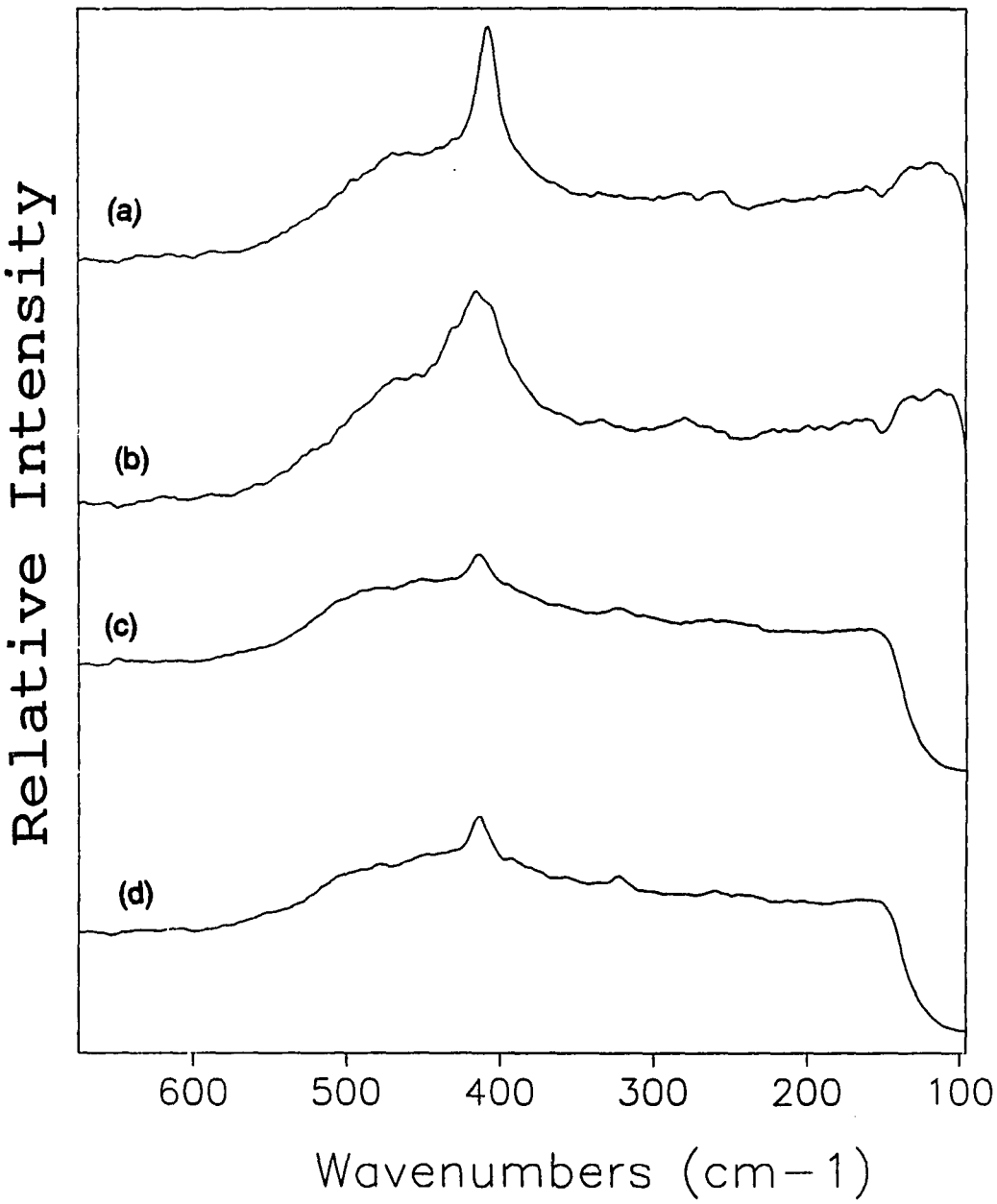

Figure 18. Raman spectra of the nitrogen-ligated adducts exhibiting the Mo-S A_{1g} mode at 408-414 cm^{-1} characteristic of a Mo_6S_8 cluster unit. The degree of crystallinity is evidenced by the sharpness of the band for the crystalline piperidine adduct (a), as compared to poorly-crystalline pyrrolidine (b), pyridine (c) and 4-methylpyridine (d).

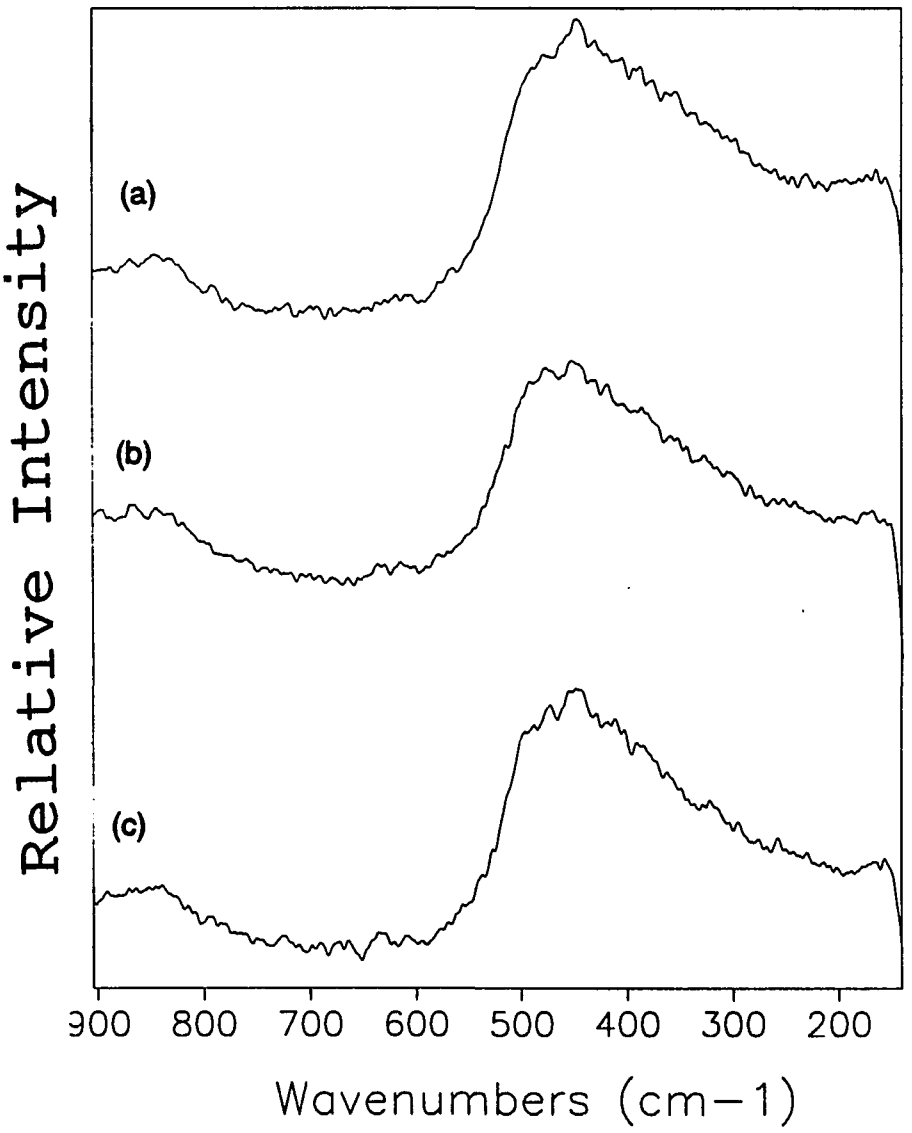

Figure 19. Raman spectra of the ligand-deficient Mo_6S_8 cluster complexes. The pyridine $Na_{2y}Mo_6S_{8+y}(py)_x$ (a), propylamine (b), and tetrahydrothiophene (c) compounds exhibit a broad Mo-S band at 448 cm^{-1}.

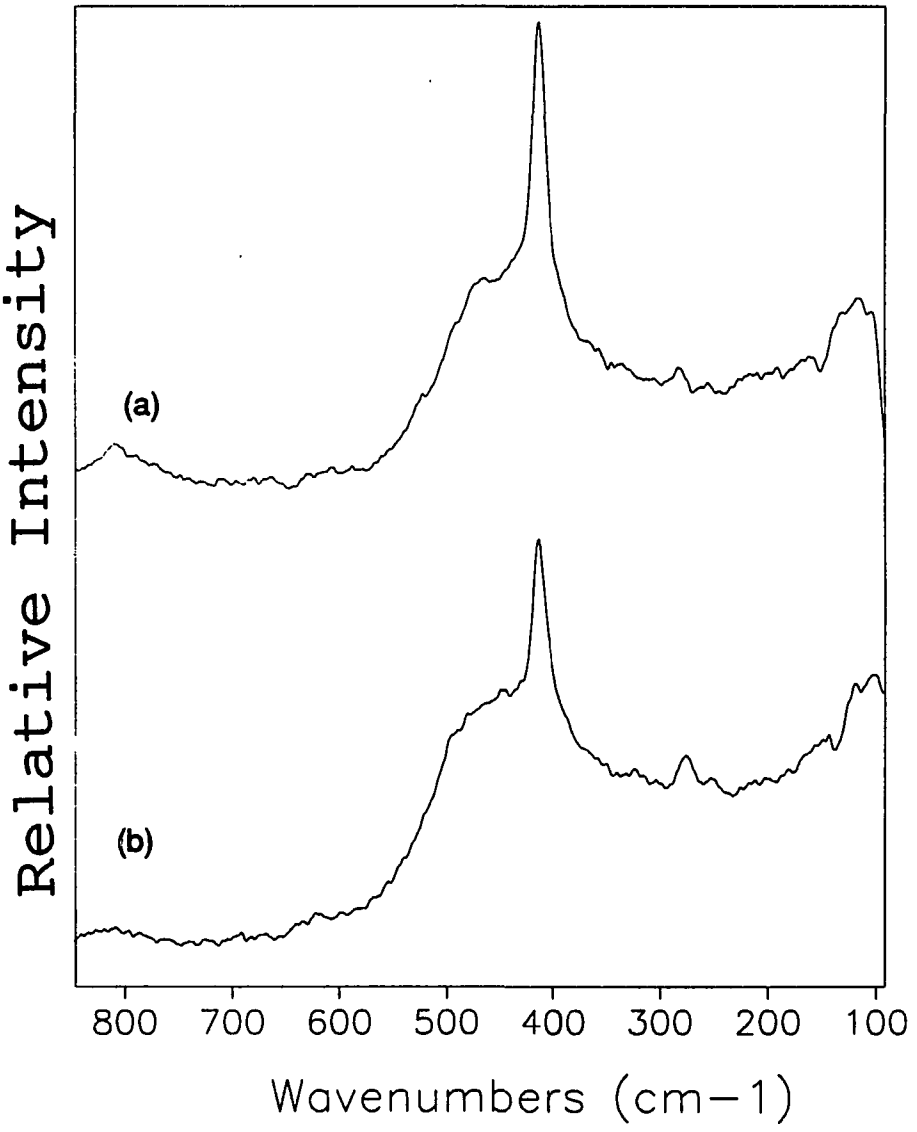

Figure 20. Raman spectra of the tetrahydrothiophine (a) and triethylphosphine (b) adducts exhibiting the sharp Mo-S A_{1g} mode at 414 cm^{-1} characteristic of a crystalline Mo_6S_8 cluster complex.

ligand-deficient cluster complexes produce a broadened Mo-S peak as observed in Figure 19. The peak center is at 448 cm^{-1} which falls almost halfway between the Mo-S peaks found for the crystalline complexes. The broadening of the Mo-S band can be understood as the result of the formation of intercluster bonds. The formation of these intercluster bonds destroys the octahedral symmetry which produced the A_{1g} mode and thus this mode is absent. However, this broad band is indicative of the cluster unit as supported by other spectroscopic techniques and will be used as a means of identifying the presence of the Mo_6S_8 cluster unit upon further deligatlon reactions.

X-ray Photoelectron Spectroscopy

This technique was also explored for the Mo_6S_8 cluster complexes in order to gain information about the materials prior to their subsequent deligation. The binding energies could be used to discover if cluster degradation was occurring and forming MoS_2 and Mo metal or whether the cluster remained intact upon heating at various temperatures. Therefore, information about the molybdenum and sulfur binding energies of the cluster complexes was obtained. It was expected that these materials should have similar binding energies since the only difference was the coordinated ligand.

The results of the XPS study are tabulated in Table 13. Previously, the only reported cluster complex, $Mo_6S_8(PEt_3)_6$, showed molybdenum binding energies at 227.8 ($3d_{5/2}$) and 231.0 eV ($3d_{3/2}$) and sulfur binding energies at 161.1 ($2p_{3/2}$) and

Table 13. X-ray photoelectron spectroscopy (XPS) data on Mo_6S_8 cluster complexes. Data has been adjusted to the C 1s binding energy of 284.6 eV.

	$(pip)_6$	$(pyrr)_y$	$(py)_y$	$(4Mepy)_y$	$(PrNH_2)_y$[a]	$(PEt_3)_6$	$(tht)_6$	$(tht)_y$[a]
Mo $3d_{5/2}$	227.7	227.7	227.6	227.2	227.7	227.8	227.7	227.5
Mo $3d_{3/2}$	230.8	230.8	230.7	230.4	230.9	230.9	230.9	230.7
S 2s	224.9	225.4	225.0	224.7	225.3	225.1	225.2	225.2
S $2p_{3/2}$	160.7	160.6	160.6	160.3	160.6	161.0	160.7	160.7
S $2p_{1/2}$[b]	161.9	161.8	161.8	161.4	161.8	162.1	161.8	161.9

[a]the propylamine and tetrahydrothiophene adducts are ligand-deficient
[b]this peak is evidenced as a shoulder on the main S $2p_{3/2}$ peak

162.1 eV ($2p_{1/2}$).[13] The cluster complexes all exhibit Mo $3d_{5/2}$ values between 227.2 and 227.8 eV and Mo $3d_{3/2}$ values between 230.4 and 230.9 eV. These values are slightly lower than reported for the triethylphosphine adduct, but still very close to each other. Likewise, the sulfur binding energies are very similar where the S $2p_{3/2}$ values lie between 160.3 and 161.0 eV and the S $2p_{1/2}$ values taken from the shoulders which lie between 161.4 and 162.1 eV. The sulfur 2s binding energies are also in a narrow range of 224.7 to 225.4 eV. These results do not differ much from the values observed for the Chevrel phases which range from 227.3-228.2 eV for the Mo $3d_{5/2}$ peak.[6,44] However, noticeable differences exist when compared to MoS_2, a decomposition product (Figure 22b). The MoS_2 binding energies for molybdenum are found to be 229.5 ($3d_{5/2}$) and 232.6 eV ($3d_{3/2}$). The values for sulfur are 226.7 (2s), 162.3 eV ($2p_{3/2}$), and 163.5 eV ($2p_{1/2}$). Similar binding energies for MoS_2 have been previously reported.[76]

The XPS spectrum for the crystalline tetrahydrothiophene adduct, $Mo_6S_8(tht)_6$, is shown in Figure 21. The XPS spectrum exhibits distinct Mo 3d peaks separated by 3.15 eV and a broad S 2s peak at slightly lower binding energies. A similar spectrum for the pyridine adduct is shown in Figure 22a. The presence of surface oxide contamination is found for this sample of the pyridine complex. As observed in Figure 21b, the tht adduct exhibits resolvable peaks for both cluster sulfide and organo-sulfur from the ligand. The organo-sulfur peaks are located at 162.9 ($2p_{3/2}$) and 164.1 eV ($2p_{1/2}$). Similar peaks are also found for the ligand-deficient tht complex at 163.1 ($2p_{3/2}$) and 164.3 eV ($2p_{1/2}$).

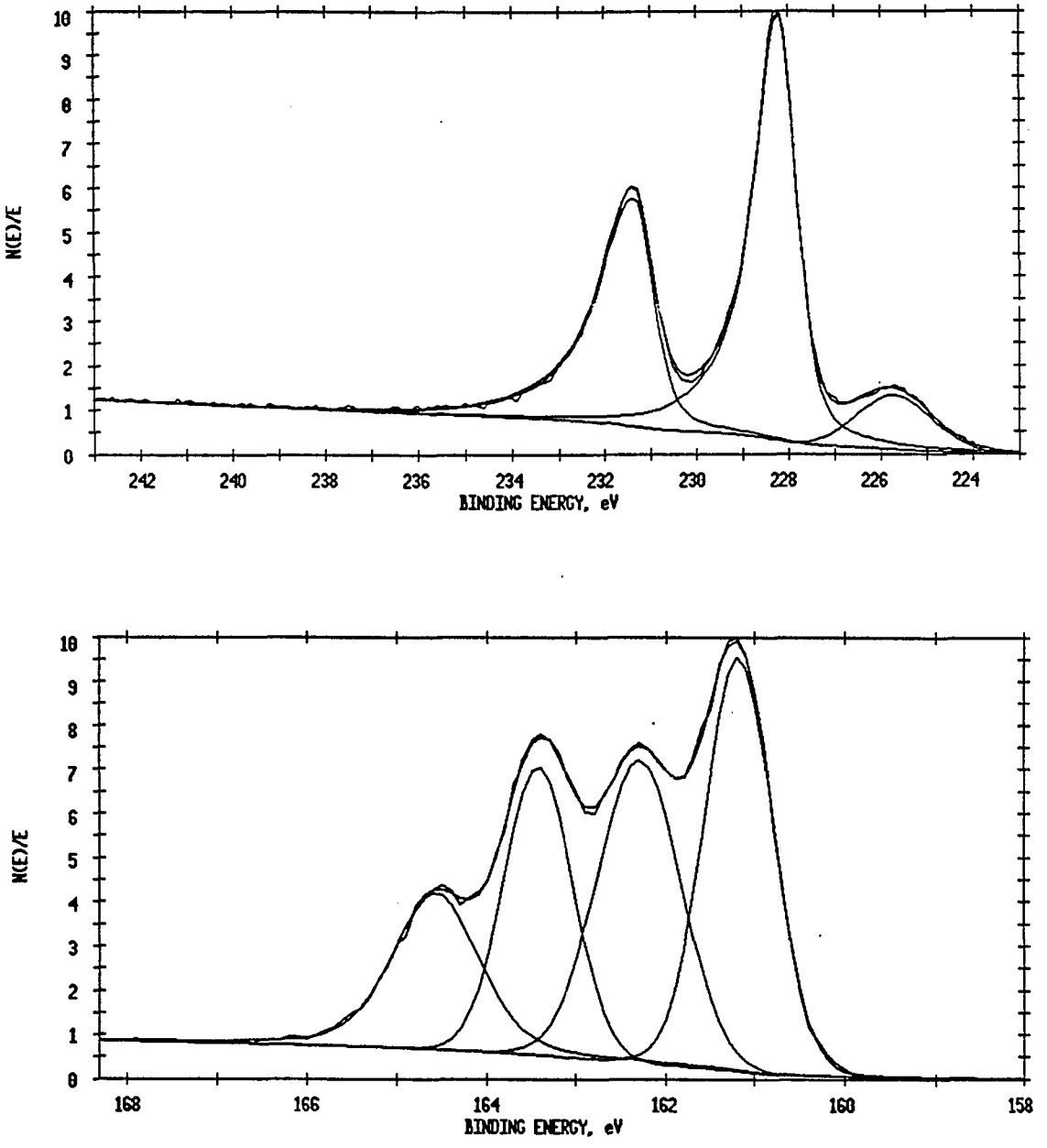

Figure 21. Uncorrected XPS spectra of the crystalline tetrahydrothiophine adduct showing the Mo 3d and S 2s bands (a). The S 2p bands (b) are resolvable into the cluster-sulfide and ligand organo-sulfur peaks.

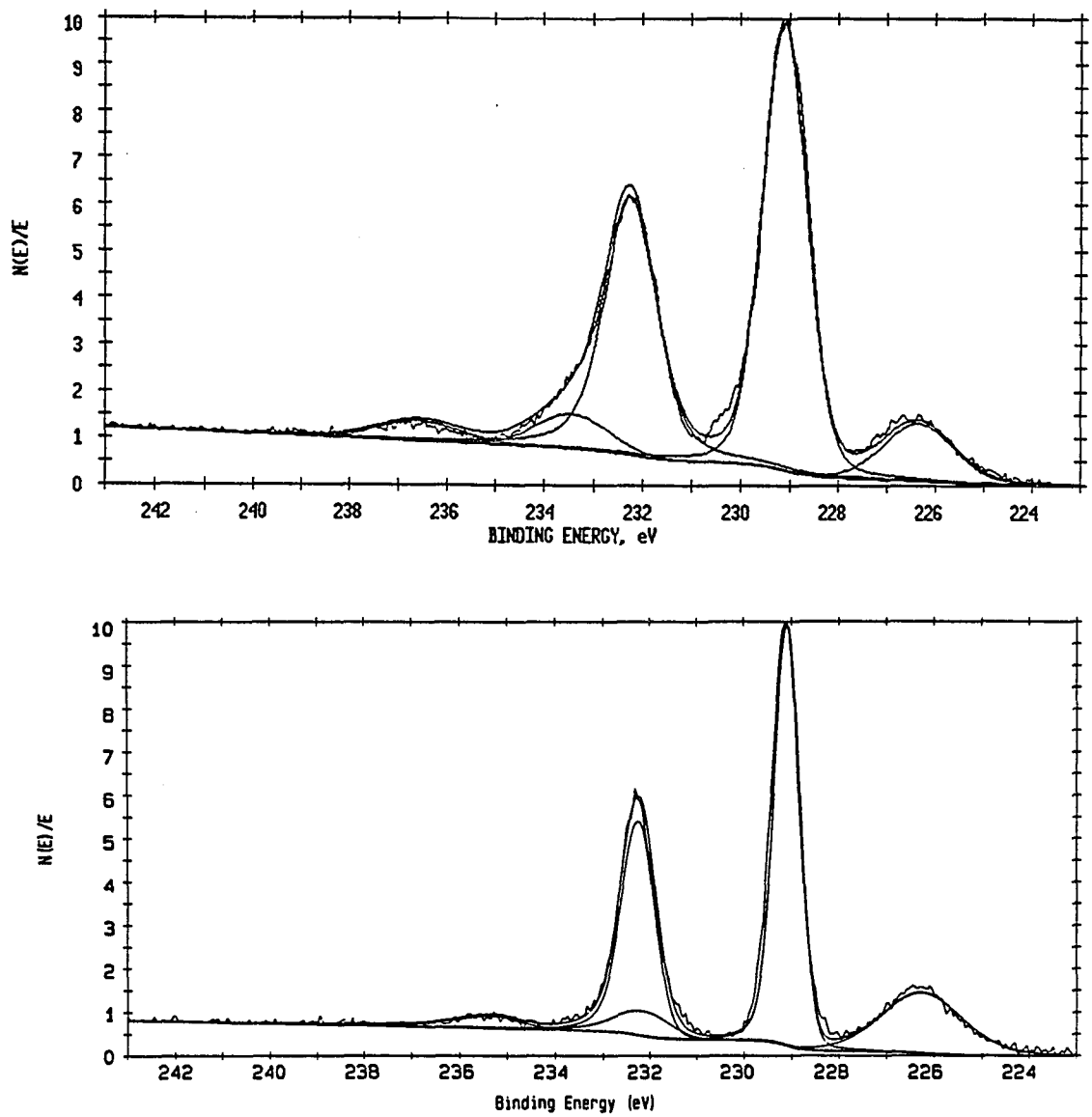

Figure 22. Uncorrected XPS spectra for the pyridine adduct (a) and MoS_2 (b) showing the Mo 3d and S 2s peaks for these compounds. Weak bands due to surface oxide contamination are evidenced in these spectra.

Crystal Structures

The molecular complexes prepared in this research all contain the hexa-molybdenum cluster unit $Mo_6S^i_8L^a_6$. This cluster unit can be viewed as an octahedron of molybdenum atoms with eight triply bridging sulfur atoms capping the octahedral faces. Each molybdenum also possesses an additional terminal coordination site located at the vertex of the octahedron, which is occupied by the nitrogen-donor ligands. The structures with pyridine, piperidine, and pyrrolidine ligands will be discussed.

The pyridine adduct was found to crystallize with two different morphologies - brown chunks and brown cubes. The chunky crystals are formulated as $Mo_6S_8(py)_6 \cdot 1.65$ py and belong to the triclinic space group $P\bar{1}$ with two molecules per unit cell. A triclinic form was evidenced previously in the tungsten sulfide cluster complex, $W_6S_8(py)_6$,[13] and the molybdenum sulfide/chloride complex, $Mo_6S_6Cl_2(py)_6$,[45] with only one molecule per unit cell. These two complexes are isostructural and contain a much smaller unit cell of about a=10.7 Å, b=11.9 Å, c=9.4 Å. This new triclinic phase contains a larger unit cell of a=11.6 Å, b=12.2 Å, c=22.0 Å.

All of the atoms in the cluster unit and the pyridine solvent are located in general positions. A diagram of the cluster complex is shown in Figure 23 and the unit cell in Figure 24. Selected bond distances and bond angles are given in Tables 14 and 15, respectively. The average Mo-Mo bond distance is 2.640(4) Å with a maximum difference of 0.026 Å. The average Mo-S bond distance is 2.453(10) Å and the average Mo-N bond distance is 2.274(36) Å.

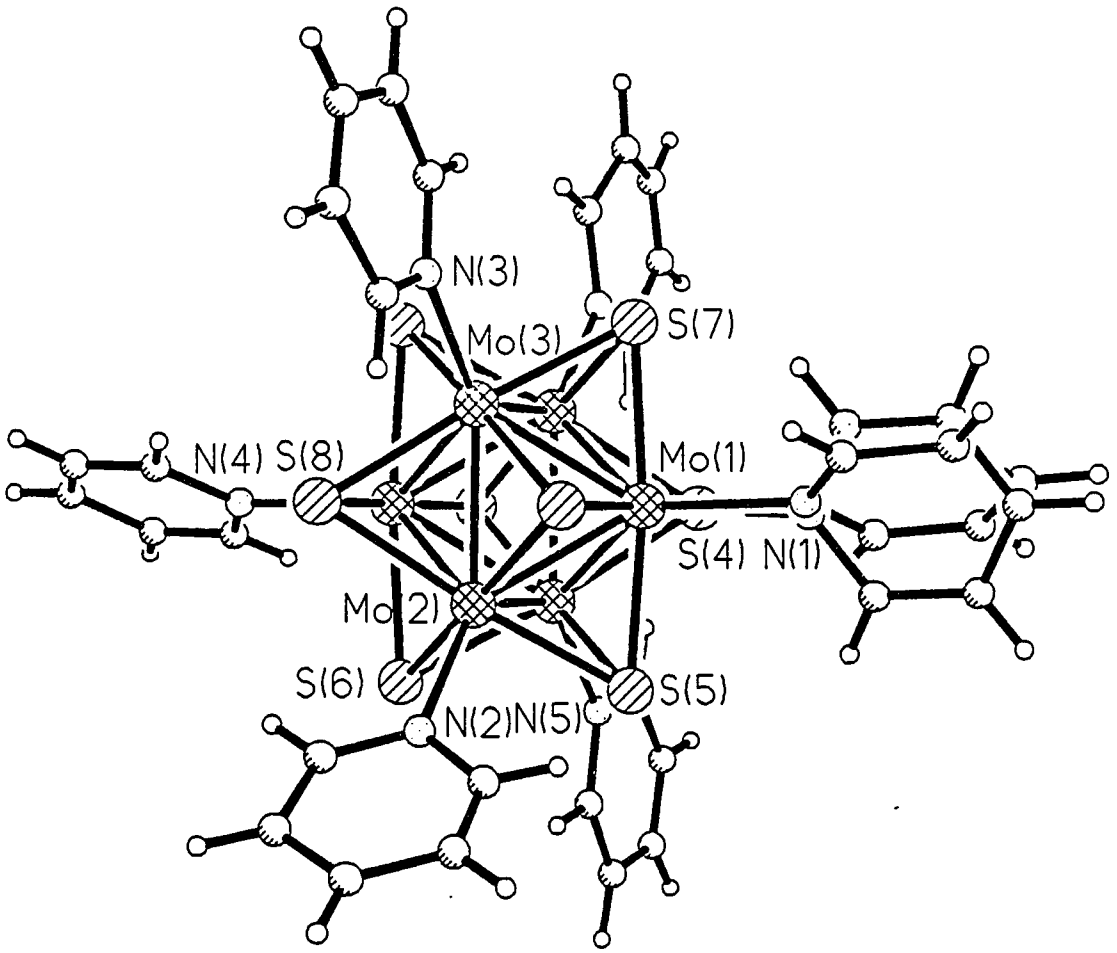

Figure 23. A ball and stick representation of the cluster unit in the triclinic $Mo_6S_8(py)_6 \cdot 1.65$ py.

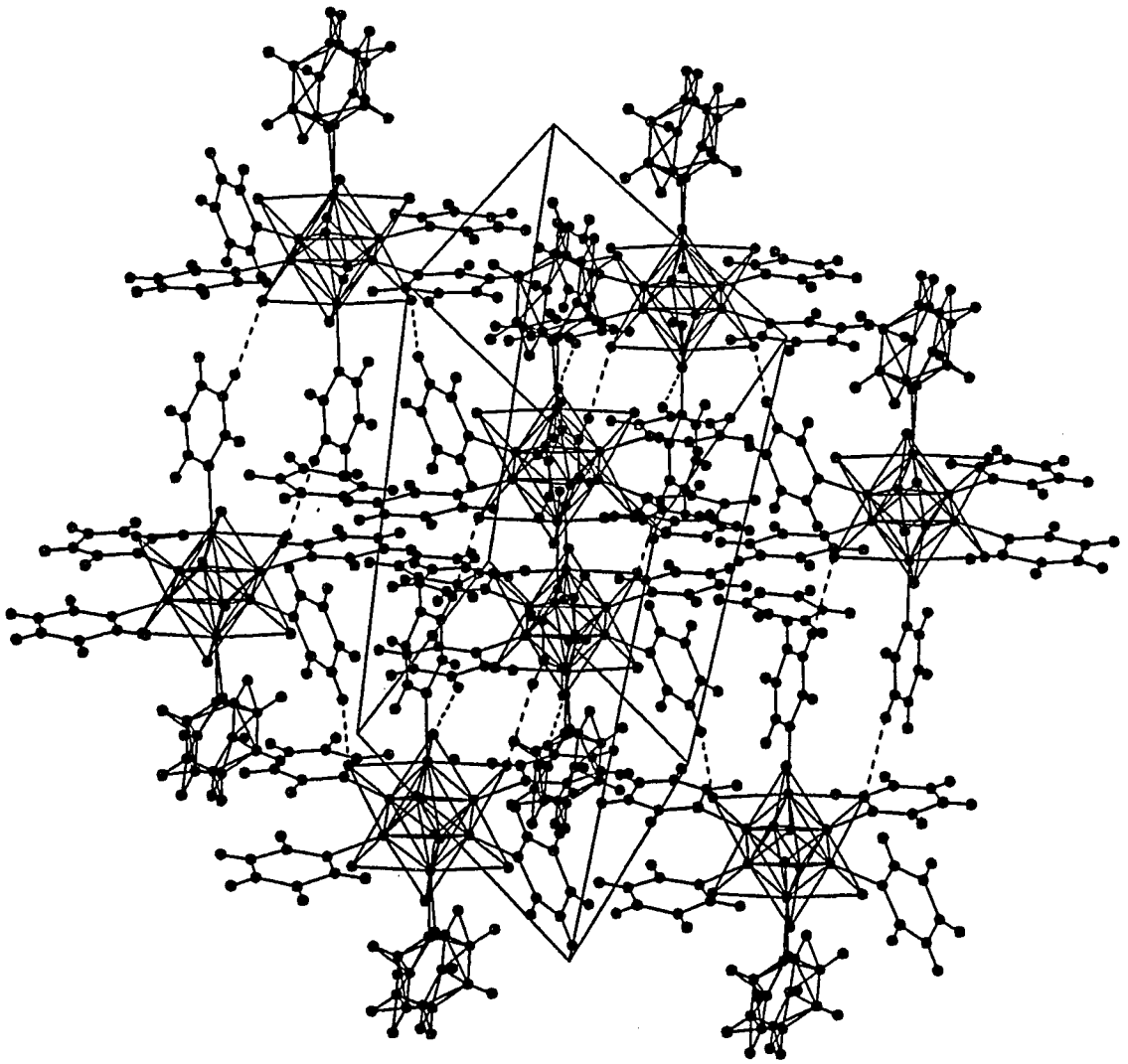

Figure 24. A view of the unit cell in the triclinic $Mo_6S_8(py)_6 \cdot 1.65$ py.

Table 14. Selected bond distances (Å) in $Mo_6S_8(py)_6 \cdot 1.65\ py$

Mo1 - Mo2	2.652 (4)	Mo1 - S1	2.459 (12)
Mo1 - Mo3	2.631 (4)	Mo1 - S4	2.450 (12)
Mo1 - Mo5	2.631 (4)	Mo1 - S5	2.457 (7)
Mo1 - Mo6	2.628 (5)	Mo1 - S7	2.451 (8)
Mo2 - Mo3	2.643 (4)	Mo2 - S1	2.460 (9)
Mo2 - Mo4	2.642 (5)	Mo2 - S5	2.440 (10)
Mo2 - Mo5	2.633 (6)	Mo2 - S6	2.460 (9)
Mo3 - Mo4	2.652 (4)	Mo2 - S8	2.457 (9)
Mo3 - Mo6	2.635 (6)	Mo3 - S1	2.450 (11)
Mo4 - Mo5	2.654 (4)	Mo3 - S2	2.457 (11)
Mo4 - Mo6	2.640 (4)	Mo3 - S7	2.443 (10)
Mo5 - Mo6	2.638 (4)	Mo3 - S8	2.456 (9)
avg Mo-Mo	2.640 (4)	Mo4 - S2	2.455 (7)
		Mo4 - S3	2.456 (13)
Mo1 - N1	2.267 (40)	Mo4 - S6	2.452 (7)
Mo1 - N1'	2.300 (39)	Mo4 - S8	2.460 (12)
Mo2 - N2	2.248 (30)	Mo5 - S3	2.454 (11)
Mo3 - N3	2.255 (26)	Mo5 - S4	2.443 (9)
Mo4 - N4	2.329 (25)	Mo5 - S5	2.444 (11)
Mo5 - N5	2.239 (25)	Mo5 - S6	2.448 (9)
Mo6 - N6	2.283 (35)	Mo6 - S2	2.470 (10)
avg Mo-N	2.274 (36)	Mo6 - S3	2.458 (10)
		Mo6 - S4	2.451 (9)
		Mo6 - S7	2.450 (10)
		avg Mo-S	2.453 (10)

Table 15. Selected bond angles (deg) in $Mo_6S_8(py)_6 \cdot 1.65$ py

Mo2 - Mo1 - Mo3	60.0 (1)	Mo1 - S1 - Mo2	65.3 (3)
Mo2 - Mo1 - Mo5	59.8 (1)	Mo1 - S1 - Mo3	64.8 (3)
Mo3 - Mo1 - Mo6	60.1 (1)	Mo2 - S1 - Mo3	65.2 (3)
Mo5 - Mo1 - Mo6	60.2 (1)	Mo3 - S2 - Mo4	65.3 (2)
Mo1 - Mo2 - Mo3	59.6 (1)	Mo3 - S2 - Mo6	64.7 (2)
Mo1 - Mo2 - Mo5	59.7 (1)	Mo4 - S2 - Mo6	64.8 (2)
Mo3 - Mo2 - Mo4	60.2 (1)	Mo4 - S3 - Mo5	65.5 (3)
Mo4 - Mo2 - Mo5	60.4 (1)	Mo4 - S3 - Mo6	65.0 (3)
Mo1 - Mo3 - Mo2	60.4 (1)	Mo5 - S3 - Mo6	65.0 (3)
Mo1 - Mo3 - Mo6	59.9 (1)	Mo1 - S4 - Mo5	65.1 (3)
Mo2 - Mo3 - Mo4	59.9 (1)	Mo1 - S4 - Mo6	64.9 (3)
Mo4 - Mo3 - Mo6	59.9 (1)	Mo5 - S4 - Mo6	65.2 (2)
Mo2 - Mo4 - Mo3	59.9 (1)	Mo1 - S5 - Mo2	65.6 (2)
Mo2 - Mo4 - Mo5	59.6 (1)	Mo1 - S5 - Mo5	64.9 (2)
Mo3 - Mo4 - Mo6	59.7 (1)	Mo2 - S5 - Mo5	65.2 (3)
Mo5 - Mo4 - Mo6	59.8 (1)	Mo2 - S6 - Mo4	65.1 (2)
Mo1 - Mo5 - Mo2	60.5 (1)	Mo2 - S6 - Mo5	64.9 (2)
Mo1 - Mo5 - Mo6	59.8 (1)	Mo4 - S6 - Mo5	65.6 (2)
Mo2 - Mo5 - Mo4	60.0 (1)	Mo1 - S7 - Mo3	65.0 (2)
Mo4 - Mo5 - Mo6	59.8 (1)	Mo1 - S7 - Mo6	64.8 (2)
Mo1 - Mo6 - Mo3	60.0 (1)	Mo3 - S7 - Mo6	65.2 (2)
Mo1 - Mo6 - Mo5	59.9 (1)	Mo2 - S8 - Mo3	65.1 (3)
Mo3 - Mo6 - Mo4	60.4 (1)	Mo2 - S8 - Mo4	65.0 (3)
Mo4 - Mo6 - Mo5	60.4 (1)	Mo3 - S8 - Mo4	65.3 (3)
avg Mo-Mo-Mo	60.0 (1)	avg Mo-S-Mo	65.1 (3)
Mo2 - Mo1 - Mo6	89.8 (1)	Mo2 - Mo4 - Mo6	89.8 (1)
Mo3 - Mo1 - Mo5	90.3 (1)	Mo3 - Mo4 - Mo5	89.4 (1)
Mo1 - Mo2 - Mo4	89.9 (1)	Mo1 - Mo5 - Mo4	90.1 (1)
Mo3 - Mo2 - Mo5	90.0 (1)	Mo2 - Mo5 - Mo6	90.0 (1)
Mo1 - Mo3 - Mo4	90.2 (1)	Mo1 - Mo6 - Mo4	90.5 (1)
Mo2 - Mo3 - Mo6	89.9 (1)	Mo3 - Mo6 - Mo5	90.1 (1)
		avg Mo-Mo-Mo	90.0 (1)

Table 15. (continued)

S1 - Mo1 - S5	89.0 (3)	S1 - Mo1 - S4	173.6 (3)
S1 - Mo1 - S7	90.0 (3)	S5 - Mo1 - S7	173.4 (3)
S4 - Mo1 - S5	90.1 (3)	S1 - Mo2 - S6	173.3 (3)
S4 - Mo1 - S7	90.2 (3)	S5 - Mo2 - S8	173.8 (4)
S1 - Mo2 - S5	89.4 (3)	S1 - Mo3 - S2	174.0 (3)
S1 - Mo2 - S8	89.5 (3)	S7 - Mo3 - S8	174.0 (3)
S5 - Mo2 - S6	90.0 (3)	S2 - Mo4 - S6	173.6 (3)
S6 - Mo2 - S8	90.4 (3)	S3 - Mo4 - S8	173.1 (3)
S1 - Mo3 - S7	90.4 (3)	S3 - Mo5 - S5	173.7 (3)
S1 - Mo3 - S8	89.8 (3)	S4 - Mo5 - S6	174.1 (3)
S2 - Mo3 - S7	90.0 (3)	S2 - Mo6 - S4	173.8 (4)
S2 - Mo3 - S8	89.2 (3)	S3 - Mo6 - S7	173.9 (4)
S2 - Mo4 - S3	90.7 (3)	avg S-Mo-S	173.7 (3)
S2 - Mo4 - S8	89.2 (3)		
S3 - Mo4 - S6	88.8 (3)		
S6 - Mo4 - S8	90.5 (3)		
S3 - Mo5 - S4	89.6 (3)		
S3 - Mo5 - S6	89.0 (3)		
S4 - Mo5 - S5	90.6 (3)		
S5 - Mo5 - S6	90.2 (3)		
S2 - Mo6 - S3	90.3 (3)		
S2 - Mo6 - S7	89.5 (3)		
S3 - Mo6 - S4	89.3 (3)		
S4 - Mo6 - S7	90.2 (3)		
avg S-Mo-S	89.8 (3)		

Difficulties in obtaining a good structure solution for the triclinic pyridine adduct prompted further study and resulted in the discovery of the brown cube-shaped crystals. This material, $Mo_6S_8(py)_6 \cdot 2py$, crystallizes in the cubic space group $Pa\bar{3}$ with four molecules per unit cell. This space group was previously observed in the molybdenum sulfide/choride double salt- $(C_5H_5NH)_3$ $[(Mo_6Cl_7S)Cl_6] \cdot 3(C_5H_5NH)Cl$ which also contained four molecules per unit cell.

The Mo_6S_8 cluster is centered on a $\bar{3}$ position (4b). One of the sulfur atoms, S1, is located on a 3-fold position (8c), while the remaining atoms are all found to reside on general positions. The pyridine solvent molecule is disordered about the center of the 3-fold position (8c). The cluster complex and unit cell diagrams are shown in Figures 25 and 26, respectively. Selected bond distances and bond angles are listed in Table 16. The average Mo-Mo bond distance is 2.644(2) Å with a maximum difference of 0.006 Å. The average Mo-S bond distance is 2.462(3) Å and the unique Mo-N distance is 2.283(9) Å.

The piperidine adduct, $Mo_6S_8(pip)_6 \cdot 7pip$, crystallizes in the tetragonal space group $I\bar{4}$ with eight molecules per unit cell. The Mo_6S_8 cluster unit is centered on a 2-fold position (4e). Also, one piperidine solvent molecule is disordered about the same 2-fold position (4e). A diagram of the cluster complex is shown in Figure 27. The coordination of the piperidine ligands by bonding through equatorial positions is evidenced in Figure 28. The unit cell diagram is shown in Figure 29. Selected bond distances and bond angles are listed in Tables 17 and 18, respectively. The average Mo-Mo bond distance is 2.649(1) Å with a maximum difference of 0.021 Å.

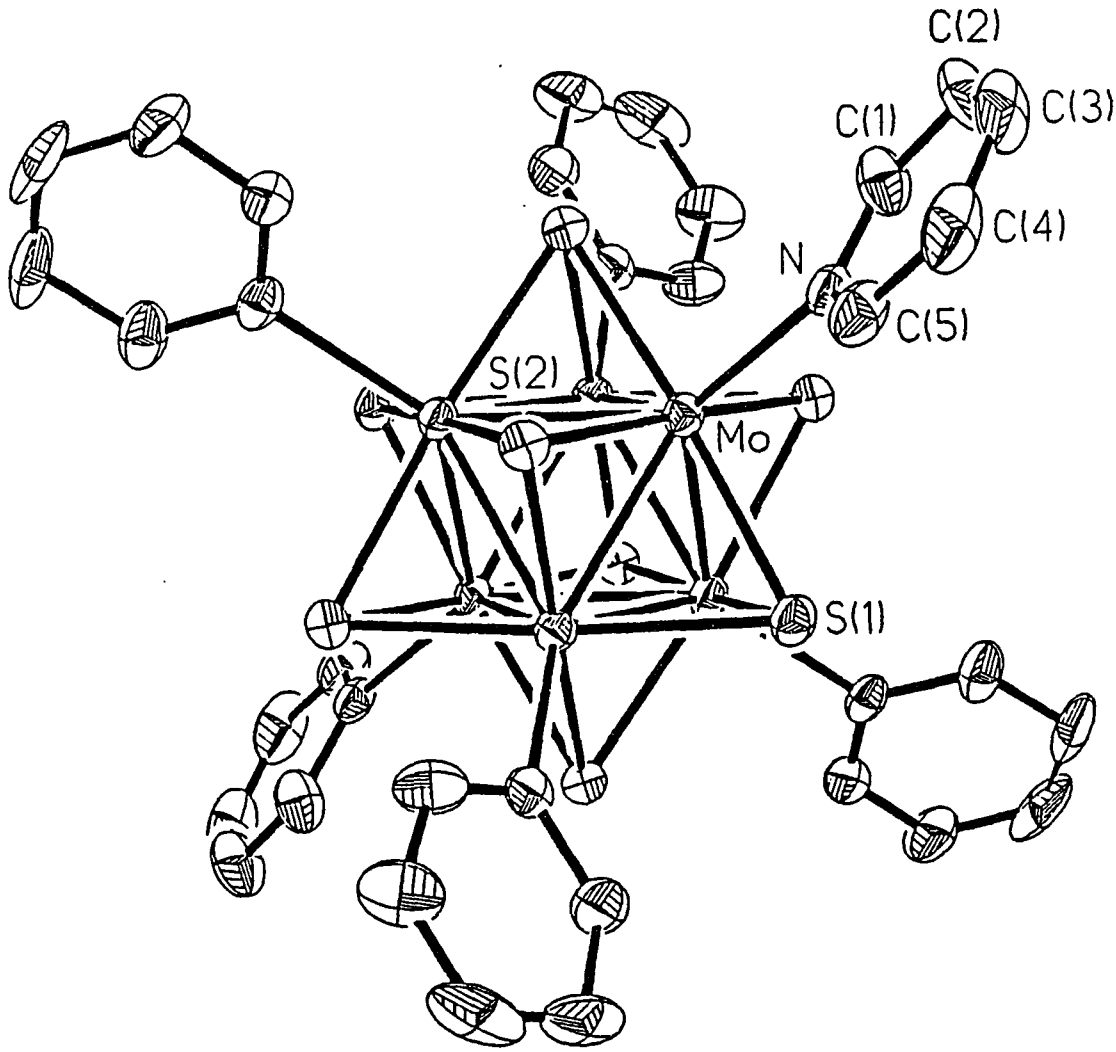

Figure 25. A view of the cluster unit in the cubic $Mo_6S_8(py)_6 \cdot 2$ py. Thermal ellipsoids are shown at the 30% probability level. Hydrogen atoms have been omitted for clarity.

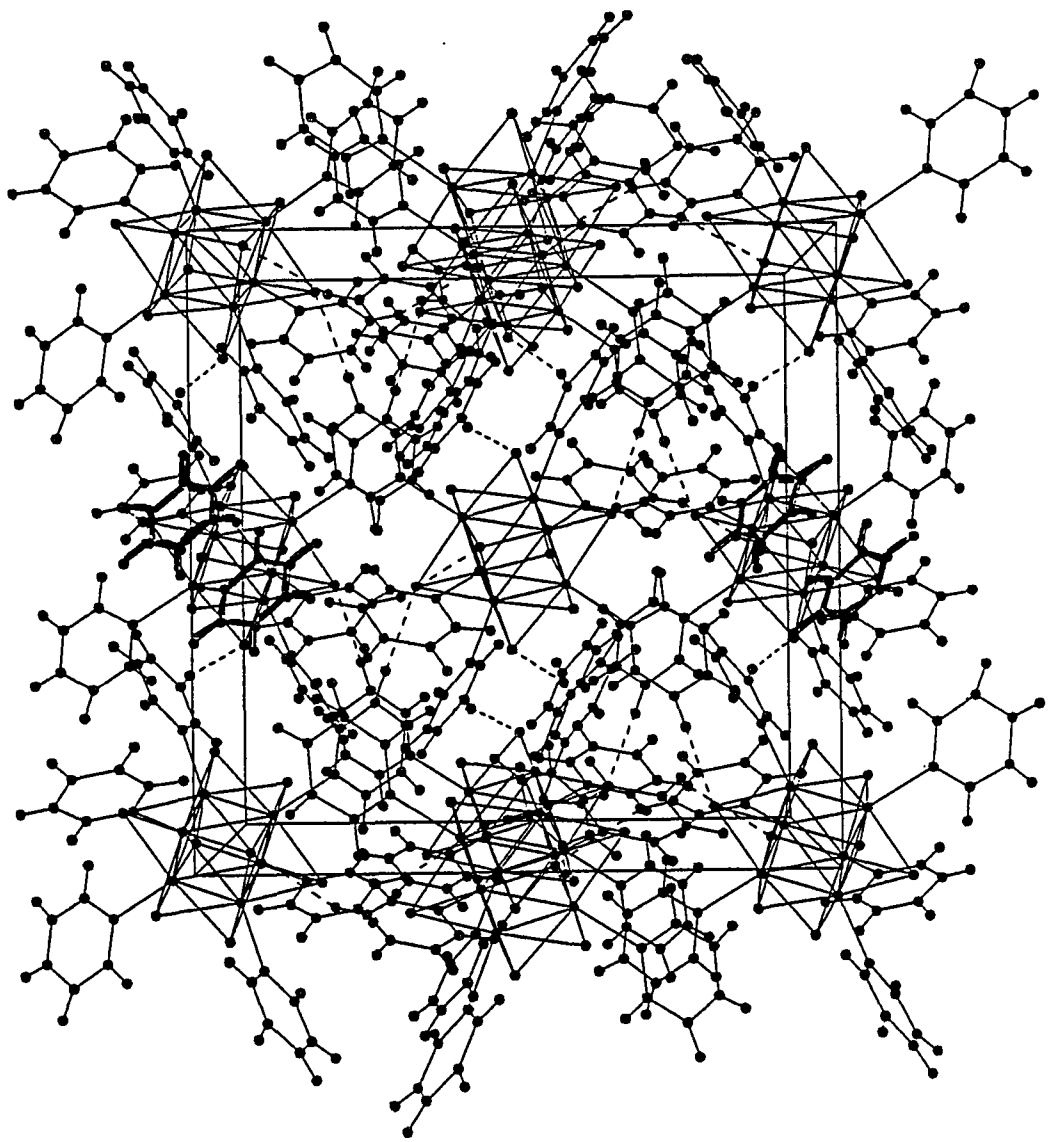

Figure 26. A view of the unit cell in the cubic $Mo_6S_8(py)_6 \cdot 2py$. The pyridine solvent molecules have been darkened to indicate their location and clusters have been omitted for clarity.

Table 16. Selected bond distances (Å) and angles (deg) in $Mo_6S_8(py)_6 \cdot 2\ py$

Mo - Mo(B)	2.641 (2)	Mo - N	2.283 (9)
Mo - Mo(D)	2.647 (2)	N - C(1)	1.340 (15)
avg Mo-Mo	2.644 (2)	N - C(5)	1.317 (16)
		avg N-C	1.328 (16)
Mo - S(2)	2.467 (3)	C(1) - C(2)	1.338 (19)
Mo - S(1A)	2.465 (2)	C(2) - C(3)	1.321 (24)
Mo - S(2A)	2.461 (3)	C(3) - C(4)	1.366 (22)
Mo - S(2B)	2.455 (3)	C(4) - C(5)	1.385 (20)
avg Mo-S	2.462 (3)	avg C-C	1.352 (21)

Mo(B) - Mo - Mo(D)	90.0 (1)	S(2) - Mo - S(1A)	90.1 (1)
Mo(B) - Mo - Mo(E)	60.0 (1)	S(1A) - Mo - S(2A)	90.2 (1)
Mo(D) - Mo - Mo(E)	60.1 (1)	S(2) - Mo - S(2B)	89.4 (1)
		S(2A) - Mo - S(2B)	89.6 (1)
Mo(A) - S(1) - Mo(C)	64.8 (1)	S(2) - Mo - S(2A)	173.6 (1)
Mo - S(2) - Mo(D)	65.1 (1)	S(1A) - Mo - S(2B)	174.2 (1)
Mo - S(2) - Mo(E)	64.8 (1)		
		S(2) - Mo - N	93.4 (2)
		S(1A) - Mo - N	93.1 (2)
		S(2A) - Mo - N	93.0 (2)
		S(2B) - Mo - N	92.7 (2)

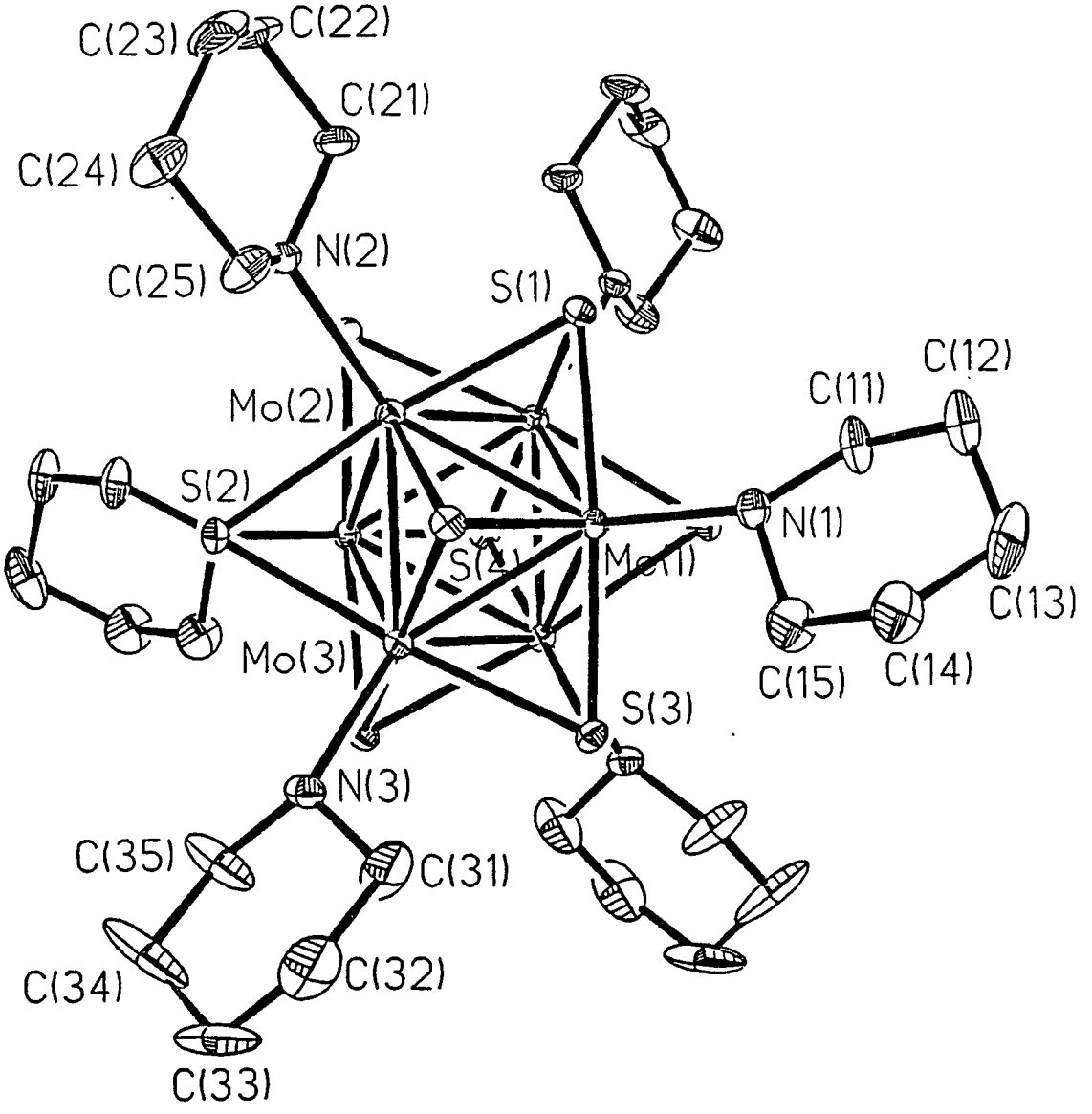

Figure 27. A view of the cluster unit in $Mo_6S_8(pip)_6 \cdot 7$ pip. Thermal ellipsoids are shown at the 30% probability level. Hydrogen atoms have been omitted for clarity.

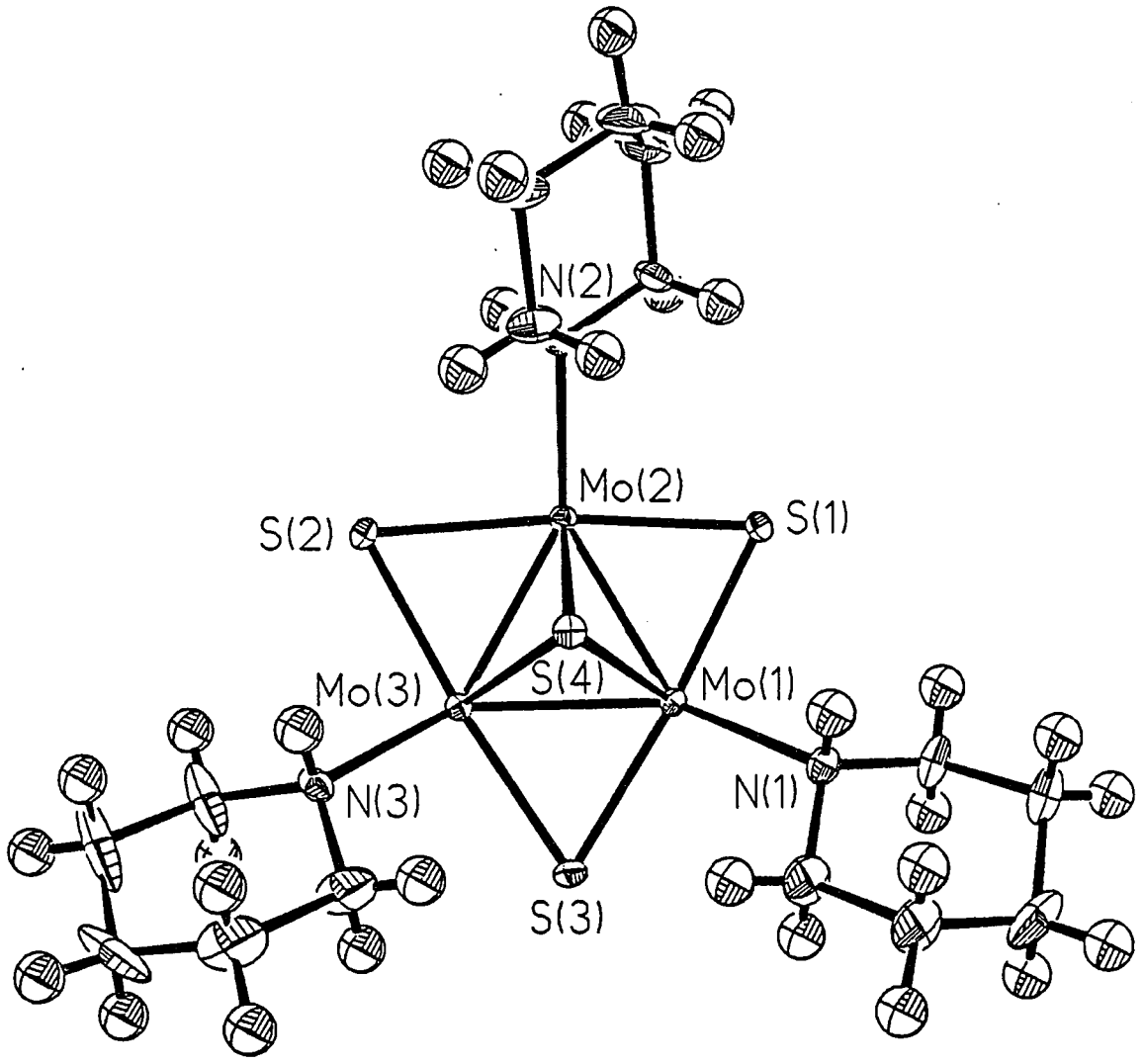

Figure 28. A view of $Mo_6S_8(pip)_6 \cdot 7$ pip showing the equatorial coordination of the piperidine ligands to the Mo_6S_8 cluster unit. Thermal ellipsoids are shown at the 30% probability level.

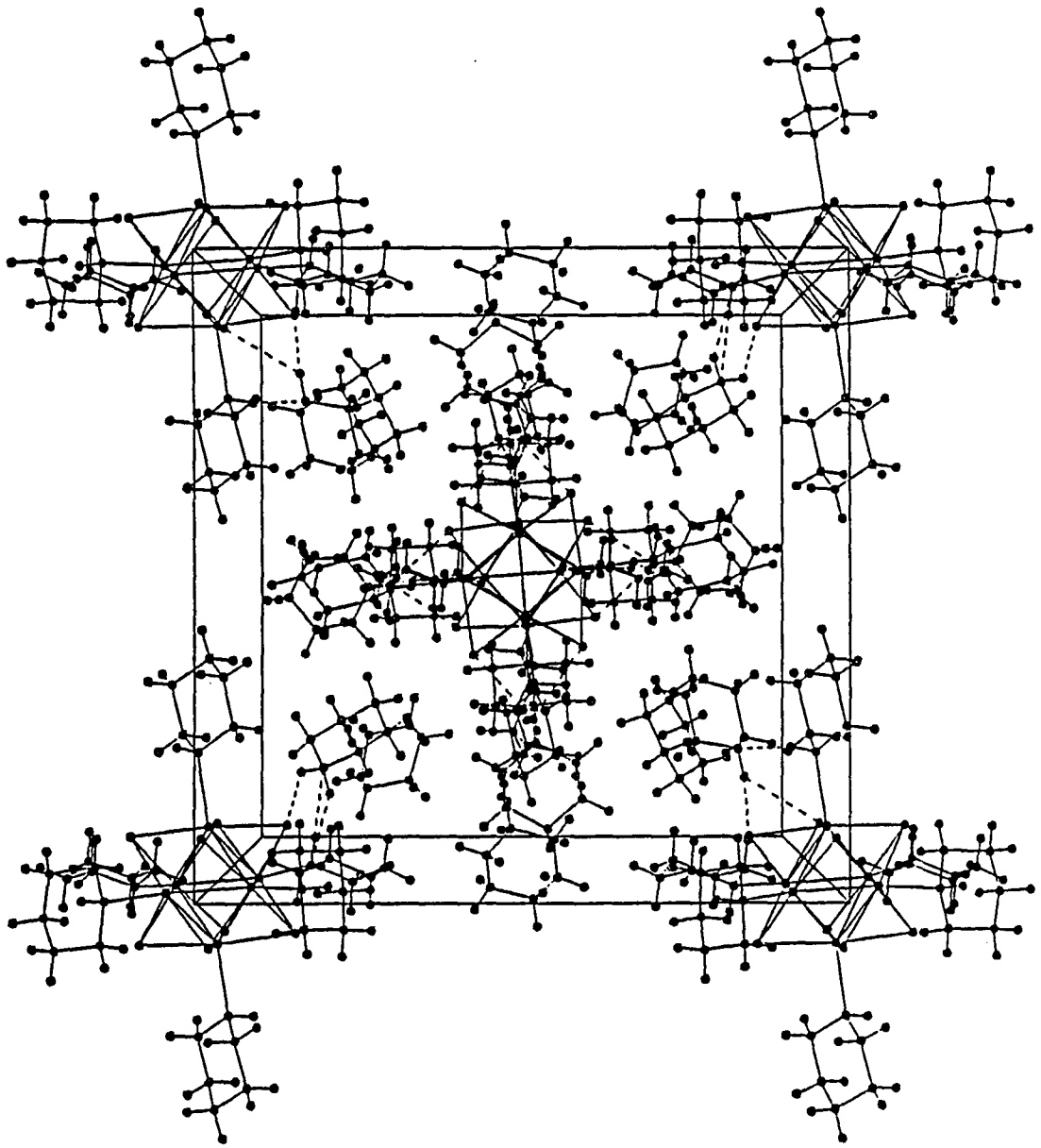

Figure 29. A view of the unit cell in $Mo_6S_8(pip)_6 \cdot 7$ pip. Clusters have been omitted for clarity.

Table 17. Selected bond distances (Å) in $Mo_6S_8(pip)_6 \cdot 7$ pip

Mo(1) - Mo(2)	2.652 (1)	Mo(1) - S(1)	2.448 (2)
Mo(1) - Mo(3)	2.640 (1)	Mo(1) - S(3)	2.446 (2)
Mo(1) - Mo(2A)	2.653 (1)	Mo(1) - S(4)	2.456 (1)
Mo(1) - Mo(3A)	2.653 (1)	Mo(1) - S(2A)	2.460 (1)
Mo(2) - Mo(3)	2.658 (1)	Mo(2) - S(1)	2.463 (2)
Mo(2) - Mo(2A)	2.637 (1)	Mo(2) - S(2)	2.456 (2)
Mo(3) - Mo(3A)	2.652 (1)	Mo(2) - S(4)	2.465 (2)
avg Mo-Mo	2.649 (1)	Mo(2) - S(1A)	2.448 (2)
Mo(1) - N(1)	2.322 (4)	Mo(3) - S(2)	2.452 (2)
Mo(2) - N(2)	2.321 (5)	Mo(3) - S(3)	2.444 (2)
Mo(3) - N(3)	2.308 (5)	Mo(3) - S(4)	2.456 (2)
avg Mo-N	2.317 (5)	Mo(3) - S(3A)	2.431 (2)
		avg Mo-S	2.452 (2)

coordinated piperidine

N(1) - C(11)	1.455 (9)	N(2) - C(21)	1.457 (8)	N(3) - C(31)	1.435 (12)
N(1) - C(15)	1.457 (10)	N(2) - C(25)	1.479 (9)	N(3) - C(35)	1.487 (12)
C(11)- C(12)	1.537 (9)	C(21)- C(22)	1.527 (10)	C(31)- C(32)	1.558 (14)
C(12)- C(13)	1.471 (13)	C(22)- C(23)	1.537 (12)	C(32)- C(33)	1.501 (19)
C(13)- C(14)	1.522 (13)	C(23)- C(24)	1.526 (12)	C(33)- C(34)	1.421 (19)
C(14)- C(15)	1.541 (10)	C(24)- C(25)	1.527 (11)	C(34)- C(35)	1.552 (15)

piperidine - solvent of crystallization

N(4) - C(41)	1.418 (14)	N(5) - C(51)	1.443 (11)	N(6) - C(61)	1.424 (10)
N(4) - C(45)	1.471 (16)	N(5) - C(55)	1.411 (11)	N(6) - C(65)	1.468 (10)
C(41)- C(42)	1.379 (18)	C(51)- C(52)	1.533 (13)	C(61)- C(62)	1.476 (12)
C(42)- C(43)	1.462 (18)	C(52)- C(53)	1.502 (12)	C(62)- C(63)	1.509 (14)
C(43)- C(44)	1.497 (19)	C(53)- C(54)	1.519 (13)	C(63)- C(64)	1.499 (14)
C(44)- C(45)	1.270 (20)	C(54)- C(55)	1.503 (13)	C(64)- C(65)	1.512 (14)

Table 18. Selected bond angles (deg) in $Mo_6S_8(pip)_6 \cdot 7$ pip

Mo(2) - Mo(1) - Mo(3)	60.3 (1)	S(1) - Mo(1) - S(4)	90.0 (1)
Mo(2) - Mo(1) - Mo(2A)	59.6 (1)	S(3) - Mo(1) - S(4)	90.6 (1)
Mo(3) - Mo(1) - Mo(3A)	60.1 (1)	S(1) - Mo(1) - S(2A)	89.4 (1)
Mo(2A)- Mo(1) - Mo(3A)	60.1 (1)	S(3) - Mo(1) - S(2A)	89.3 (1)
Mo(1) - Mo(2) - Mo(3)	59.6 (1)	S(1) - Mo(2) - S(4)	89.4 (1)
Mo(3) - Mo(2) - Mo(1A)	60.0 (1)	S(2) - Mo(2) - S(4)	89.3 (1)
Mo(1) - Mo(2) - Mo(2A)	60.2 (1)	S(1) - Mo(2) - S(1A)	91.0 (1)
Mo(1A)- Mo(2) - Mo(2A)	60.2 (1)	S(2) - Mo(2) - S(1A)	89.5 (1)
Mo(1) - Mo(3) - Mo(2)	60.1 (1)	S(2) - Mo(3) - S(4)	89.6 (1)
Mo(2) - Mo(3) - Mo(1A)	59.9 (1)	S(3) - Mo(3) - S(4)	90.6 (1)
Mo(1) - Mo(3) - Mo(3A)	60.2 (1)	S(2) - Mo(3) - S(3A)	89.8 (1)
Mo(1A)- Mo(3) - Mo(3A)	59.7 (1)	S(3) - Mo(3) - S(3A)	89.1 (1)
avg Mo-Mo-Mo	60.0 (1)	avg S-Mo-S	89.8 (1)
Mo(3) - Mo(1) - Mo(2A)	90.2 (1)	S(1) - Mo(1) - S(3)	173.3 (1)
Mo(2) - Mo(1) - Mo(3A)	89.9 (1)	S(4) - Mo(1) - S(2A)	173.3 (1)
Mo(1) - Mo(2) - Mo(1A)	89.8 (1)	S(1) - Mo(2) - S(2)	173.0 (1)
Mo(3) - Mo(2) - Mo(2A)	90.2 (1)	S(4) - Mo(2) - S(1A)	173.5 (1)
Mo(1) - Mo(3) - Mo(1A)	90.1 (1)	S(2) - Mo(3) - S(3)	173.0 (1)
Mo(2) - Mo(3) - Mo(3A)	89.8 (1)	S(4) - Mo(3) - S(3A)	173.6 (1)
avg Mo-Mo-Mo	90.0 (1)	avg S-Mo-S	173.3 (1)
Mo(1) - S(1) - Mo(2)	65.4 (1)	S(1) - Mo(1) - N(1)	90.6 (2)
Mo(1) - S(1) - Mo(2A)	65.6 (1)	S(3) - Mo(1) - N(1)	96.1 (2)
Mo(2) - S(1) - Mo(2A)	64.9 (1)	S(4) - Mo(1) - N(1)	89.3 (1)
Mo(2) - S(2) - Mo(3)	65.6 (1)	S(2A)- Mo(1) - N(1)	97.3 (1)
Mo(2) - S(2) - Mo(1A)	65.3 (1)	S(1) - Mo(2) - N(2)	94.0 (1)
Mo(3) - S(2) - Mo(1A)	65.4 (1)	S(2) - Mo(2) - N(2)	93.0 (1)
Mo(1) - S(3) - Mo(3)	65.4 (1)	S(4) - Mo(2) - N(2)	97.6 (1)
Mo(1) - S(3) - Mo(3A)	65.9 (1)	S(1A)- Mo(2) - N(2)	88.9 (1)
Mo(3) - S(3) - Mo(3A)	65.9 (1)	S(2) - Mo(3) - N(3)	92.7 (1)
Mo(1) - S(4) - Mo(2)	65.2 (1)	S(3) - Mo(3) - N(3)	94.4 (1)
Mo(1) - S(4) - Mo(3)	65.0 (1)	S(4) - Mo(3) - N(3)	91.5 (1)
Mo(2) - S(4) - Mo(3)	65.4 (1)	S(3A)- Mo(3) - N(3)	94.8 (1)
avg Mo-S-Mo	65.4 (1)	avg S-Mo-N	93.4 (1)

The average Mo-S bond distance is 2.452(2) Å and the average Mo-N distance is 2.317(5) Å.

The pyrrolidine adduct $Mo_6S_8(pyrr)_6 \cdot 1pyrr$, crystallizes in the tetragonal space group $I4_1/a$ with sixteen molecules per unit cell. Two independent cluster units are found in the asymmetric unit where cluster 1 is located on a 2-fold position (8e) and cluster 2 is positioned on an inversion center (8d). The two cluster units are shown in Figure 30. Again, difficulties were observed in the refinement of the pyrrolidine carbon positions which led to the large errors in the observed bond lengths (Table 19) and bond angles (Table 20). This disorder can also be observed for the pyrrolidine rings found in the unit cell diagram shown in Figure 31. The average Mo-Mo bond distance is 2.649(3) Å with a maximum difference of 0.030 Å. The average Mo-S bond distance is 2.446(6) Å and the average Mo-N distance is 2.309(21) Å.

The bond distances for these nitrogen ligand based $Mo_6S_8L_6$ cluster complexes can be compared to the previously reported rhombohedral triethylphosphine ($R\bar{3}$) and cubic tetrahydrothiophene (Ia3) complexes. The distances are tabulated in Table 21. The reported bond distances for Mo-Mo of 2.640-2.658 Å and Mo-S of 2.430-2.462 Å are very similar for these complexes and indicate that the Mo_6S_8 octahedron is relatively unperturbed by the differing ligands. A distinct difference can be noted when comparing the undistorted octahedra in the $Mo_6S_8L_6$ clusters with the trigonally distorted cluster units found in the Chevrel phase compounds.

In the Chevrel phases, the octahedra are elongated along the 3-fold axis which result in a shortening of the Mo-Mo bonds in the Mo_3 triangles which lie perpendicular

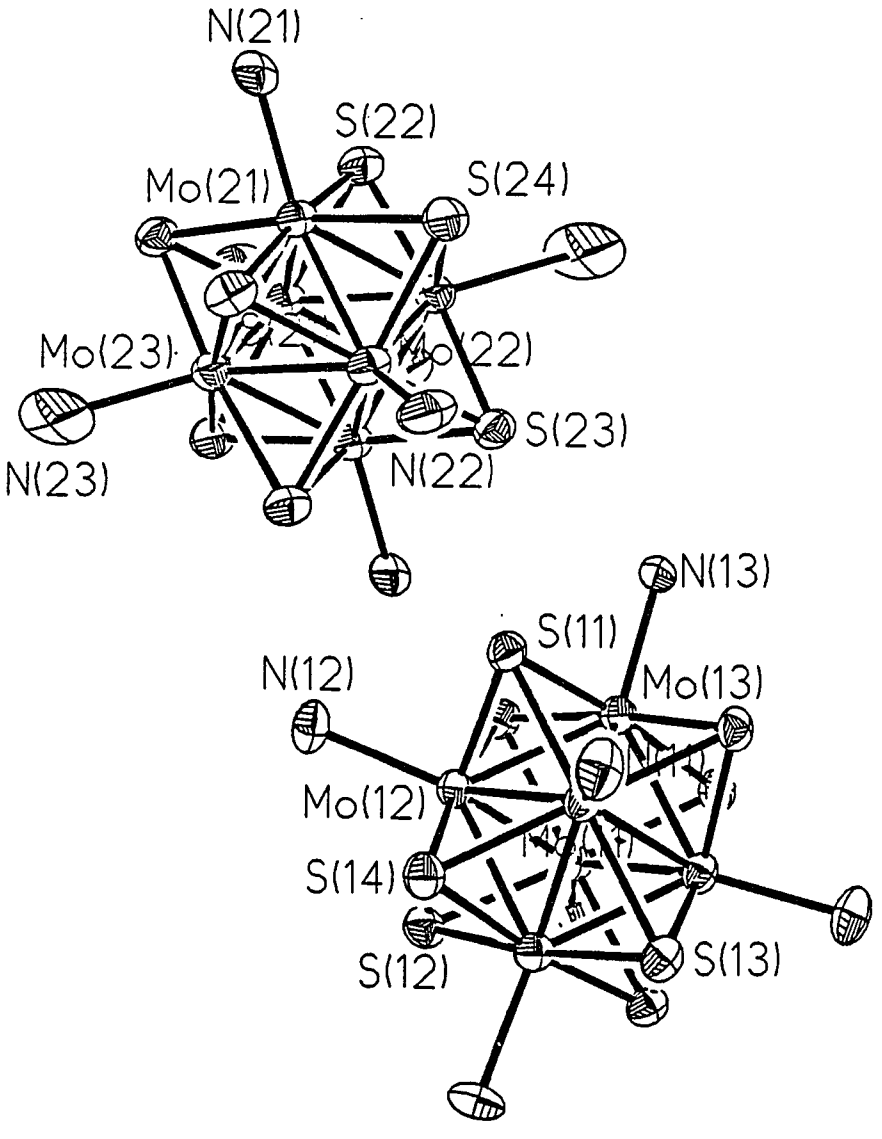

Figure 30. A view of the two cluster units found for $Mo_6S_8(pyrr)_6 \cdot 1$ pyrr. Thermal ellipsoids are shown at the 30% probability level. Only the nitrogens of the pyrrolidine ligands are indicated.

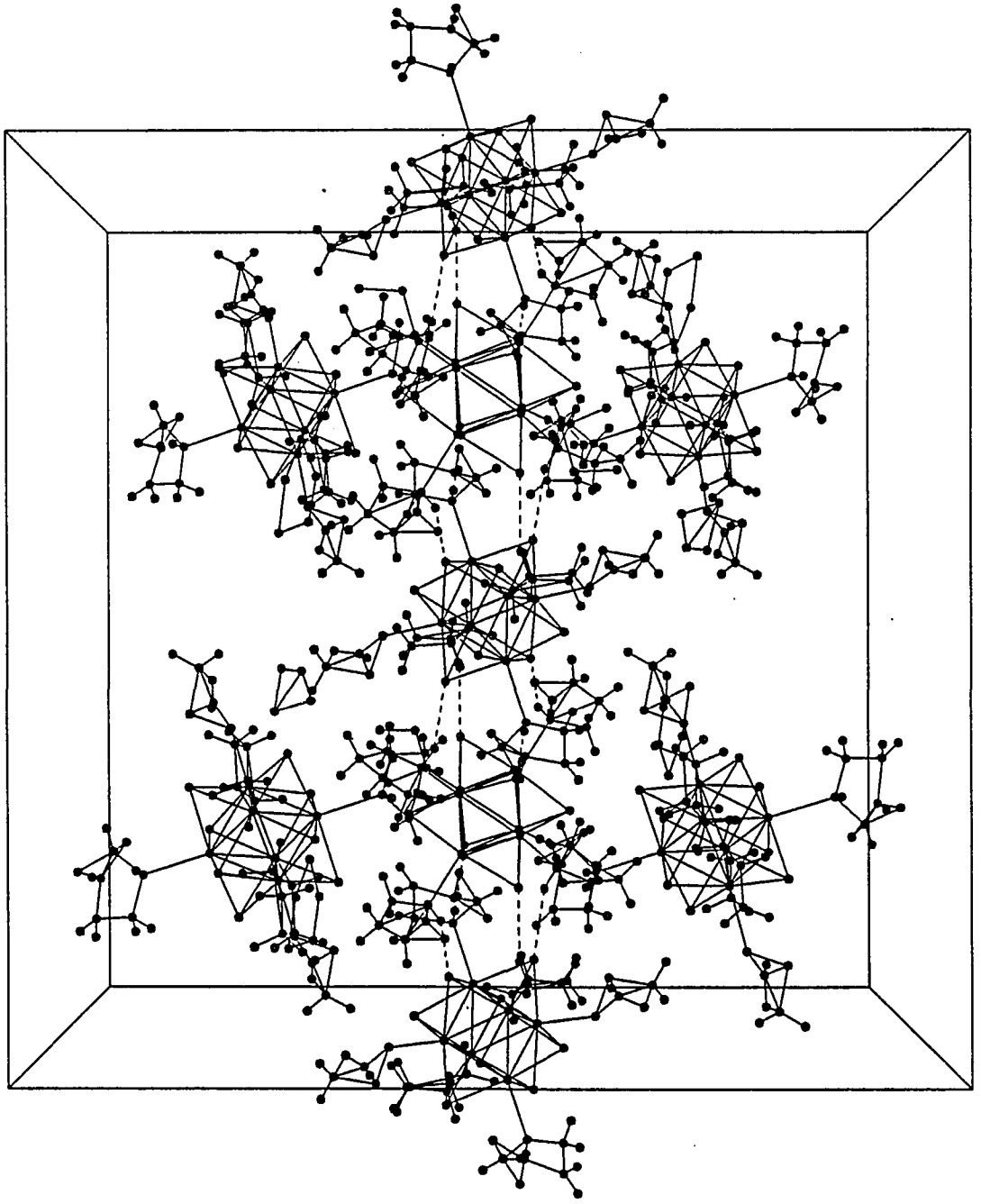

Figure 31. A view of the unit cell in $Mo_6S_8(pyrr)_6 \cdot 1$ pyrr. Clusters have been omitted for clarity.

Table 19. Selected bond distances (Å) in $Mo_6S_8(pyrr)_6 \cdot 1$ pyrr

Mo11 - Mo12	2.645 (3)	Mo21 - Mo22	2.646 (3)
Mo11 - Mo13	2.666 (3)	Mo21 - Mo23	2.642 (3)
Mo11 - Mo11A	2.636 (4)	Mo21 - Mo22A	2.662 (3)
Mo11 - Mo13A	2.644 (3)	Mo21 - Mo23A	2.649 (3)
Mo12 - Mo13	2.637 (3)	Mo22 - Mo23	2.643 (3)
Mo12 - Mo12A	2.670 (4)	Mo22 - Mo23A	2.651 (3)
Mo12 - Mo13A	2.649 (3)	avg Mo-Mo	2.649 (3)
Mo11 - S11	2.464 (6)	Mo21 - S21	2.422 (7)
Mo11 - S13	2.446 (6)	Mo21 - S22	2.449 (7)
Mo11 - S14	2.437 (6)	Mo21 - S24	2.450 (6)
Mo11 - S13A	2.438 (6)	Mo21 - S23A	2.447 (6)
Mo12 - S11	2.452 (6)	Mo22 - S21	2.422 (7)
Mo12 - S12	2.458 (6)	Mo22 - S23	2.451 (7)
Mo12 - S14	2.435 (6)	Mo22 - S24	2.440 (7)
Mo12 - S12A	2.442 (6)	Mo22 - S22A	2.450 (6)
Mo13 - S11	2.451 (6)	Mo23 - S21	2.436 (7)
Mo13 - S12A	2.446 (6)	Mo23 - S22A	2.466 (6)
Mo13 - S13A	2.454 (6)	Mo23 - S23A	2.444 (6)
Mo13 - S14A	2.434 (6)	Mo23 - S24A	2.467 (7)
		avg Mo-S	2.446 (6)
Mo11 - N11	2.286 (19)	Mo21 - N21	2.293 (18)
Mo12 - N12	2.290 (18)	Mo22 - N22	2.236 (21)
Mo13 - N13	2.286 (18)	Mo23 - N23	2.425 (32)
		avg Mo-N	2.303 (21)

Table 20. Selected bond angles (deg) in $Mo_6S_8(pyrr)_6 \cdot 1$ pyrr

Mo12 - Mo11 - Mo13	59.6 (1)	Mo22 - Mo21 - Mo23	60.0 (1)
Mo12 - Mo11 - Mo13A	60.1 (1)	Mo22 - Mo21 - Mo23A	60.1 (1)
Mo13 - Mo11 - Mo11A	59.8 (1)	Mo23 - Mo21 - Mo22A	60.0 (1)
Mo11A- Mo11 - Mo13A	60.6 (1)	Mo22A-Mo21 - Mo23A	59.7 (1)
Mo11 - Mo12 - Mo13	60.6 (1)	Mo21 - Mo22 - Mo23	59.9 (1)
Mo11 - Mo12 - Mo13A	59.9 (1)	Mo21 - Mo22 - Mo23A	60.0 (1)
Mo13 - Mo12 - Mo12A	59.9 (1)	Mo23 - Mo22 - Mo21A	59.9 (1)
Mo12A- Mo12 - Mo13A	59.4 (1)	Mo21A- Mo22 - Mo23A	59.6 (1)
Mo11 - Mo13 - Mo12	59.8 (1)	Mo21 - Mo23 - Mo22	60.1 (1)
Mo11 - Mo13 - Mo11A	59.5 (1)	Mo21 - Mo23 - Mo22A	60.4 (1)
Mo12 - Mo13 - Mo12A	60.7 (1)	Mo22 - Mo23 - Mo21A	60.4 (1)
Mo11A- Mo13 - Mo12A	60.0 (1)	Mo21A- Mo23 - Mo22A	59.9 (1)
		avg Mo-Mo-Mo	60.0 (1)
Mo12 - Mo11 - Mo11A	90.4 (1)	Mo22 - Mo21 - Mo22A	90.1 (1)
Mo13 - Mo11 - Mo13A	89.8 (1)	Mo23 - Mo21 - Mo23A	89.7 (1)
Mo11 - Mo12 - Mo12A	89.6 (1)	Mo21 - Mo22 - Mo21A	89.9 (1)
Mo13 - Mo12 - Mo13A	90.2 (1)	Mo23 - Mo22 - Mo23A	89.6 (1)
Mo11 - Mo13 - Mo12A	89.6 (1)	Mo21 - Mo23 - Mo21A	90.3 (1)
Mo12 - Mo13 - Mo11A	90.4 (1)	Mo22 - Mo23 - Mo22A	90.4 (1)
		avg Mo-Mo-Mo	90.0 (1)
Mo11 - S11 - Mo12	65.1 (1)	Mo21 - S21 - Mo22	66.1 (2)
Mo11 - S11 - Mo13	65.7 (1)	Mo21 - S21 - Mo23	65.7 (2)
Mo12 - S11 - Mo13	65.1 (1)	Mo22 - S21 - Mo23	65.9 (2)
Mo12 - S12 - Mo12A	66.0 (2)	Mo21 - S22 - Mo22A	65.8 (2)
Mo12 - S12 - Mo13A	65.4 (2)	Mo21 - S22 - Mo23A	65.2 (2)
Mo12A - S12 - Mo13A	65.3 (2)	Mo22A - S22 - Mo23A	65.0 (2)
Mo11 - S13 - Mo11A	65.3 (2)	Mo22 - S23 - Mo21A	65.8 (2)
Mo11 - S13 - Mo13A	65.3 (1)	Mo22 - S23 - Mo23A	65.6 (2)
Mo11A - S13 - Mo13A	66.0 (1)	Mo21A - S23 - Mo23A	65.4 (2)
Mo11 - S14 - Mo12	65.8 (1)	Mo21 - S24 - Mo22	65.5 (2)
Mo11 - S14 - Mo13A	65.8 (1)	Mo21 - S24 - Mo23A	65.2 (2)
Mo12 - S14 - Mo13A	65.9 (1)	Mo22 - S24 - Mo23A	65.4 (2)
		avg Mo-S-Mo	65.6 (2)

Table 20. (continued)

S11 - Mo11 - S14	90.0 (2)	S21 - Mo21 - S24	89.2 (2)
S11 - Mo11 - S13A	88.5 (2)	S21 - Mo21 - S23A	90.1 (2)
S13 - Mo11 - S14	90.4 (2)	S22 - Mo21 - S24	90.6 (2)
S13 - Mo11 - S13A	90.3 (2)	S22 - Mo21 - S23A	89.2 (2)
S11 - Mo12 - S14	90.3 (2)	S21 - Mo22 - S24	89.7 (2)
S11 - Mo12 - S12A	90.5 (2)	S21 - Mo22 - S22A	90.5 (2)
S12 - Mo12 - S14	89.8 (2)	S23 - Mo22 - S24	90.0 (2)
S12 - Mo12 - S12A	88.5 (2)	S23 - Mo22 - S22A	89.1 (2)
S11 - Mo13 - S12A	90.5 (2)	S21 - Mo23 - S22A	89.8 (2)
S11 - Mo13 - S13A	88.4 (2)	S21 - Mo23 - S23A	90.1 (2)
S12A - Mo13 - S14A	90.1 (2)	S22A - Mo23 - S24A	89.8 (2)
S13A - Mo13 - S14A	90.2 (2)	S23A - Mo23 - S24A	89.5 (2)
		avg S-Mo-S	89.9 (2)
S11 - Mo11 - S13	173.0 (2)	S21 - Mo21 - S22	173.1 (2)
S14 - Mo11 - S13A	173.2 (2)	S24 - Mo21 - S23A	173.1 (2)
S11 - Mo12 - S12	173.0 (2)	S21 - Mo22 - S23	172.9 (2)
S14 - Mo12 - S12A	173.0 (2)	S24 - Mo22 - S22A	173.6 (2)
S11 - Mo13 - S14A	173.3 (2)	S21 - Mo23 - S24A	172.9 (2)
S12A - Mo13 - S13A	172.8 (2)	S22A - Mo23 - S23A	173.1 (2)
		avg S-Mo-S	173.1 (2)
S11 - Mo11 - N11	97.6 (5)	S21 - Mo21 - N21	95.9 (5)
S13 - Mo11 - N11	89.3 (5)	S22 - Mo21 - N21	91.0 (5)
S14 - Mo11 - N11	94.8 (5)	S24 - Mo21 - N21	96.3 (5)
S13A - Mo11 - N11	92.0 (5)	S23A - Mo21 - N21	90.5 (5)
S11 - Mo12 - N12	89.9 (5)	S21 - Mo22 - N22	95.0 (6)
S12 - Mo12 - N12	98.1 (5)	S23 - Mo22 - N22	92.1 (6)
S14 - Mo12 - N12	94.1 (5)	S24 - Mo22 - N22	94.1 (5)
S12A - Mo12 - N12	92.8 (5)	S22A - Mo22 - N22	92.4 (5)
S11 - Mo13 - N13	91.9 (5)	S21 - Mo23 - N23	99.8 (9)
S12A - Mo13 - N3	89.9 (6)	S22A - Mo23 - N23	100.0 (8)
S13A - Mo13 - N13	97.2 (6)	S23A - Mo23 - N23	86.7 (8)
S14A - Mo13 - N13	94.8 (5)	S24A - Mo23 - N23	87.2 (9)
		avg S-Mo-N	93.4 (6)

Table 21. Bond distances and bond order calculations for the $Mo_6S_8L_6$ cluster complexes.

formula	Mo-Mo	Mo-S	Mo-L	est. Mo-L[a]	BO(Mo-Mo)[b]	BO(Mo-L)[c]
$Mo_6S_8(PEt_3)_6 \cdot 2DCM$	2.6584 (5)	2.446 (1)	2.524 (1)	2.50	0.843 (1)	0.91 (1)
$Mo_6S_8(tht)_6$	2.640 (4)	2.430 (8)	2.576 (8)	2.44	0.905 (14)	0.59 (2)
$Mo_6S_8(py)_6 \cdot 1.65py$	2.640 (4)	2.453 (10)	2.274 (36)	2.11	0.905 (14)	0.53 (7)
$Mo_6S_8(py)_6 \cdot 2py$	2.644 (2)	2.462 (3)	2.283 (9)	2.11	0.891 (7)	0.53 (2)
$Mo_6S_8(pip)_6 \cdot 7pip$	2.649 (1)	2.454 (2)	2.317 (5)	2.11	0.874 (3)	0.45 (1)
$Mo_6S_8(pyrr)_6 \cdot 1pyrr$	2.649 (3)	2.446 (6)	2.309 (21)	2.11	0.874 (10)	0.47 (4)

[a]Estimated single bond distance from Pauling covalent radii r(N), r(S), and the calculated covalent radius of the molybdenum atom r(Mo) = d(Mo-S) - r(S), where d(Mo-S) distance is the value from the table.

[b]Estimated bond order from Pauling bond order equation, d(n) = d(1) - 0.6 log n, where d(n) is the observed Mo-Mo distance and d(1) is the estimated Mo-Mo single bond distance, 2.614 Å.

[c]Estimated bond order from Pauling bond order equation, d(n) = d(1) - 0.6 log n, where d(n) is the observed Mo-L distance and d(1) is the estimated Mo-L single bond.

to the 3-fold axis. The Mo-Mo bond distances within the Mo_3 triangles range from 2.654 ($ErMo_6S_8$) to 2.698 Å (Mo_6S_8) and the distances between triangles range from 2.681 ($Cu_{3.66}Mo_6S_8$) to 2.862 Å (Mo_6S_8).[1,2] This distortion results from a close approach between cluster units and formation of a weak intercluster Mo-Mo bond as evidenced by the distance of 3.084 Å for the highly distorted Mo_6S_8. The isolated $Mo_6S_8L_6$ cluster units show no intercluster Mo-Mo bonding and negligible distortion of the octahedron. The Chevrel phases exhibit average Mo-S distances of about 2.44 to 2.46 Å which are very similar to the distances observed for the $Mo_6S_8L_6$ cluster units.

The application of bond order calculations has proven useful in understanding the stability of the cluster unit relative to the loss of ligands in subsequent deligation studies. The bond order for metal-metal or metal-ligand bonds can be determined by using Pauling's bond order equation[46] shown below in equation 2,

$$d(n) = d(1) - 0.6 \log n \qquad (2)$$

where d(n) is the observed bond distance, d(1) is the single bond distance, and n is the bond order. The calculations for the Mo-Mo and Mo-L bond orders are given in Table 21. The estimated Mo-Mo bond distance, d(n), for the Mo_6S_8 unit was found to be 2.662 Å, where d(1) = 2.614 Å was used as the Mo-Mo single bond value and n = 20/24 = 0.833 was used as the bond order. The calculated Mo-Mo bond orders for the $Mo_6S_8L_6$ complexes were observed to range from 0.843 to 0.905, which are in reasonable agreement with the expected value of 0.833 for the 20 electron cluster compounds.

Bond order calculations for the Mo-L bonds indicate that the strength of the bonding between the cluster and coordinated ligands differs significantly depending upon the terminal ligand. The value for the triethylphosphine adduct is much greater than what is observed for the sulfur- or nitrogen-donor ligands. Also, it is noted that the nitrogen-based ligands, with piperidine in particular, show the weakest Mo-L bonding and thus should be the easiest ligands to remove upon deligation. The Mo-L bond order values for $Mo_6S_8L_6$ complexes are quite similar to the values that were previously reported for the tungsten cluster complexes[13] as evidenced in Table 22.

Table 22. Bond distances and bond order calculations for the $W_6S_8L_6$ cluster complexes.

formula	W-W	W-S	W-L	est. W-L[a]	BO (W-L)[b]
$W_6S_8(PEt_3)_6 \cdot 1.44DCM$	2.6732 (3)	2.452 (3)	2.513 (1)	2.51	1.00
$W_6S_8(tht)_6$	2.653 (3)	2.440 (6)	2.548 (9)	2.45	0.68
$W_6S_8(py)_6$	2.6617 (2)	2.458 (3)	2.255 (5)	2.11	0.56

[a]Estimated single bond distance from Pauling covalent radii r(P), r(S), r(N), and the calculated covalent radius of the tungsten atom r(W) = d(W-S) - r(S), where d(W-S) is the average distance 2.45 Å in these clusters.

[b]Estimated bond order from Pauling bond order equation, d(n) = d(1) - 0.6 log n, where d(n) is the observed W-L distance and d(1) is the estimated W-L single bond distance, 2.630 Å.

CONCLUSIONS

This paper describes the preparation and characterization of molecular $Mo_6S_8L_6$ cluster complexes. Previously reported adducts of pyridine, propylamine, and tetrahydrothiophene were studied in order to improve their preparation for higher yields or to gain information by further characterization. New complexes were found with the nitrogen-donor ligands of 4-methylpyridine, pyrrolidine, and piperidine.

In an attempt to improve the two-step preparative route to the completely sulfur-substituted cluster, $Mo_6S_8(py)_x$, it was discovered that this compound had been misformulated. Both the previous two-step route and the new one-step method with higher stoichiometric amounts of the sulfiding agent, NaSH, resulted in a similar product which contained sodium, $Na_{2y}Mo_6S_{8+y}(py)_x$. In this procedure, the pyridine content was found to be variable and depended upon the reaction conditions.

This pyridine-deficient material was quite amenable to undergoing ligand exchange reactions. Further reaction in neat pyridine produced the crystalline hexapyridine complex which existed in two different morphologies. The chunk-like crystals possessed triclinic symmetry which was also observed for the pyridine adducts of the tungsten and molybdenum sulfide/chloride compounds. Furthermore, a new form was also structured which showed cubic symmetry in the space group $Pa\bar{3}$.

Reaction of the pyridine-deficient material with n-propylamine resulted in the formation of the reactive propylamine adduct. The propylamine ligands were found

to be more weakly bound to the Mo_6S_8 cluster unit, which allowed for facile ligand exchange and the preparation of new complexes with pyrrolidine and piperidine. These adducts crystallized in tetragonal space groups. Also, they were soluble in organic solvents which allowed for study by NMR spectroscopy. The complexes showed spectra consistent with the presence of both coordinated and "free" ligands. The free ligands appear to result from strong hydrogen bonding interactions and remain in the complexes even after extended drying under dynamic vacuum. Two-dimensional NMR studies on the piperidine adduct have resulted in tentative assignments for the protons. Also, the structure solution has shown that the piperidine ligands are coordinated via equatorial positions.

Characterization of these molecular $Mo_6S_8L_6$ cluster complexes has been developed beyond elemental analyses and infrared spectra. Further information has been gained from Raman and XPS spectra. Characteristic bands can be detected in the spectra by these techniques which corroborate the presence of the Mo_6S_8 cluster unit. SEM-EDS has been employed as a means of gaining qualitative elemental information. Structural information on the nitrogen-donor ligands has shown them to possess the weakest Mo-L bonds as evidenced in relatively low bond orders. The results indicate that these complexes should be the best materials for further deligation studies to prepare the Chevrel phase compounds.

Further research is needed in the preparation of single crystals of the propylamine adduct, as well as better single crystal structural solutions for the triclinic pyridine and tetragonal pyrrolidine complexes. Similarly, useful information could be

gained from a crystal structure of the 4-methylpyridine adduct. Pyrrole should be explored as a replacement for pyrrolidine, since disorder problems with this ligand would be greatly diminished by ring conjugation. Likewise, further efforts should be employed in the preparation and characterization of new adducts which might lead to even more interesting cluster complexes. Possible materials to study include the above mentioned pyrrole (or substituted pyrroles), imidazole, pyrazole, dimethylformamide, and bulkier amines like isobutylamine. Further study of mixed ligand compounds could prove fruitful in better understanding the exchange process which is occurring.

Recent research has led to a method for improving the yield of the crystalline tetrahydrothiophene complex. The predominant product from the tht reaction, the insoluble tht-deficient solid, was stirred with n-propylamine and resulted in nearly complete dissolution of the solid and formation of a $PrNH_2$/tht adduct. After stripping of the n-propylamine solution, a brown/black solid was obtained. This material was further reacted with neat tetrahydrothiophene for 2-3 hours at reflux and resulted in a much larger quantity of the crystalline tht complex.

REFERENCES

1. Yvon, K. Current Topics in Materials Science, 1st ed., Kaldis, E., Ed.; North-Holland: New York, 1978; Vol. 3, Ch. 2.

2. Chevrel, R.; Sergent, M. Topics in Current Physics, Fischer, Ø. and Maple, M.B., Eds.; Springer-Verlag: Heidelberg, 1982; Vol. 32, Ch. 2.

3. Schöllhorn, R.; Kümpers, M.; Besenhard, J.O. *Mater. Res. Bull.* **1977**, *12*, 781.

4. Mulhern, P.J.; Haering, R.R. *Can. J. Phys.* **1984**, *62*, 527.

5. McCarty, K.F.; Schrader, G.L. *Ind. Eng. Chem. Prod. Res. Dev.* **1984**, *23*, 519.

6. McCarty, K.F.; Anderegg, J.W.; Schrader, G.L. *J. Catal.* **1985**, *93*, 375.

7. Nanjundaswamy, K.S.; Vasanthacharya, N.Y.; Gopalakrishnan, J.; Rao, C.N.R. *Inorg. Chem.* **1987**, *26*, 4286.

8. Rabiller-Baudry, M.; Sergent, M.; Chevrel, R. *Mater. Res. Bull.* **1991**, *26*, 519.

9. Spink, D.A. PhD. Dissertation, Iowa State University, Ames, IA, 1989.

10. McCarley, R.E.; Laughlin, S.K.; Spink, D.A.; Hur, N. Abstract of Papers, 3rd Chemical Congress of North America, Toronto, Ontario (Canada), 1988.

11. McCarley, R.E.; Zhang, X.; Spink, D.A.; Hur, N. Abstracts of Papers, 199th National Meeting of the American Chemical Society; Boston, MA, 1990.

12. McCarley, R.E.; Hollingshead, J.A.; Hilsenbeck, S.J.; Zhang, X. Abstracts of Papers, 204th National Meeting of the American Chemical Society; Washington, D.C., 1992.

13. Zhang, X. PhD. Dissertation, Iowa State University, Ames, IA, 1991.

14. Saito, T.; Yamamoto, N.; Yamagata, T.; Imoto, H. *J. Am. Chem. Soc.* **1988**, *110*, 1646.

15. Saito, T.; Yamamoto, N.; Nagase, T.; Tsuboi, T.; Kobayashi, K.; Yamagata, T.; Imoto, H.; Unoura, K. *Inorg. Chem.* **1990**, *29*, 764.

16. Koknat, F.W.; Adaway, T.J.; Erzerum, S.I.; Syed, S. *Inorg. Nucl. Chem. Lett.* **1980**, *16*, 307.

17. Brauer, G. Handbuch der Preparativen Anorganischen Chemie; Ferdinand Enke Verlag: Stuttgart, 1975; p. 371.

18. Elwell, W.T.; Wood, D.F. Analytical Chemistry of Molybdenum and Tungsten; Pergamon Press: New York, 1971.

19. Oneida Research Services, Inc., Whitesboro, New York.

20. SHELXTL-PLUS, Siemans Analytical Xray, Inc., Madison, WI.

21. Laughlin, S.K. M.S. Thesis, Iowa State University, Ames, IA, 1986.

22. Breuer, E.; Melumad, D. *J. Org. Chem.* **1973**, *38*, 1601.

23. Abraham, R.J.; Bedford, G.R.; Wright, B. *Org. Magn. Reson.* **1983**, *21*, 637.

24. Gill, N.S.; Nuttall, R.H.; Scaite, D.E.; Sharp, D.W. *J. Inorg. Nucl. Chem.* **1961**, *18*, 79.

25. Thornton, D.A. *Coord. Chem. Rev.* **1990**, *104*, 251.

26. Cotton, F.A.; Wing, R.M.; Zimmerman, R.A. *Inorg. Chem.* **1967**, *6*, 11.

27. Akyüz, S.; Davies, J.E.D.; Holmes, K.T. *J. Molec. Struct.* **1977**, *42*, 59.

28. Fan, K.; Boggs, J.E. *Tetrahedron* **1986**, *42*, 1265.

29. Sato, N.; Hamada, Y.; Tsuboi, M. *Spectrochim. Acta* **1987**, *43A*, 943.

30. Ogura, T.; Hamachi, T.; Kawaguchi, S. *Bull. Chem. Soc. Jpn.* **1968**, *41*, 892.

31. Bandiwar, R.; Schrivastava, O.P.; Soni, N.K. *J. Indian Chem. Soc.* **1983**, *60*, 825.

32. Sheinker, Y.A.; Peresleni, E.M. *Zh. Fiz. Chim.* **1958**, *32*, 2112.

33. Barvinok, M.S.; Lukina, L.G. *Russ. J. Inorg. Chem.* **1979**, *24*, 397.

34. Muldagaliev, K.K.; Ignatev, I.S. *Russ. J. Phys. Chem.* **1983**, *57*, 1507.

35. Giorgini, M.G.; Paliani, G.; Cataliotti, R. *Spectrochim. Acta* **1977**, *33A*, 1083.

36. Lewis, J.; Miller, J.R.; Richards, R.L.; Thompson, A. *J. Chem. Soc.* 1965, 5850.

37. Green, J.H.S. *Spectrochim. Acta* 1968, *24A*, 137.

38. Shobatake, K.; Nakamoto, K. *J. Am. Chem. Soc.* 1970, *92*, 3332.

39. Csaszar, A.G.; Fogarasi, G.A. *Spectrochim. Acta* 1989, *45A*, 845.

40. Nakashima, M.; Mikuriya, M.; Muto, Y. *Bull. Chem. Soc. Jpn.* 1985, *58*, 968.

41. Verble, J.L.; Wieting, T.J. *Phys. Rev. Lett.* 1970, *25*, 362.

42. Müller, A.; Jostes, R.; Eltzner, W.; Nie, C.; Diemann, E.; Bögge, H.; Zimmermann, M.; Dartmann, M.; Reinsch-Vogell, U.; Che, S.; Cyvin, S.J.; Cyvin, B.N. *Inorg. Chem.* 1985, *24*, 2872.

43. Müller, A.; Sarkar, S.; Dommröse, A.; Filgueira, R. *Z. Naturforsch* 1980, *35B*, 1592.

44. Yashonath, S.; Hegde, M.S.; Sarode, P.R.; Rao, C.N.R.; Umarji, A.M.; Subba Rao, G.V. *Solid State Commun.* 1981, *37*, 325.

45. Michel, J.B. PhD. Dissertation, Iowa State University, Ames, IA, 1979.

46. Pauling, L. The Nature of the Chemical Bond, 3rd ed.; Cornell University Press: Ithaca, New York, 1960; p. 400.

PAPER 2.

DELIGATION OF COORDINATED LIGANDS FROM THE MOLECULAR $Mo_6S_8L_6$ CLUSTER COMPLEXES

INTRODUCTION

Ternary molybdenum chalcogenides of the general formula $M_xMo_6Y_8$ (M=ternary metal cation; Y=chalcogenide), known as Chevrel phases, have been extensively studied and have been shown to possess interesting physical and chemical properties.[1-6] These properties are related to the structures of the compounds which consist of Mo_6Y_8 clusters interlinked to form three-dimensional networks. The production of the Chevrel phases has generally involved solid state reactions at high temperatures (1000-1300°C). Recently, though, lower temperature routes using polythiomolybdates and metal chlorides as solution precursors have been reported.[7,8] Likewise, a major focus of the McCarley research group has been on the preparation of $M_6S_8L_6$ (M = Mo, W) cluster complexes as low temperature precursors to the Chevrel phases.[9-13]

Previous attempts at deligation of the $M_6S_8L_6$ cluster complexes have been explored for the triethylphosphine adduct of the molybdenum complexes[9] and the pyridine adduct of the tungsten analogue.[13] For the triethylphosphine adduct, partial deligation was found by using phosphine acceptors like $Co_2(CO)_8$, $Mo(CO)_6$, or CuCl. The use of propylene sulfide to alter the phosphine ligand resulted in the formation of coordinated triethylphosphine sulfide.

For the deligation of the tungsten pyridine adduct, thermal decomposition below 350°C resulted in partial pyridine removal and heating to 640°C produced complete

deligation, but also disproportionation to tungsten and tungsten disulfide. The pyridine adduct was reacted with metallic lead powder in an attempt to form the lead Chevrel phase. Heating at temperatures up to 350°C produced partial deligation and unreacted lead. An attempt to remove pyridine by forming an aluminum chloride-pyridine complex also resulted in only partial deligation. Solution reactions with trifluoromethanesulfonic acid formed oily residues or products showing triflate anion coordination. Likewise, the solution reaction with the boron trifluoride-diethyl ether complex produced a solid which showed BF_3 coordination.

These results indicated that more weakly ligated adducts should be studied if complete deligation is to be reached. Therefore, in this paper, the deligation of a variety of the cluster complexes will be explored in an attempt to produce the metastable Mo_6S_8 phase and other Chevrel phase compounds.

EXPERIMENTAL

Materials

The reagents and products involved in this work appear to be air and moisture sensitive. Therefore, special precautions were taken to ensure the maintenance of a dry, inert atmosphere. All manipulations were performed by the use of an inert atmosphere drybox, a high-vacuum manifold, and Schlenk techniques, unless otherwise stated. All glassware was thoroughly dried prior to use by its placement in an oven at 140°C for at least 4 hours.

The molecular complexes $Mo_6S_8L_x$ were prepared according to procedures discussed in Paper 1. Anhydrous ammonia (99.9%) was obtained from Matheson Gas Products and condensed onto finely-divided sodium metal before further use. Trifluoromethanesulfonic acid (Aldrich Co.) was syringed from a side-arm flask into the reaction under a nitrogen purge. The tetrafluoroboric acid-diethyl ether complex (85%, Aldrich Co.) was syringed from a Nalgene container under a nitrogen purge.

All solvents were purified and dried prior to use. Also, the solvents were deoxygenated by use of the freeze-thaw process: freeze to liquid nitrogen temperature, evacuate the gaseous material, and then thaw. This process was repeated three times prior to the distillation of the purified solvent onto 3 or 4 Å molecular sieves and storage under vacuum or a nitrogen atmosphere. Diethyl ether was purified by refluxing over calcium hydride for at least 4 hours. Methanol was

dried by refluxing over sodium methoxide. When used, the solvents were vacuum distilled or syringed under a flowing nitrogen gas atmosphere.

Analytical Procedures

Molybdenum was determined gravimetrically either as the trioxide (if ternary metal cations were not present) or as the 8-hydroxyquinolate. For the trioxide method, samples were placed in tared crucibles and decomposed initially with dilute (3M) nitric acid. Concentrated nitric acid was then added to ensure complete oxidation and the samples evaporated to dryness. After ignition in a muffle furnace at 520°C, the resulting MoO_3 solid was weighed. For the 8-hydroxyquinolate method,[14] the samples were dissolved in basic solutions with the aid of hydrogen peroxide. The solutions were neutralized with dilute sulfuric acid to pH = 4-6. EDTA (5%) and acetic acid/ammonium acetate buffer solutions were added. The analyte, $MoO_2(ONC_9H_6)_2$, was precipitated by the addition of 8-hydroxyquinoline solution and filtered through tared filters. After washing with hot distilled water, the materials were dried to constant weight at 140°C.

Additional microanalyses for carbon, hydrogen, nitrogen, and sodium were obtained from Oneida Research Services.[15] The C,H,N analyses were found to be lower than expected based on the molybdenum analyses. This problem could arise from a loss of ligand prior to the analyses or from incomplete combustion since samples known to have excess ligand like pyrrolidine were always found to be ligand-deficient. Therefore, less confidence was placed in these elemental percentages.

Physical Measurements

Infrared spectroscopy

Infrared spectra (4000-200 cm^{-1}) were obtained by using an IBM IR/98 Fourier Transform Infrared Spectrometer and a Bomem MB-102 Fourier Transform Infrared Spectrometer manufactured by Hartmann and Braun. Samples were prepared as Nujol mulls and the mulls were pressed between cesium iodide plates. The sample chamber was continuously purged with dry, compressed air and reference spectra were collected in the empty chamber.

Raman spectroscopy

Raman spectra were obtained with the help of Jeanne Wynn in Professor Therese Cotton's group. A Spex Triplemate spectrometer with a Princeton Applied Research Corp. (PARC) intensified SiPD detector cooled to -40°C was used to record the spectra. The excitation source was a Coherent Ar^+ 200 series laser at the wavelength of 514.5 nm and the scattered radiation was collected in a backscattering geometry. The laser power at the sample was approximately 30 mW and the integration time was 200 s. The Raman spectra were obtained at room temperature from solid samples packed in capillary tubes.

X-ray photoelectron spectroscopy

XPS spectra were collected by James Anderegg at room temperature with a Physical Electronics Industries 5500 muititechnique surface analysis system. This

system was equipped with a hemispherical analyzer, a toroidal monochromator, and multichannel detector which sampled a 2 mm^2 area. The samples were placed on an indium substrate and excited with monochromatic Al K-α radiation (1486.6 eV) at the power of 300 W. The binding energies were calibrated with C 1s = 284.6 eV.

Nuclear magnetic resonance spectroscopy

Proton spectra were collected on the Nicolet NT-300 MHz instrument. The samples were handled in an inert atmosphere solvent drybox and dissolved in deuterated benzene just prior to the NMR study.

X-ray powder diffraction

An Enraf Nonius Delft FR552 Guinier camera was used to obtain x-ray powder diffraction patterns. A General Electric XRD-5 generator with an AEG fine focus tube and a copper target were used to generate the x-rays. Air-sensitive samples were ground thoroughly and then placed between strips of cellophane tape in the drybox. Powdered NBS silicon was added as an internal standard.

Scanning Electron Microscopy-Energy Dispersive Spectroscopy (SEM-EDS)

This technique was employed to obtain qualitative elemental information on the sample. A Cambridge S-200 Scanning Electron Microscope coupled to a Tracor Northern Micro Z-II Energy Dispersive Spectrometer with a beryllium window was used. The samples were placed onto a metal disk backed with double-stick Scotch

tape and then sputter-coated with gold or carbon. The molybdenum L series and sulfur K series peaks fell at almost identical energies and thus were not resolvable by this technique.

Thermal analysis (TG/DTA)

Thermal analysis curves were obtained from a Seiko TG/DTA 300 located in Professor Mufit Akinc's group. The samples were loaded into aluminum (T_{max}=600°C) or platinum pans with brief exposure to the atmosphere. Under flowing argon gas (100 cm^3/min), the samples were then heated (10°C/min) to 600°C or 800°C depending upon the experiment.

Mass spectroscopy

Spectra were collected by Jan Beane of Chemistry Instrument Services on a Finnigan 4000 Gas Chromatograph/EI-CI Mass Spectrometer System. The samples were heated at a controlled rate (30-50°C/min) and the spectra were collected at several intervals during the experiments. Electron ionization of 70 eV was used.

Synthetic Procedures

This study focused on the deligation of nitrogen-donor cluster complexes, especially the propylamine, pyridine-deficient and piperidine adducts. Some additional work has involved the tetrahydrothiophene adducts since only the deligation

of the triethylphosphine adduct was previously explored for the Mo_6S_8 cluster compounds.[9] Likewise, only the pyridine adduct deligation has been studied for the tungsten analogues.[13] These previous studies indicated that the deligation of the complexes was very difficult and complete removal of the ligands was not achieved. Routes designed to remove the ligands were explored by both solid state reactions and those in solution.

An initial step in studying the deligation of the cluster complexes was to explore the thermolysis of these materials by TG/DTA.

Thermal deligation

Similar reaction conditions were employed for all thermal decomposition reactions. In a typical preparation, the sample was placed in a Pyrex tube equipped with a standard ball-joint and adapter. The tube was then evacuated and heated to the desired temperature under dynamic vacuum. The following adducts were studied by this method: pyridine, 4-methylpyridine, propylamine, pyrrolidine, piperidine, and tetrahydrothiophene. The temperatures were varied from 100-500°C and the reaction was usually held at the desired temperature for a period of 1-2 days. Infrared spectra were always collected. Depending upon the product, x-ray powder diffraction data, elemental analyses, mass spectra, and other spectral data (Raman, XPS, and NMR) were also obtained.

Reactions with ternary metals

Reactions of the pyridine-deficient compound were explored by heating in the presence of ternary metal powders like tin and lead. The general reaction sequence involved heating the mixture at 500-700°C for 1-4 days under dynamic vacuum to remove the organic ligands and then further heating at 700-900°C for 4-7 days in a sealed tube. The reaction of the pyridine-deficient compound with an excess of tin at 700°C for 1 day resulted in an amorphous black powder. XPS data were collected on this material. Further heating to 900°C produced a black/grey powder in which the x-ray powder pattern indicated the presence of $SnMo_6S_8$, Sn, and MoS_2. Similar reactions were repeated with stoichiometric ratios of reactants and also resulted in a mixture of the desired Chevrel phase compound and MoS_2.

Alternatively, the pyridine-deficient compound was first heated to 500°C for 2 days under dynamic vacuum before further reaction with the ternary metal. The resulting black powder was amorphous and exhibited a featureless infrared spectrum. Anal. Calc. for $NaMo_6S_{8.5}$: Mo, 66.67%. Found: Mo, 61.82%. This material was then further reacted with lead powder at 700-900°C for 5-7 days. The x-ray powder pattern of the resulting product indicated the presence of the lead Chevrel phase along with lead and MoS_2 impurities.

Reactions with ammonia gas

In an attempt to exchange ammonia for propylamine in the cluster complex, the idea of using flowing ammonia gas to aid in cluster deligation was pursued. The

initial reaction involved placing 0.3 g of the propylamine adduct on a fritted disk in a Pyrex gas dispersion tube and heating to 150°C for 4 hours under flowing ammonia. The resulting black product was insoluble in neat n-propylamine. Infrared and Raman spectra were obtained. The reaction was repeated at 200°C and resulted in a similar infrared spectrum. Also, XPS data were obtained for this product.

Reactions with ammonia were also explored with the pyrrolidine and piperidine adducts. The pyrrolidine sample was heated to 250°C for 4 hours in flowing ammonia. Infrared and Raman spectra were obtained for the black, amorphous powder. The piperidine adduct was first heated to 200°C for 5 hours under flowing ammonia and an infrared spectrum was collected. A second piperidine sample was then heated to 300°C for 5 hours in flowing NH_3 and infrared and Raman spectra were collected. Anal. Found on the piperidine sample heated to 300°C: Mo, 58.06%.

Reaction of $Mo_6S_8(PrNH_2)_y$ with trifluoromethanesulfonic acid

Reactions of the cluster complex with this strong acid were explored in an attempt to protonate the propylamine ligand and thus make it a better leaving group. A general reaction involved placing 0.5 g of the propylamine adduct into a 100 mL reaction flask. Methanol (25 mL) was distilled onto the solid, followed by the addition via syringe of CF_3SO_3H (0.26 mL, 6 equiv.), and the mixture was refluxed for 1 day. After filtration and drying under dynamic vacuum, a black solid was obtained. Infrared spectra were collected on these products.

Reaction of $Mo_6S_8(PrNH_2)_y$ with tetrafluoroboric acid-diethyl ether complex

Similar reactions were explored with $HBF_4 \cdot Et_2O$ in both methanol and diethyl ether solutions. Generally, 0.2-0.3 g of the propylamine adduct was placed in a 100 mL reaction flask with 25-30 mL of the organic solvent and then 6 equivalents of the acid were added (0.15-0.3 mL). The mixtures were then refluxed for 1 day and after filtering and drying under dynamic vacuum, black solids were obtained. Infrared spectra were collected for the two materials. Anal. Found on product in methanol solution: Mo, 54.72%; C, 3.92%; H, 1.41%.

RESULTS AND DISCUSSION

Thermal Deligation

The method of thermal deligation was the first route explored for the cluster complexes. Ideally, the molybdenum-ligand bond would be weaker than the corresponding cluster molybdenum-sulfur bonds and, upon cleavage, the ligand would be displaced and result in intercluster molybdenum-sulfur linkages and formation of the binary Chevrel phase Mo_6S_8. This process is indicated by reaction 1:

$$Mo_6S_8L_6 \rightarrow Mo_6S_8 + 6L \qquad (1)$$

However, ligand fragmentation was also a possible outcome, which would result in the random blocking of intercluster linkages and produce a disordered material. Also, as a precautionary measure, deligation temperatures were limited to those below about 450-500°C because the binary Mo_6S_8 phase has been shown to undergo disproportionation above 500°C to the more thermodynamically stable products of molybdenum and molybdenum disulfide.[16,17]

Propylamine

The first step in understanding the thermal deligation process was to study pyrolysis via TG/DTA. The initial cluster complex chosen for study was the propylamine adduct and the resulting TG/DTA curve is shown in Figure 1. As

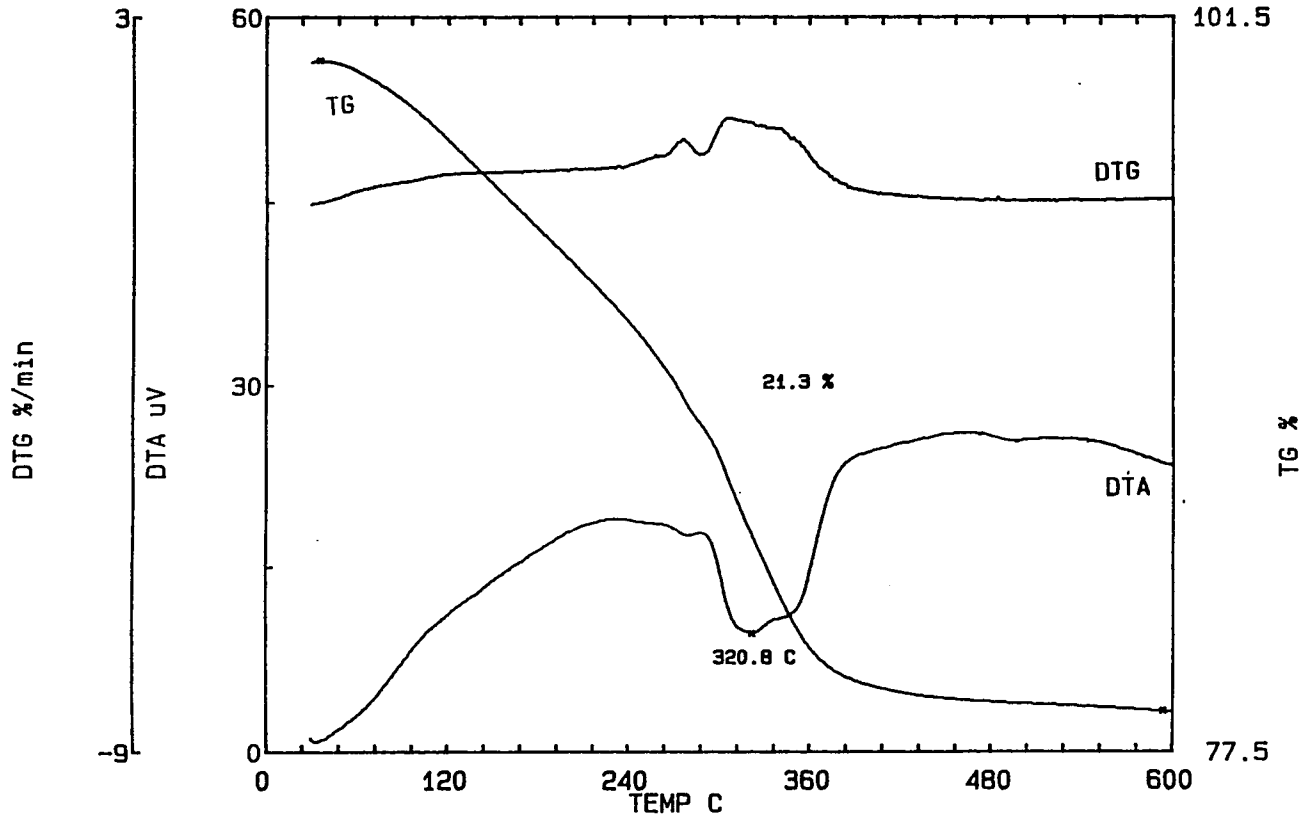

Figure 1. TG/DTA curve for the propylamine adduct - $Mo_6S_8(PrNH_2)_y$

observed in this figure, weight loss occurs quite quickly (T_{onset}~50°C) and shows a steady weight loss to almost 400°C before levelling off. The observed weight loss of 21.3% corresponds to the removal of about 4 propylamine ligands and this black product exhibits a featureless infrared spectrum.

Based on the TG/DTA findings, deligation was explored under dynamic vacuum. A lower temperature of 250°C was initially chosen and resulted in the formation of a shiny, grey-black amorphous solid. The far-infrared spectrum of this product is shown in Figure 2a and exhibits a very weak and broad peak centered about 386 cm^{-1}. Also, the mid-IR region is completely devoid of propylamine bands. The Mo analyses on this material (62.13% Mo) were lower than that calculated for Mo_6S_8 (69.18%). The XPS spectrum corroborated that this material contained the cluster unit and that MoS_2 was not present.

Further heating of the propylamine adduct to 350°C again resulted in the formation of a shiny, yet amorphous, grey-black solid. The mid/far-infrared spectrum (Figure 2b) exhibits only several weak bands in the range of 406-347 cm^{-1}. The spectrum indicates that the weak, broad Mo-S stretching mode is being lost amongst the bands caused by trace amounts of water in the IR purge gas. Molybdenum analyses (67.99% Mo) on this product indicated that some organic residue must be present. This result can be understood as probably arising from fragmentation of the propylamine ligand, since, during pyrolysis, a noticeable pressure increase at about 300°C was observed. This increase in pressure could only be due to volatile gases like methane or hydrogen which would not condense in the liquid nitrogen trap.

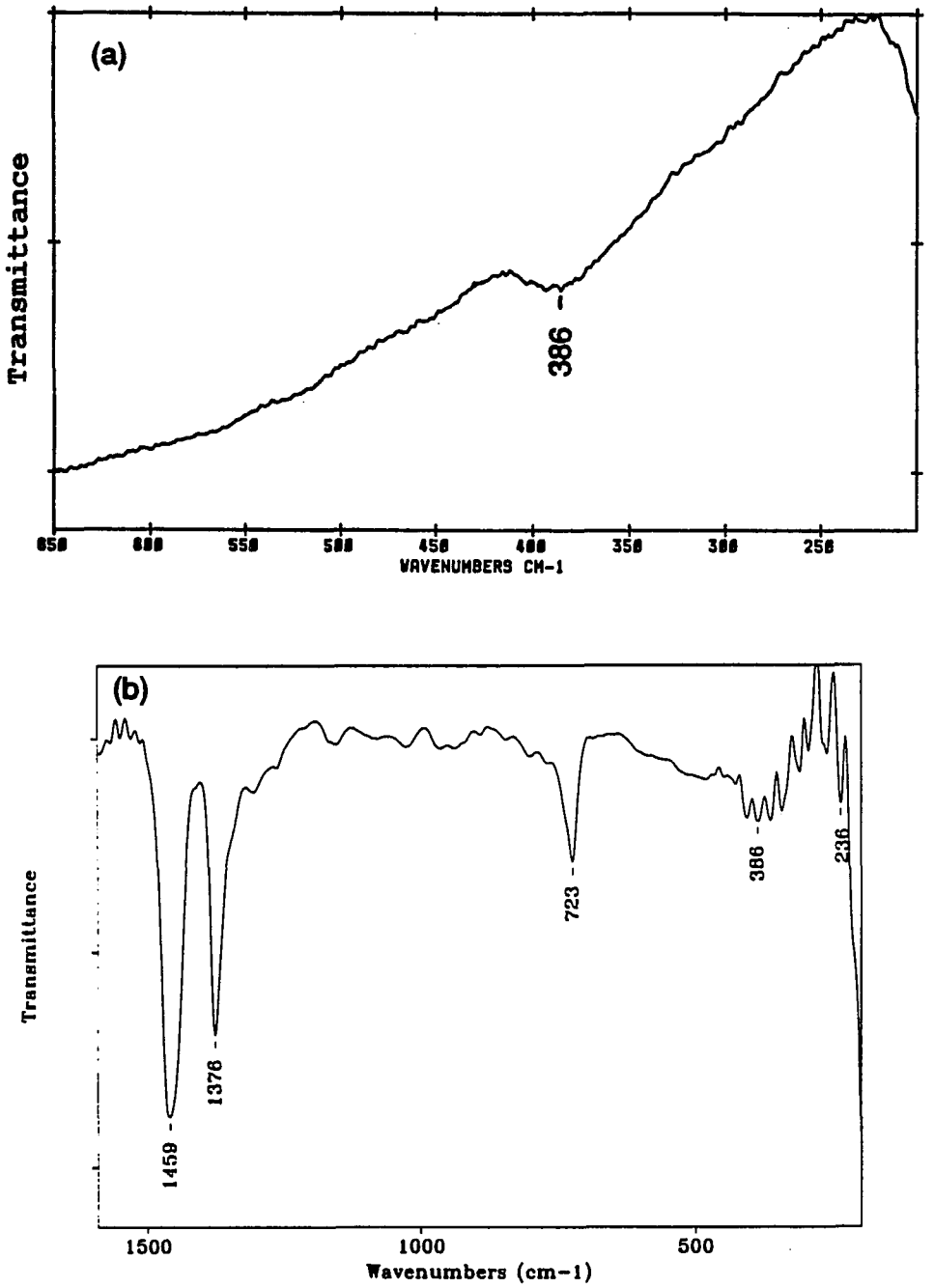

Figure 2. Infrared spectra (Nujol) of the propylamine adduct deligation products at 250°C (a) and at 350°C (b) by heating under dynamic vacuum

The Raman spectra for the initial propylamine cluster complex and the product of deligation at 350°C are shown in Figure 3. The presence of the broad band centered at 448 cm^{-1} in these spectra indicates that the Mo_6S_8 cluster unit has been retained after thermolysis.

Pyridine compounds

Thermolysis of the pyridine-deficient compound, formulated as $Na_{2y}Mo_6S_{8+y}(py)_x$, was also explored. Since this compound was nearly deligated already, it was reasoned that further heating might readily lead to the ternary Chevrel phase - $Na_xMo_6S_8$ (x=1-3). The TG/DTA curve is shown in Figure 4. The material which was examined by TG/DTA contained more pyridine since it was not reactive upon the brief air contact necessary in loading samples for thermal analysis; however, other samples often exhibited smoking or flaming of the material prior to the TG/DTA experiment. This curve shows an uneven weight loss regime which indicates a complex thermolysis process. Unlike the propylamine adduct, heating did not produce a levelling of the weight loss and probably indicates the start of cluster degradation. The sodium Chevrel phase is metastable since it can only be prepared by the electrochemical insertion of sodium into the binary phase Mo_6S_8,[3,18] and thus should show disproportionation to Mo and MoS_2 at these temperatures (800°C).

Attempts at thermal deligation under dynamic vacuum at 250°C and 500°C were explored for the pyridine-deficient compound. Deligation at 250°C produced a black powder which exhibited only a broad Mo-S band centered at 393 cm^{-1} in the far-IR

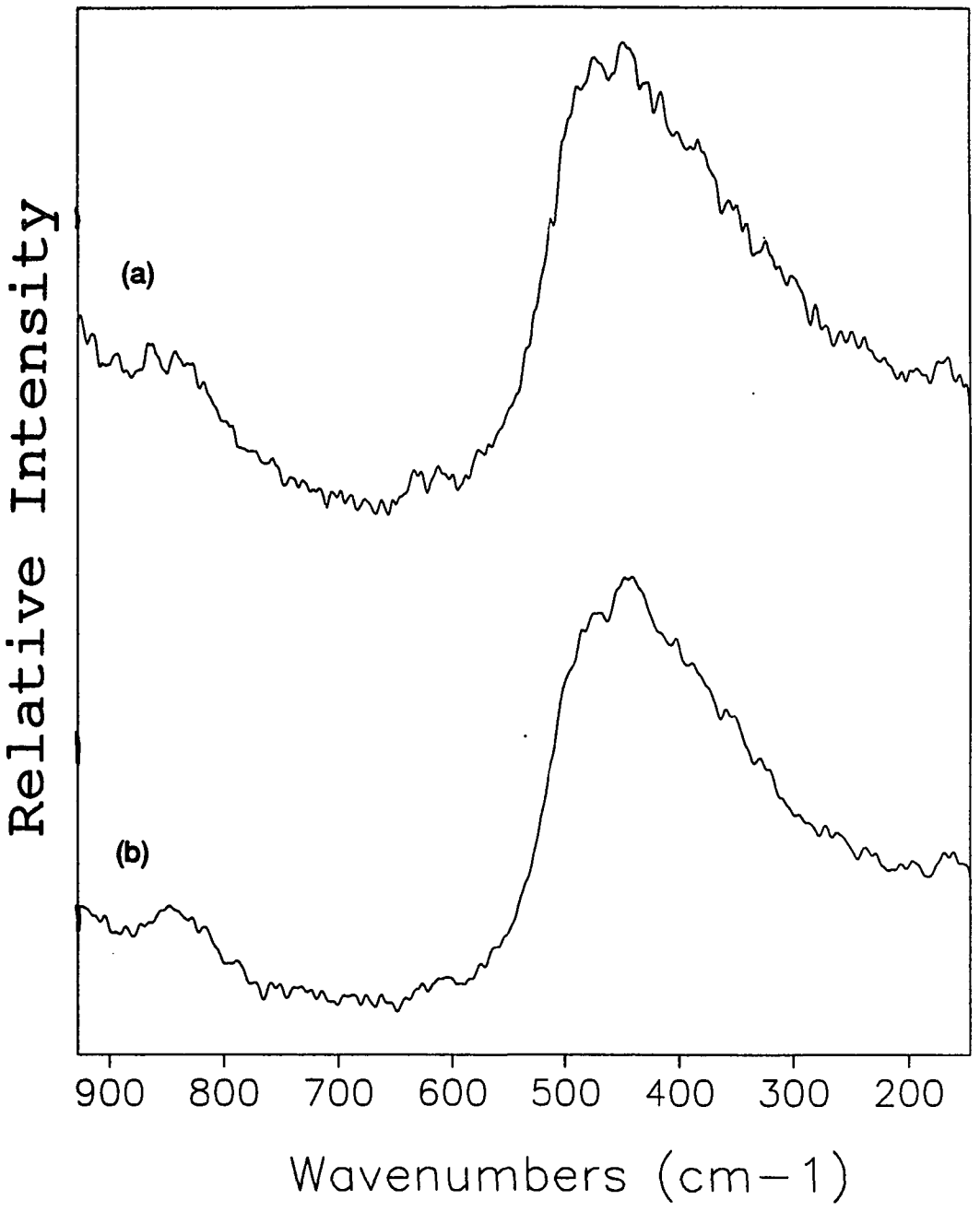

Figure 3. Raman spectra of $Mo_6S_8(PrNH_2)_y$ (a) and the deligation product (b) from heating at 350°C under dynamic vacuum. The peaks are centered at about 448 cm^{-1}.

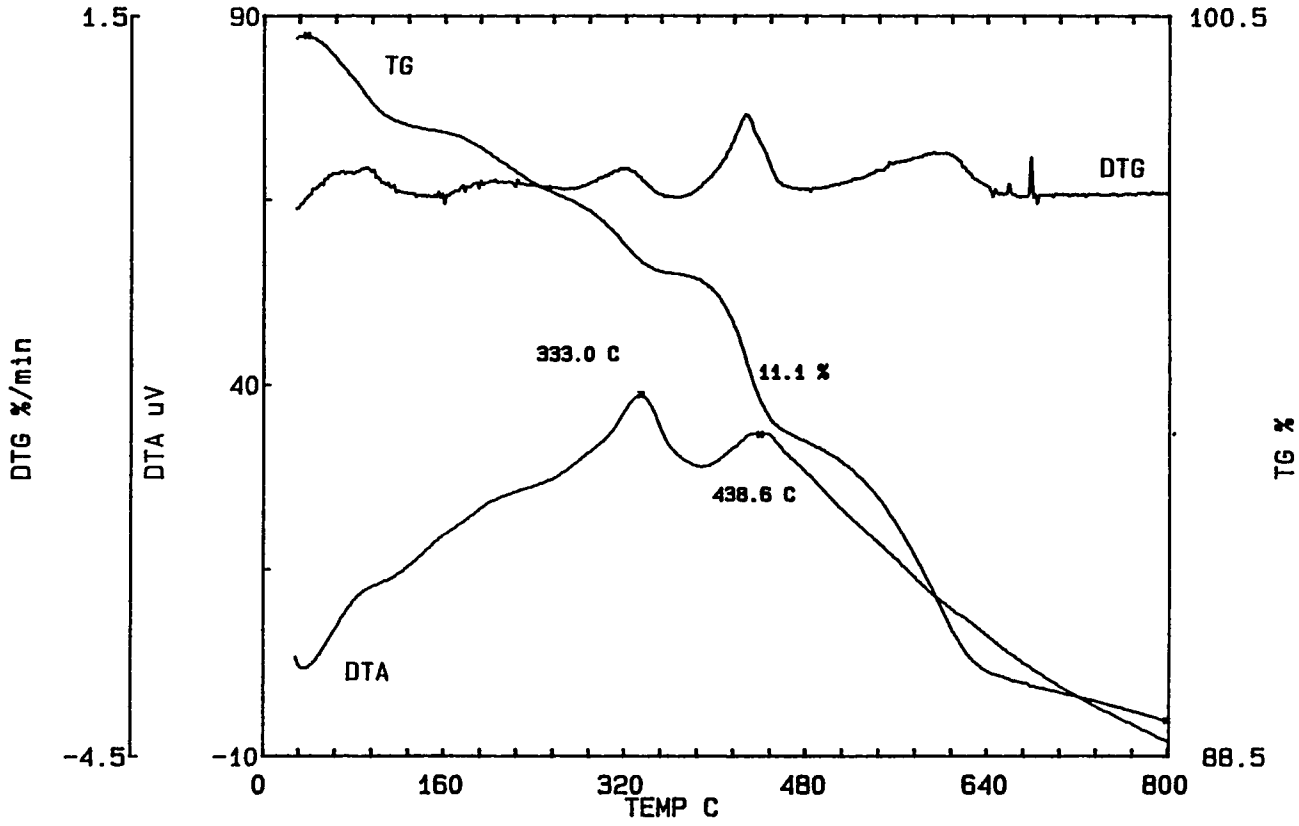

Figure 4. TG/DTA curve for $Na_{2y}Mo_6S_{8+y}(py)_x$

region. An XPS study on this material gave further evidence for retention of the Mo_6S_8 cluster unit, as shown in Table 1. Heating of the pyridine-deficient material to 500°C resulted in the formation of an amorphous black powder which possessed a featureless infrared spectrum. The Raman spectrum of this material (Figure 5) shows a broad peak centered at about 445 cm^{-1} which is indicative of the Mo_6S_8 unit. Molybdenum analyses (61.82% Mo) were lower than expected for the sodium Chevrel phases (Calc. for $Na_3Mo_6S_8$: Mo, 63.88%) or for the ternary sodium molybdenum sulfides (Calc. for $Na_2Mo_6S_9$: - Mo, 63.25%) which might indicate incomplete deligation. Further reaction of this material with lead powder will be found in the discussion of the reactions with ternary metals.

Similar TG/DTA curves are noted for the pyridine and 4-methylpyridine adducts (Figure 6). Both curves indicate complex deligation processes; however, the TG/DTA spectrum for the pyridine adduct shows a cessation of weight loss above 640°C, while the 4-methylpyridine curve exhibits weight loss over the entire region. The pyridine weight loss of 32.5% corresponds to the removal of 5.5 pyridine ligands and the 4-Mepy weight loss of 29.0% indicates the loss of about four 4-methylpyridine ligands. Each of these materials contains sodium, as discussed in Paper 1, which also leads to the potential of forming the sodium Chevrel phases. The resulting black products were not analyzed since, at these pyrolysis temperatures, MoS_2 should be formed.

Table 1. XPS data for deligation products[a]

	$Na_{2y}Mo_6S_{8+y}(py)_x$	$Na_{2y}Mo_6S_{8+y}(py)_x$ heated to 250°C	$Na_{2y}Mo_6S_{8+y}(py)_x$ reacted with Sn by heating to 700°C	$SnMo_6S_8$[b]
Mo $3d_{5/2}$	227.5	227.4	227.4	228.1
Mo $3d_{3/2}$	230.6	230.6	230.6	231.4
S 2s	225.4	225.3	225.3	-
S $2p_{3/2}$	161.1 br	161.0 br	161.4	161.7
S $2p_{1/2}$	-	-	162.6 sh	-

[a]values adjusted to C 1s = 284.6 eV; br = broad, sh = shoulder
[b] data from reference 6

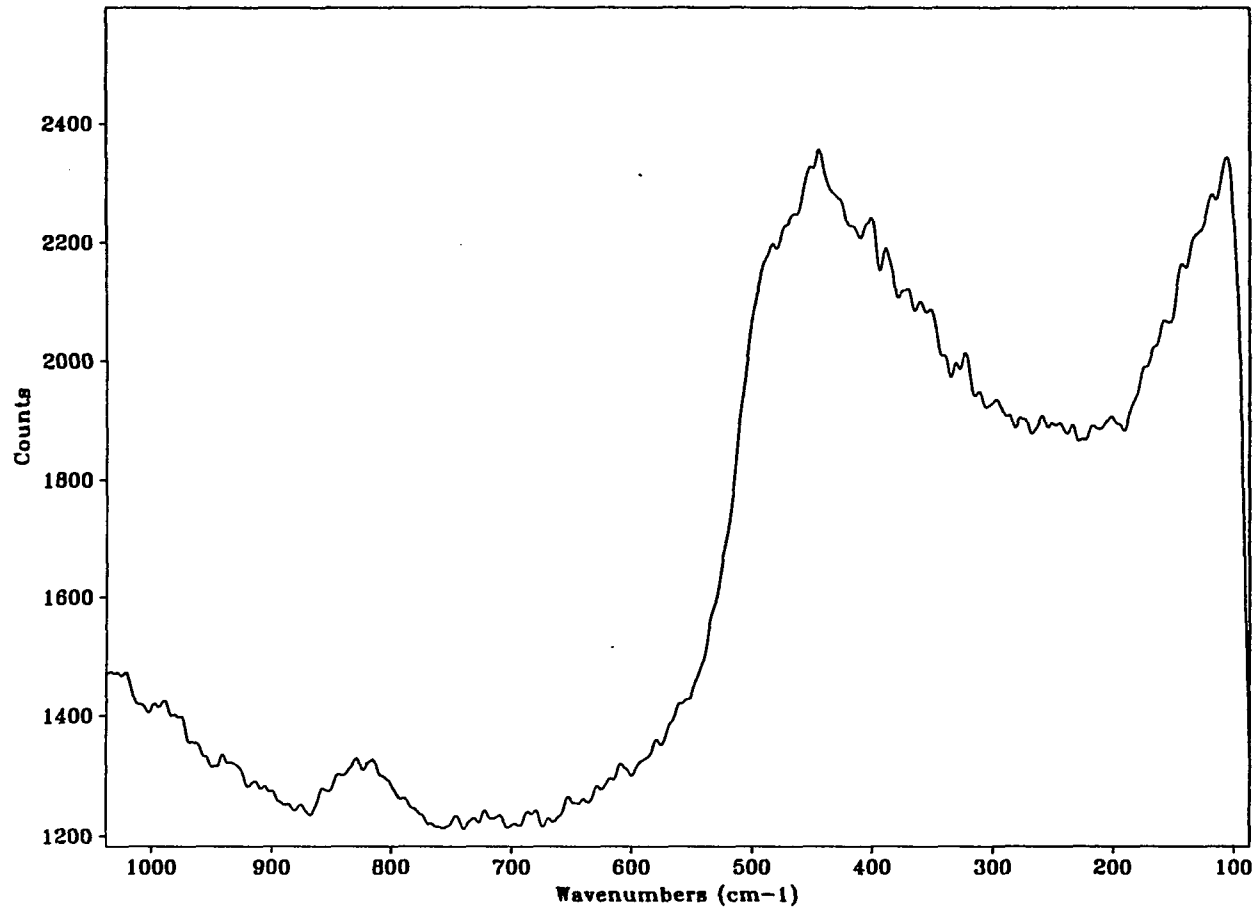

Figure 5. Raman spectrum for the product from the deligation of the pyridine-deficient compound at 500°C under dynamic vacuum

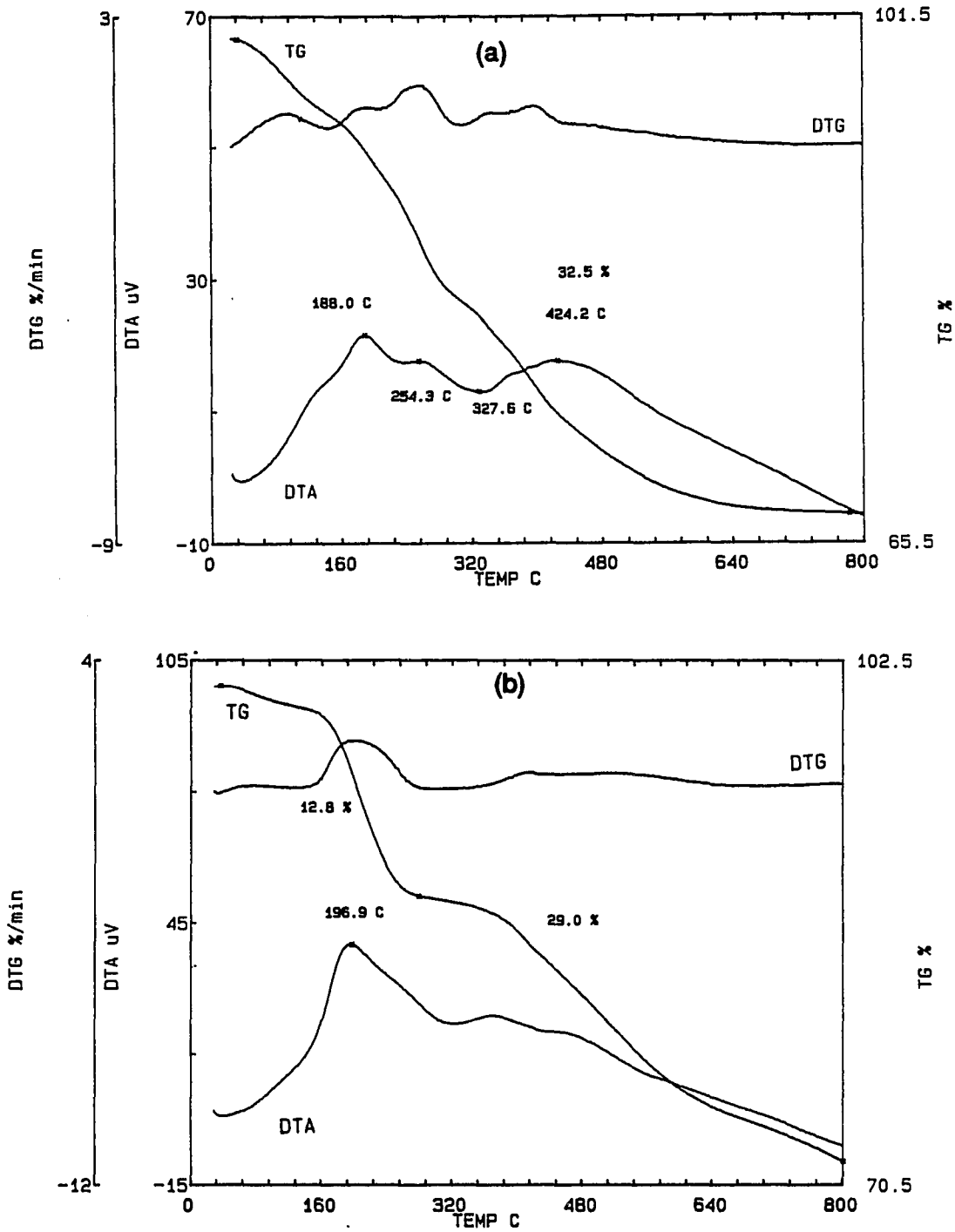

Figure 6. TG/DTA curves for $Mo_6S_8(py)_y$ (a) and $Mo_6S_8(4Mepy)_x$ (b)

Tetrahydrothiophene

TG/DTA curves for the crystalline adduct and ligand-deficient complex are shown in Figure 7. The crystalline adduct is quite stable up to about 160°C before undergoing a sharp weight loss of 18.6% (approx. 3 tht ligands). A stability range of about 70°C is present before the material undergoes a further two-step weight loss. The weight loss levels off at about 500°C and then indicates the start of a weight gain as the temperature nears 600°C. This weight gain can be understood as arising from the uptake of oxygen since the whitish TG/DTA product is MoO_3. This result obviously indicates that the system contains oxygen contaminants and leads to oxidation of the cluster unit. The total weight loss of 39.0% corresponds to complete removal of the 6 tetrahydrothiophene ligands.

The TG/DTA curve for the ligand-deficient tetrahydrothiophene complex exhibits ligand loss from the onset of the experiment to about 350°C where the weight loss levels off. The total weight loss of 19.9% corresponds to removal of almost all of the tht ligands (about 2.5 tht) and the resulting infrared spectrum shows only the presence of MoS_2 peaks at 384 and 469 cm^{-1}. The observed decomposition of the deligated Mo_6S_8 cluster units at 600°C would be expected since the metastable Mo_6S_8 is known to disproportionate at around 450-500°C.

Thermal deligation under vacuum was explored at 250°C for both the crystalline adduct and the ligand-deficient complexes. The resulting black products exhibited a very similar "metallic" appearance; however, powder x-ray diffraction showed both to be amorphous. The far-infrared spectra, shown in Figure 8, possibly exhibit weak,

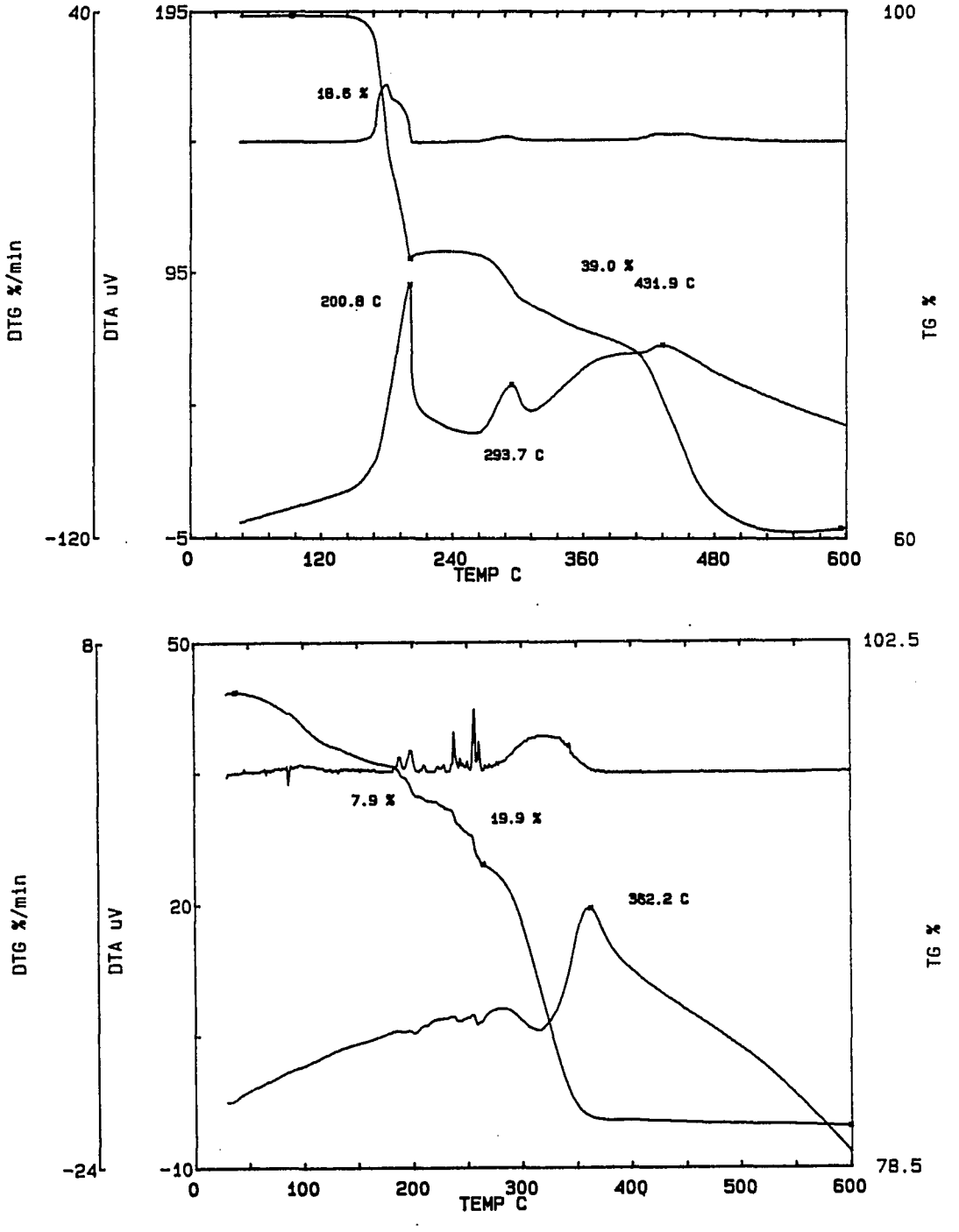

Figure 7. TG/DTA curves for the crystalline $Mo_6S_8(tht)_6$ (a) and the ligand-deficient $Mo_6S_8(tht)_y$ (b) complexes

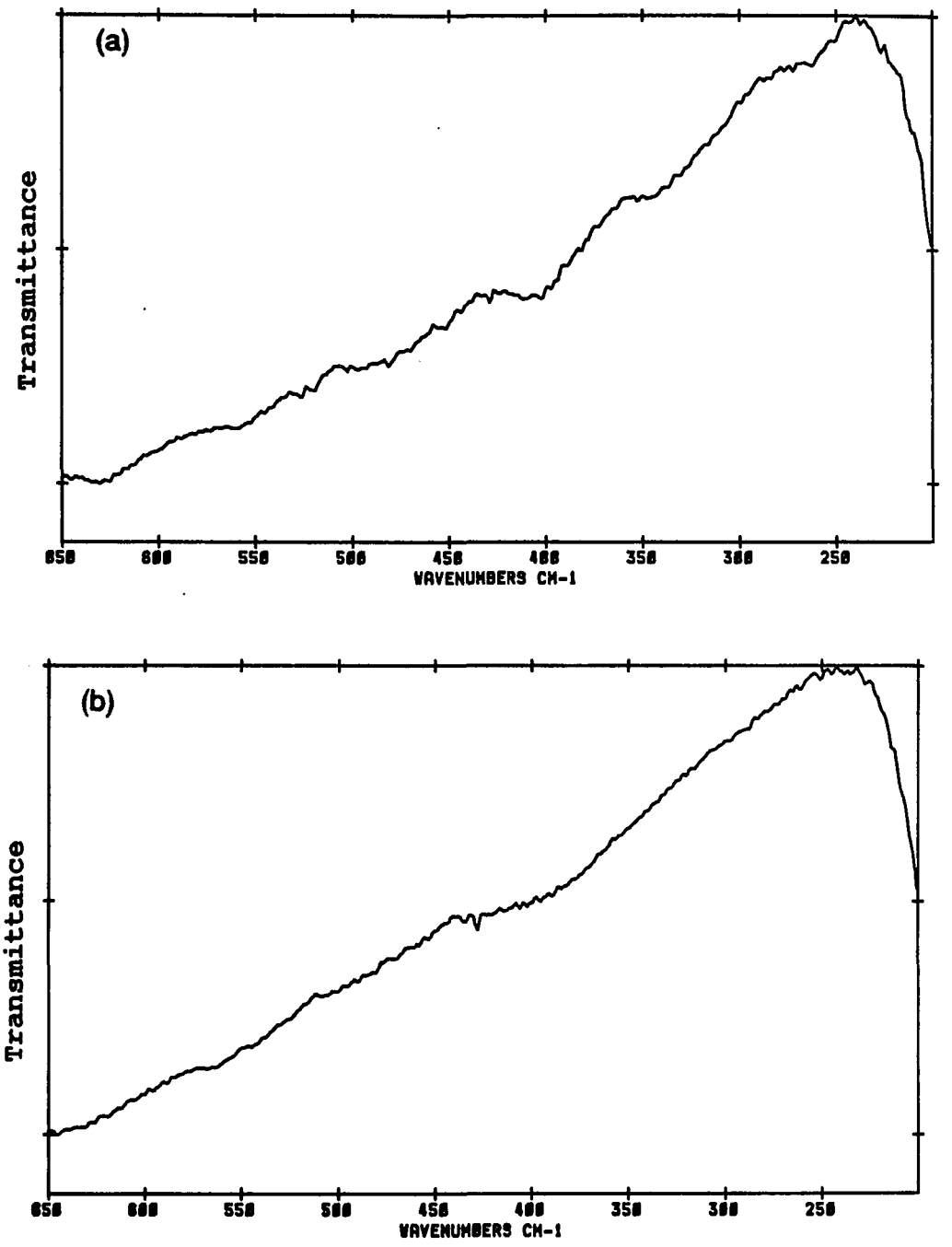

Figure 8. Infrared spectra (Nujol) for the deligation of the tetrahydrothiophene adducts at 250°C under dynamic vacuum. Products from reactions of the crystalline (a) and ligand-deficient complexes (b) are shown.

broad Mo-S bands about 400 cm^{-1}. The mid-IR region was featureless. Figure 9 shows the Raman spectra for these deligation products. These spectra indicate the presence of the Mo_6S_8 cluster unit as identified by the broad peak centered at about 445 cm^{-1}. The tetrahydrothiophene-deficient compound was also heated to 350°C under dynamic vacuum and resulted in the formation of an amorphous, black powder. The infrared spectrum was featureless, however, the Raman spectrum was virtually identical to that observed in Figure 9b.

In order to better understand the deligation process for the tetrahydrothiophene adducts, mass spectroscopy was employed. Studying the mass spectra of the products obtained upon heating would show whether intact tetrahydrothiophene was lost or if some fragmentation process was occurring which left coordinated sulfide or organo-sulfides bound to the molybdenum. Similar results were observed for both materials and showed that tetrahydrothiophene deligated intact, as indicated by the strong presence of the tht parent peak. Figure 10 shows the mass spectrum observed (with very slight variations that depended upon the temperature) for the crystalline tht adduct and a plot of the relative ion current versus scan number. Temperatures along the curve can be calculated and the plot can be understood as a thermal analysis curve showing the largest loss at about 240°C. The observed mass spectra all exhibited the same peaks for tht and fragments of this parent: 88 amu for C_4H_8S (tht), 60 for $C_2H_4S^+$ (largest peak), 54-56 for butene and butadiene, and 46 for CH_2S^+. As the temperature increased, less tht was observed (80 $\rightarrow$ 60 relative %), more HDS products (54-56 amu) were found; yet, very little H_2S was detected.

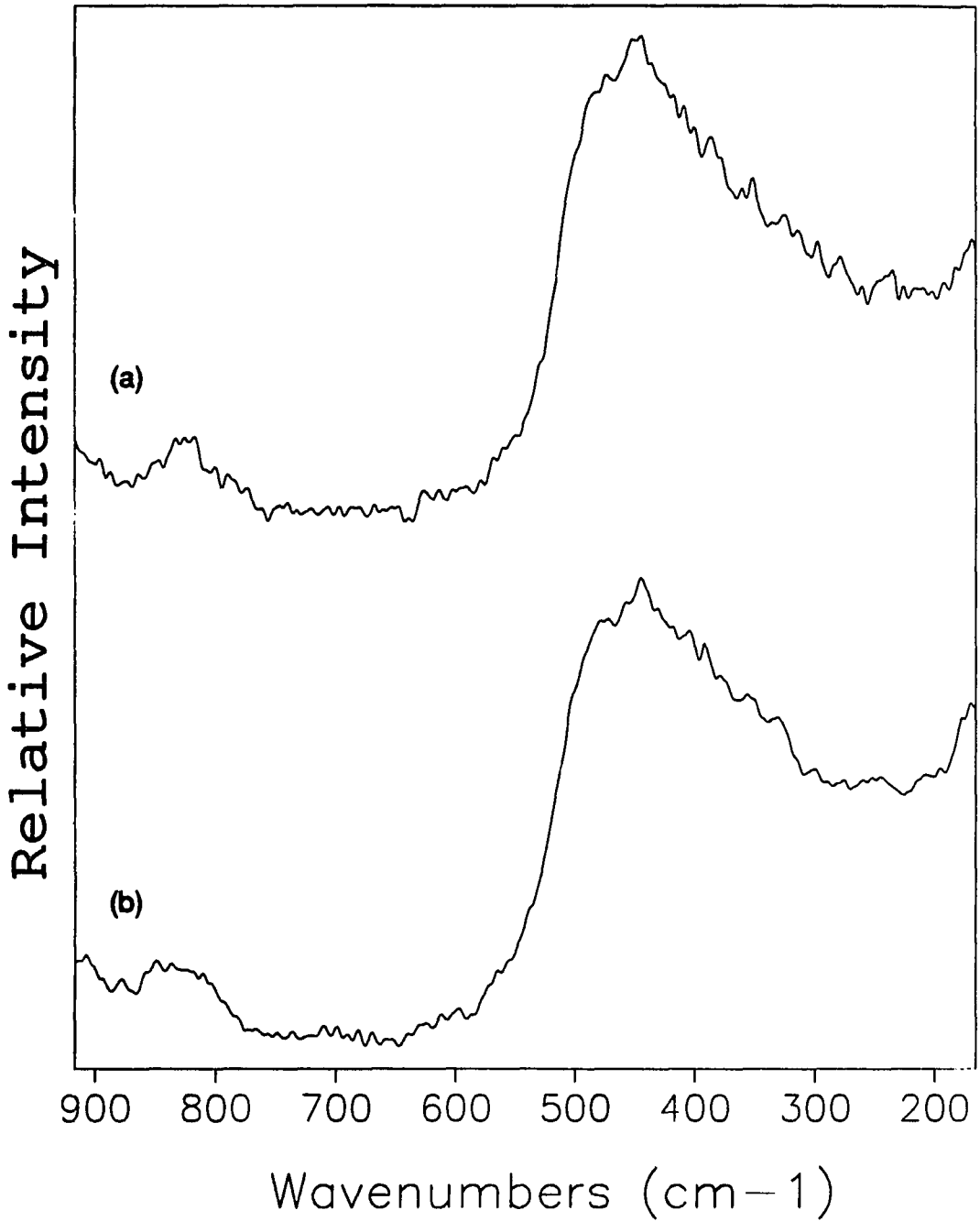

Figure 9. **Raman spectra for the deligation of the tetrahydrothiophene adducts at 250°C under dynamic vacuum. The products from reactions of the crystalline (a) and the ligand-deficient complexes (b) are shown.**

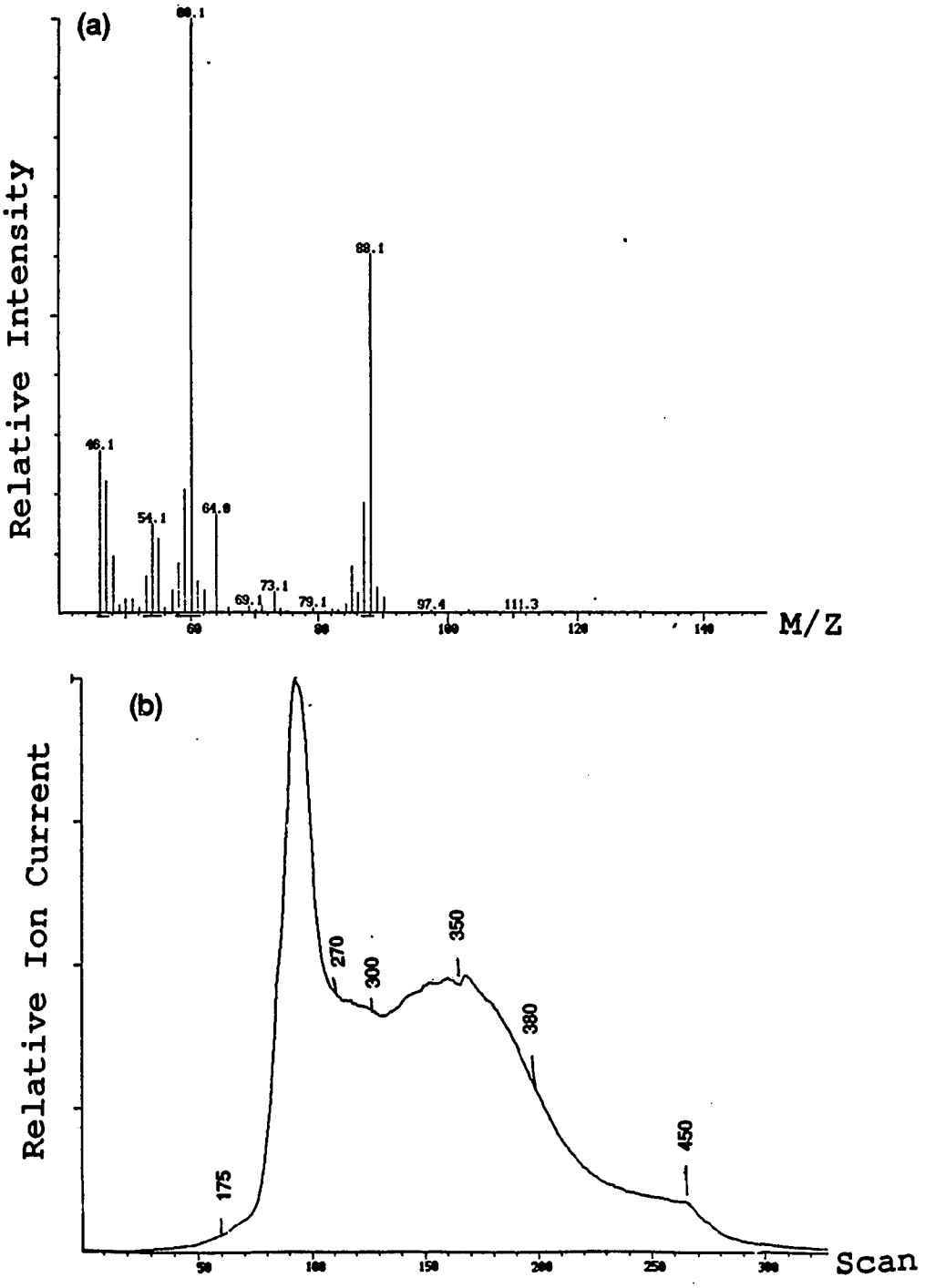

Figure 10. EI-mass spectrum for the tetrahydrothiophene adducts (a) showing the parent peak (M/Z 88) and fragmentation peaks. The plot of the relative ion current vs. scan number (b) provides a thermal analysis curve with the largest loss at about 240°C (temperatures on plot).

Similar mass spectra vs. temperature curves were observed for the ligand-deficient complex. A difference was noted in that there was very little change in relative intensities of the various peaks at the different temperatures of the measured spectra. Also, no larger fragments (M/Z 100-850) were detected in either experiment, which indicated that the Mo_6S_8 cluster unit remained intact up to about 500°C.

Pyrrolidine

The TG/DTA curve for the pyrrolidine adduct is shown in Figure 11. The curve exhibits initial stability from 25-100°C before undergoing a sharper weight loss over the region 120-300°C and then a steady loss through the rest of the experiment. The total weight loss of 23.6% corresponds to 4.4 pyrrolidine lost. The resulting product was an amorphous black powder.

Thermal deligation was explored *in vacuo* at 200, 350, and 450°C. Heating to 200°C produced an amorphous black powder with probable pyrrolidine peaks in the mid-infrared region and split peaks at 395 and 380 in the far-IR region. A similar black, amorphous powder was obtained by heating to 350°C. The far-infrared spectrum of this solid (Figure 12a) showed a broad Mo-S band centered at 395 cm^{-1}. Further heating of the same material to 450°C also resulted in a black, amorphous powder with two broad bands in the far-infrared spectrum at 486 and 402 cm^{-1} (Figure 12b). Molybdenum analyses of 63.91% Mo were found for the pyrrolidine adduct heated at 450°C which again is lower than the value calculated for Mo_6S_8 (69.18% Mo). This result indicates that some organic residue remains.

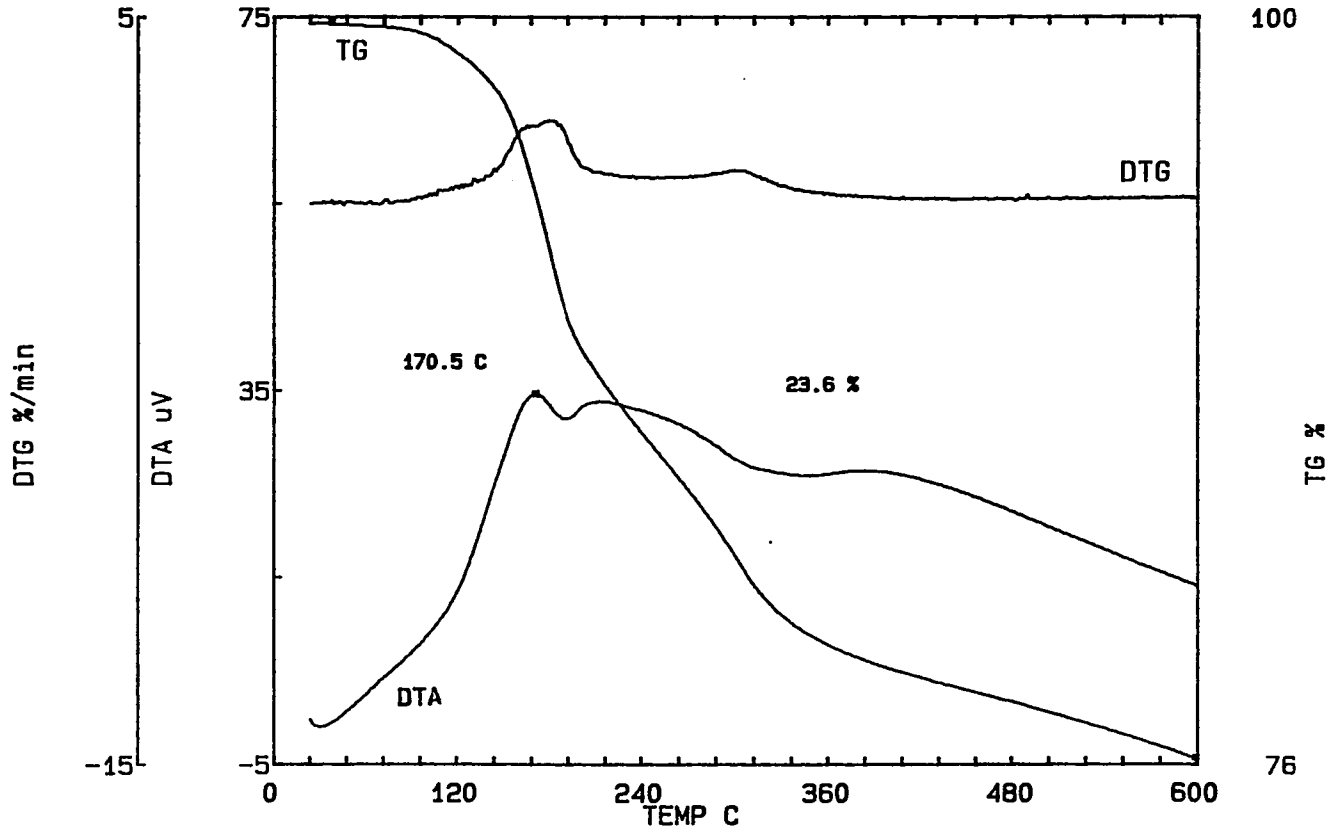

Figure 11. TG/DTA curve for the pyrrolidine adduct - $Mo_6S_8(pyrr)_x$

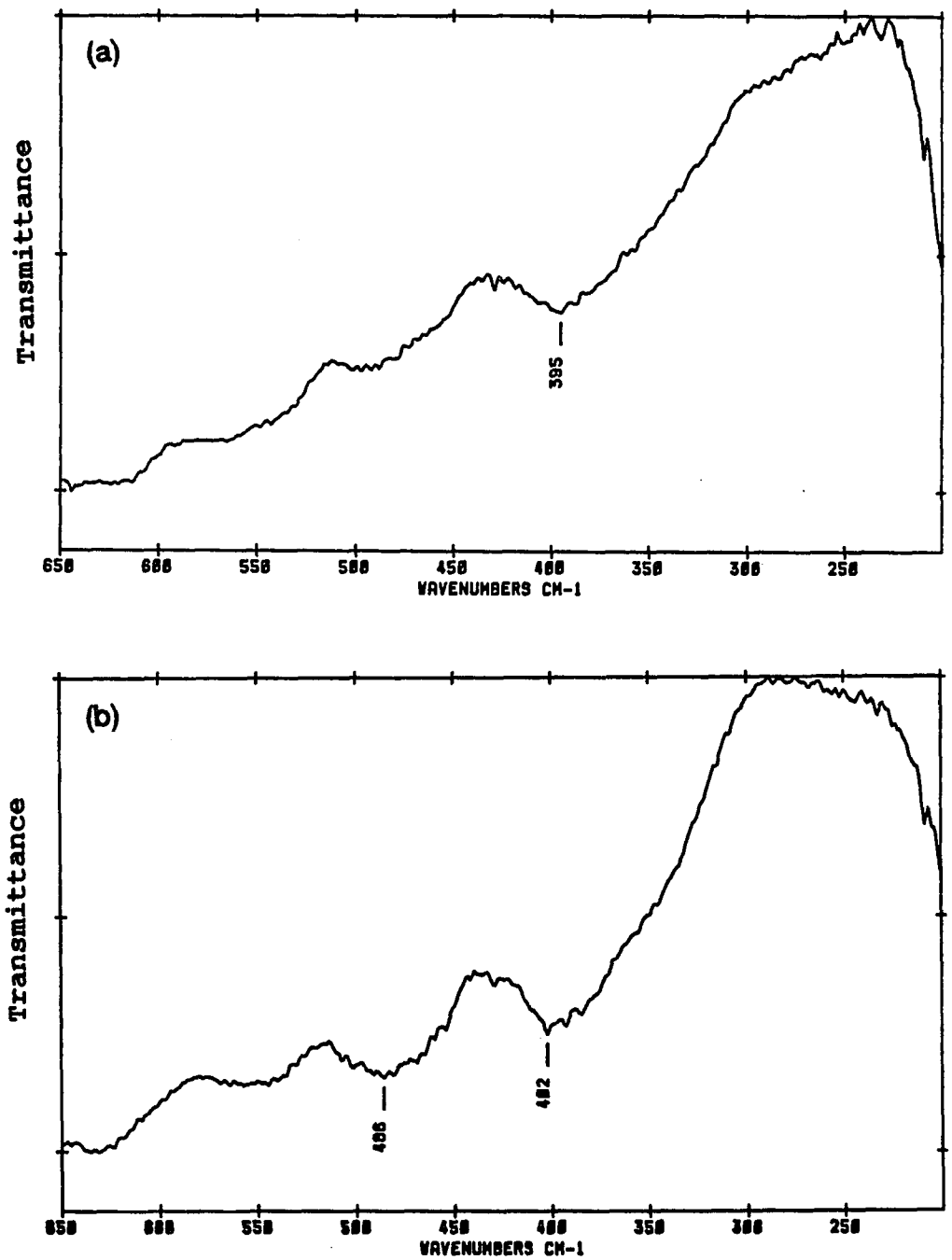

Figure 12. Infrared spectra (Nujol) for the products of the pyrrolidine adduct deligation at 350°C (a) and at 450°C (b) under dynamic vacuum

Piperidine

TG/DTA curves are shown for the crystalline adduct and the red powder resulting from the reaction of larger quantities of the propylamine adduct with neat piperidine (Figure 13). Both curves show almost immediate weight loss as would be expected considering that about 7 "free" piperidine per cluster reside in the lattice. The crystalline adduct exhibits a sharp loss over the region 30-100°C (25.7% - about 6 pip). A slower weight loss of 6.7% (approx. 1.5 pip) is found from 100-160°C and then continuous weight loss is seen over the rest of the region. The total weight loss of 56.5% corresponds to all 13 piperidine being removed. The resulting product from the TG/DTA experiment was a brown/black powder.

The TG/DTA of the red solid shows a rapid weight loss of 27.3% (about 6 piperidine) from 30-100°C before slowly losing more weight over the rest of the region. The total weight loss of 40.3% only corresponded to the removal of 9 piperidine ligands and probably indicated that some piperidine must still be present in the sample. The resulting product was a grey/black powder. Earlier TG/DTA curves exhibited a brief plateau region from 120-140°C.

Based on the large initial loss of piperidine, attempts were made to form this intermediate by heating of the adduct at 100°C under dynamic vacuum. The product of this reaction was an amorphous brown powder whose infrared spectrum showed the presence of coordinated piperidine and a shifting of the Mo-S peak from 382 to 387 cm^{-1} (Figure 14a). The solid was found to be soluble in toluene; therefore, a NMR spectrum was obtained in deuterated benzene. The material was not as soluble

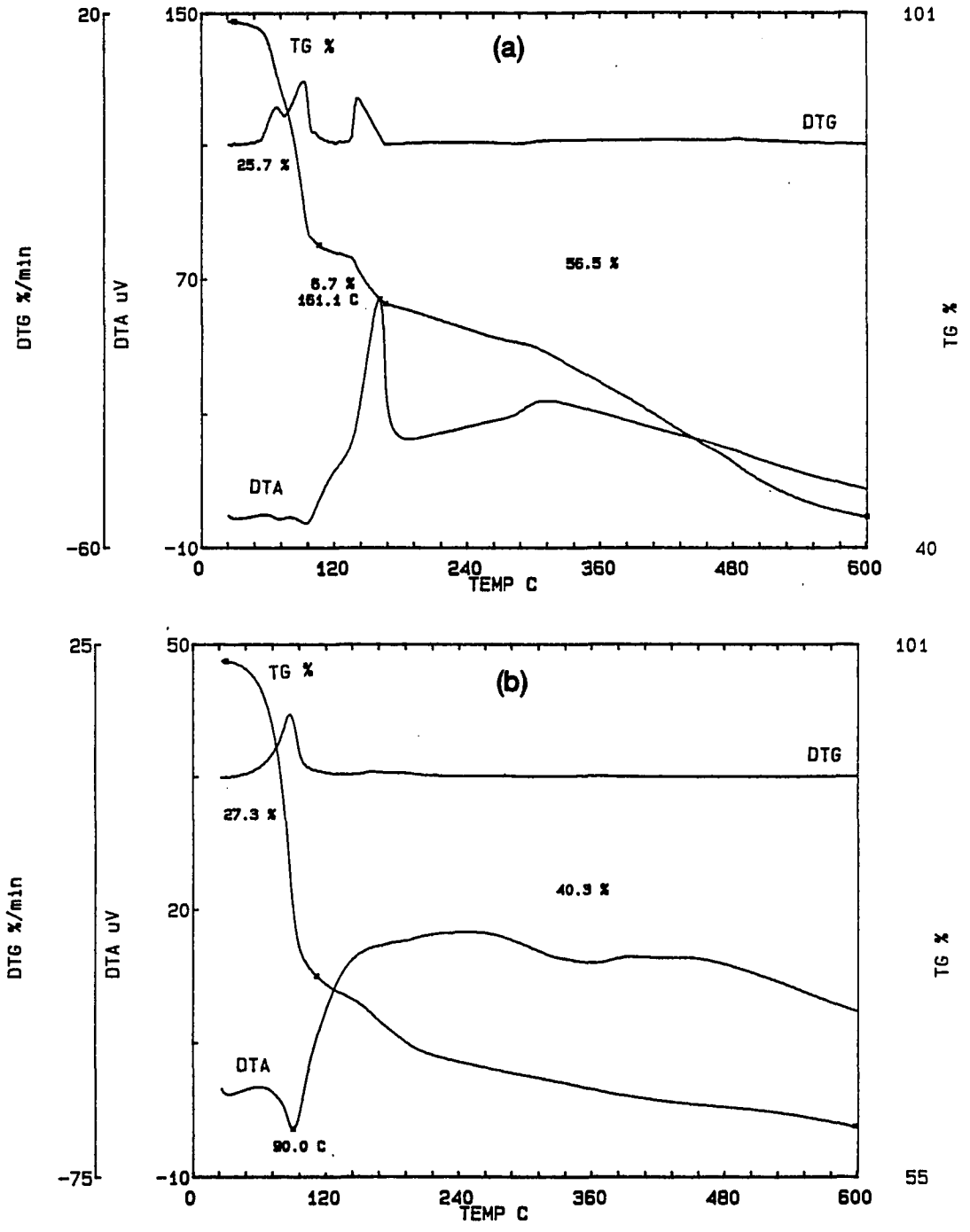

Figure 13. TG/DTA curves for the crystalline $Mo_6S_8(pip)_6 \cdot 7pip$ complex (a) and the red $Mo_6S_8(pip)_x$ product (b) from larger reaction batches

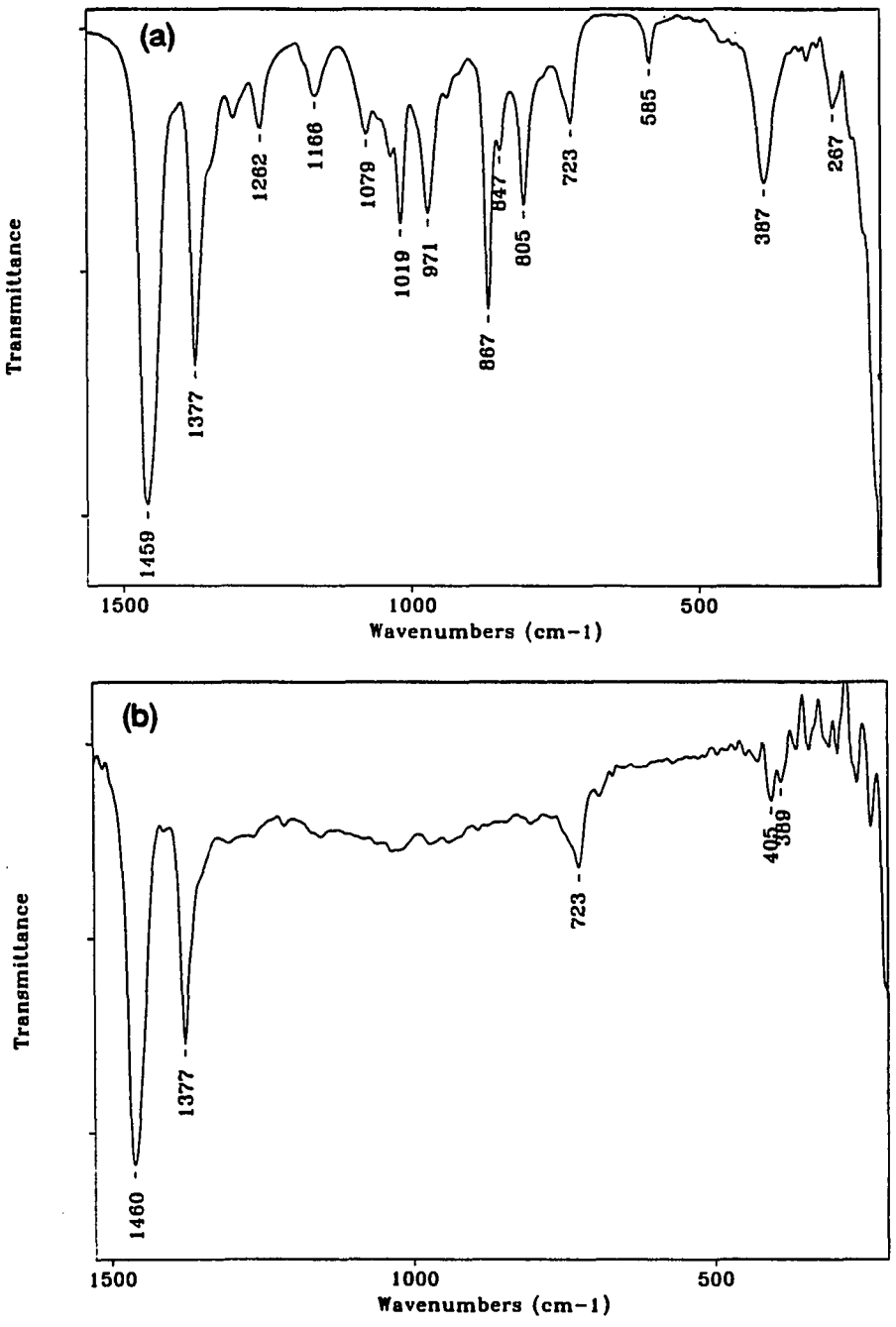

Figure 14. Infrared spectra (Nujol) for the deligation of the piperidine adduct at 100°C (a) and at 300°C (b) by heating under dynamic vacuum

as before the heating, but, the NMR spectrum showed bands identifiable as both coordinated and free piperidine (as discussed in Paper 1). The bands for free piperidine were much weaker than before; however, their presence indicated that the heating of this material to 100°C for 1 day under dynamic vacuum caused only partial removal of the "free" piperidine trapped in the lattice. This heated material dissolved in neat piperidine and resulted in the formation of a pinkish-red solution from which small crystals of the adduct could be grown.

Heating of the piperidine adduct to 300°C was also explored. During heating at 300°C, a pressure loss due to the formation of gaseous products was observed. The thermolysis product was found to be an amorphous black powder whose infrared spectrum is shown in Figure 14b. The infrared spectrum possibly indicates the presence of the Mo_6S_8 cluster unit with weak, split Mo-S bands at 389 and 405 cm^{-1}. Attempts to dissolve this material in either neat piperidine or benzene (for NMR study) showed that it was insoluble. A Raman spectrum was obtained for this product which also confirmed that the Mo_6S_8 unit remained (Figure 15).

Reactions with Ternary Metals

The pyridine-deficient compound was reacted with tin and iron powder in an attempt to prepare the ternary Chevrel phases. The reactions proceeded initially under dynamic vacuum at 700°C to remove the ligated pyridine and resulted in amorphous black or black/grey powders. The XPS data for the reaction of excess

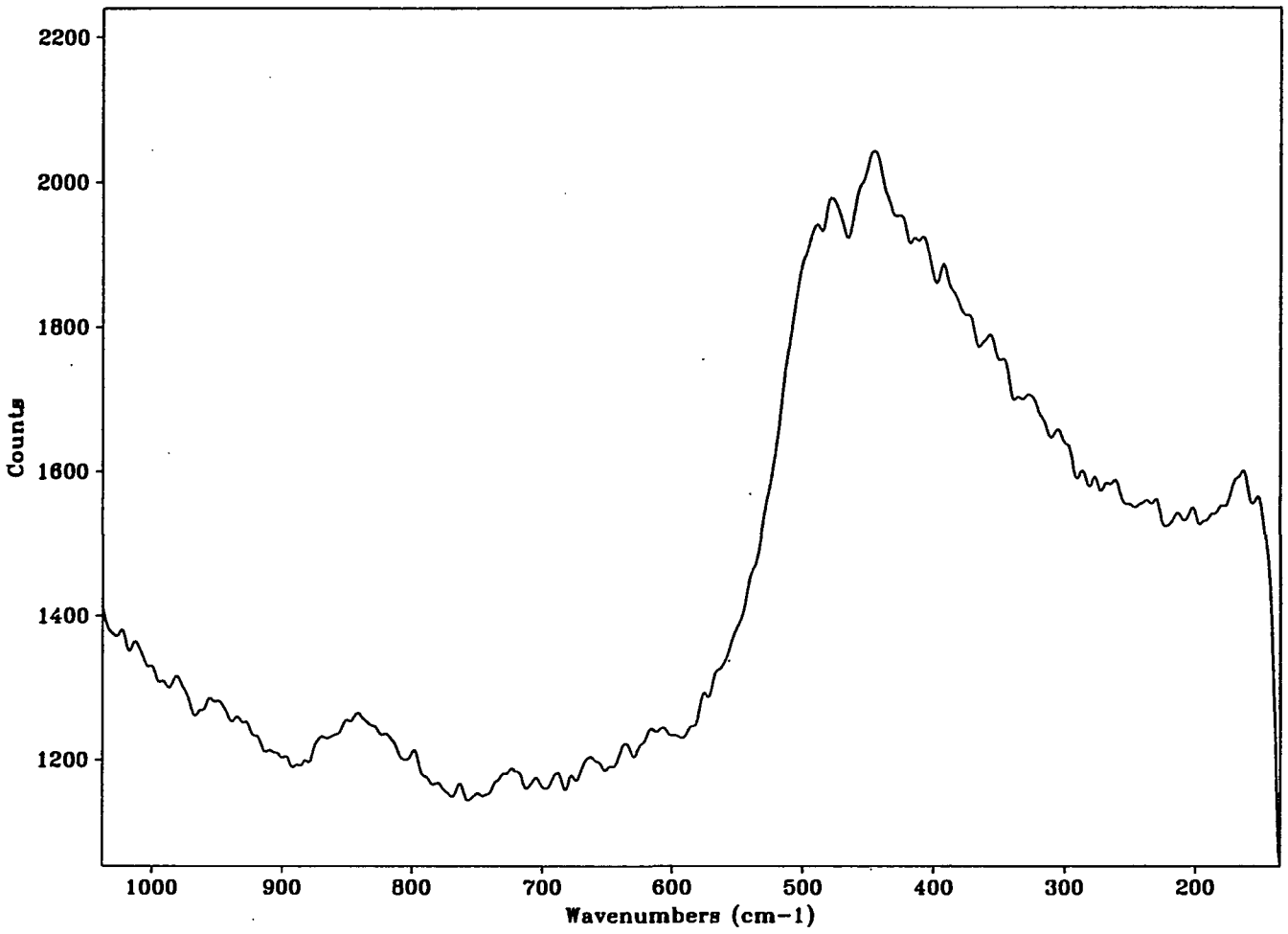

Figure 15. Raman spectrum for the product from the deligation of the piperidine adduct at 300°C under dynamic vacuum

tin powder with the pyridine-deficient compound is shown in Table 1. The observed molybdenum and sulfur binding energies indicate that the Mo_6S_8 unit is retained - no disproportionation to MoS_2 and molybdenum metal. However, the binding energies of this reaction product are shifted from those observed for the tin Chevrel phase and probably indicate this material is some intermediate phase. This conclusion is further supported by the amorphous nature of the product.

The observation that these reactions led to amorphous products prompted further heating of the solids to 900°C in a sealed tube. The powder x-ray diffraction patterns of the resulting products showed lines indicative of the desired ternary Chevrel phases, as well as the MoS_2 disproportionation product.

An alternative method was to deligate the pyridine-deficient compound first by heating to 500°C under dynamic vacuum and then reacting this material with the ternary metal powders. The reactions which were explored involved heating with lead powder and resulted in the formation of $PbMo_6S_8$, MoS_2, and Pb phases as identified by the powder x-ray diffraction patterns.

Reactions with Ammonia Gas

The deligation of the propylamine adduct was explored in the presence of flowing ammonia gas and resulted in a black, amorphous powder. The infrared and Raman spectra for the deligation reaction at 150°C are shown in Figure 16. The spectra indicate that the Mo_6S_8 cluster unit is retained as evidenced by the Mo-S band at 448 cm^{-1} in the Raman spectrum and the split Mo-S bands at 381 and 367 cm^{-1} in the

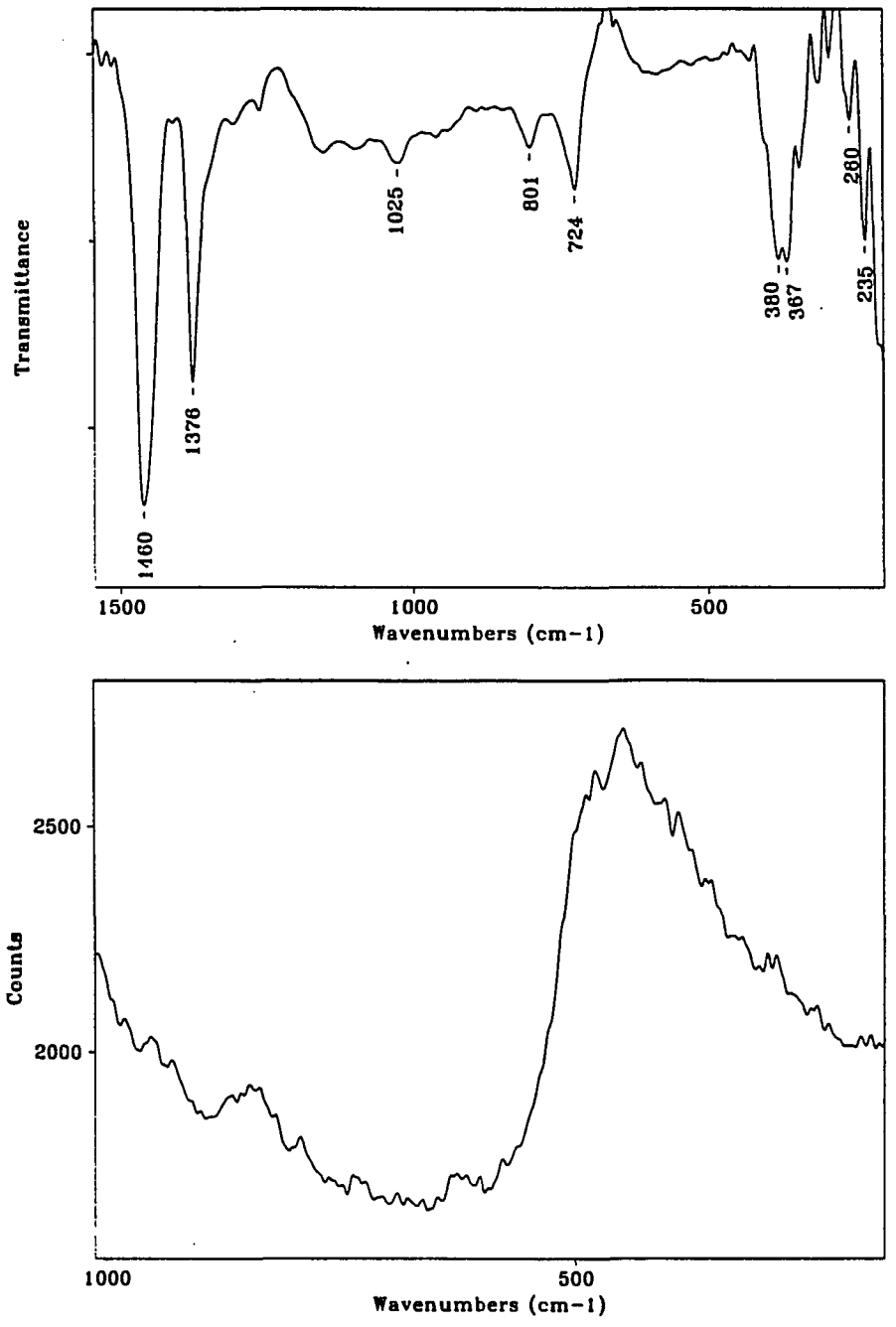

Figure 16. Infrared (a) and Raman (b) spectra for the product from the deligation of the propylamine adduct at 150°C in flowing ammonia

infrared spectrum. The bands in the mid-IR region are due exclusively to the presence of contaminating stopcock grease; no peaks identifiable as propylamine bands are found. Likewise, no bands for coordinated NH_3 were detected. Similar results were obtained for the reaction at 200°C. The XPS spectrum (Figure 17) shows binding energy values of 227.6 (Mo $3d_{5/2}$), 230.7 (Mo $3d_{3/2}$), 225.3 (S 2s), 160.8 (S $2p_{3/2}$), and 161.8 eV (S $2p_{1/2}$). The Mo $3d_{5/2}$ value is close to that found for Mo_6S_8 of 227.5 eV (all data corrected for C1s).[19] The spectrum also exhibits higher Mo binding energy peaks indicative of surface oxide contamination.

A comparison between heating under dynamic vacuum and in flowing ammonia at 150°C for 4 hours was made. As discussed previously, the reaction in flowing ammonia resulted in an infrared spectrum with no detectable propylamine bands. However, the infrared spectrum of the sample heated at 150°C under dynamic vacuum showed distinctive propylamine bands. These observations further indicated that heating under flowing ammonia does aid in the deligation of the coordinated propylamine ligands.

Deligation under flowing ammonia gas was also explored for the pyrrolidine and piperidine adducts. Heating of the pyrrolidine adduct to 250°C for 4 hours resulted in the formation of a black, amorphous powder. The infrared spectrum (shown in Figure 18a) shows only bands attributable to stopcock grease in the mid-IR region and a distinct Mo-S band at 386 cm^{-1}. Heating of the piperidine adduct to 200°C in ammonia resulted in incomplete deligation, as indicated by the presence of coordinated piperidine bands in the mid-infrared spectrum. However, heating to

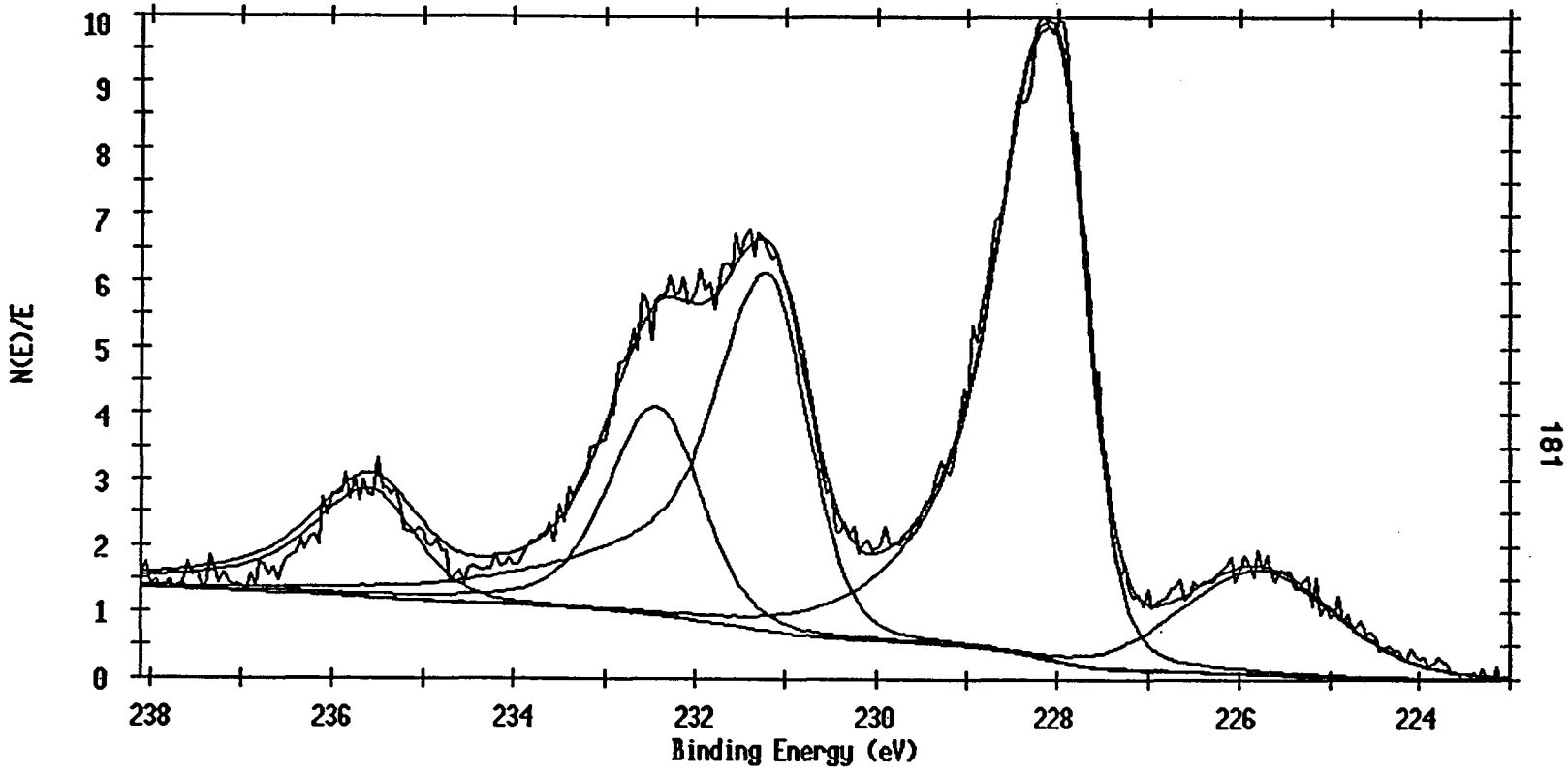

Figure 17. Uncorrected XPS spectrum showing Mo 3d and S 2s bands for the product from the deligation of the propylamine adduct at 150°C in flowing ammonia. Oxide contamination is evidenced by the presence of the bands at higher binding energies.

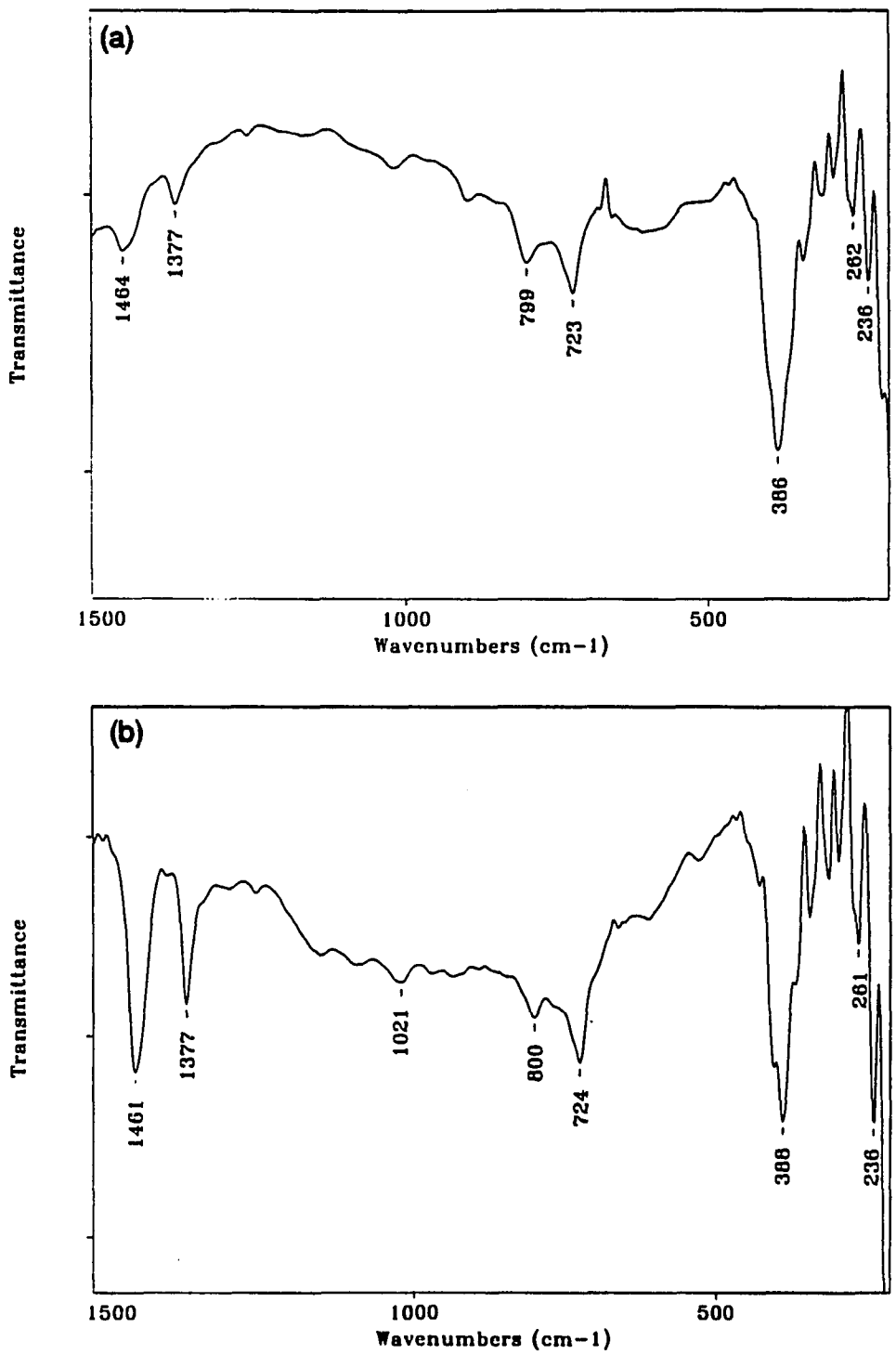

Figure 18. Infrared spectra (Nujol) for the deligation of the pyrrolidine adduct at 250°C (a) and the piperidine adduct at 300°C (b) by heating in the presence of flowing ammonia

300°C produced an amorphous black solid with a featureless mid-IR and a Mo-S band at 388 cm^{-1} in the far-infrared region, as shown in Figure 18b. Raman spectra (Figure 19) for the deligation of the pyrrolidine and piperidine adducts in flowing ammonia show the presence of a broad peak centered at about 445 cm^{-1} which is indicative of the Mo_6S_8 cluster unit. The molybdenum analysis on the piperidine adduct heated to 300°C, 58.06%, indicated that some type of organic or nitride residue remained in this material.

Solution Deligation Studies

Reactions with trifluoromethanesulfonic acid

The propylamine adduct was reacted with trifluoromethanesulfonic acid in methanol in an attempt to protonate the amine and thus make it a better leaving group. Reactions resulted in the production of an amorphous black solid whose far infrared spectrum is shown in Figure 20a. The mid-IR region is nearly featureless except for the band observed at 631 cm^{-1}. The far-IR region shows the same band at 631 cm^{-1}, as well as, a broad Mo-S stretching mode at 400 cm^{-1}. The coordination of the triflate anion ($CF_3SO_3^-$) was previously observed in the deligation attempts with the tungsten cluster complex $W_6S_8(py)_6$, yet, the presence of triflate anion cannot be confirmed by this spectrum. Further reaction of this material with pyridine in an attempt to prepare the pyridine-ligated material produced a spectrum that showed both coordinated pyridine and triflate. Therefore, work was discontinued in attempting to deprotonate the cluster with trifluoromethanesulfonic acid.

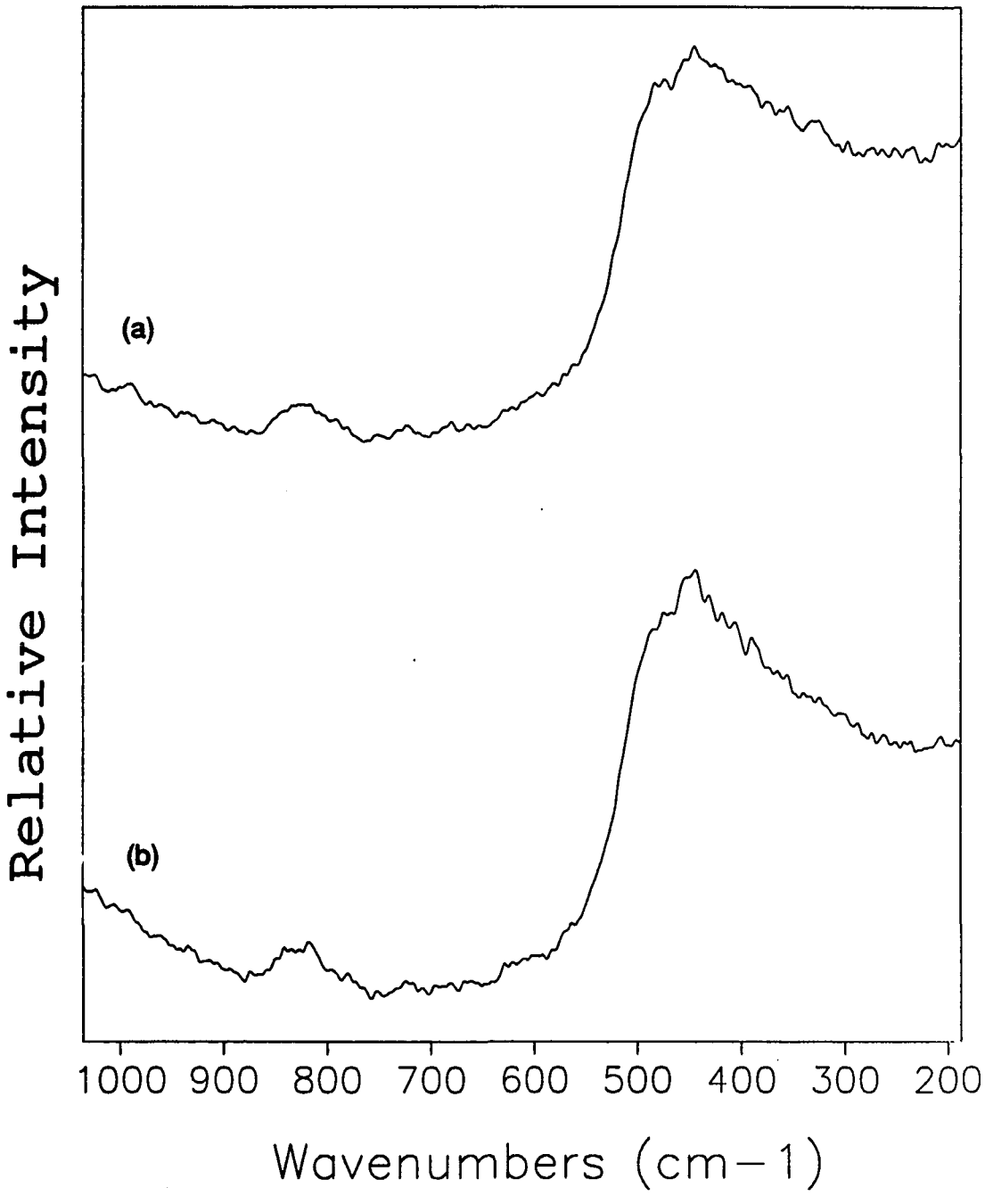

Figure 19. Raman spectra for the deligation of the pyrrolidine adduct at 250°C (a) and the piperidine adduct at 300°C (b) by heating in the presence of flowing ammonia

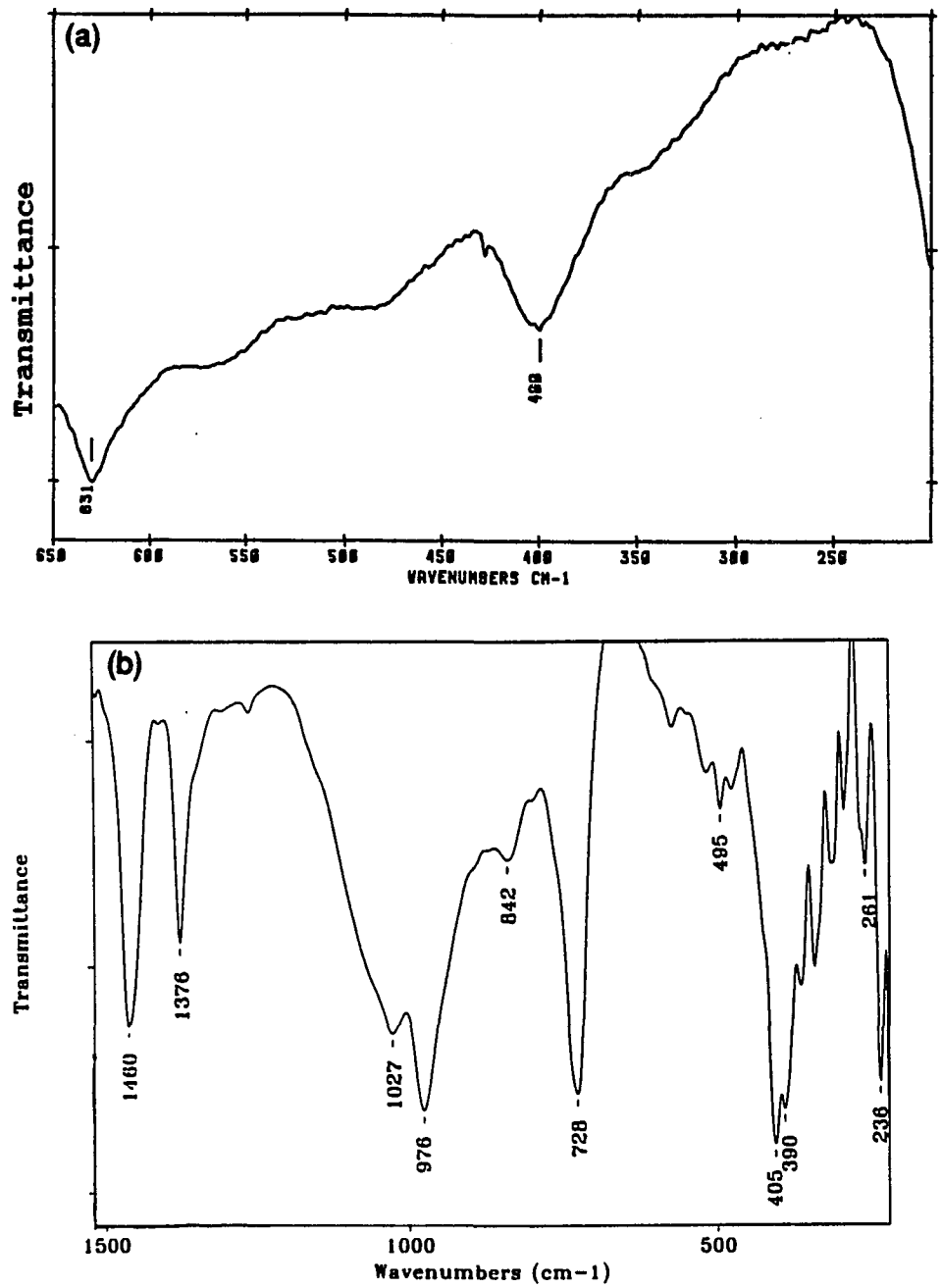

Figure 20. Infrared spectra (Nujol) for the solution deligation of the propylamine adduct with trifluoromethanesulfonic acid (a) and with tetrafluoroboric acid-diethyl ether complex (b) in methanol

Reactions with tetrafluoroboric acid-diethyl ether complex

Similar deprotonation reactions of the propylamine adduct were attempted with $HBF_4 \cdot Et_2O$ in both diethyl ether and methanol. The reactions in diethyl ether resulted in products that showed distinct bands for BF_3 or BF_4^-. The reactions in methanol resulted in black solids whose infrared spectrum is shown in Figure 20b. This spectrum exhibits two distinct bands at 1027 and 976 cm^{-1} which probably result from coordinated methanol. An infrared spectrum of the methanol filtrate showed bands attributable to $PrNH_3^+BF_4^-$ which indicated the acid was succeeding in deprotonating the ligand. Elemental analyses on the black solid indicated the presence of carbon fragments (3.92% C, 1.41% H). The hydrogen to carbon ratio of 4.3:1 is reasonable for methanol; however, comparison of the C:Mo_6 ratio of 3.4:1 to the observed elemental percentages suggests possible coordination of fluoroborate. Currently, though, there is no evidence for any remaining BF_3 or BF_4^-.

CONCLUSIONS

This paper describes the deligation of coordinated ligands from the molecular $Mo_6S_8L_8$ cluster complexes. A variety of cluster complexes were studied under the conditions of thermal deligation, reactions with ternary metals, reactions in flowing ammonia gas, and solution reactions. The emphasis was on the deligation of the nitrogen-donor complexes since crystallographic structure determinations have indicated that these ligands show the weakest bonding to the Mo_6S_8 cluster.

Thermal analysis by TG/DTA provided initial temperature ranges where deligation was occurring; however, the upper heating limit was fixed at about 450-500°C since Mo_6S_8 disproportionates to Mo and MoS_2 at these temperatures. Direct heating under dynamic vacuum for all the complexes resulted in incomplete deligation, as evidenced by low molybdenum analyses. It was reasoned that ligand fragmentation had occurred at temperatures above 300°C, since a noticeable increase in pressure was observed at these temperatures. This pressure increase must result from the production of volatile gases like methane or hydrogen which would not have condensed in the liquid nitrogen trap. The pyridine-deficient compound could be heated to at least 500°C without cluster degradation as evidenced by the Raman spectrum. This extra stabilization must result from the presence of the ternary sodium cations.

Reactions of the pyridine-deficient compound with the ternary metals tin and lead were attempted to prepare the corresponding Chevrel phases. An amorphous solid

resulted from the heating with tin to 700°C. The XPS spectrum indicated that the material was Chevrel phase-like, but not $SnMo_6S_8$. Also, the spectrum showed that this product had not disproportionated to form MoS_2. The tin Chevrel phase and MoS_2 could by produced by further heating to 900°C. Similar reactions were evidenced with lead metal and produced the lead Chevrel phase, lead, and MoS_2. These reactions are the first which show that the molecular Mo_6S_8 cluster complexes can be reacted to form the desired Chevrel phases.

Thermolysis reactions in the presence of flowing ammonia gas have resulted in what appears to be complete deligation of the propylamine adduct at much lower temperatures than are observed by direct heating under dynamic vacuum. The infrared spectrum for heating at 150°C indicated propylamine deligation in the ammonia reaction, while distinct propylamine bands were observed for the sample heated *in vacuo*. Similar reactions at higher temperatures for the pyrrolidine and piperidine adducts have not resulted in complete deligation.

Attempts at deligation were explored by solution reactions with strong acids in an attempt to protonate the propylamine ligand and thus make it a better leaving group. Reactions in trifluoromethanesulfonic acid led to removal of the ligand; however, coordination of the triflate anion was observed. Reactions with the tetrafluoroboric acid/diethyl ether complex in diethyl ether led to coordination of BF_3 or BF_4^-. Further reactions in methanol removed the propylamine ligand and the infrared spectra showed only methanol coordination, yet the analyses do not clearly indicate complete deligation.

Areas of further study in the deligation of the $Mo_6S_8L_6$ cluster complexes include better characterization of the reaction products through further elemental analyses and techniques like EXAFS, XPS and Raman spectroscopy. Further examination is needed on the reactions of the cluster complexes with ammonia gas and in the methanol solution with tetrafluoroboric acid/diethyl ether complex. Initial study has indicated that these reactions may lead to nearly complete deligation, however, further proof is necessary.

Further study of the higher temperature heating with ternary metals should be explored, especially reactions in a reducing hydrogen atmosphere. Interesting metals to study include cobalt, nickel, copper, and zinc. Likewise, other types of intercalation reactions should be studied, such as reactions with R_2Zn, $R_4(Pb,Sn)$, n-BuLi, Zn(Hg), Na(Hg), CaH_2, and metal halides like MX_2 (M=Pb,Cu, Sn, Zn) and LiX.

REFERENCES

1. Yvon, K. Current Topics in Materials Science, 1st ed., Kaldis, E., Ed.; North-Holland: New York, 1978; Vol. 3, Ch. 2.

2. Chevrel, R.; Sergent, M. Topics in Current Physics, Fischer, Ø. and Maple, M.B., Eds.; Springer-Verlag: Heidelberg, 1982; Vol. 32, Ch. 2.

3. Schöllhorn, R.; Kümpers, M.; Besenhard, J.O. *Mater. Res. Bull.* 1977, *12*, 781.

4. Mulhern, P.J.; Haering, R.R. *Can. J. Phys.* 1984, *62*, 527.

5. McCarty, K.F.; Schrader, G.L. *Ind. Eng. Chem. Prod. Res. Dev.* 1984, *23*, 519.

6. McCarty, K.F.; Anderegg, J.W.; Schrader, G.L. *J. Catal.* 1985, *93*, 375.

7. Nanjundaswamy, K.S.; Vasanthacharya, N.Y.; Gopalakrishnan, J.; Rao, C.N.R. *Inorg. Chem.* 1987, *26*, 4286.

8. Rabiller-Baudry, M.; Sergent, M.; Chevrel, R. *Mater. Res. Bull.* 1991, *26*, 519.

9. Spink, D.A. PhD. Dissertation, Iowa State University, Ames, IA, 1989.

10. McCarley, R.E.; Laughlin, S.K.; Spink, D.A.; Hur, N. Abstract of Papers, 3rd Chemical Congress of North America, Toronto, Ontario (Canada), 1988.

11. McCarley, R.E.; Zhang, X.; Spink, D.A.; Hur, N. Abstracts of Papers, 199th National Meeting of the American Chemical Society; Boston, MA, 1990.

12. McCarley, R.E.; Hollingshead, J.A.; Hilsenbeck, S.J.; Zhang, X. Abstracts of Papers, 204th National Meeting of the American Chemical Society; Washington, D.C., 1992.

13. Zhang, X. PhD. Dissertation, Iowa State University, Ames, IA, 1991.

14. Elwell, W.T.; Wood, D.F. Analytical Chemistry of Molybdenum and Tungsten; Pergamon Press: New York, 1971.

15. Oneida Research Services, Inc., Whitesboro, New York.

16. Chevrel, R.; Sergent, M.; Prigent, J. *Mater. Res. Bull.* 1974, *9*, 1487.

17. Schöllhorn, R.; Kümpers, M.; Plorin, D. *J. Less-Common Metals* **1978**, *58*, 55.

18. Aleshin, V.G.; Kharlamov, A.I. *Russ. J. Inorg. Chem.* **1980**, *25*, 1128.

19. Müller, A.; Sarkar, S.; Dommröse, A.; Filgueira, R. *Z. Naturforsch* **1980**, *35B*, 1592.

PAPER 3.

NOVEL PREPARATIVE ROUTES TO TERNARY MOLYBDENUM SULFIDES VIA SODIUM MOLYBDENUM SULFIDE

INTRODUCTION

Ternary molybdenum chalcogenides of the general formula $M_xMo_6Y_8$ (M=ternary metal cation; Y=chalcogenide), known as Chevrel phases, have been extensively studied and have been shown to possess interesting physical and chemical properties.[1-4] The most recent focus has been on the catalytic properties of the Chevrel phases, especially the development of these compounds as heterogeneous catalysts for hydrodesulfurization (HDS).[5-9]

The importance of this catalytic process is evidenced by the fact that over 60 million barrels of oil per day undergo HDS before further processing.[10] The typical HDS catalyst is produced from molybdenum oxides with a promoter metal such as cobalt supported on high surface area alumina (γ-Al_2O_3).[11] Recently, a number of Chevrel phase compounds have been shown to possess higher HDS activities than the commonly used Co-Mo-S catalysts. The Chevrel phases were also found to be more selective catalysts since these materials exhibited less 1-butene hydrogenation.[5-9]

The largest drawback concerning these Chevrel phase catalysts is their low surface area (0.1-1.5 m^2/g) relative to the supported Co-Mo-S catalysts on γ-Al_2O_3 (100 m^2/g). It is commonly observed in these types of catalytic processes that the activity increases with surface area; therefore, there is a need for the development of supported Chevrel phases.

In order to produce supported Chevrel phase compounds, a variety of methods have been attempted including evaporation,[12] sputtering,[13] and chemical vapor transport.[14] Recently, though, lower temperature routes using polythiomolybdates and metal chlorides as solution precursors have been reported.[15,16] Also, the first example of an alumina-supported Chevrel phase compound has been published.[17]

The discovery that sodium was present in the pyridine-deficient cluster compounds prompted the exploration of similar reactions without the addition of pyridine to the reaction mixture. The resulting ternary sodium molybdenum sulfides should more closely resemble the desired Chevrel phase compounds and open another avenue for preparing a variety of different materials via cation exchange reactions. The focus of this paper is on a new preparative route to the ternary Chevrel-like phases via sodium molybdenum sulfide. Characterization of these new phases and the preliminary studies as to their HDS catalytic activity will be discussed.

EXPERIMENTAL

Materials

The reagents and products involved in this work appear to be air and moisture sensitive. Therefore, special precautions were taken to ensure the maintenance of a dry, inert atmosphere. All manipulations were performed by the use of an inert atmosphere drybox, a high-vacuum manifold, and Schlenk techniques, unless otherwise stated. All glassware was thoroughly dried prior to use by the placement in an oven at 140°C for at least 4 hours.

Mo_6Cl_{12} was prepared by the high temperature comproportionation method described by Koknat *et al.*[18] Sodium hydrosulfide (NaSH) was prepared by the method described by Brauer.[19] In this method, hydrogen sulfide gas was bubbled through a solution of sodium ethoxide in ethanol and the desired product was precipitated by the addition of diethyl ether. Sodium butoxide (NaOBu) was prepared by the reaction of n-butanol with sodium metal, and used as the solid. The metal dichlorides of cobalt, tin, and lead were dehydrated by heating under dynamic vacuum and the resulting solids were stored in the drybox. Holmium trichloride was prepared at the Ames Lab Rare-Earth Center by the heating of holmium oxide with an excess of ammonium chloride to 275°C. The excess ammonium chloride was sublimed at 350°C and the $HoCl_3$ was stored in the drybox.

All solvents were purified and dried prior to use. Also, the solvents were deoxygenated by use of the freeze-thaw process: freeze to liquid nitrogen temperatures, evacuate the gaseous material, and then thaw. This process was repeated three times prior to the distillation of the purified solvent onto 3 or 4 Å molecular sieves and storage under vacuum or a nitrogen atmosphere. N-propylamine was purified by refluxing over calcium hydride for at least 4 hours. Without heating, 1-butanol was stirred with sodium metal. Methanol was dried by refluxing over sodium methoxide. N,N-dimethylformamide (dmf) was purified by refluxing with barium oxide. When used, the solvents were vacuum distilled or syringed under a flowing nitrogen gas atmosphere.

Analytical Procedures

The presence of the transition metal cations interfered with the normal molybdenum analysis procedure, therefore, it became necessary to separate the metal cations prior to further analysis. The separation of cobalt[20] was relatively easy and was incorporated into the procedure discussed below. Cobalt was determined as the oxide, Co_2O_3, while molybdenum was determined as the 8-hydroxyquinolate.[21] In this adapted procedure, the samples were dissolved in basic solutions with the aid of hydrogen peroxide. The cobalt oxide precipitated while the molybdenum remained in solution. The cobalt oxide was collected by filtration using tared Gooch crucibles and then ignited at 520°C in a muffle furnace to constant weight. The solutions containing molybdenum were then neutralized with dilute sulfuric acid to pH = 4-6.

EDTA (5%) and acetic acid/ammonium acetate buffer solutions were added. The analyte, $MoO_2(ONC_9H_6)_2$, was precipitated by the addition of the 8-hydroxyquinoline solution and filtered through tared filters. After washing with hot distilled water, the materials were dried to constant weight at 140°C. A similar procedure was employed for the analysis of holmium. Additional microanalyses for sodium and cobalt were obtained from Oneida Research Services.[22]

Chlorine was determined by the potentiometric titration of neutralized solutions with a standardized silver nitrate solution. A silver/silver chloride electrode was used as the working electrode and a silver electrode as the reference. The endpoint was determined by using the second derivative method.

Physical Measurements

Infrared spectroscopy

Infrared spectra (4000-200 cm^{-1}) were obtained by using an IBM IR/98 Fourier Transform Infrared Spectrometer and a Bomem MB-102 Fourier Transform Infrared Spectrometer manufactured by Hartmann and Braun. Samples were prepared as Nujol mulls and the mulls were pressed between cesium iodide plates. The sample chamber was continuously purged with dry, compressed air and reference spectra were collected in the empty chamber.

Raman spectroscopy

Raman spectra were obtained with the help of Jeanne Wynn in Professor

Therese Cotton's group. A Spex Triplemate spectrometer with a Princeton Applied Research Corp. (PARC) intensified SiPD detector cooled to -40°C was used to record the spectra. The excitation source was a Coherent Ar^+ 200 series laser at the wavelength of 514.5 nm and the scattered radiation was collected in a backscattering geometry. The laser power at the sample was approximately 30 mW and the integration time was 200 s. The Raman spectra were obtained at room temperature from solid samples packed in capillary tubes.

X-ray photoelectron spectroscopy

XPS spectra were collected by Jim Anderegg at room temperature with a Physical Electronics Industries 5500 multitechnique surface analysis system. This system was equipped with a hemispherical analyzer, a toroidal monochromator, and multichannel detector which sampled a 2 mm^2 area. The samples were placed on an indium substrate and excited with monochromatic Al K-α radiation (1486.6 eV) at the power of 300 W. The binding energies were calibrated with C 1s = 284.6 eV.

X-ray powder diffraction

An Enraf Nonius Delft FR552 Guinier camera was used to obtain x-ray powder diffraction patterns. A General Electric XRD-5 generator with an AEG fine focus tube and a copper target were used to generate the x-rays. Air-sensitive samples were ground thoroughly and then placed between strips of cellophane tape in the drybox. Powdered NBS silicon was added as an internal standard.

Scanning Electron Microscopy-Energy Dispersive Spectroscopy (SEM-EDS)

This technique was employed to obtain qualitative elemental information on the sample. A Cambridge S-200 Scanning Electron Microscope coupled to a Tracor Northern Micro Z-II Energy Dispersive Spectrometer with a beryllium window was used. The samples were placed onto a metal disk backed with double-stick Scotch tape and then sputter-coated with gold or carbon. The molybdenum L series and sulfur K series peaks fell at almost identical energies and thus were not resolvable by this technique.

BET surface area

Surface area measurements were obtained with the help of Michael Columbia on a Micromeritics 2100E Accusorb instrument located in Professor Glenn Schrader's group. Krypton gas was used as the adsorbate at liquid nitrogen temperatures and the samples were outgassed overnight at about 120°C before analysis. Surface areas were calculated from the data by using a least squares fitting program.

HDS catalytic activity

Catalytic activity measurements were obtained with the help of Michael Columbia by using a micro fixed-bed reactor located in Professor Glenn Schrader's group. Thiophene gas was used as the model sulfur-containing compound. The reactor was heated from room temperature to 400°C in a helium stream and, at 30 minute intervals, pulses of 2 mol % thiophene in hydrogen were injected into the reactor.

The desulfurization products were separated and analyzed by a gas chromatography-mass spectroscopy system.[23]

Synthetic Procedures

The general procedure for the preparation of the Mo_6S_8 cluster unit was similar to that discussed previously in Paper 1 for $Na_{2y}Mo_6S_{8+y}(py)_x$, except for the absence of pyridine as a coordinating ligand. These reactions were studied in neat 1-butanol in an attempt to prepare compounds that more closely resembled the ternary Chevrel phases. Changes in reaction stoichiometry and conditions were explored in order to facilitate the preparation of these ternary molybdenum sulfides.

Reactions with 1:12:6 stoichiometry

A typical procedure involved the placement of 4.00 g Mo_6Cl_{12} (4 mmol), 2.69 g NaSH (48 mmol), and 2.30 g NaOBu (24 mmol) into a reaction flask and the addition by syringe of 75 mL of 1-butanol. The mixture was then heated to reflux for a period of 2-3 days. After cooling, a blackish solid and faint colored filtrate were separated by filtration. The resulting solid was extracted with methanol to remove the sodium chloride by-product. After the extraction, no evidence of chlorine was detected by chlorine analyses. The presence of sodium was confirmed by using SEM-EDS. Also, it was observed that the methanol content was quite variable from one reaction to another. The product was found to be insoluble in non-coordinating solvents and

amorphous to x-rays. Spectral data (infrared, Raman, XPS) and elemental analyses were obtained. A surface area measurement and HDS catalytic activity study were explored. Analyses are given for the product of one preparation - Calc. for $Na_{2.8}Mo_6S_{9.4}(MeOH)_{4.2}$: Na, 5.98%; Mo, 53.50%. Found: Na, 5.98%; Mo, 53.43%; Na/Mo_6 = 2.80.

Reactions with 1:11:7 stoichiometry

Similar reactions to prepare $Na_{2y}Mo_6S_{8+y}$ were explored with a different stoichiometry. A typical reaction involved the placement of 2.00 g Mo_6Cl_{12} (2 mmol), 1.24 g NaSH (22 mmol), and 1.34 g NaOBu (14 mmol) into a reaction flask and the addition by syringe of 60 Ml of 1-butanol. The resulting reaction product, a blackish solid, was extracted with methanol to remove the sodium chloride by-product. After the extraction, no evidence of chlorine was detected by chlorine analyses. The presence of sodium was confirmed by using SEM-EDS. Spectral data (infrared, Raman, XPS) and elemental analyses were obtained. Anal. Found: Mo, 51.99%.

Reaction of $Na_{2y}Mo_6S_{8+y}$ with n-propylamine

The sodium molybdenum sulfide compound was readily converted by extraction with neat n-propylamine. A typical preparation involved the placement of 0.1-0.3 g of the solid onto the frit of an extractor and the distillation of 25-30 mL of n-propylamine into the receiving flask. After approximately 4 hours of extraction, the blackish solid was completely solubilized and provided a dark black/brown solution.

After drying under dynamic vacuum, a black, "glassy" solid was obtained. This product was identified by its infrared spectrum as $Mo_6S_8(PrNH_2)_y$. SEM-EDS on the product indicated an absence of sodium, thus it was reasoned that the propylamine insoluble sodium sulfide by-product remained on the frit after the extraction.

Cation Exchange Reactions

Reaction of $Na_{2y}Mo_6S_{8+y}$ with cobalt dichloride

A general preparation involved the reaction of 1.00 g of the ternary sodium molybdenum sulfide with an excess of cobalt dichloride (0.74 g) in methanol (30 mL). The reactions were studied at room temperature or under reflux conditions for a period of 1-2 days. Upon filtration, a blackish solid and blue filtrate were observed. The solid was extracted with solvent distilled from the filtrate to remove the NaCl by-product and any unreacted $CoCl_2$. After drying under dynamic vacuum, a black amorphous powder was obtained. The product showed a variable reactivity upon contact with air - some samples were highly pyrophoric, while others showed no apparent reactivity. SEM-EDS indicated that complete exchange of Co^{2+} for Na^+ had occurred as evidenced by the detection of only cobalt. Infrared spectra, XPS, and elemental analyses were obtained. A surface area measurement and HDS catalytic activity study were explored. Analyses are given for the product of one preparation - Calc. for $Co_{0.8}Mo_6S_{8.8}(MeOH)_{3.9}$: Co, 4.58%; Mo, 55.89%. Found: Co, 4.54%; Mo, 55.82%; $Co/Mo_6 = 0.79$.

Reaction of $Na_{2y}Mo_6S_{8+y}$ with tin dichloride

A general preparation involved the reaction of 1.00 g of the ternary sodium molybdenum sulfide with an excess of tin dichloride (1.07 g) in methanol (30 mL). The reactions were studied at room temperature or under reflux conditions for a period of 1-2 days. Upon filtration, a blackish solid and light yellow filtrate were observed. The solid was extracted with solvent distilled from the filtrate to remove the NaCl by-product and any unreacted $SnCl_2$. After drying under dynamic vacuum, a black amorphous powder was obtained. SEM-EDS indicated that complete exchange had occurred as evidenced by the detection of only tin and absence of sodium. XPS, infrared, and Raman spectra were obtained.

Reaction of $Na_{2y}Mo_6S_{8+y}$ with lead dichloride

A general preparation involved the reaction of 1.00 g of the ternary sodium molybdenum sulfide with an excess of lead dichloride (1.56 g) in N,N-dimethyl-formamide (30 mL). The reactions were studied at room temperature or under reflux conditions for a period of 1-2 days. The blackish product was extracted with methanol (30 mL) to remove the NaCl by-product and dried *in vacuo*. If chlorine analyses indicated that chlorine was still present, the sample was stirred further with dmf to remove any unreacted lead dichloride. The black powder was amorphous and highly pyrophoric upon air contact. Infrared and Raman spectra were obtained.

Reaction of $Na_{2y}Mo_6S_{8+y}$ with holmium trichloride

A general preparation involved the reaction of 1.00 g of the ternary sodium molybdenum sulfide with an excess of holmium trichloride (1.53 g) in methanol (30 mL). The reactions were studied at room temperature or under reflux conditions for a period of 1-2 days. Upon filtration, a blackish solid and pinkish filtrate were observed. The solid was extracted with solvent distilled from the filtrate to remove the NaCl by-product and any unreacted $HoCl_3$. After drying under dynamic vacuum, a black amorphous powder was obtained. The product was highly pyrophoric upon air contact. SEM-EDS indicated that exchange had occurred as evidenced by the absence of sodium and the detection of holmium. XPS, infrared, and Raman spectra and elemental analyses were obtained. Analyses are given for the product of one preparation - Calc. for $Ho_{0.3}Mo_6S_{8.45}(MeOH)_{4.4}$: Ho, 4.77%; Mo, 55.52%. Found: Ho, 4.98%; Mo, 55.58%; Ho/Mo_6 = 0.31.

Thermolysis Reactions

The sodium and tin molybdenum sulfides were explored by heating in an attempt to prepare the known Chevrel phases. $Na_{2y}Mo_6S_{8+y}$ was heated to 800°C in a sealed tube for 8 days and resulted in the formation of MoS_2 as detected by powder x-ray diffraction. Likewise, the heating of the tin molybdenum sulfide to 800°C for 4 days in a sealed tube resulted in the detection of the tin metal and MoS_2. Heating of the tin molybdenum sulfide under flowing hydrogen gas to about 1000°C resulted in the formation of the tin Chevrel phase $SnMo_6S_8$ and molybdenum metal.

A Raman spectrum was obtained on the tin molybdenum sulfide heated to 1000°C under flowing hydrogen gas and compared to a spectrum from the 900°C heating of $Na_{2y}Mo_6S_{8+y}(py)_x$ and tin metal which produced $SnMo_6S_8$ and MoS_2.

RESULTS AND DISCUSSION

Sodium Molybdenum Sulfides

Compounds of the general formula $Na_{2y}Mo_6S_{8+y}$ can be prepared via the reaction of Mo_6Cl_{12}, NaSH, and NaOBu in refluxing butanol. The presence or absence of a coordinating ligand like pyridine seems to have little effect in these types of reactions. Both the reaction in pyridine/butanol and neat butanol produce similar products - blackish amorphous powders which show very little ligand coordination. A comparison of the infrared spectra are shown in Figure 1. For $Na_{2y}Mo_6S_{8+y}$, a broad band at about 969 cm^{-1} indicates the presence of an alcohol in this material. This alcohol is most likely occluded methanol which was trapped in the compound during the extraction to remove the NaCl reaction by-product. The broad Mo-S stretching mode can be evidenced at 381 cm^{-1}. Likewise, the Raman spectra (Figure 2) are virtually identical, showing a broad Mo-S band centered at about 448 cm^{-1}. Also, the reactions of $Na_{2y}Mo_6S_{8+y}$ and the pyridine-deficient compound $Na_{2y}Mo_6S_{8+y}(py)_x$ with n-propylamine produced the same propylamine adduct - $Mo_6S_8(PrNH_2)_y$. The infrared spectra for the products of these reactions with n-propylamine are shown in Figure 3. Bands attributable to coordinated propylamine are labelled, as well as the broad Mo-S stretching mode centered at 384 cm^{-1}. XPS data for these materials are listed in Table 1 and an XPS spectrum of the sodium molybdenum sulfide compound is shown in Figure 4a. These results indicate that the pyridine-deficient ternary compound and $Na_{2y}Mo_6S_{8+y}$ are very similar.

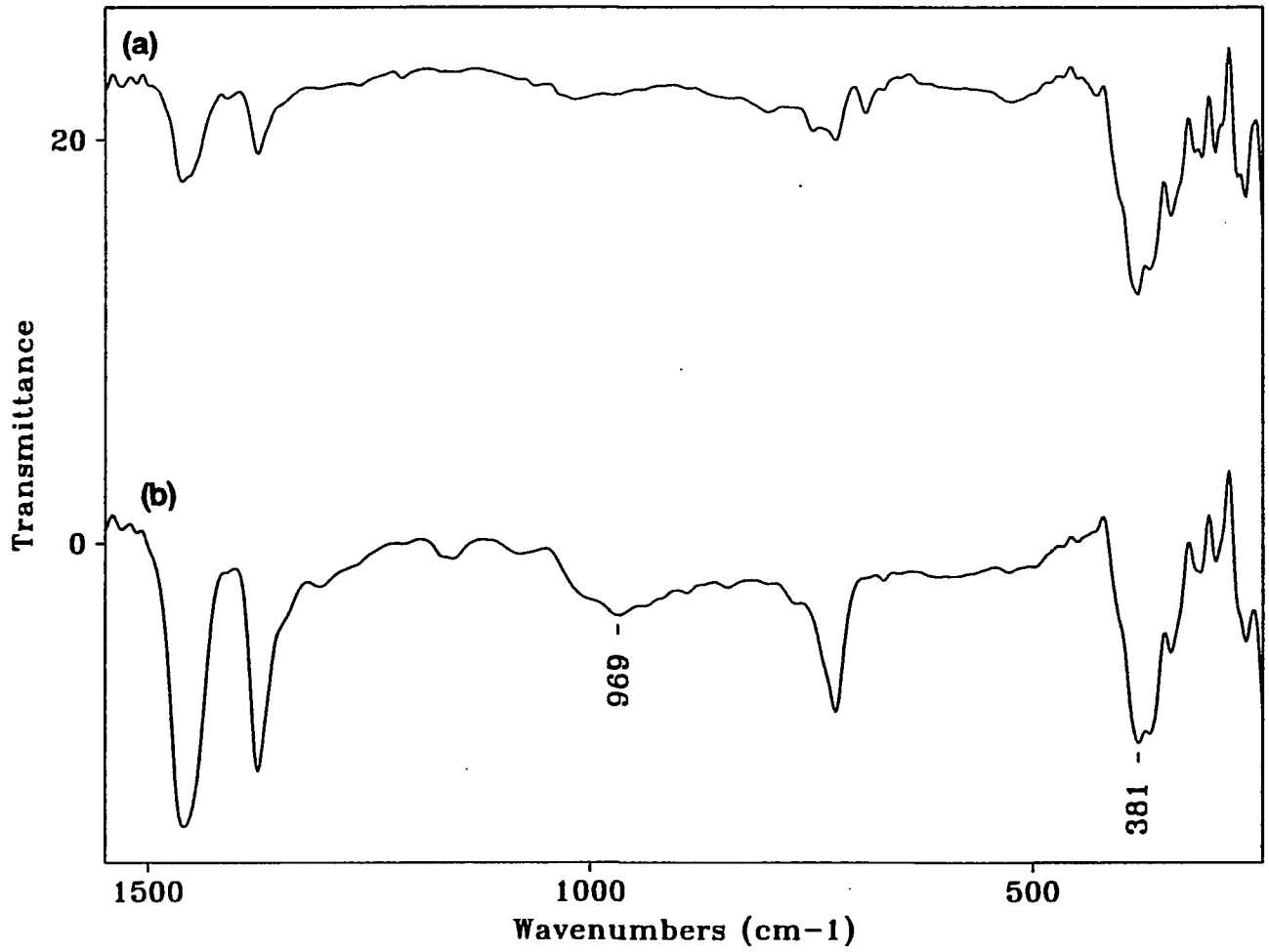

Figure 1. Infrared spectra (Nujol) for the pyridine-deficient compound $Na_{2y}Mo_6S_{8+y}(py)_x$ (a) and the ternary sodium molybdenum sulfide $Na_{2y}Mo_6S_{8+y}$ (b)

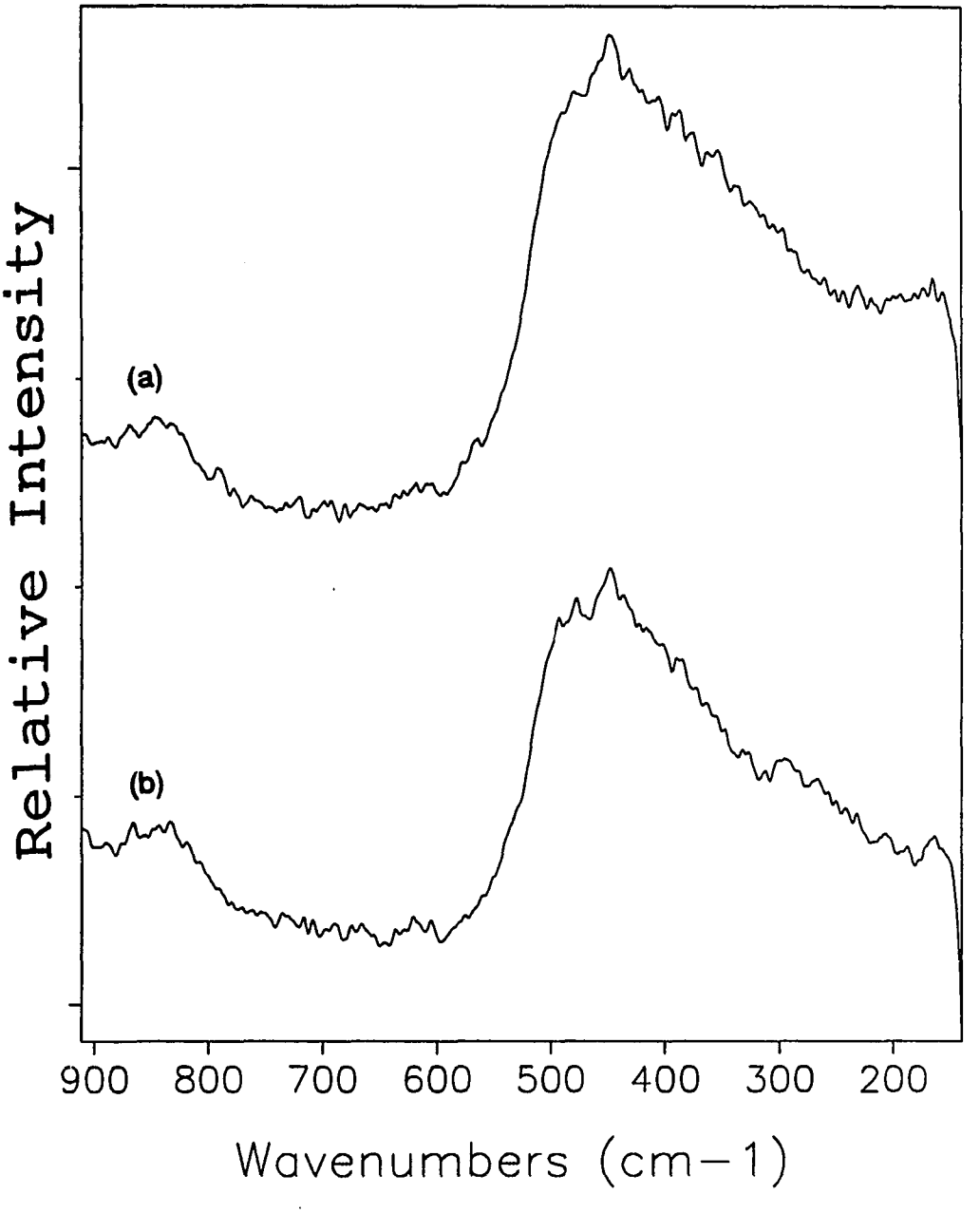

Figure 2. Raman spectra for the pyridine-deficient $Na_{2y}Mo_6S_{8+y}(py)_x$ (a) and the sodium molybdenum sulfide $Na_{2y}Mo_6S_{8+y}$ (b)

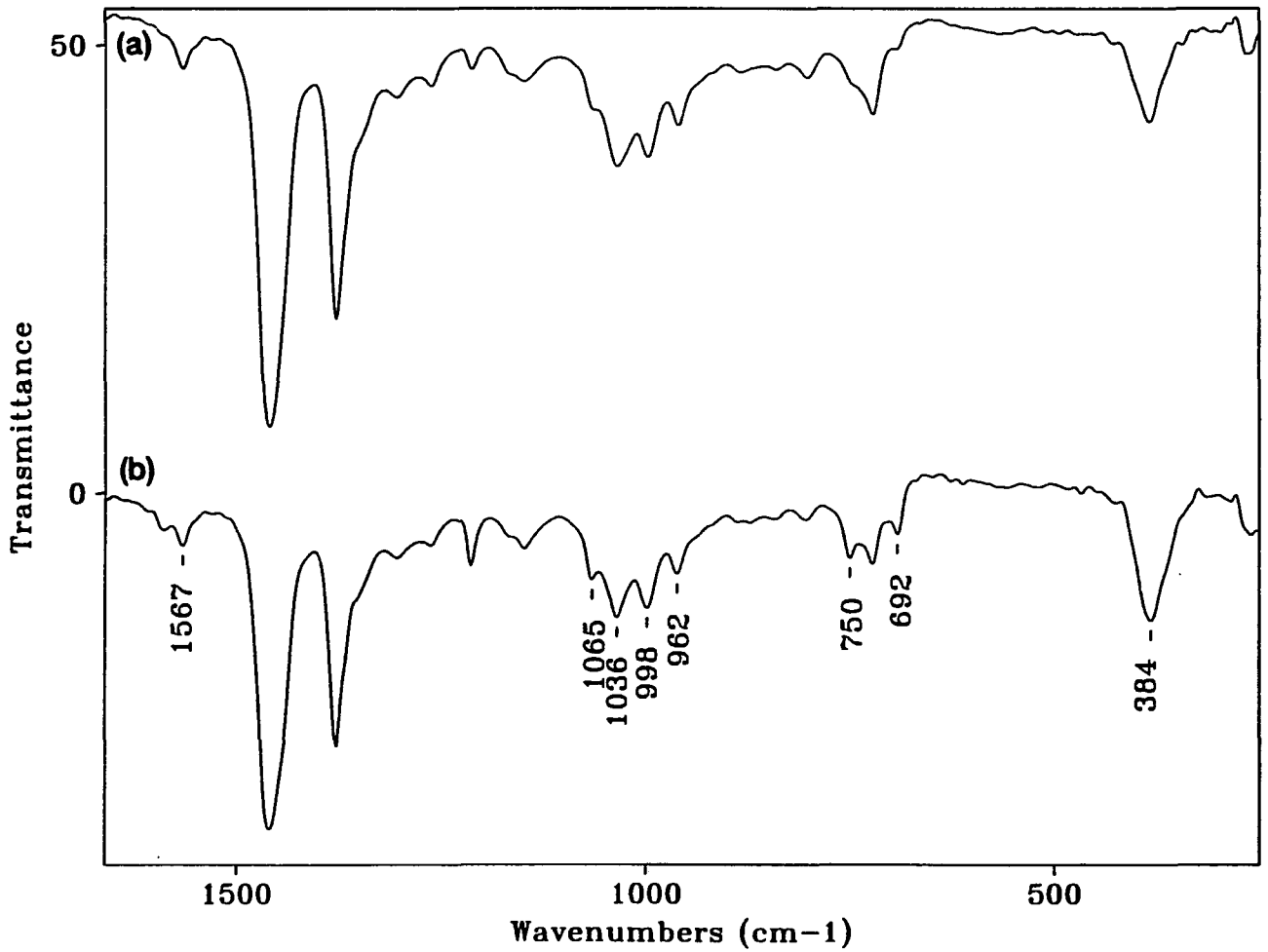

Figure 3. Infrared spectra (Nujol) for the propylamine adducts produced from the reaction of neat propylamine with the pyridine-deficient $Na_{2y}Mo_6S_{8+y}(py)_x$ (a) and $Na_{2y}Mo_6S_{8+y}$ (b)

Table 1. X-ray photoelectron spectroscopy (XPS) data[a]

	$Na_{2y}Mo_6S_{8+y}(py)_x$	$Na_{2y}Mo_6S_{8+y}$	$Co_yMo_6S_{8+y}$[b]	$Sn_yMo_6S_{8+y}$[c]	$Ho_{2y}Mo_6S_{8+3y}$
Mo $3d_{5/2}$	227.5	227.2	227.9	227.5	227.2
Mo $3d_{3/2}$	230.6	230.4	231.1	230.6	230.5
S 2s	225.4	225.0	225.8	225.4	225.0
S $2p_{3/2}$	161.1 br	160.6	161.3	161.8 br	161.1 br
S $2p_{1/2}$	-	161.8 sh	162.5 sh	-	-

[a]values adjusted to C 1s = 284.6 eV; br = broad, sh = shoulder
[b]small peaks observed at Mo $3d_{5/2}$ 228.6 eV and Mo $3d_{3/2}$ 231.8 eV
[c]ternary metal data - Sn $3d_{5/2}$ 487.0 eV, Sn $3d_{3/2}$ 495.4 eV

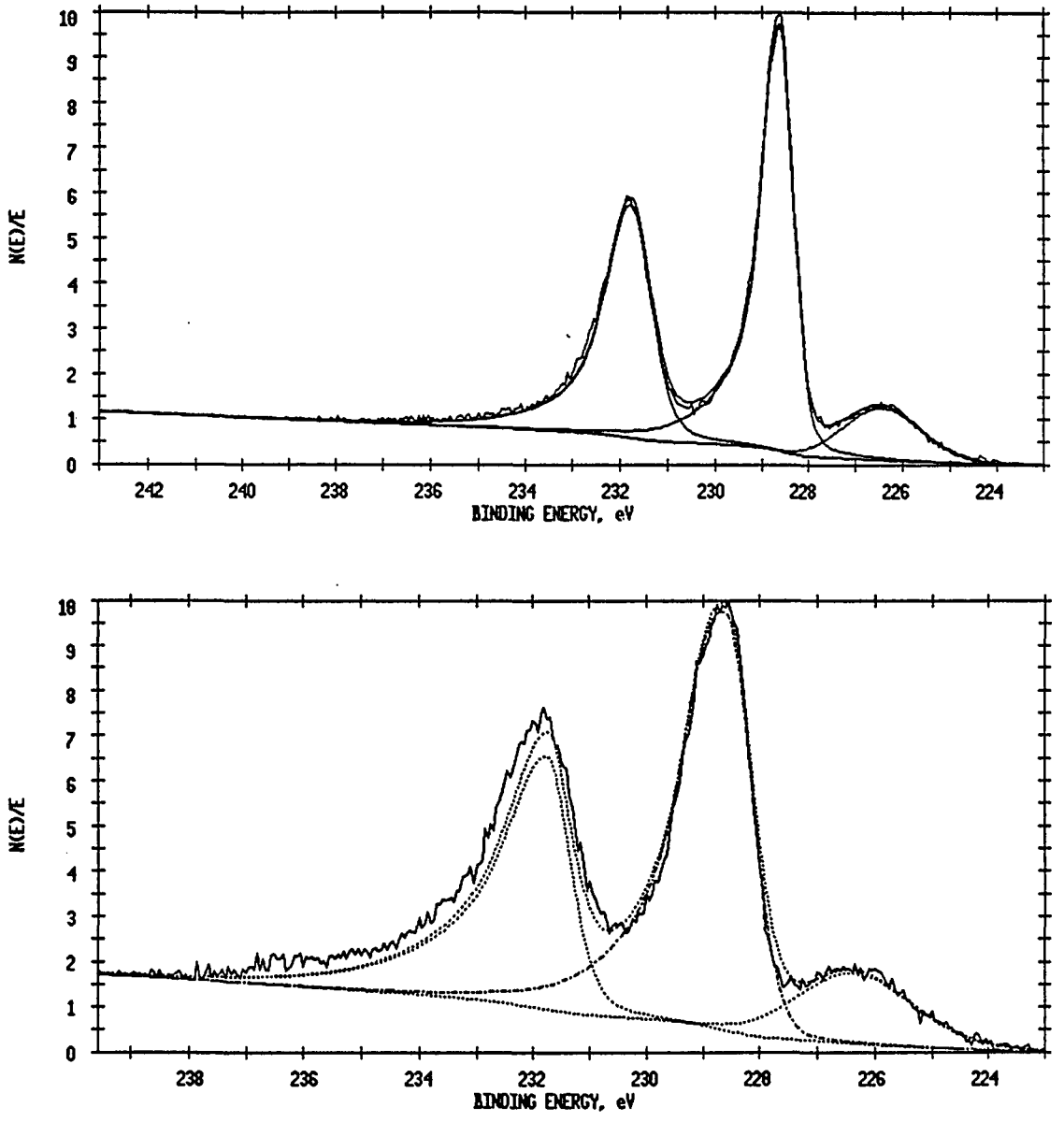

Figure 4. Uncorrected XPS spectra for the sodium (a) and tin (b) molybdenum sulfides showing the Mo 3d and S 2s bands

Elemental analyses on this ternary sodium molybdenum sulfide result in the formulation of this material as $Na_{2.8}Mo_6S_{9.4}(MeOH)_{4.2}$. The previously reported sodium Chevrel phase compounds $Na_xMo_6S_8$ were found over the range x = 1 to 4, but they did not contain extra sulfide in the terminal positions of the cluster.

Similar products were observed upon changing the reaction stoichiometry from 1:12:6 to 1:11:7 (Mo_6Cl_{12}:NaSH:NaOBu). The infrared spectra, Raman spectra, and XPS data were almost identical in nature.

Cation Exchange Reactions

The sodium in the sodium molybdenum sulfide compounds could be readily exchanged with a variety of other metal cations. This exchange occurred by the reaction of $Na_{2y}Mo_6S_{8+y}$ with the desired metal chloride in methanol or dmf (for lead dichloride) either at room temperature or under reflux conditions to produce the cobalt, tin, lead, and holmium ternary molybdenum sulfides. The products were amorphous, blackish powders which often showed a high degree of air reactivity - pyrophoric upon air contact. Complete exchange could be observed by the presence of the desired ternary metal and the lack of detectable sodium in the SEM-EDS spectrum. The infrared spectra which were obtained are shown in Figure 5. These spectra indicate the presence of weak methanol bands around 950-1000 cm^{-1} and a weak, broad Mo-S stretching mode at 380-400 cm^{-1}. The lead molybdenum sulfide compound shows bands for coordinated dimethylformamide at 1630, 1103, 893, and 658 cm^{-1}. The Raman spectra shown in Figure 6 for the ternary molybdenum sulfides

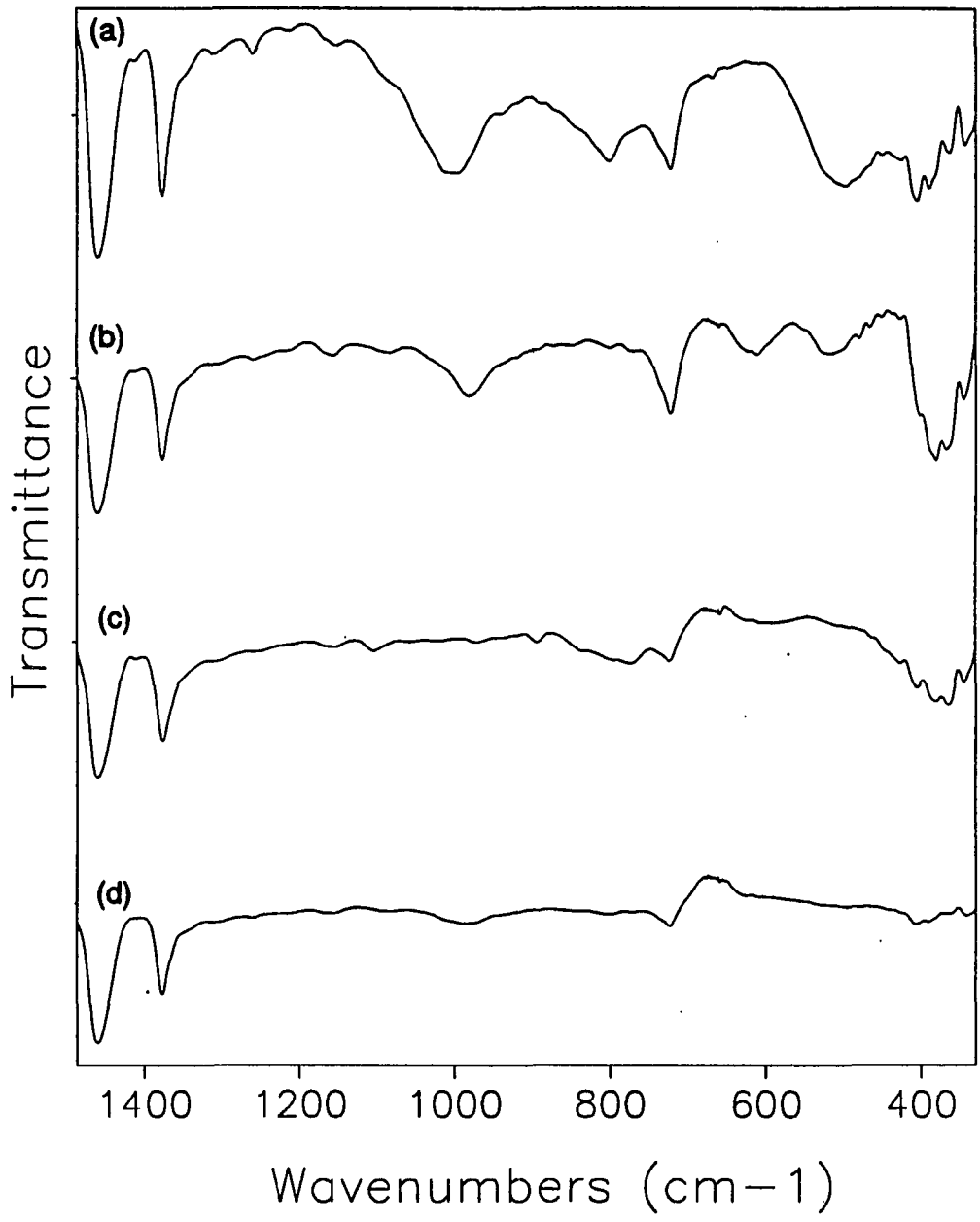

Figure 5. Infrared spectra (Nujol) for the ternary molybdenum sulfide compounds with cobalt (a), tin (b), lead (c), and holmium (d)

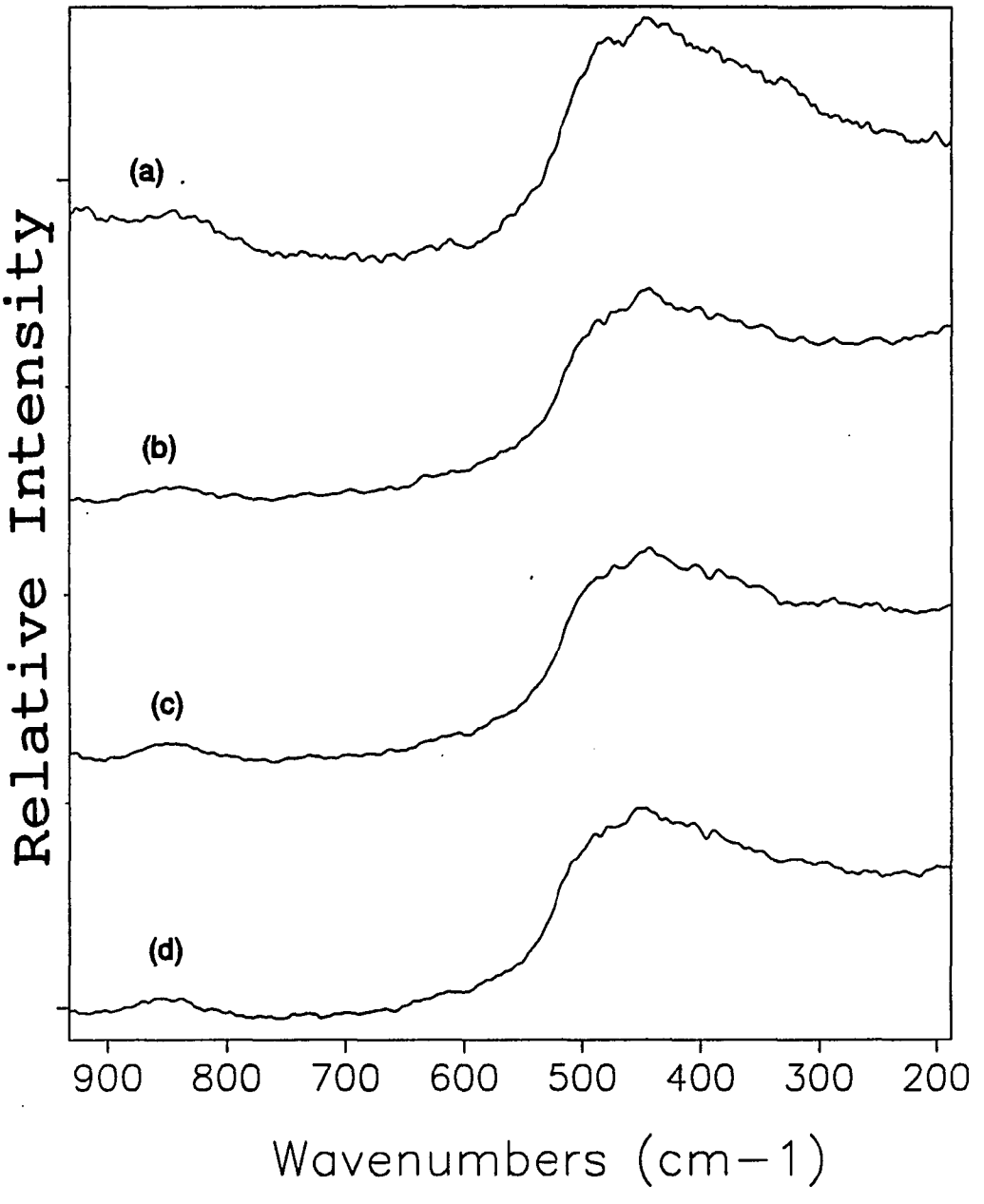

Figure 6. Raman spectra for the ternary molybdenum sulfide compounds with cobalt (a), tin (b), lead (c), and holmium (d)

exhibit a broad band centered at about 445-450 cm^{-1}, which is indicative of the Mo_6S_8 unit.

The XPS data listed in Table 1 further support the presence of the Mo_6S_8 unit. The XPS spectrum for the tin molybdenum sulfide is shown in Figure 4b. The Mo $3d_{5/2}$ values all lie within the range of 227.2 - 227.9 eV. Likewise, the data for the cobalt and tin molybdenum sulfides are very similar to those observed for the Chevrel phase compounds - $Co_{1.6}Mo_6S_8$ (Mo $3d_{5/2}$, 227.8; S 2p, 161.9 Ev) and $SnMo_6S_8$ (Mo $3d_{5/2}$, 228.1; S 2p, 161.7 eV).[6]

Elemental analyses on the cobalt and holmium molybdenum sulfides result in the formulation of $Co_{0.8}Mo_6S_{8.8}(MeOH)_{3.9}$ and $Ho_{0.3}Mo_6S_{8.45}(MeOH)_{4.4}$ for these materials. These values indicate that the cation exchanged ternary molybdenum sulfides contain much less ternary metal than the corresponding Chevrel phases.

Thermolysis Reactions

Preliminary attempts to prepare the Chevrel phases by heating of the sodium and tin molybdenum sulfides were explored. Direct heating of either compound to 800°C in a sealed tube resulted in oxidation or disproportionation of the cluster unit and the detection of MoS_2 by powder x-ray diffraction. However, heating to about 1000°C under a reducing hydrogen gas flow produced the desired tin Chevrel phase along with molybdenum metal. These results indicate the necessity of having a reducing atmosphere present in the reactions, while lower temperature heating should aid in preparing single phase Chevrel compounds.

The Raman spectrum for the heating of tin molybdenum sulfide under a reducing hydrogen atmosphere is shown in Figure 7a and compared to the spectrum from the heating to 900°C of $Na_{2y}Mo_6S_{8+y}(py)_x$ and tin metal which contains the tin Chevrel phase and MoS_2 (Figure 6b). Both spectra show that the tin Chevrel phase compound, $SnMo_6S_8$, exhibits a broad band centered at about 445 cm^{-1} which is also seen in the Raman spectra of the ternary molybdenum sulfides. Pronounced MoS_2 bands are observed in Figure 7b at 405 cm^{-1} and 380 cm^{-1} which has been identified as the Mo-S A_{1g} and $E_{2g}{}^1$ modes.[24]

Thermogravimetric analysis (TG/DTA) was explored for several samples, however, problems with oxygen contamination were evidenced by an initial increase in weight and the detection of MoO_2 in the powder x-ray diffraction patterns of these TG/DTA products.

HDS Catalytic Activity

Preliminary catalytic activity measurements were made on the sodium and cobalt molybdenum sulfide compounds. These materials exhibited higher surface areas and thiophene conversion percentages than any reported Chevrel phase compounds, however, the HDS activities were not as high as any of the Chevrel phases. The results of this study are tabulated in Table 2 and are compared with several Chevrel phase compounds and the unsupported catalyst "Co-Mo-S".

The lower HDS activity could be the result of ternary metal cation size. McCarty *et al.* previously reported that the small ternary metal cation Chevrel phases exhibited

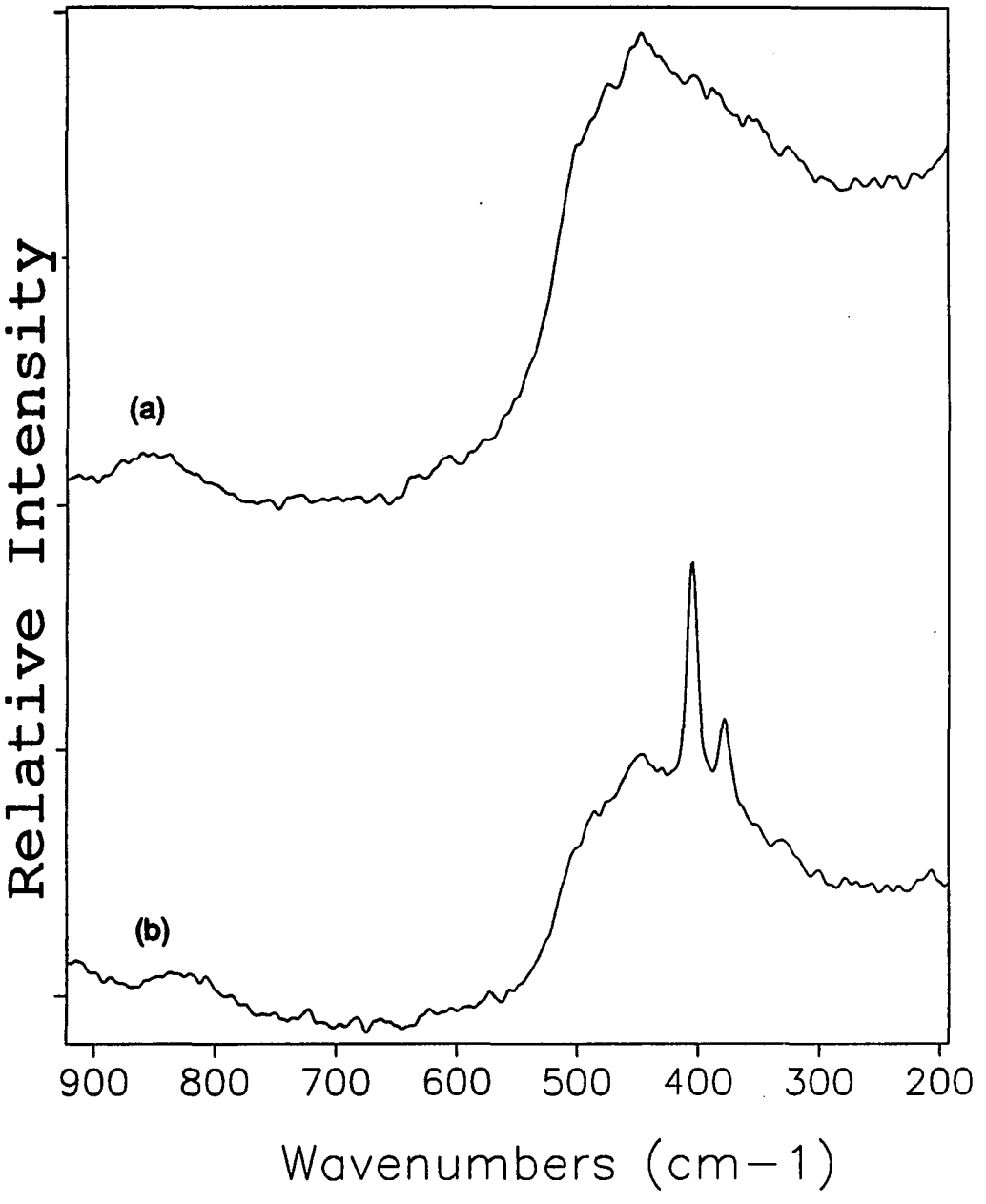

Figure 7. Raman spectra for the tin molybdenum sulfide compound heated to 1000°C under flowing hydrogen gas (a) and the pyridine-deficient compound with tin metal heated to 900°C in a sealed tube (b). Both spectra exhibit a broad band centered at about 445 cm^{-1}, while sharp bands for MoS_2 can be observed at 405 and 380 cm^{-1} in (b).

Table 2. Thiophene hydrodesulfurization (HDS) activities after reaction at 400°C[a,b]

	Surface area (m^2/g)	% thiophene conversion	HDS Rate ($x10^8$ mol/m^2s)
$Na_{2y}Mo_6S_{8+y}$	4.30	1.19	0.27
$Co_yMo_6S_{8+y}$	6.95	3.67	0.52
$Ho_{1.2}Mo_6S_8$	0.58	2.20	11.23
$PbMo_{6.2}S_8$	0.40	1.28	6.68
$SnMo_{6.2}S_8$	0.39	1.72	3.24
$Co_{1.6}Mo_6S_8$	0.10	0.47	1.02
$Co_{0.25}$-Mo-S	10.83	0.77	2.92

[a]Chevrel phases and $Co_{0.25}$-Mo-S data are from reference 6
[b]Sodium compound heated for 4 hours, cobalt compound heated for 5 hours, remaining compounds were heated for 10 hours

lower activity than those with large cations.[5-6] It was reasoned that the large cations have little mobility which results in structural stability and thus catalytic stability. However, the high mobility of the small cations, as observed in their high ion conductivity, allows these cations to "retreat" from the surface into the bulk structure. This movement makes the material less catalytically active and opens sites to surface oxidation and subsequent destabilization by forming MoS_2.

Further support for this reasoning can be observed in the XPS spectra for the cobalt molybdenum sulfide as prepared and after the HDS experiment (Figure 8). The initial cobalt compound shows the distinctive Mo $3d_{5/2}$ peak at 227.9 eV which is supportive of the Mo_6S_8 cluster unit, as well as smaller peaks due to surface oxidation. After hydrodesulfurization, the largest Mo $3d_{5/2}$ peak resides at 228.5 eV which indicates oxidation of the material's surface (MoO_2-like binding energy). A much smaller peak is also observed at 227.7 eV (Mo $3d_{5/2}$), the normal binding energy for the cobalt compound. The cobalt molybdenum sulfide material shows only a trace peak for cobalt at 778 eV ($2p_{3/2}$) after HDS which further supports only a very small amount of cobalt remaining on the surface. Similar observations have been reported for the cobalt Chevrel phase $Co_{1.6}Mo_6S_8$.[6]

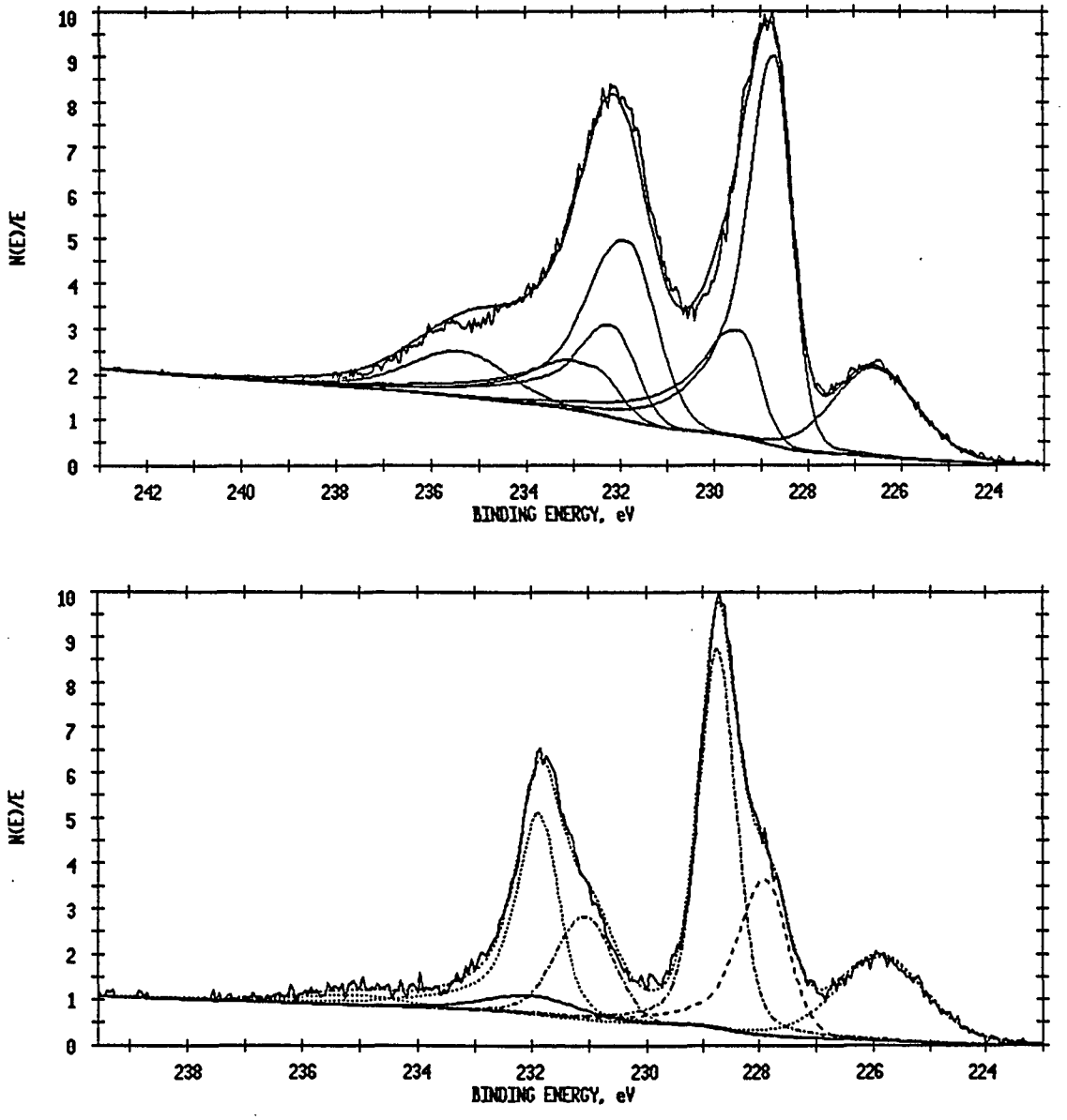

Figure 8. Uncorrected XPS spectra for the cobalt molybdenum sulfide as prepared (a) and the product after hydrodesulfurization (b). The spectra show Mo 3d and S 2s bands for the Mo_6S_8 cluster unit as well as surface oxidation of the material.

CONCLUSIONS

This paper describes new preparative routes to ternary molybdenum sulfides by cation exchange reactions with sodium molybdenum sulfide. A wide range of compounds have been prepared with the ternary metals of cobalt, tin, lead, and holmium. These compounds are similar to the Chevrel phases in that they both contain Mo_6S_8 cluster units. Raman spectroscopy and XPS support the presence of the cluster units. These Mo_6S_8 units are not as strongly interconnected at the lower preparation temperatures which allows for the extraction of individual clusters via the reaction with propylamine as evidenced for the sodium molybdenum sulfide.

Elemental analyses have indicated that the cobalt and holmium molybdenum sulfides contain much less ternary metal than what is evidenced for the corresponding Chevrel phases. These compounds are formulated as $Co_{0.8}Mo_6S_{8.6}(MeOH)_{3.9}$ and $Ho_{0.3}Mo_6S_{8.45}(MeOH)_{4.4}$. The presence of the ternary metal and absence of sodium has been confirmed by XPS and SEM-EDS, while methanol is detected in the infrared spectra of these products.

The tin Chevrel phase, $SnMo_6S_8$, has been prepared by the high temperature heating of the tin molybdenum sulfide in the presence of flowing hydrogen gas. Direct heating of the same material in a sealed tube leads to the detection of MoS_2 which indicates cluster degradation either by oxidation or disproportionation.

Hydrodesulfurization (HDS) studies have been explored to discover if the ternary molybdenum sulfides show similar activities to the Chevrel phases. Preliminary

studies on the sodium and cobalt compounds indicate that these materials possess larger surface areas and thiophene conversion percentages than the corresponding Chevrel phases, however, the ternary molybdenum sulfides show a slower HDS rate. The small cation Chevrel phases were previously found to exhibit lower HDS rates, which was explained by the movement of the cations away from the surface and subsequent surface oxidation. Similar observations were noted for the cobalt molybdenum sulfides. XPS spectra on the solids after HDS showed the presence of surface oxides and very little cobalt was detected on the surface. Distinct differences should be observed with the larger cation ternary molybdenum sulfides since these cations are not considered to be very mobile.

Raman spectroscopy has developed into an important tool for studying the ternary molybdenum sulfides. A broad, yet distinctive, Mo-S band is always detected at about 445-450 cm^{-1}. Further study on samples containing $SnMo_6S_8$ have also shown that this Chevrel phase produces a similar band in the Raman spectrum. Samples containing MoS_2, as detected in the powder x-ray diffraction patterns, show distinct Raman bands that are separated from the Mo_6S_6 cluster Mo-S band.

Further development is needed on these ternary molybdenum sulfides, especially, better characterization of the existing compounds and exploration into the preparation of new compounds. Likewise, catalytic activity studies on the reported tin, lead, and holmium molybdenum sulfides are of great interest in order to discover if these large cation compounds show similar HDS properties to the Chevrel phases. Also, research is needed to better understand the conditions necessary to convert these

materials into single phase Chevrel compounds via the hydrogen reduction process. Further reactions should be explored in order to increase the metal cation concentration in the ternary molybdenum sulfides prepared by cation exchange. Finally, other routes to these ternary molybdenum sulfides should be considered. Possible ideas include the reaction of the propylamine adduct with sodium hydrosulfide or sodium borohydride in solution or by sealed tube heating. A metal or metal halide could be added to the reaction mixture. Higher temperature reduction in hydrogen gas would probably be needed to form the desired products.

Further methods of characterization like EXAFS or diffuse scattering should be explored for these ternary molybdenum sulfides, especially as they compare to the Chevrel phase compounds. Also, Raman spectra should be collected for Mo_6S_8 and other Chevrel phases to verify that this technique can detect the Mo-S stretch for these compounds. Furthermore, a variable temperature x-ray diffraction study could prove interesting in the detection of the temperature region where these ternary molybdenum sulfides are converted to the Chevrel phases.

REFERENCES

1. Yvon, K. Current Topics in Materials Science, 1st ed., Kaldis, E., Ed.; North-Holland: New York, 1978; Vol. 3, Ch. 2.

2. Chevrel, R.; Sergent, M. Topics in Current Physics, Fischer, Ø. and Maple, M.B., Eds.; Springer-Verlag: Heidelberg, 1982; Vol. 32, Ch. 2.

3. Schölihorn, R.; Kümpers, M.; Besenhard, J.O. *Mater. Res. Bull.* 1977, *12*, 781.

4. Mulhern, P.J.; Haering, R.R. *Can. J. Phys.* 1984, *62*, 527.

5. McCarty, K.F.; Schrader, G.L. *Ind. Eng. Chem. Prod. Res. Dev.* 1984, *23*, 519.

6. McCarty, K.F.; Anderegg, J.W.; Schrader, G.L. *J. Catal.* 1985, *93*, 375.

7. McCarty, K.F.; Schrader, G.L. *J. Catal.* 1987, *103*, 261.

8. Ekman, M.E.; Anderegg, J.W.; Schrader, G.L. *J. Catal.* 1989, *117*, 246.

9. Kareem, S.A.; Miranda, R. *J. Molec. Catal.* 1989, *53*, 275.

10. *Oil and Gas Journal* 1991, *89*, 25.

11. Weisser, O.; Landa, S. Sulphide Catalysts: Their Properties and Applications; Pergamon Press: Oxford, 1973.

12. Webb, R.J.; Goldman, A.M.; Kang, J.H.; Maps, J.; Schmidt, M.F. *IEEE Trans. Magn.* 1985, *MAG-21*, 835.

13. Banks, C.K.; Kammerdiner, L.; Luo, H. *J. Solid State Chem.* 1975, *15*, 271.

14. Hinode, H.; Yamamoto, S.; Wakihara, M.; Taniguchi, M. *Mater. Res. Bull.* 1985, *20*, 611.

15. Nanjundaswamy, K.S.; Vasanthacharya, N.Y.; Gopalakrishnan, J.; Rao, C.N.R. *Inorg. Chem.* 1987, *26*, 4286.

16. Rabiller-Baudry, M.; Sergent, M.; Chevrel, R. *Mater. Res. Bull.* 1991, *26*, 519.

17. Rabiller-Baudry, M.; Sergent, M.; Chevrel, R.; Prouzet, E.; Dexpert, H. *Eur. J. Solid State Inorg. Chem.* 1992, *29*, 593.

18. Koknat, F.W.; Adaway, T.J.; Erzerum, S.I.; Syed, S. *Inorg. Nucl. Chem. Lett.* 1980, *16*, 307.

19. Brauer, G. Handbuch der Preparativen Anorganischen Chemie; Ferdinand Enke Verlag: Stuttgart, 1975; p. 371.

20. Young, R.S. The Analytical Chemistry of Cobait; Pergamon Press: Oxford, 1966; pp. 37-38.

21. Elwell, W.T.; Wood, D.F. Analytical Chemistry of Molybdenum and Tungsten; Pergamon Press: New York, 1971.

22. Oneida Research Services, Inc., Whitesboro, New York.

23. Specific details about the HDS catalytic activity equipment and measurements can be found in McCarty, K.F. PhD. Dissertation, Iowa State University, Ames, IA, 1985.

24. Verble, J.L.; Wieting, T.J. *Phys. Rev. Lett.* 1970, *25*, 362.

GENERAL SUMMARY

The goal of this dissertation has been to develop and characterize $Mo_8S_8L_6$ cluster complexes as precursors for the low temperature synthesis of the Chevrel phase compounds, $M_xMo_6S_8$. Subsequently, deligation of these cluster complexes has been explored in order to prepare the desired Chevrel phases. In conjunction, a new synthetic route for the preparation of ternary molybdenum sulfides has been discovered. Cation exchange reactions with $Na_{2y}Mo_6S_{8+y}$ have resulted in the formation of materials that are related to the Chevrel phase compounds.

An improved method for the preparation of $Na_{2y}Mo_6S_{8+y}(py)_x$ was discovered by the reaction of Mo_6Cl_{12} with higher stoichiometric ratios of sodium hydrosulfide and sodium butoxide in 1-butanol/pyridine. This pyridine-deficient compound was quite soluble in neat pyridine (py) and resulted in the formation of the crystalline hexapyridine complex. This adduct exhibited two different crystal modifications which were structurally characterized as the triclinic $Mo_6S_8(py)_6 \cdot 1.65py$ and cubic $Mo_6S_8(py)_6 \cdot 2py$.

Further reaction of the pyridine-deficient compound with n-propylamine ($PrNH_2$) resulted in the formation of the reactive, ligand-deficient $Mo_6S_8(PrNH_2)_y$ complex. Subsequent ligand exchange reactions with pyrrolidine (pyrr) and piperidine (pip) produced the tetragonal $Mo_6S_8(pyrr)_6 \cdot 1pyrr$ and $Mo_6S_8(pip)_6 \cdot 7pip$ complexes. Solubility of the piperidine adduct allowed for two-dimensional NMR studies and

proton assignments. The structural solution showed that the piperidine ligands were coordinated via equatorial positions on the N-atom with respect to chair conformation.

Spectroscopic studies have resulted in the observation of characteristic bands for the Mo_6S_8 cluster unit. Infrared bands can be noted for the Mo-S stretching mode at 378-392 cm^{-1}. Sharp Raman bands for the Mo-S A_{1g} mode are observed at 408-415 cm^{-1} in the crystalline complexes and, upon ligand loss, a broad band is found at 445-450 cm^{-1}. XPS bands are observed at 227.2-227.8 eV ($Mo3d_{5/2}$), 230.4-230.9 Ev ($Mo3d_{3/2}$), 224.7-225.4 eV (S2s), 160.3-161.0 eV ($S2p_{3/2}$), and 161.4-162.1 eV ($S2p_{1/2}$). Structural determinations for the nitrogen-donor complexes exhibit Mo-Mo and Mo-S bond distances which are nearly identical to previous complexes with sulfur-or phosphorus-donor ligands. However, these nitrogen-donor ligands show much weaker bonding to the cluster units and thus were excellent candidates for deligation studies to remove the ligands and form the binary Chevrel phase Mo_6S_8.

Deiigation studies were explored by a variety of methods including direct heating of the compounds, reactions with tin and lead metal, thermolysis reactions in the presence of ammonia gas, and solution reactions with strong acids. Direct thermolysis reactions resulted in incomplete deligation and ligand fragmentation at temperatures above 300°C. Under dynamic vacuum conditions, this fragmentation was indicated by the observation of an increase in pressure at these temperatures. This pressure increase must have resulted from the production of volatile gases like methane or hydrogen which would not be condensed in the liquid nitrogen trap.

The reaction of the pyridine-deficient compound with the ternary metals resulted in the formation of the desired Chevrel phases along with an MoS_2 impurity phase. Heating of the materials to 700°C under dynamic vacuum produced an amorphous material whose XPS spectrum indicated the compound was Chevrel phase-like. The Chevrel phase compounds could be produced by further heating to 900°C.

Thermolysis reactions in the presence of ammonia gas have resulted in what appears to be complete deligation of the propylamine adduct at much lower temperatures than observed by direct heating under dynamic vacuum. The infrared spectrum after heating at 150°C in ammonia showed the absence of propylamine, while distinct propylamine bands were observed for the sample heated *in vacuo*.

Solution reactions in the presence of strong acids were studied in an attempt to protonate the ligands and thus make them better leaving groups. Reactions in trifluoromethanesulfonic acid led to removal of the ligands; however, coordination of the triflate anion was observed. Reactions with tetrafluoroboric acid/diethyl ether complex in diethyl ether indicated coordination of BF_3 or BF_4^-. Reactions in methanol removed the propylamine ligands and the infrared spectra showed only methanol coordination, yet the analyses do not clearly indicate complete deligation.

A new preparative route has been developed for ternary molybdenum sulfides. Cation exchange reactions with sodium molybdenum sulfide were used to prepare the cobalt, tin, lead, and holmium compounds. Raman and XPS spectroscopy have indicated that these compounds contain the Mo_6S_8 cluster units. These cluster units

are not as strongly interconnected as the Chevrel phases at these lower preparation temperatures, which allows for the extraction of individual clusters via reaction with propylamine to form the ligand-deficient $Mo_6S_8(PrNH_2)_y$ complex.

Elemental analyses have indicated that these complexes contain much less ternary metal than is observed for the Chevrel phases. The presence of the ternary metal and absence of sodium was confirmed by SEM-EDS and XPS. The tin Chevrel phase can be prepared by the high temperature heating of the tin molybdenum sulfide in the presence of flowing hydrogen gas. Furthermore, this product shows the broad, yet characteristic, band at about 445-450 cm^{-1} in the Raman spectrum. Direct heating of the same material in a sealed tube leads to the formation of MoS_2 and indicates cluster degradation. Preliminary hydrodesulfurization (HDS) studies on the sodium and cobalt compounds showed that these materials possess larger surface areas and thiophene conversion percentages than the Chevrel phases; however, these ternary molybdenum sulfides exhibit lower HDS rates.

REFERENCES

1. Yvon, K. Current Topics in Materials Science, 1st ed., Kaldis, E., Ed.; North-Holland: New York, 1978; Vol. 3, Ch. 2.

2. Chevrel, R.; Sergent, M. Topics in Current Physics, Fischer, Ø. and Maple, M.B., Eds.; Springer-Verlag: Heidelberg, 1982; Vol. 32, Ch. 2.

3. Schöllhorn, R.; Kümpers, M.; Besenhard, J.O. *Mater. Res. Bull.* **1977**, *12*, 781.

4. Mulhern, P.J.; Haering, R.R. *Can. J. Phys.* **1984**, *62*, 527.

5. McCarty, K.F.; Schrader, G.L. *Ind. Eng. Chem. Prod. Res. Dev.* **1984**, *23*, 519.

6. McCarty, K.F.; Anderegg, J.W.; Schrader, G.L. *J. Catal.* **1985**, *93*, 375.

7. McCarty, K.F.; Schrader, G.L. *J. Catal.* **1987**, *103*, 261.

8. Ekman, M.E.; Anderegg, J.W.; Schrader, G.L. *J. Catal.* **1989**, *117*, 246.

9. Kareem, S.A.; Miranda, R. *J. Molec. Catal.* **1989**, *53*, 275.

10. *Oil and Gas Journal* **1991**, *89*, 25.

11. Aksenov, V.S.; Kamyanov, V.F. Organic Sulfur Chemistry, Freidina, R.Kh. and Skorova, A.E., Eds.; Pergamon Press: New York, 1981; p. 201.

12. Gates, B.C.; Katzer, J.R.; Schuit, G.C.A. Chemistry of Catalytic Processes; McGraw-Hill: New York, 1979.

13. Weisser, O.; Landa, S. Sulphide Catalysts: Their Properties and Applications; Pergamon Press: Oxford, 1973.

14. Topsøe, H.; Clausen, B.S.; Candia, R.; Wivel, C.; Mørup, S. *J. Catal.* **1981**, *68*, 433.

15. Tauster, S.J.; Pecoraro, T.A.; Chianelli, R.R. *J. Catal.* **1980**, *63*, 515.

16. Webb, R.J.; Goldman, A.M.; Kang, J.H.; Maps, J.; Schmidt, M.F. *IEEE Trans. Magn.* **1985**, *MAG-21*, 835.

17. Banks, C.K.; Kammerdiner, L.; Luo, H. *J. Solid State Chem.* **1975**, *15*, 271.

18. Hinode, H.; Yamamoto, S.; Wakihara, M.; Taniguchi, M. *Mater. Res. Bull.* **1985**, *20*, 611.

19. Nanjundaswamy, K.S.; Vasanthacharya, N.Y.; Gopalakrishnan, J.; Rao, C.N.R. *Inorg. Chem.* **1987**, *26*, 4286.

20. Rabiller-Baudry, M.; Sergent, M.; Chevrel, R. *Mater. Res. Bull.* **1991**, *26*, 519.

21. Rabiller-Baudry, M.; Sergent, M.; Chevrel, R.; Prouzet, E.; Dexpert, H. *Eur. J. Solid State Inorg. Chem.* **1992**, *29*, 593.

22. Schäfer, H.; von Schnering, H.G. *Angew. Chem.* **1964**, *20*, 833.

23. Michel, J.B.; McCarley, R.E. *Inorg. Chem.* **1982**, *21*, 1864.

24. Michel, J.B. PhD. Dissertation, Iowa State University, Ames, IA, 1979.

25. Laughiin, S.K. M.S. Thesis, Iowa State University, Ames, IA, 1986.

26. Spink, D.A. M.S. Thesis, Iowa State University, Ames, IA, 1986.

27. Spink, D.A. PhD. Dissertation, Iowa State University, Ames, IA, 1989.

28. McCarley, R.E.; Laughlin, S.K.; Spink, D.A.; Hur, N. Abstract of Papers, 3rd Chemical Congress of North America, Toronto, Ontario (Canada), 1988.

29. McCarley, R.E.; Zhang, X.; Spink, D.A.; Hur, N. Abstracts of Papers, 199th National Meeting of the American Chemical Society; Boston, MA, 1990.

30. Saito, T.; Yamamoto, N.; Yamagata, T.; Imoto, H. *J. Am. Chem. Soc.* **1988**, *110*, 1646.

31. Saito, T.; Yamamoto, N.; Nagase, T.; Tsuboi, T.; Kobayashi, K.; Yamagata, T.; Imoto, H.; Unoura, K. *Inorg. Chem.* **1990**, *29*, 764.

32. Zhang, X. PhD. Dissertation, Iowa State University, Ames, IA, 1991.

33. Chevrel, R.; Sergent, M.; Prigent, J. *J. Solid State Chem.* **1971**, *3*, 515.

34. Peňa, O.; Sergent, M. *Prog. Solid St. Chem.* **1989**, *19*, 165.

35. Chevrel, R.; Sergent, M.; Prigent, J. *Mater. Res. Bull.* **1974**, *9*, 1487.

36. Schöllhorn, R.; Kümpers, M.; Plorin, D. *J. Less-Common Metals* **1978**, *58*, 55.

37. Guillevic, J.; Bars, O.; Grandjean, D. *J. Solid State Chem.* **1973**, *7*, 158.

38. Tarascon, J.M.; Waszczak, J.V.; Hull, G.W.; DiSalvo, F.J.; Blitzer, L.D. *Solid State Comm.* **1983**, *47*, 973.

39. Tarascon, J.M.; DiSalvo, F.J.; Murphy, D.W.; Hull, G.W.; Rietman, E.A.; Waszczak, J.V. *J. Solid State Chem.* **1984**, *54*, 204.

40. Nohl, H.; Klose, W.; Andersen, O.K. Topics in Current Physics, Fischer, Ø. and Maple, M.B., Eds.; Springer-Verlag: Heidelberg, 1982; Vol. 32, Ch. 6.

41. Hughbanks, T.; Hoffman, R. *J. Am. Chem. Soc.* **1983**, *105*, 1150.

42. Perrin, A.; Sergent, M.; Fischer, Ø. *Mater. Res. Bull.* **1978**, *13*, 259.

43. Sergent, M. Thése de Doctorat d'Etat, Rennes, France, 1969.

44. Behlock, R.J.; Robinson, W.R. *Mater. Res. Bull.* **1983**, *18*, 1069.

45. Nanjundaswamy, K.S.; Gopalakrishnan, J. *J. Solid State Chem.* **1987**, *68*, 188.

46. Schäfer, H.; von Schnering, H.G.; Tillack, J.; Kuhnen, F.; Wohrle, H.; Baumann, H. *Z. Anorg. Ailg. Chem.* **1967**, *353*, 281.

47. Perrin, C.; Sergent, M.; Le Traon, F.; Le Traon, A. *J. Solid State Chem.* **1978**, *25*, 197.

ACKNOWLEDGEMENTS

I would like to express my appreciation and thanks to Dr. R.E. McCarley for his guidance and instruction during my graduate years at Iowa State. I will always remember the brainstorming sessions we had when this work seemed to produce more and more questions and very few answers. I always left those times with new insights and renewed motivation. Thanks, Doc.

I would also like to thank the past and present members of the McCarley group. Special appreciation goes to George Schimek - you have been both a great roommate and friend. Thanks for continuing to challenge me.

This research would not have been possible without the aid of the following people and their expertise:

Dr. Victor Young for x-ray crystallography
James Anderegg for x-ray photoelectron spectroscopy data
Jeane Wynn for Raman spectroscopy data
Dave Scott for 2-dimensional NMR studies
Mike Columbia for HDS catalytic activity studies

I would like to thank my family for the support and love they have shown me and the encouragement to work to the best of my abilities in all that I do. You taught me to enjoy the good times and persevere through the tough times and to find joy in each of them. Thanks, I love you!

I would like to thank the many friends I have gained during these years in Ames. You have taught me what it means to grow in community and to serve others. You will always be in my thoughts, memories, and prayers.

Finally, I would like to acknowledge the ONE who made all possible - my Lord and Savior Jesus Christ. I praise You and thank You for the opportunities to learn and grow during my graduate studies.

This work was performed at the Ames Laboratory under contract no. W-7405-eng-82 with the U. S. Department of Energy. The United States government has assigned the DOE Report number IS-T 1609 to this dissertation.